PUBLICAÇÃO ESPECIAL Nº 03
1988

PROPRIEDADES GERAIS DE GALÁXIAS LENTICULARES E ELÍPTICAS

Reinaldo R. de Carvalho

Tese de Doutorado
Rio de Janeiro, Janeiro/88

CONSELHO NACIONAL DE DESENVOLVIMENTO CIENTÍFICO E TECNOLÓGICO
OBSERVATÓRIO NACIONAL
DEPARTAMENTO DE ASTRONOMIA

PROPRIEDADES GERAIS DE GALÁXIAS LENTICULARES E ELÍPTICAS

REINALDO RAMOS DE CARVALHO

TESE DE DOUTORADO
RIO DE JANEIRO, JANEIRO 1988

Agradecimentos

Ao Dr. L. N. da Costa pela orientação segura com a qual conduziu este trabalho e pela sua participação ativa em todas as etapas deste projeto. Aproveito para enfatizar o meu reconhecimento de que sua inestimável ajuda se traduziu não somente no aprendizado dos temas aqui apresentados mas também na minha formação profissional como um todo. Ao amigo L.N. da Costa por tudo o que fez.

Ao colega P.S. Pellegrini pela sua participação em várias etapas deste trabalho e pelo estímulo sempre presente nas discussões mantidas durante o preparo desta tese.

Ao colega C. Rité pelo suporte nas atividades computacionais ao longo de todo este trabalho. Além disso, pelo incentivo demonstrado em todos os momentos.

Ao Dr. D. Latham por ter tornado possível a realização do "Redshift Survey", que constituiu a base de dados espectrocópicos utilizados nesta tese.

Ao Dr. S. Djorgovski pelas inúmeras sugestões que contribuiram de maneira significativa para alguns dos tópicos aqui discutidos.

Ao colega C. Willmer pela leitura cuidadosa dos textos submetidos a publicação.

Ao colega M. A. Nunes pelo apoio dispensado no desenvolvimento e manutenção do microdensitômetro PDS do Observatório Nacional, fundamental para a obtenção dos dados aqui analisados.

Ao colega D. Nascimento pelo suporte ao "hardware" que permitiu manter um funcionamento continuo e eficiente durante a redução e análise dos dados.

INDICE

I- INTRODUÇÃO

Nos últimos anos uma grande quantidade de dados observacionais vem sendo acumulado para as galáxias elípticas e lenticulares o que tem proporcionado a realização de inúmeros trabalhos relevantes relacionados a estes objetos. A principal motivação deste esforço é porque estes sistemas são os mais simples ao longo da sequência de Hubble e portanto podem fornecer importantes informações sobre os processos de formação e evolução de galáxias.

O estudo sistemático das propriedades estruturais de galáxias S0 teve seu início a partir do trabalho realizado por Freeman (1970) que demonstrou que a distribuição de luz destas galáxias poderia ser dividida em duas componentes principais com propriedades bem definidas (BOJO e DISCO). O bojo teria uma distribuição de luz semelhante a das galáxias elípticas, enquanto a componente disco segueria uma lei exponencial, similar aos discos de espirais. É bom lembrar que além destas, outras componentes são também observadas nestes sistemas como, barras, lentes, anéis internos e externos etc., cuja presença pode manifestar, e em alguns casos ser responsável pela evolução dinâmica destas galáxias.

Durante muitos anos acreditou-se que os bojos de S0's seriam similares aos das galáxias elípticas, tendo em vista as semelhanças de suas distribuições de brilho (Kormendy 1977). Por outro lado, Freeman (1970) mostrou que as componentes disco de galáxias lenticulares seguem uma lei exponencial, semelhante ao observado em galáxias espirais, sugerindo que as galáxias S0 pareciam ser nada mais do que galáxias espirais sem

atividade de formação estelar.

Estas informações sugeriam em primeiro lugar que o processo de formação dos bojos de sistemas disco seria semelhante ao das elípticas e que as galáxias S0's teriam evoluido a partir de galáxias espirais por processos de remoção de gás. Vários processos foram propostos para esta remoção, tais como: ventos galácticos (Mathews e Baker 1971), "sweeping" (Gunn e Gott 1972) e evaporação térmica (Cowie e Songaila 1977). Entretanto, estudos mais recentes têm revelado que as galáxias elípticas parecem ser objetos de natureza triaxial, mantidos por uma distribuição de velocidades anisotrópica, enquanto as observações cinemáticas de bojos de S0's favorecem a interpretação de que a rotação é a principal causa do achatamento observado desta componente. Estes resultados sugerem, portanto, que as semelhanças são apenas aparentes com os bojos e as elípticas formando sistemas dinamicamente distintos (e.g. Kormendy 1980). Outra evidência contrária ao modelo de formação de S0's a partir de espirais vem do trabalho de Dressler (1980) sobre as propriedades estruturais de galáxias em aglomerados. Este estudo revelou a existência de diferencas significativas entre as características estruturais de galáxias S0 e espirais, indicando que estas últimas não poderiam dar origem às galáxias lenticulares pela simples remoção do gás. Por outro lado, Dressler (1980) demonstrou a existência de uma forte relação entre as propriedades das galáxias S0 e a densidade galáctica, indicando a possível importância de interações entre galáxias após a fase de formação, ou das condições físicas primordiais do ambiente de formação, na determinação de suas características morfológicas.

A importância destes resultados para as teorias de formação de galáxias e o fato de que os dados utilizados por Dressler (1980), embora estatisticamente adequados, eram imprecisos, motivaram o estudo apresentado no capítulo II. Neste capítulo são apresentados os resultados da fotometria superficial de galáxias S0 no aglomerado de Fornax. Esta região foi escolhida por ser representativa de um ambiente de alta densidade galáctica, permitindo examinar alguns dos resultados obtidos por Dressler (1980). Um importante resultado desta análise foi verificar que os discos das S0 estudadas possuem baixa luminosidade, sendo que alguns destes objetos apresentam um brilho superficial central muito "fraco", quando comparados com as S0's de "campo" observadas por Burstein (1979a). Este resultado veio confirmar que o brilho central das componentes disco não se concentra em torno de 21.65 mag arcsec^{-2}, como sugerido originalmente por Freeman (1970), corroborando os trabalhos de Kormendy (1979) e Burstein (1979a). Foi também verificado que os bojos das galáxias S0 em Fornax apresentam luminosidades compatíveis com os bojos observados em baixa densidade galáctica, sugerindo que a correlação entre a razão de luminosidades do disco e do bojo e a densidade galáctica reflete simplesmente o decréscimo da luminosidade do disco com a densidade galáctica, como proposto por Kent (1981). Um possível mecanismo para explicar este comportamento, se baseia no modêlo de formação lenta do disco proposto por Larson et al. (1980) para explicar a formação de galáxias S0 pela interrupção da formação do disco pela remoção do reservatório de gás associado a galáxia. Uma característica observável prevista por este modelo seria a existência de um corte abrupto na distribuição de brilho da componente disco, como observado por van der Kruit e Searle (1981) em sua série de

trabalhos sobre galáxias espirais vistas de perfil. Infelizmente, estes cortes ocorrem a brilhos superficiais bastante "fracos" para serem observados em galáxias pouco inclinadas. Por esta razão, o estudo das galáxias S0 em Fornax foi complementado com a análise da distribuição de brilho da galáxia NGC 1381 apresentada no capítulo III.

Além de sua orientação adequada para este estudo, a galáxia NGC 1381 apresenta outras características que a torna de grande interesse para as teorias de estrutura e evolução galáctica, como por exemplo: uma região nuclear do tipo "box-shaped" e uma aparência retangular nas regiões mais externas, semelhante a distribuição de brilho que levou Burstein (1979b) a sugerir a existência de uma terceira componente galáctica, denominada disco "espesso". Embora vários processos tenham sido propostos para a formação desta componente (Spitzer e Schwarzschild 1953, Monet et al. 1981, Binney 1981, Jones e Wise 1983), no caso particular da galáxia NGC 1381 a aparência retangular foi interpretada como sendo simplesmente um efeito de projeção associado a possível existência de um anel externo neste sistema. A forma do núcleo apresenta características que parecem refletir a evolução dinâmica do sistema, causada pela presença de uma barra, consistente com o resultado de simulações numéricas de Combes e Sanders (1981). Finalmente, como mostrado no capítulo III, foi encontrada evidência de um corte na distribuição do disco "fino", consistente com o que seria esperado pelo modêlo de Larson et al. (1980).

Complementando o estudo dos sistemas "early-type", no capítulo IV são apresentados os resultados de um levantamento fotométrico de galáxias elIpticas no hemisfério sul. As galáxias selecionadas fazem parte da

amostra do "Southern Sky Redshift Survey" (SSRS) recém completado por da Costa et al. (1988). O objeto principal deste estudo foi obter dados fotométricos homogêneos e de boa qualidade, com o propósito de investigar as propriedades estruturais destas galáxias, extendendo os recentes programas de fotometria superficial realizados por Djorgovski (1985) e Schombert (1986). Estes levantamentos são essenciais para a geração de uma amostra estatística que permita estabelecer correlações entre os parâmetros observáveis que revelem as propriedades intrínsecas destes objetos.

Uma das questões examinadas no capítulo IV é a variedade de perfís apresentados pelas galáxias elípticas, já que estes perfís podem fornecer informações importantes sobre a dinâmica interna destas galáxias. É bom lembrar que nenhum modelo dinâmico proposto até agora tem se mostrado satisfatório na descrição da distribuição de brilho destas galáxias. Tradicionalmente, a lei empírica de de Vaucouleurs é utilizada para descrever os perfís observados. Entretanto, como discutido no capítulo IV, esta lei é apenas uma simples descrição paramétrica dos perfís observados que em sua grande maioria apresentam desvios significativos desta lei. Estes desvios são importantes principalmente na parte externa, pois podem revelar entre outras coisas a existência de efeitos de maré e também a existência de discos tênues que poderiam indicar uma continuidade entre as famílias de elípticas e S0's. Além disto, o exame da distribuição bidimensional permite examinar a existência de variações do ângulo de posição das isofotas, que podem esclarecer se os "twists" são de origem intrínseca, associado a forma triaxial das elípticas, ou devido a interação galáxia-galáxia. No capítulo IV é investigada a

possibilidade da existência de uma correlação entre o "twist" observado e a densidade galáctica e os resultados obtidos, embora preliminares, sugerem que estas variações estejam associadas à forma intrínseca destes objetos e não a agentes externos que, se presentes, só seriam detectados a niveis isofotais mais "fracos" (Aguillar e White 1987). Outra possível maneira de obter informações sobre a forma intrínseca das galáxias elípticas, a partir dos dados fotométricos apresentados no capítulo IV, seria examinar a possível correlação entre a elipticidade e o brilho superficial (Richstone 1979), o que se pretende realizar em um trabalho futuro.

Medidas cinemáticas na região central de galáxias elípticas são importantes para complementar as informações provenientes da fotometria. Em particular, Dressler et al. (1987) e Djorgovski e Davis (1987) demonstraram, recentemente, que a família de galáxias elípticas obedecem a uma lei bem definida envolvendo os parâmetros estruturais e dinâmicos observados ("plano fundamental"), sugerindo uma certa regularidade no processo de formação destes objetos. Os dados espectrocópicos podem tambem ser utilizados para investigar a forma real das galáxias elípticas através do exame da correlação entre a elipticidade e a velocidade de dispersão, como sugerido por Merrit (1982).

Tendo em vista a importância dos dados cinemáticos, medidas de velocidade de dispersão foram obtidas para aproximadamente 200 galáxias "early-type" da amostra do SSRS. No capítulo V é apresentada uma análise da qualidade destes dados, a partir da comparação feita com as medidas disponíveis em trabalhos anteriores (Tonry e Davis 1981,

Whitmore et al. 1985, Davies et al. 1987) e observações ainda não publicadas realizadas no Observatório de Las Campanas. Um importante resultado desta análise foi verificar a existência de desvios sistemáticos entre as nossas medidas e as de Davies et al. (1987), que podem ter implicações importantes no estudo do campo de velocidades peculiares, como discutido no capítulo VI.

No capítulo VI os dados fotométricos e espectrocópicos obtidos nos capítulos anteriores são utilizados para reexaminar o "plano fundamental" das galáxias elípticas, determinado por Dressler et al. (1987) e Djorgovski e Davis (1987). O reexame desta relação é importante pois ela estabelece um indicador de distancia que permite investigar os desvios do movimento das galáxias em relação a lei de Hubble. O uso das relações determinadas anteriormente implicou na conclusão da existência de um campo de velocidades peculiares local com uma amplitude típica da ordem de 700 km/s, bem maior do que o esperado, por exemplo, pelo modelo de formação de estruturas no Universo envolvendo a existência de matéria "fria" no Universo. Tendo em vista as implicações destes resultados, é de grande interesse examinar a relação usada na determinação de distâncias utilizando dados independentes. Além disso, é importante estabelecer a influência que o meio ambiente e o modelo teórico assumido para o campo de velocidade tem na determinação do "plano fundamental". Um estudo detalhado destas questões é apresentado no capítulo VI.

Finalmente, no capítulo VII são revistos os principais resultados desta tese, assim como um esboço dos trabalhos em andamento.

Referências

Aguillar, L.A., e White, S.D.M. 1986, Ap. J. 307, 97.

Binney, J. 1981, Mon. Not. R. Astr. Soc. 196, 455.

Burstein, D. 1979a, Ap. J. 234, 435.

Burstein, D. 1979b, Ap. J. 234, 829.

Combes, F., e Sanders, R.H. 1981, Astr. Ap. 164, 173.

Cowie, L.L., e Songaila, A. 1977, Nature 266, 501.

da Costa, L.N., Pellegrini, P.S., Sargent, W.L.W., Tonry, J., Davis, M., Meiksin, A., e Latham, D. 1988, Ap. J. no prelo.

Davies, R.L., Burstein, D., Dressler, A., Faber, S.M., Lynden-Bell, D., Terlevich, R., e Wegner, G. 1987, Ap. J. Suppl. 64, 581.

Djorgovski, S. 1985, Ph. D. Thesis, U. C. Berkeley.

Djorgovski, S., e Davis, M. 1987, Ap. J. 313, 59.

Dressler, A. 1980, Ap. J. 236, 351.

Dressler, A., Lynden-Bell, D., Burstein, D., Davies, R.L., Faber, S.M., Terlevich, R., e Wegner, G. 1987, Ap. J. 313, 42.

Freeman, K.C. 1970, Ap. J. 160, 811.

Gunn, J.E., e Gott, J.R. 1972, Ap. J. 176, 1.

Jones, B.J.T., e Wise, R.F.G. 1983, Astr. Ap. 120, 165.

Kent, S.M. 1981, Ap. J. 245, 805.

Kormendy, J. 1977, Ap. J. 218, 333.

Kormendy, J. 1979, Ap. J. 227, 714.

Kormendy, J. 1980, Proc. ESO Workshop on Two-dimensional Photometry, eds. P. Crane e K. Kjar (Leiden: Sterrenacht Leiden), p. 191.

Kruit, P.C. van der, e Searle, L. 1981, Astr. Ap. 95, 105.

Larson, R.B., Tinsley, B.M., e Caldwell, C.N. 1980, Ap. J. 237, 692.

Mathews, W.G., e Baker, J.C. 1971, Ap. J. 170, 241.

Merrit, D. 1982, A. J. 87, 1279.

Monet, D.G., Richstone, D.O., e Schechter, P.L. 1981, Ap. J. 245, 454.

Richstone, D.O. 1979, Ap. J. 234, 825.

Schombert, J.M. 1986, Ap. J. 60, 603.

Spitzer, L., e Schwarzschild, M. 1953, Ap. J. 118, 106.

Tonry, J.L., e Davis, M. 1981, Ap. J. 246, 666.

Whitmore, B., McElroy, D., e Tonry, J.L. 1985, Ap. J. Suppl. 59, 1.

II- Estrutura de Galáxias S0 nas Regiões Centrais do Aglomerado de Fornax

Como mencionado no capítulo I, as galáxias S0 têm sido motivo de várias investigações no que concerne às suas propriedades estruturais e dinâmicas. Este interesse se deve ao fato destes sistemas apresentarem características intermediárias entre as galáxias elípticas e as espirais, o que torna as S0 um importante caso teste para as teorias de formação e evolução de galáxias. Em particular, o estudo dos sistemas lenticulares serve também para avaliar a importância relativa dos efeitos ambientais sobre os processos que atuam durante a época de formação de galáxias, na definição do tipo morfológico das galáxias.

Neste capítulo, é mostrado um estudo sobre as propriedades estruturais de galáxias S0 localizadas nas regiões centrais do aglomerado de Fornax, que complementa, de certa forma, trabalhos anteriores que consideraram principalmente galáxias de "campo". Através de uma análise detalhada da distribuição bi-dimensional de luz, foi possível determinar os parâmetros característicos das componentes fundamentais destas S0's, apesar de muitas apresentarem componentes secundárias de relativa importância. Um importante resultado desta análise foi encontrar exemplos de galáxias com componentes disco pouco luminosas e de baixo brilho superficial central. Além do mais, estas galáxias apresentam bojos com luminosidades típica de ambientes de baixa densidade galáctica. Estes fatos sugerem que isto seja uma característica geral das galáxias em regiões de alta densidade galáctica, responsável pela correlação encontrada por Dressler (1980) entre a razão das luminosidades do disco e do bojo (D/B) e a

densidade de galáxias.

Além das componentes bojo e disco, neste capítulo são também determinados os parâmetros característicos das principais componentes secundárias presentes nestes sistemas, a partir do exame cuidadoso das distribuições de luz ao longo do eixo-maior destas galáxias. Desta análise é possível determinar o tamanho, o brilho característico e a importância relativa de componentes como barras e lentes na determinação das propriedades globais dos sistemas discos. Estes dados são importantes para o desenvolvimento de teorias que tentam explicar o papel desempenhado por estas componentes na evolução dinâmica de sistemas disco.

Astron. Astrophys. 149, 449–458 (1985)

ASTRONOMY AND ASTROPHYSICS

Structure of S0 galaxies in the central regions of the Fornax cluster

R. R. de Carvalho, L. N. da Costa, and P. S. Pellegrini

Department of Astronomy, CNPq-Observatório Nacional, Rua General Bruce, 586, São Cristóvão, Rio de Janeiro, Brasil

Received August 13, 1984; accepted February 14, 1985

Summary. We present surface photometry observations of S0 galaxies located in the central regions of the nearby Fornax cluster of galaxies. The two-dimensional brightness distribution of the program galaxies were obtained using high-resolution plates, taken at the 60-in. telescope of the Observatório Nacional (ON), to observe the details of the light distribution near the center, and were extended to low surface brightness values using the ESO(B) and ESO/SRC (J) Sky Surveys on film. Comparison with published photoelectric observations suggests that the procedure is sufficiently accurate to justify its use in more extensive surface photometry programs. We have applied standard decomposition techniques to analyse the major-axis profiles of the sample galaxies, deriving the structural parameters for each separate component. An important result of this analysis was to find examples of galaxies with very faint and diffuse disks. We suggest that this may be a general characteristic of disks in high galactic density regions and it is perhaps the primary cause for the correlation between the bulge-to-disk luminosity ratio and galactic density observed by Dressler (1980) for disk galaxies.

Key words: galaxies: lenticular – galaxies: structure

1. Introduction

A major challenge to theories on the formation and evolution of galaxies has been to account for the origin of S0 galaxies and their well-known tendency to occur in dense regions of space (e.g. Oemler, 1974). In particular, the question of whether they represent an intrinsically distinct class of objects or form a parallel-sequence of gas-poor spirals has motivated much of the recent theoretical and observational work on the subject, recently reviewed by Kormendy (1982). The distinction between these alternatives may be essential not only to explain the origin of S0 galaxies, but it may also lead to a better understanding of the phenomenon of galaxy formation in general.

Until recently the bulk of the observational evidence seemed to argue in favor of parallel-sequence theories which suggest that environmental effects, resulting from either galaxy-galaxy close encounters (Spitzer and Baade, 1951) or the interaction of a galaxy with the intergalactic medium (e.g. Gunn and Gott, 1972; Cowie and Songaila, 1977), are responsbile for the evolution of spiral galaxies into S0's. Among the various mechanisms that have been proposed, ram-pressure stripping was favored by many workers to explain the transformation of spirals into S0 galaxies. However, in the past few years new data on the structural properties of S0's and their relationship with the surrounding environment have challenged this interpretation. First, as pointed out by Burstein (1979b), there seems to be fundamental differences in the internal structure of S0's and spirals, inconsistent with a scenario involving the simple removal of the gas from the disk of a spiral to form a S0 galaxy. Further observational evidences of these differences were presented by Dressler (1980), in particular showing that S0's tend to have not only lower disk to bulge luminosity ratios (D/B) but also more luminous bulges than spirals. Since gas removal mechanisms are not expected to affect the internal structure of a galaxy, Dressler's results are a strong evidence against the hypothesis that S0's are simply gas-poor spirals. Second, the galactic content of a cluster seems to be primarily a function of the local density of galaxies and independent of the global properties of the cluster (Dressler, 1980). This behaviour was interpreted by Dressler (1980) as an additional evidence that S0's are not produced by the removal of gas from spiral galaxies by either ram-pressure stripping or gas evaporation.

Most of Dressler's observational findings can be explained by the model recently advanced by Larson et al. (1980) for the formation of S0 galaxies. The basic hypothesis is that the formation of disks results from the slow accumulation of infalling gas from a gaseous halo surrounding a galaxy. According to these authors, S0's would be formed from the progenitors of present-day spiral galaxies which at some point in their evolutionary history lost their loosely bound gas-rich envelopes, due to interactions with other galaxies, thereby truncating the disk formation. One possible objection to this model is that it fails to account for the observed differences in the bulge luminosity distributions of S0's and spirals mentioned earlier. However, considering the crude nature of Dressler's data, it seems worthwhile to investigate in more detail the structural properties of S0 galaxies in high galactic density regions in order to verify some of his findings and to look for vestiges in the disk structure which may reveal the interruption of its growth as proposed in this scenario.

In this paper we present the preliminary results of photographic surface photometry observations of S0 galaxies in the central regions of the compact Fornax cluster. Our primary goal in the present work was to evaluate the accuracy of the new procedure adopted here to derive galaxy profiles, which makes

Send offprint requests: R.R. de Carvalho

use of high-resolution plates taken on a medium size telescope, to detail the structure of the galaxies near the center and the ESO (B) and ESO/SRC (J) film copies to derive its brightness distribution at faint light levels. Our main motivation was to find out whether we could use the vast photographic material of the Sky Atlas for moderate precision photometric work, thereby eliminating the need of multiple exposures of the same galaxy. This is one of the major drawbacks in the realization of photographic surface photometry programs and partly accounts for the limited number of well-studied galaxies presently available for statistical analysis, such as that undertaken by Dressler (1980). In Sect. 2 we describe the data reduction techniques and compare our derived light profiles with available photoelectric data. In Sect. 3 we present the results of the profile analysis, comparing the parameters obtained for the bulge and the disk with those of previous studies. The main results of this paper are presented in Sect. 4.

2. Data reduction

In the present work we have selected S0 galaxies (Lauberts, 1982) in the central regions of the Fornax cluster, at an adopted distance of 27 Mpc (Ho = 50 km/s/Mpc). The basic data on the program galaxies are given in Table 1. The morphological types are from the Revised Shapley-Ames Catalog of Bright Galaxies (RSA) (Sandage and Tamman, 1981) and from the Second Reference Catalogue of Bright Galaxies (RC2) (de Vaucouleurs et al., 1976). The coordinates, total apparent blue magnitudes B_T and heliocentric velocities v are from the RSA except NGC 1380B, for which all the information comes from the RC2. Note that our sample includes both transition type galaxies, like NGC 1351 and 1380, and galaxies classified as ellipticals by some investigators such as NGC 1374, 1380B and 1389 (cf. Table 1, Sandage and Visvanathan, 1978). Most of our program galaxies were studied earlier by Hodge (1978), who presented isophotal maps and east-west profiles in the V passband, obtained using surface photometry techniques different from those presented here. They were intentionally included in our sample for a qualitative comparison but were not used to determine the accuracy of our photometry.

A total of 5 plates were taken of the three fields containing all the program galaxies using the Observatório Nacional 60-in. telescope (scale 13.0″ mm^{-1}), in the photographic B passband (GG 385 filter + IIa-O plates), with typical exposures varying from 30 to 60 min. All plates were developed for 15 min in D-76 and the best quality exposures were selected for data reduction. In order to cover the outermost parts of the galaxy we have used the film copies of the ESO (B) (scale 67.4″ mm^{-1}) and ESO/SRC (J) (scale 67.2″ mm^{-1}) for the field 358 which includes all the program galaxies, except the comparison galaxy NGC 1316 located in the field 301. Details on the original Sky Atlas can be found in West and Schuster (1982) and a discussion about the quality of the glass and film copies of the ESO/SRC (J) Atlas is presented by Sim (1981). Recently, we have undertaken a more extensive analysis of the photometric properties of the film copies of both surveys and the results will be presented elsewhere.

The photographic material was scanned on the Observatório Nacional PDS microdensitometer. For each galaxy 3 two-dimensional data arrays (200 × 200 pixels) were generated in the following manner: an "inner" array consisting of density readings of the high-resolution ON plates, each pixel 50 μ (=0.67″) square; an "intermediate" array measured on the ESO (B) copy, each pixel 50 μ (=3.37″) square; an "outer" array measured on the ESO/SRC (J) copy, each pixel 100 μ (=6.72″) square.

In order to convert density d into intensity I we have used the sensitometric spots on each ON plate (9 spots) and in the field 358 of the ESO/SRC (J) copy (7 spots). The spot densities were least-squares fitted to the function (de Vaucouleurs, 1968)

$$\log I = \sum_{i=0}^{n} a_i (\log w)^i \qquad (1)$$

where $w = 10^{(d-d_f)} - 1$ and d_f is the fog chemical density.

The value of n was chosen depending on the density domain covered by the spot set available on each individual plate material. For the ON plates we used $n = 3$ which adequately re-

Table 1. Basic data for program galaxies. The sources of the photoelectric data are: SV – Sandage and Visvanathan (1978); G – Griersmith (1978); GD – Green and Dixon (1980).

NGC	R.A.	Dec. (1950.0)	Type	B_T	v (km s)$^{-1}$	Sources
1351	03 28 38	−35 02.0	SO_1(6)/E6 SAO uncertain	12.65	1506	SV
1374	03 33 21	−35 23.5	EO EO	12.30	1201	SV
1380	03 34 31	−35 08.4	SO_3(7)/Sa SAO	11.10	1774	SV,G
1380B	03 35 06	−35 21.0	— SO^+ uncertain	—	1779	SV,G
1387	03 35 02	−35 40.2	SBO_2(pec) SO^-	11.83	1184	SV,GD,G
1389	03 35 17	−35 54.5	SO_1(5)/SBO_1 E4 uncertain	12.39	979	SV,G

produces the linear part of the characteristic curve covered by the spots, while for the ESO/SRC (J) material we used $n = 5$ to follow the curvature of the characteristic curve at the high density end. Unfortunately, standard procedures to obtain a characteristic curve cannot be applied to the ESO (B) material because only a small number of fields have sensitometric spots available. Therefore we have employed the procedure of combining characteristic curves similar to that successfully used by Burstein (1979c) for 103 a-O emulsions and Davoust (1981) for II a-O emulsions. The results of these earlier experiments partly justifies our assumption that the procedure will also be valid for the film copies of the II a-O emulsions specially considering the quality control under which the Sky Atlas was prepared. In order to derive this combined curve we examined all the available spot sets (16 fields), and measured the spot densities for 12 fields, discarding 4 because of various problems with the sensitometry. The data for each individual set were fitted by the function given in Eq. (1) with $n = 1$. The fits were then shifted along the intensity scale until the linear part of the several characteristic curves coincided. The combined characteristic curve was finally obtained by refitting Eq. (1) to the data points of all available spot sets, using $n = 5$ for the final fit because of a slight curvature in the high density region. From the overall scatter about the combined curve we estimate that the error in the density-intensity conversion should be ~ 0.06 mag in the linear part of the characteristic curve. We note that an alternative method for obtaining characteristic curves for the ESO Blue Survey has been discussed by Lauberts (1983). All galaxy density arrays were converted to intensity arrays utilizing the fits determined for each individual photographic material.

The final step in the processing of the data arrays was to subtract the contribution of the sky background. The method employed for the sky determination is similar to the technique used by Burstein (1979a) and described in more detail by Burstein (1979c). The method consists of the following steps: (1) areas containing the galaxy and nearby bright objects, which may consist of stars and neighboring galaxies, are excluded from the determination of the sky background; (2) a histogram of density values for all pixels outside the excluded areas is generated and the pixels with density values in the high-density tail of the distribution are discarded; (3) either a first or second order two-dimensional polynomial is then fitted to the remaining data and subtracted from the original raster, generating a histogram of residuals; (4) the distribution of residuals is tested for symmetry and how closely it approaches to a gaussian distribution. If these conditions are not satisfactorily met, the pixels corresponding to large ($> 3\sigma$) positive residuals are eliminated and a new fit is attempted. Usually, a maximum of 3 iterations are necessary to obtain satisfactory fits; (5) as a final check, the data and the corresponding polynomial fit are plotted along different directions for inspection. Using the sky determination procedure outlined, we find that the mean value of the residual distribution is typically 0.02 mag, implying that the galaxy profiles may suffer from systematic errors starting at ~ 27.5 mag arcsec^{-2}.

The zero-point of the magnitude scale was determined for each galaxy using the available photoelectric data from the sources listed in the last column of Table 1. Since the aperture diameters normally used in the photoelectric observations are typically > 30 arcsec, the instrumental intensities were calibrated using the intermediate raster. However, since the program galaxies are slightly overexposed near the center in the ESO Blue Survey, we simulated annular apertures integrating the instrumental intensities within two consecutive diaphragms. The difference between these integrated values was compared to the value derived in a similar fashion from the photoelectric data to determine the calibrating constant. Whenever more than two annular apertures were available the average value of the different calibration constants was used to define the zero-point level. Although the calibration based on annular apertures should be less precise, the good agreement between the zero-points obtained for different galaxies using data from several independent sources suggests that the zero-point is accurate to ~ 0.1 mag.

Isophotal maps for the program galaxies are shown in Fig. 1, over the brightness range $19.5 < \mu_B < 24.5$ except NGC 1380B (cf. figure caption). In general, the maps obtained in the present work resemble those of Hodge (1978) for the galaxies in common. However, the differences are substantial enough, especially in the outer regions, to justify a direct comparison of profiles.

The light profiles along the principal axes of the galaxies (defined at the isophotal level $\mu_B \sim 25.0$) were obtained for each raster and combined into a single profile. Near the center we used the profile obtained from the inner raster data matching it to the intermediate profile before it became too noisy. The match was made over a radii range which avoided the saturation problems of the external profile and it was performed by shifting the inner uncalibrated profile by an amount determined by the average value of the differences in brightness of the two profiles, within the overlap region. Exactly the same technique was used to extend the galaxy profile to the outermost parts of the galaxy, joining the profiles derived from the data in the intermediate and outer arrays. In this fashion we generated four profiles: a pair on each side of the major axis and a corresponding pair for the minor axis. The light distribution along each axis was finally obtained by averaging the values of intensity at the same galactocentric distance on each side of the galaxy. This was done except in regions where the presence of faint stars or galaxy images affected one of the profiles, in which case we used the intensity values of the uncontaminated side. A good example is that of NGC 1374 whose outer regions are strongly contaminated by the foreground galaxy NGC 1375. The final brightness profiles along the major axis used in all the subsequent analysis are shown in Fig. 2.

The best check on the accuracy of the present data and the techniques utilized to derive the galaxy profiles is to compare them with published surface brightness measurements. For the galaxies in common with Hodge (1978) only a qualitative comparison was justified in view of the limited information given for these objects. An exception is NGC 1399 for which Hodge (1978) reports the results of CTIO photoelectric surface brightness observations. The intensity values reported in the V passband were converted to the B band assuming $B\text{-}V = 1.0$, as given by Hodge (1978). Figure 3 shows the difference between our measured surface brightnesses and the photoelectric measurements as a function of surface brightness for this comparison galaxy. We find a zero-point difference of approximately 0.4 mag arcsec^{-2} for $\mu_B > 19.0$ while for $\mu_B < 19$ the photoelectric data falls below our photographic profile, probably due to the smaller resolution of the CTIO observations. However, in the range $19.0 < \mu_B < 25.0$ we find that the differences between the two profiles are less than 0.2 mag arcsec^{-2}, aside from the zero-point discrepancy.

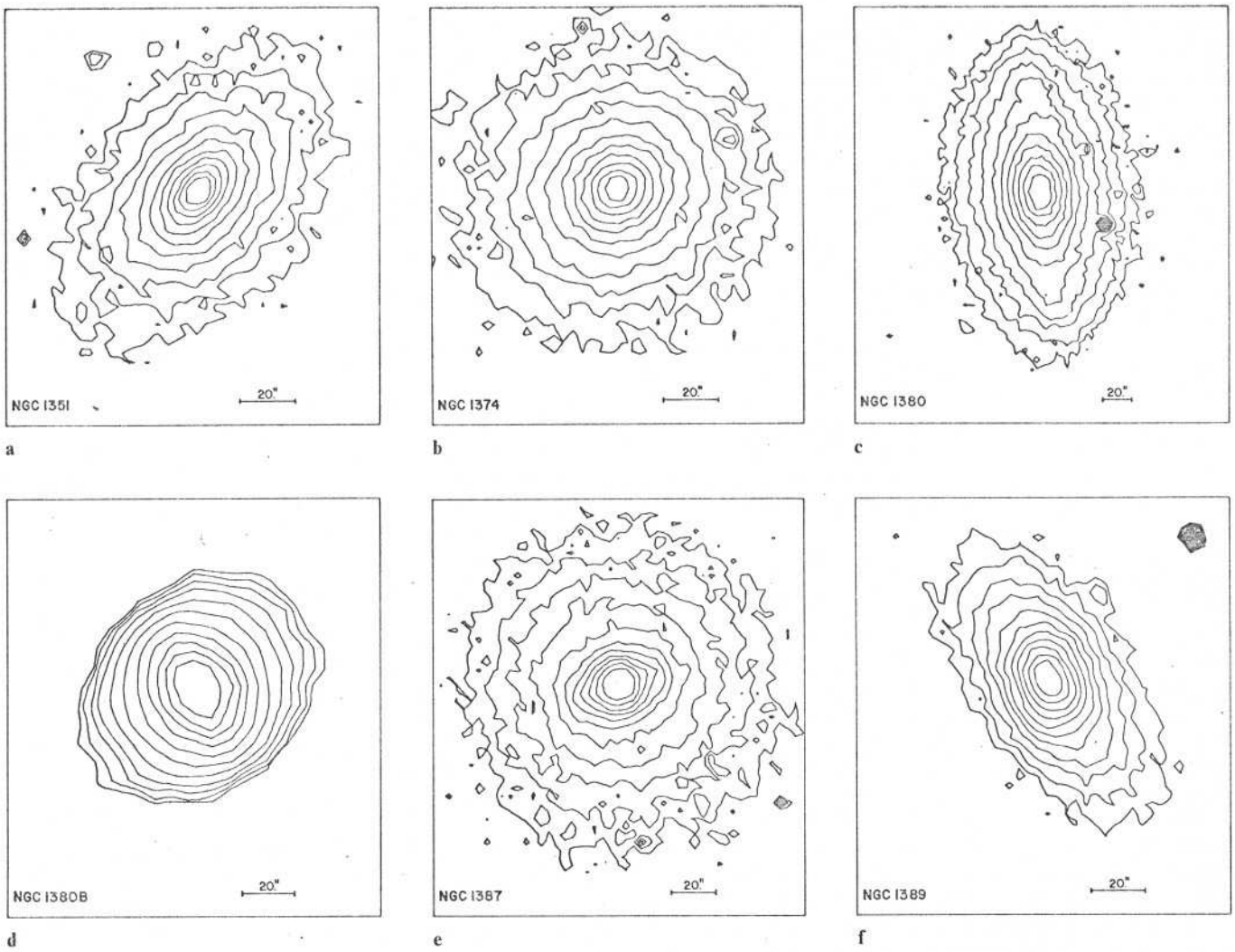

Fig. 1. Isophotal maps for the program galaxies from 19.5 to 24.5 mag arcsec^{-2} at 0.5 mag arcsec^{-2} intervals. These contours were drawn from the data in the intermediate raster (ESO(B)) except for NGC 1380B. For the latter galaxy we used the outer raster (ESO/SRC(J)) in order to show more clearly the isophotal twist. The contours are in this case from 21.5 to 26.5 mag arcsec^{-2} at 0.5 mag arcsec^{-2} intervals. The maps have north up and east at the left

By far the most reliable data for comparison are the photoelectric spot measurements along the east-west axis obtained by Schweizer (1980) for the giant spiral NGC 1316, shown in Fig. 3. Unfortunately, we do not have ON plates for this galaxy and since its central region is saturated in the ESO (B) Atlas the comparison cannot cover the entire brightness range of our photographic data. Inspection of Fig. 3 shows that, at least within the range $19.5 < \mu_B < 25.5$, our profile for NGC 1316 shows no systematic deviations relative to the photoelectric measurements, with the zero-point difference between the two data sets being less than 0.1 mag arcsec^{-2}. It is important to note that the calibration for this galaxy was established independently, using the multiaperture observations of Sandage (1975). Neglecting the zero-point offset the differences between the profiles are less than 0.25 mag arcsec^{-2}. Based on these preliminary results we estimate that our photometry is accurate to about 0.2 mag arcsec^{-2}, although a more extensive comparison would be desirable.

3. Data analysis

3.1. Profile decomposition

In order to study the structural properties of the observed galaxies, the profiles along the major axis were analyzed using the iterative decomposition method originally proposed by Kormendy (1977a). The method assumes that the two major galactic structures, the bulge and the disk, are adequately described by analytical fitting functions. As usual, we assume that the spheroidal component is well represented by the empirical $r^{1/4}$ law (de Vaucouleurs, 1948) given by

$$\mu_{\text{bulge}} = B_0(V) + 8.325\,((r/r_0)^{1/4} - 1) \qquad (2)$$

where r is the galactocentric distance, r_0 is the de Vaucouleurs radius and $B_0(V)$ is the brightness at that radius. The light distribution of the disk is assumed to follow the exponential law (Freeman, 1970)

$$\mu_{\text{disk}} = B_c(0) + 1.0857\,\alpha\, r \qquad (3)$$

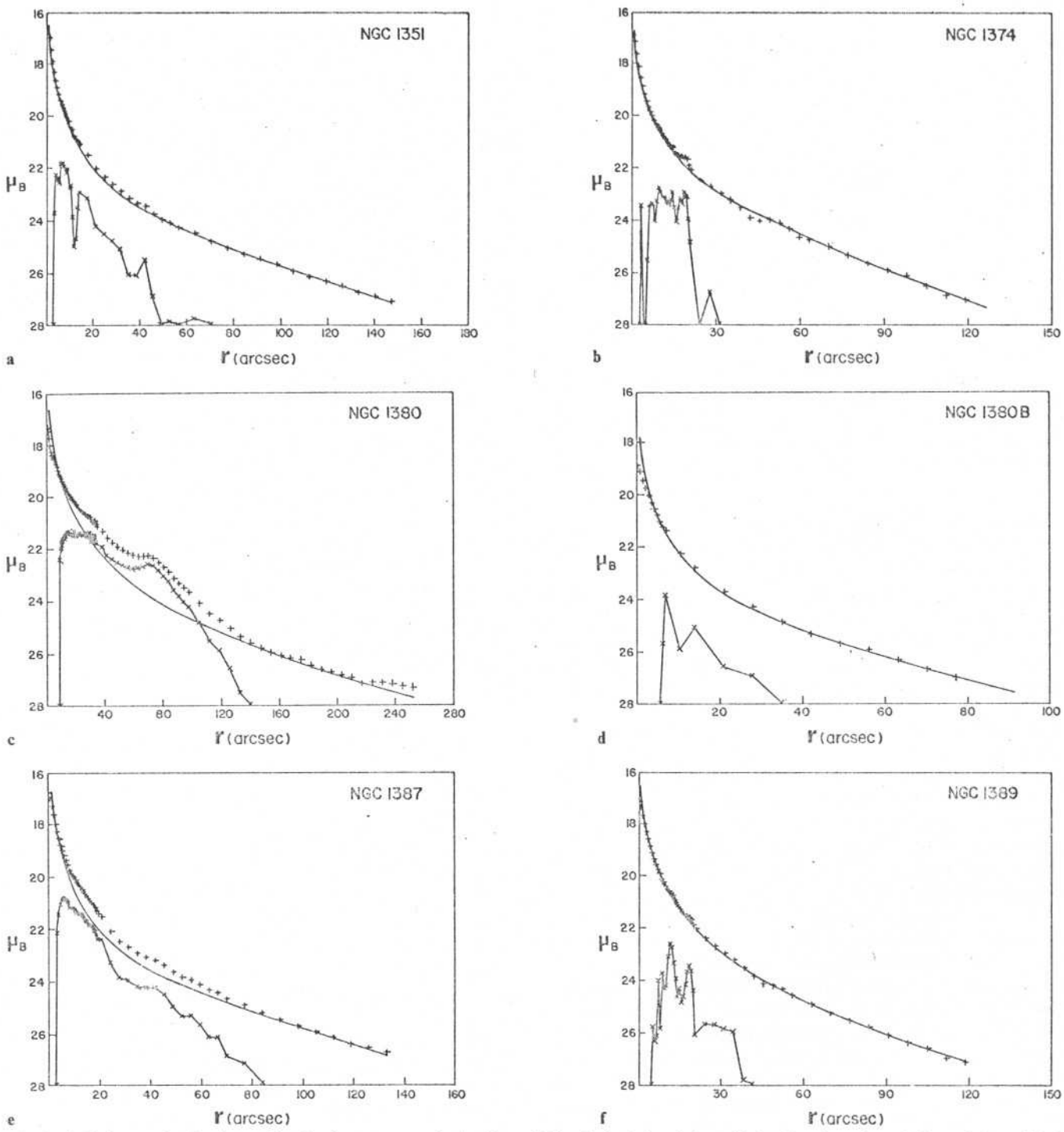

Fig. 2a–f. Major-axis luminosity profiles for the program galaxies. The solid line is the bulge-disk model fit. Also shown in each figure is the residual light distribution (x connected by a line) after the subtraction of the bulge-disk model from the observed profile. The following domains were used in the fit: a NGC 1351: $r = 1.9''$–$3.1''$ for the bulge, $r = 60''$–$144''$ for the disk. b NGC 1374: $r = 2.4''$–$4.5''$ for the bulge, $r = 68''$–$121''$ for the disk; c NGC 1380: $r = 7.4''$–$9.0''$ for the bulge, $r = 151''$–$220''$ for the disk; d NGC 1380B: $r = 4.5''$–$6.0''$ for the bulge, $r = 38''$–$79''$ for the disk; e NGC 1387, $r = 3.1''$–$4.6''$ for the bulge, $r = 108''$–$142''$ for the disk; f NGC 1389: $r = 3.9''$–$5.3''$ for the bulge, $r = 74''$–$108''$ for the disk

where α^{-1} is the disk scale length and $B_c(0)$ is the central surface brightness. A number of objections have been raised against applying such technique to study the structural properties of disk galaxies, particularly when either the bulge or the disk dominates the light distribution or whenever there are more than two components present (e.g. Kormendy, 1982). In both cases the major difficulty is to select two radii ranges, one in which the bulge dominates the light distribution and one in which the disk clearly contributes most of the light. For systems with extreme values of the ratio D/B or relatively prominent underlying

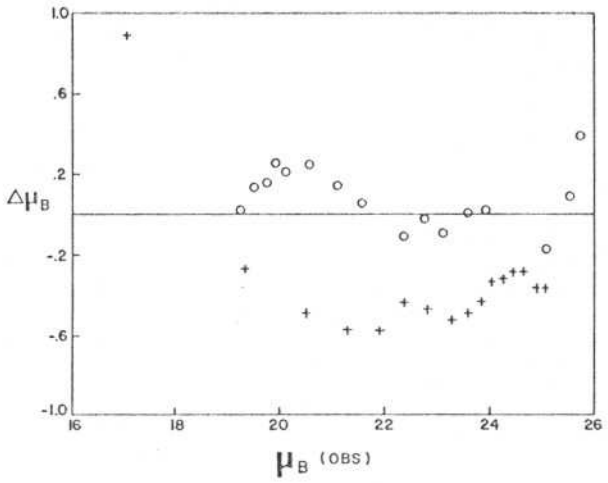

Fig. 3. Comparison of surface brightness measurements of NGC 1316 (O) and NGC 1399 (+). The quantity $\Delta\mu_B$ represents the difference between our measurements and photoelectric measurements made by Schweizer (1980) for NGC 1316 and CTIO for NGC 1399 (Hodge, 1978)

components, contributing with significant amounts of light in the bulge and disk domains, the results of modelling become sensitive to the choice of these radii ranges. Moreover, the presence of a third component increases the degree of freedom of the models, and can lead in some cases to unphysical solutions which may nevertheless be good fits to the data. On the other hand, any representative sample of S0's is expected to include galaxies of these types for the following reasons. First, as pointed out by Burstein (1979a) even in a sample of S0's chosen by their apparent normality one finds a substantial fraction of galaxies which show some sort of peculiarity. Second, Dressler (1980) has shown that S0 galaxies in high galactic density regions usually have small D/B ratios, implying bulge dominated galaxies.

Our sample is a good example of the situation described above with all galaxies showing some sort of feature in their profiles and small values of D/B. However, in view of the importance of studying systems typical of dense regions, we have in the present work attempted to investigate the properties of the sample galaxies using standard decomposition techniques, despite the known limitations of the method for systems such as the ones considered here. In order to verify the internal physical consistency of the solutions obtained by the iterative method we have also investigated the structural properties of the components which are interpreted as being responsible for the light excesses above the model fits. These results are compared with the sparse information presently available for the galactic components such as lenses and bars known to exist in disk galaxies. Although this procedure cannot be considered as a totally independent check, since the underlying components never occur in isolation, it provides a method of evaluating how realistic the fits might be.

The final bulge-disk model fits are shown in Fig. 2 with the domains used in the profile decomposition of each galaxy indicated in the figure caption. These domains were selected examining the individual profiles plotted either as a function of r, to define the best disk domain, or as a function of $r^{1/4}$ to select the bulge region. The selection of the radial interval for the bulge fit is particularly critical in our case due to the presence of probable secondary components in all galaxies, which restricts the radii range over which one can reliably assume that the bulge light dominates. In order to avoid as much as possible the effects of contamination from subcomponents, which will tend to make the bulge light distribution less steep, we adopted the following criteria to select the bulge domain. Each individual profile, plotted against $r^{1/4}$, was examined to define the radii range over which the light distribution approached a straight line. The bulge domain was then selected as the radial interval over which we could obtain the steepest linear fit to the available data points. In principle this criteria should minimize the effects of light contamination, although in some cases it leads to very small bulge domains, increasing the uncertainty of the model fits. The model fits shown in Fig. 2 are for most galaxies a fair representation of the observed luminosity profile both in the bulge region and in the outermost parts of the galaxy where the disk dominates. The poor quality of the fit for the bulges of NGC 1380 and 1380B is discussed in more detail below. We note that the innermost data points ($r < 1.5''$) were discarded because the light profiles were not corrected for seeing effects. At intermediate distances the presence of extra light is indicative of the contribution from separate components, with NGC 1380 showing the most prominent feature. In fact this galaxy, classified as a transition type galaxy (cf. Table 1), has a very complex structure with features that make model fitting particularly difficult, being by far the worst case to analyse in the present sample. Near the center the presence of dust lanes prevents a satisfactory fit of the bulge, while the extent of the features in the intermediate region and the presence of an outer component, probably associated with the spiral-arms like features visible in long exposure plates, hampers the definition of the disk domain. Finally, we note that for the face-on galaxy NGC 1387 the major axis profile was taken to be along the short axis of the bar, in order to minimize its effects in the final fitted model. However, the presence of the bar still affects the bulge parameters probably causing the bulge luminosity to be overestimated.

A first result that stands out is that the luminosity profiles of the S0's studied here show no evidence of systematic deviations from the exponential law for $\mu_B < 26.5$, in contrast to earlier works which have found several examples of non-exponential disks. In particular, there is no indication of inner-disk cutoffs similar to those observed by Kormendy (1977a) in compact S0's. In the outer parts of the disk there are local deviations from the exponential law but they are generally small ($\Delta\mu_B < 0.15$). An examination of all the available data shows that the exponential behavior extends to fainter light levels ($\mu_B \sim 27.5$) except in NGC 1380 and 1380B, the latter showing some evidence for an outer-disk cutoff at $\mu_B \sim 27$. However, at this faint light level, systematic errors in the sky determination may have already become important thus casting some doubt on whether this feature is real.

3.2. *Bulge and disk parameters*

The main results of the present model analysis are sumarized in Table 2 where we list the bulge and disk parameters derived from the profile decomposition of each galaxy. In columns 2 and 3 we list the bulge parameters r_0 and $B_0(V)$, the latter corrected for inclination following Burstein (1979b). In column 4 we list the estimated intrinsic axial ratio for the bulge, q_{int}, derived from the apparent axial ratio of the central isophotes ($\mu_B < 20$) and the appropriate expressions for an oblate spheroid given by

Table 2. Structural parameters for SO galaxy sample

NGC	r_0 (kpc)	$B_0(V)$ (mag arcsec^{-2})	q_{int}	α^{-1} (kpc)	$B_c(0)$ (mag arcsec^{-2})	D/B
1351	1.20	20.63	0.65	5.16	23.64	0.32
1374	1.18	20.62	—	3.43	22.37	0.47
1380B	0.83	21.45	0.71	3.55	24.41	0.34
1387	0.73	19.15	—	4.95	23.02	0.36
1389	1.39	20.92	0.56	3.98	24.46	0.09

Binggelli (1980). In columns 5 and 6 we give the values derived for the disk scale length, α^{-1}, and the central surface brightness, $B_c(0)$, corrected for inclination. The value of the inclination was derived from the apparent axial ratio in the isophotal range 25–26 mag arcsec^{-2}, assuming round disks. Finally, in column 7 we list the derived disk-to-bulge ratio D/B, following Burstein (1979b). Because of the difficulties in the bulge-disk model fit for NGC 1380 parameters for this galaxy are uncertain and are not presented.

A comparison of our bulge parameters with those of previous studies is illustrated in Fig. 4 where we show the distribution of the observed bulge parameters in the $B_0(V)$–$\log r_0$ plane. The data shown includes the parameters derived by Kormendy (1977a) for the compact S0 galaxies and the results of Burstein (1979b) for a sample of "normal" S0 galaxies typical of the general field. As a comparison we also show the point representing the parameters derived in the present analysis from the $r^{1/4}$ law fit of the elliptical galaxy NGC 1399. An examination of Fig. 4 shows that the bulge luminosities derived here are within the normal range of luminosities and that the bulge parameters derived lie close to the general $B_0(V)$–$\log r_0$ relation found by Kormendy (1977b) for normal ellipticals. The bulges of NGC 1351, 1374, 1380B and 1389 are slightly more diffuse than ellipticals of the same magnitude, a general trend also observed by Burstein (1979b) and usually interpreted as evidence of the relative importance of rotation in the bulges of disk galaxies. As a final note about the bulges we should mention that the intrinsic axial ratios listed in Table 2 are also in agreement with the range 0.35–0.70 found by Hamabe (1982) for a sample of edge-on galaxies.

The disk structure of our sample galaxies is compared with the available data in the $B_c(0)$–$\log \alpha^{-1}$ plane shown in Fig. 5. A noticeable feature of the disks studied here is their tendency to lie on the low-luminosity end of the normal range of disk luminosities ($-17 > M_B > -21$). Among the S0 galaxies studied to date only NGC 4592 has a disk luminosity as low as the extreme cases of NGC 1380B and 1389. Although all the derived disk scale lengths lie within the typical range of 2–10 kpc, the disks show a clear tendency of being large for their magnitudes, resembling the diffuse disks found by Kormendy (1977a) for the compact S0 galaxies. In particular, the values obtained for the central disk brightness span a larger domain than that observed by both Burstein (1979b) and Boroson (1981) who found values of $B_c(0)$ between 20 and 23 mag arcsec^{-2}. The disk of NGC 1351, 1380B and 1389 are especially faint, although Kormendy (1977a) and Romanishin et al. (1982) have reported values of $B_c(0)$ close to those obtained in the present work. A

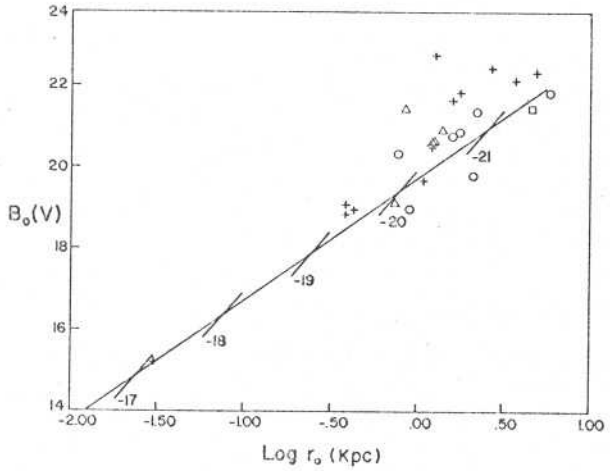

Fig. 4. Bulge parameters for the galaxies in Table 2 are shown in the $B_0(V)$–$\log r_0$ plane, similar to that given by Burstein (1979b). Open circles are data from Kormendy (1977a), crosses are the parameters of the S0's studied by Burstein (1978b) and triangles are for the S0's of the present work. For comparison we also show the parameters obtained from the $r^{1/4}$ law fit of the elliptical galaxy NGC 1399 (□). Also indicated in the figure are the straight-line relation found by Kormendy (1977b) for normal ellipticals and lines of constant absolute blue magnitude. Note that the bulge parameters obtained in this study lie within the normal range found in previous works

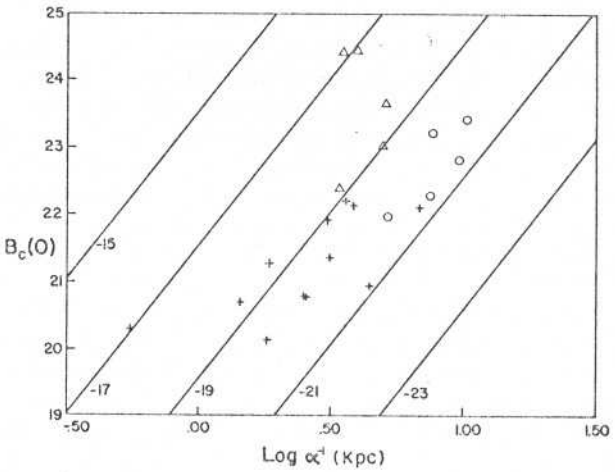

Fig. 5. Exponential disk parameters for the galaxies in Table 2 are shown in the $B_c(0)$–$\log \alpha^{-1}$ plane. The symbols are the same as those described in Fig. 4. Lines of constant absolute blue magnitude are also indicated. Note that the disks of the present sample are characterized by low luminosities and faint central surface brightnesses

distinguishing property of the galaxies studied here is that their disks are both less luminous and more diffuse than previously observed disks, placing them in a distinct region of the $B_c(0)$ - $\log \alpha^{-1}$ diagram. One important implication of this result is that it weakens the evidence in favor of the correlation between disk parameters suggested by Hamabe (1982), which could in principle place strong constraints on the theories of galactic disk formation.

The above conclusions should be taken with caution for at least two reasons. First, the observed galaxies have very low D/B ratios and the low values derived for the disk brightness could simply manifest the inadequacy of the profile decomposition method. Second, we have observed disks in galaxies like NGC 1374, 1380B and 1389 which have been in the past classified as ellipticals. The case of NGC 1374 is especially noteworthy since it has the largest D/B ratio of the sample. In order to check the results obtained from the major-axis analysis we describe below some tests applied to the data.

One potentially serious problem of our model fits is, as mentioned earlier, the small domains usually used for the bulge fits. To investigate how sensitive our final results were on this choice, new fits were obtained using more extended bulge domains, including all points interior to the radial distance where a significant deviation from the $r^{1/4}$ law, due to the presence of a subcomponent, was noticeable in the plots. In general the use of these larger domains, typically 3 times larger than those given in the figure caption, produces models that show both a decrease in the brightness and an increase in the size of the corresponding bulges and disks, without any significant change in the magnitude of these components. The variations in the structural parameters are relatively small and do not qualitatively alter our results. The bulge domain is critical only for NGC 1380B for which $B_0(V)$ and $B_c(0)$ decrease by about 1 mag arcsec^{-2} and the ratio D/B decreases to 0.17. It is interesting that the new model does not significantly improve the quality of the fit in the inner parts of the galaxy over that shown in Fig. 2d.

Another possible way of testing our fit procedure could be to use a recognized elliptical galaxy to check whether the decomposition technique used can artificially introduce a disk component, depending on the selected fit domains. This test would be important to corroborate the results of our analysis which have revealed the existence of faint disks in galaxies classified earlier as ellipticals. However, Kormendy (1977b) has shown that the profiles of ellipticals do not all have the same shape and in some cases are not well described by a single $r^{1/4}$ law. In particular, ellipticals with nearby companions tend to have bright envelopes above the extrapolation of an $r^{1/4}$ law fit to the inner parts, which can resemble an exponential disk profile. This is the case, for instance, of NGC 1399 (cf. Sect. 2) which exhibits a bright outer envelope like the cD-type profiles observed by Oemler (1976). Therefore, the use of NGC 1399 or any other elliptical to determine how reliable are the faint disks found in this paper by the decomposition technique would not be conclusive raising, instead, other issues beyond the scope of the present paper.

In spite of the problems mentioned above we have investigated whether a de Vaucouleurs law fitted over the inner region could adequately describe the whole profile of the galaxies classified earlier as ellipticals. For NGC 1374 the residual light clearly reveals an underlying disk and a third component in the inner portions, suggesting that it was probably misclassified in the past. For NGC 1380B the situation is much less clear because even though there seems to be a systematic deviation from the $r^{1/4}$ law which resembles a disk, this departure occurs at faint light levels and shows a strong dependence on the domain chosen for the fit. Therefore it is very difficult to say anything more definite about the real nature of this galaxy based on this result alone. Finally, the light residual for NGC 1389 showed the likely presence of a faint disk and of a relatively prominent inner component, giving support to our claim that it is an example of a S0 galaxy with a faint disk.

Unfortunately, it seems unlikely that any procedure adopted to test our results could completely eliminate the use of subjective criteria in the decomposition of the light distribution of a galaxy, a major weakness of this type of investigation. Moreover, it seems that each galaxy has to be analyzed on an individual basis utilizing all the information that can be gathered not only from the major-axis analysis but also from the results obtained along the minor-axis and the characteristics of its two-dimensional structure, as discussed in the next section. Nevertheless, based on these preliminary results we can state with some degree of confidence that NGC 1351, 1374, 1380, 1387 and probably NGC 1389 are disk galaxies. The most difficult case to interpret is NGC 1380B because the structural parameters derived for it are quite sensitive to on how the profile is decomposed. In particular, the disk brightness varies from 24.4 mag arcsec^{-2} to the unlikely low value of 25.6 mag arcsec^{-2}, depending on the bulge domain used. On the other hand, for several reasons the interpretation of NGC 1380B as an elliptical galaxy is also not very satisfactory. First, it shows an unusually large (90°) isophotal twist for an elliptical galaxy, as it can be seen in Fig. 1d. Second, the de Vaucouleurs law does not adequately describe its light distribution both in the central regions and at large radii where it exhibits a large drop below the fit. Third, the parameters derived for the bulge using the $r^{1/4}$ law places the spheroidal component of NGC 1380B quite far from the region of normal ellipticals. All of these characteristics show the peculiar nature of this galaxy which may deserve a more careful study in the future.

Finally, we note that all galaxies in the present sample have $D/B < 1$, consistent with their location in the central regions of a cluster. Except for NGC 1351 all galaxies are within a projected distance of 0.25 Mpc from the nominal center of the Fornax cluster and have radial velocities within 2σ of its mean velocity of 1395 km s^{-1} (Jones and Jones, 1980).

3.3. *Other components*

In the present work we have also attempted to examine some of the basic properties of the structures associated with the residual light distributions obtained by subtracting the bulge-disk fits from the observed profiles. Our primary intention was to determine whether their properties were consistent with the limited information presently available regarding the general characteristics of lenses and bars, the most prominent features normally encountered in S0 galaxies.

For most of the program galaxies the presence of secondary components can readily be detected in the isophotal maps (Fig. 1) either by noticeable twists of the isophotes or by variations in their ellipticities. Based on these maps one can also detect a significant variation of the position angle of the major axis determined at different isophotal levels suggesting that the underlying components are probably triaxial. The presence of

subcomponents can also, in most cases, be clearly seen by the features they produce in the galaxy profiles especially when they are plotted against $r^{1/4}$.

An examination of the residual light distributions (Fig. 2) shows that they are all very noisy and that their shapes are clearly affected by small errors in the fits, especially in the bulge region. Furthermore, small wiggles in the original profile may create spikes which in some cases can be misinterpreted as additional structures. Nevertheless, the overall shape of the profiles roughly resembles the qualitative description given in the literature for lenses (e.g. Kormendy, 1982). In the case of NGC 1387 in addition to a more extended lens component there is a light excess near the center associated with the bar, clearly seen in all plates. For NGC 1380 the lens is the inner plateau structure inside 40 arcsec. In view of the quality of the data no attempt has been made to fit an analytical function to the data points as recently done by Duval and Athanassoula (1983) for the galaxies NGC 5383 and UGC 8877. Despite the uncertainties we estimate that the lenses have central brightnesses typically around 23 mag arcsec^{-2} while the bar in NGC 1387 has a value of $\sim$21 mag arcsec^{-2}.

Another valuable information that can also be used to characterize the secondary components is their intrinsic equatorial axial ratios. In order to determine this quantity for triaxial structures the profiles should ideally be analyzed along their apparent principal axes, as it was done in the case of the face-on galaxies NGC 1374 and 1387. However, for the other galaxies of the sample this ratio has been estimated simply as the ratio of the characteristic sizes of the structures as determined along the principal axes of the galaxy. We believe that for the purpose of the present work this determination is sufficient to characterize the nature of these structures.

The decomposition of the minor axis profiles could in principle follow the same scheme adopted to analyse the light distributions along the major axis. However, for systems at higher inclinations, the components tend to contaminate each other making it even more difficult to identify radii ranges, along the minor axis, where a single component contributes with most of the light. Therefore it is important to use as much as possible the information derived from the major-axis profile analysis such as the disk scale-length and the central brightness to determine the disk profile along the minor axis, taking into account the inclination of the galaxies. One further constraint that could be used would be to fix the bulge central brightness. However, since this quantity is poorly determined and small errors in the bulge fit can have a large effect on the photometric properties of the underlying component, this information was not used except to verify the final result. The technique finally adopted to decompose the minor axis profile was to subtract the disk contribution, constructed on the basis of the information obtained from the major-axis analysis, and to adjust $r^{1/4}$ laws to the remaining light distribution until the central brightness of the underlying structure on both principal axes approximately matched. A possible criticism to the above method is that the $r^{1/4}$ law may be in fact a poor description of the bulge structure along directions close to its rotation axis (e.g. Jensen and Thuan, 1982).

As expected, the shape of the residual light profiles along the minor axis are qualitatively similar to those of the major axis, although the cutoffs occur at different radii as a consequence of the intrinsic equatorial axial ratio of the components and the inclination of the corresponding galaxies. The size of these structures on both principal axes were measured in the brightness range 25–26 mag arcsec^{-2} of the residual light distribution. Utilizing these values and the assumption that lenses and bars are thin (e.g. Tisikoudi, 1979; Burstein, 1979b) we estimated their intrinsic axial ratios. For all galaxies we obtained axial ratios in the range 0.8–0.9 consistent with the average value of 0.85 found by Athanassoula et al. (1982) based on a statistical study of the apparent axial ratio distribution of lenses. For the bar in NGC 1387 we derived a ratio of 0.35, slightly larger than typical values (Kormendy, 1982). However, considering the uncertainties involved in the determination of these ratios, the above discrepancy is not too serious especially since equatorial ratios as large as 0.35 for bars have already been reported. We note that the values obtained for the central brightness and axial ratio of the components are slightly dependent on the fit domains, especially that used for the bulge. As a rule, larger domains give weaker and more elongated components.

Altogether the results presented above seem to indicate that the model fits obtained here are a fair description of the physical structure of the galaxies analyzed, partly justifying the use of the iterative decomposition method even for these low D/B S0 galaxies.

4. Conclusion

Our primary goal in this preliminary work was to determine the quality of our surface photometry data obtained utilizing the ESO (B) and ESO/SRC (J) film copies. For that purpose we have compared our final composed photographic profiles with available photoelectric data for the giant spiral NGC 1316 (Schweizer, 1980) and the elliptical galaxy NGC 1399 (Hodge, 1978). The results obtained from these comparisons indicate that the precision of our photographic profiles is $\sim$0.2 mag arcsec^{-2} between the brightness limits $21.0 < \mu_B < 25.5$ where the different data can be compared. Furthermore, the separation of the profiles into their intrinsic components yields results consistent with those obtained by other investigators, apparently justifying the use of the film copies for detailed surface photometry programs.

In this paper we have applied the method presented in Sect. 2 to investigate the properties of S0's typical of high galactic density regions and with independent components other than the bulge and the disk. In a way our sample complements that utilized in previous investigations that have considered primarily galaxies in the general field. Despite the large uncertainties, the photometric properties of the extra components were investigated and compared with available information. The results obtained from this comparison show in general a good agreement, lending further support to our model fits.

Perhaps the most interesting result of the present work is the tendency of the disks studied to have low luminosity and to find examples of very low surface brightness disks. Moreover, these galaxies have bulge luminosities typical of low density environments, despite their location in a dense region. This result may argue in favor of the idea that the correlation of D/B with galactic density simply reflects the decrease of the disk luminosity with density, as proposed by Kent (1981). One possible mechanism to explain this behavior is for example the slow disk formation model recently proposed by Larson et al. (1980). Interestingly, the disks show no evidence of outer cutoffs, a possible signature of the sudden removal of the gaseous halo which according to Larson et al. (1980) would lead to the formation of S0 galaxies.

Our preliminary results suggest that further photometry of S0 galaxies in dense environments may be worthwhile and will contribute towards a better understanding of the physical processes that have led to their formation.

The methodology developed in this paper, making extensive use of the ESO and ESO/SRC film copies, provides a powerful tool to significantly increase the currently available database of S0 galaxies with detailed surface photometry observations. A statistical sample based on reliable photometric data will be invaluable to further investigate some fundamental topics such as: (1) the reason for the variety of observed disk profile shapes; (2) to confirm our suggestion that disks in high density regions are less luminous and are the primary cause for the variation of D/B with density; (3) whether the disk parameter correlations claimed by Boroson (1981) and Hamabe (1982) can be verified for a larger and more representative sample of S0 galaxies. Progress on the theories of galactic disk formation and the origin of S0 galaxies will depend to a great extent on these observational results.

Acknowledgments. We wish to thank M.A. Nunes and D. Nascimento for their dedication in keeping our data acquisition system working. We are also very grateful to C. Rite for his enormous contribution in the development of the software. We also thank C. Willmer for his careful reading of the manuscript.

References

Athanassoula, E., Bosma, A., Crézé, M.: 1982 *Aston. Astrophys.* **107**, 101
Binggeli, B.: 1980, *Astron. Astrophys.* **82**, 289
Boroson, T.: 1981, *Astrophys. J. Suppl.* **46**, 177
Burstein, D.: 1979a, *Astrophys. J. Suppl.* **41**, 435
Burstein, D.: 1979b, *Astrophys. J.* **234**, 435
Burstein, D.: 1979c, A. A. S. PhotoBull. no. 20, 6
Cowie, L.L., Songaila, A.: 1977, *Nature* **266**, 501
Davoust, E.: 1981, in Astronomical Photography 1981 Meeting of the IAU Working Group on Photographic Problems, Eds. M.E. Sim and J.L. Heudier, p. 19
de Vaucouleurs, G.: 1948, *Ann. Astrophys.* **11**, 247
de Vaucouleurs, G.: 1968, *Appl. Optics* **7**, 1513
de Vaucouleurs, G., de Vaucouleurs, A., Corwin, H.C.: 1976, Second Reference Catalogue of Bright Galaxies, University of Texas Press (RC2)
Dressler, A.: 1980, *Astrophys. J.* **236**, 351
Duval, M.F., Athanassoula, E.: 1983, *Astron. Astrophys.* **121**, 297
Freeman, K.C.: 1970, *Astrophys. J.* **160**, 811
Green, M.R., Dixon, K.L.: 1978, *The Observatory* **98**, 166
Griersmith, D.: 1980, *Astron. J.* **85**, 789
Gunn, J.E., Gott, J.R.: 1972, *Astrophys. J.* **176**, 1
Hamabe, M.: 1982, *Publ. Astron. Soc. Japan* **34**, 423
Hodge, P.W.: 1978, *Astrophy. J. Suppl.* **37**, 429
Jensen, E.B., Thuan, T.X.: 1982, *Astrophy. J. Suppl.* **50**, 421
Jones, J.E., Jones, B.J.T.: 1980, *Monthly Notices Roy. Astron. Soc.* **191**, 685
Kent, S.M.: 1981, *Astrophys. J.* **245**, 805
Kormendy, J.: 1977a, *Astrophy. J.* **217**, 406
Kormendy, J.: 1977b, *Astrophys. J.* **218**, 333
Kormendy, J.: 1982, Morphology and Dynamics of Galaxies, 10th Advanced Course Swiss Society of Astronomy and Astrophysics, Eds. L. Martinet and M. Mayor, p. 113
Larson, R.B., Tinsley, B.M. Caldwell, C.N.: 1980, *Astrophys. J.* **237**, 692
Lauberts, A.: 1982, ESO/Uppsala Survey of the ESO (B) Atlas, private communication
Lauberts, A., Valentijn, E.A.: 1983, The Messenger, no. 34, 10
Oemler, A.: 1974, *Astrophys. J.* **194**, 1
Oemler, A.: 1976, *Astrophys. J.* **209**, 693
Romanishin, W., Strom, S.E., Strom, K.M.: 1982, *Astrophys. J.* **258**, 77
Sandage, A.: 1975, *Astrophys. J.* **202**, 563
Sandage, A., Visvanathan, N.: 1978, *Astrophys. J.* **223**, 707
Sandage, A., Tammann, G.: 1981, A Revised Shapley-Ames Catalog of Bright Galaxies, Carnegie Institution of Washington (RSA)
Schweizer, F.: 1980, *Astrophys. J.* **237**, 303
Sim, M.E.: 1981, in Astronomical Photography 1981 Meeting of the IAU Working Group on Photographic Problems, Eds. M.E. Sim and J.L. Heudier, p. 179
Spitzer, L., Baade, W.: 1951, *Astrophys. J.* **113**, 413
Tsikoudi, V.: 1979, *Astrophys. J.* **234**, 842
West, R.M., Schuster, H.E.: 1982, *Astron. Astrophys. Suppl.* **49**, 577

III- Fotometria Superficial da Galáxia "edge-on" NGC 1381

O papel dos efeitos ambientais na estrutura das galáxias S0 tem sido motivo de extensas investigaçõoes como por exemplo o trabalho de Dressler (1980). Um dos principais resultados deste trabalho foi o estabelecimento da correlação entre a razão D/B e a densidade local de galáxias, o que é usado como argumento contra a idéia de que as S0's são o produto de galáxias espirais que tiveram o gás de seu disco removido.

No capítulo anterior foi mostrado que as galáxias S0 localizadas na região central do aglomerado de Fornax apresentam bojos similares aos das S0's observadas em ambientes de baixa densidade galáctica e portanto os baixos valores da razão D/B obtidos refletem a baixa luminosidade da componente disco, como esperado pelo modelo de formação lenta do disco proposto por Larson et al. (1981). Entretanto, as galáxias S0 estudadas em Fornax não apresentaram nenhuma evidência de cortes externos no perfil de brilho, o que seria uma outra evidência a favor deste modelo. Assim torna-se importante o estudo de galáxias "edge-on", principalmente em regiões de alta densidade galáctica, porque neste caso podemos observar a maiores distâncias ao longo do plano do disco galáctico e assim verificar a presença ou não de cortes externos nesta componente.

Complementando o estudo apresentado no capítulo anterior, aqui são apresentados os resultado da análise da distribuição de luz da galáxia de perfil NGC 1381, também no aglomerado de Fornax. Outro importante aspecto da observação de galáxias de perfil é que nestes casos é possível

investigar a estrutura vertical dos discos e obter informações que podem contribuir para a nossa compreensão sobre o processo de formação e evolução desta componente.

A estrutura da galáxia NGC 1381, descrita a seguir, confirma o resultado obtido no capítulo anterior de que os discos de S0's em regiões de alta densidade galáctica são menos luminosos do que os observados em galáxias de "campo". Outro resultado importante é a possível existência de um corte externo no disco de NGC 1381, consistente com a teoria de Larson et al. (1980). Portanto, um estudo sistemático de S0's de perfil em regiões de diferentes regimes de densidade é fundamental para o esclarescimento das principais questões pertinentes aos processos de formação de discos galácticos.

Astron. Astrophys. 171, 66–76 (1987)

ASTRONOMY AND ASTROPHYSICS

Surface photometry of the edge-on galaxy NGC 1381

R.R. de Carvalho and L.N. da Costa

Department of Astronomy, CNPq, Observatório Nacional, Rua General Bruce, 586, São Cristóvão, 20921, Rio de Janeiro, Brazil

Received June 20, accepted July 2, 1986

Summary. We present surface photometry of the edge-on S0 galaxy NGC 1381. Examination of the brightness profiles parallel and perpendicular to the equatorial plane indicates that this galaxy has several distinct components, including a bar and an outer ring. In contrast to earlier expectations we find no evidence of a thick disk population and argue that the overall box-shaped appearance of the galaxy is probably due to the projection of the outer ring onto the plane of the sky. Support to our model comes from the fact that the existence of an outer ring and a box-shaped nucleus are consistent with the results of theoretical investigations on the dynamical evolution of barred galaxies.

From the decomposition of the observed light distribution into separate components we have obtained the photometric parameters that characterize each of these components. In particular, we find that NGC 1381 has a low-luminosity disk similar to those found in other neighboring S0 galaxies in the central regions of the Fornax cluster. This finding is in agreement with the hypothesis that the relationship between disk-to-bulge luminosity ratio and galaxy density is due primarily to variations in the disk luminosity. We also find evidence that the disk can be described by a truncated exponential model similar to that found in edge-on spirals. The importance of this result is that the existence of an outer disk edge in an S0 galaxy may be, if the picture of the slow disk formation is correct, a relic of the epoch when the galaxy lost its gas reservoir. Therefore, a systematic study of edge-on S0's may provide insight into the process of disk formation.

Key words: galaxies: lenticular – structure of galaxies

1. Introduction

In recent years the interest in the photometric and kinematic properties of S0 galaxies has grown primarily because of the general recognition that these studies may contribute to our understanding of the formation and evolution of galaxies. Lenticular galaxies are particularly important in this context since they are an intermediate case between the extremes of purely spheroidal systems, with no discernible disk, and spiral galaxies with small bulges and disks which are still actively forming stars. Clearly, an understanding of the origin of S0 galaxies may help to determine the relative importance of environmental effects and the physical conditions at the epoch of galaxy formation in establishing the present-day structure of galaxies.

Send offprint requests to: R.R. de Carvalho

The structure of S0's has been investigated by detailed surface photometry measurements and decomposition of the light distribution into distinct components (e.g. Burstein, 1979a, b; Tsikoudi, 1979, 1980; Hamabe, 1982; Kent, 1985). Additional information has come from statistical studies of the global properties of the secondary galactic components, using the data available from morphological surveys (e.g. Kormendy, 1979; de Vaucouleurs and Buta, 1980). These data combined with recent measurements of the rotation and dispersion velocity profiles (see Kormendy, 1982 for a review) have greatly increased our knowledge of the internal structure and dynamics of S0 galaxies. They have also motivated detailed numerical simulations which have attempted to explain the dynamical evolution of disk galaxies and the origin of features like bars, lenses, inner and outer rings, frequently observed in these systems.

The role of environmental effects in the structure of S0's has been investigated by Dressler (1980) and one of the main results of that work was to find a well-defined relationship between the disk-to-bulge luminosity ratio (D/B) and the local galaxy density. The existence of this correlation has become a strong argument against the idea that S0's have simply evolved from spirals by means of some type of gas removal mechanism. Other important questions have, however, remained unanswered such as the possible variation of the bulge luminosity with the galactic density which, if real, would have important implications for galaxy formation theories as discussed by Dressler (1980).

Motivated by these questions, we have recently presented surface photometry data for a sample of galaxies located in the central regions of the Fornax cluster (de Carvalho et al., 1985, Paper I). In selecting our S0 sample we made no restrictions concerning the structure of the galaxies in an attempt to include all possible examples of S0's in dense environments. As a result the observed galaxies had, in general, a complex structure with prominent underlying components. Nevertheless, by carefully utilizing standard techniques of decomposition of light profiles, we were able to derive the structural parameters of the bulge and the disk, as well as some information on the secondary components like lenses and bars. An important result of that investigation was to find that the observed bulges were very similar to those found in S0's of the general field and that the small values obtained for D/B were due to the low luminosities of the disks. As pointed out in Paper I, this behavior is consistent with the scenario proposed by Larson et al. (1980) which argues that the formation of a galactic disk is a slow process and that S0 galaxies originate from spirals that somehow had the growth of their disks inhibited at some point during their lifetime. We note, however, that in contrast to normal spirals, the disks of the

galaxies studied in Paper I showed no evidence of outer cutoffs which could be, in principle, an expected signature of the sudden loss of the galaxy's gas reservoir. In this context, the study of the structure of disks in lenticular galaxies, especially edge-on systems in high-density regions, may provide important clues about the process of disk formation and may eventually contribute to the progress of more detailed theoretical models, which are at the present time still very schematic (e.g. Gunn, 1981).

In the study of the structural properties of disks, edge-on galaxies are particularly useful since with them it is possible to investigate the vertical structure of the various galactic components and to probe larger distances along the fundamental plane. Therefore we complement our earlier work on S0 galaxies in dense regions (Paper I) investigating here the properties of the edge-on system NGC 1381. This galaxy is particularly interesting because at faint light levels it has the characteristic box-shaped form that led Burstein (1979b) to introduce the concept of thick disk. The true nature and the possible origin of thick disks is still highly controversial and several interpretations have been advanced since their detection. Burstein's (1979b) original hypothesis was that thick disks were a distinct galactic component only present in S0 galaxies. However, recent work on edge-on spirals (van der Kruit and Searle, 1981a) has shown that these systems also exhibit light excesses above the galactic plane, very similar to those observed in S0's. From the theoretical point of view the following models have been proposed to account for this component: 1. it is formed during the initial collapse of the galaxy and precedes the formation of the bulge and the thin disk, the latter being formed from infalling gas produced by stars in the thick disk (Jones and Wyse, 1983); 2. it simply reflects the response of the bulge to the gravitational potential of a flat thin disk (e.g. Freeman, 1979; van der Kruit and Searle, 1981a; Monet et al., 1981; Barnes and White, 1984); 3. it is associated to the secular evolution of a thin disk driven by the interaction of stars with interstellar clouds (Spitzer and Schwarzschild, 1953) or by resonant coupling between z-oscillations with a time-dependent asymmetric potential like that produced by a rotating bar (e.g. Binney, 1981; Pfenniger, 1985).

Another interesting feature displayed by NGC 1381 is the box-shaped appearance of its nucleus, clearly seen in short-exposure plates (Burstein, 1979c). Similar shapes have been observed in other edge-on galaxies and in three-dimensional N-body simulations, and it is believed that it is also associated to resonances between the bar motion and the z-oscillations of disk stars (e.g. Combes and Sanders, 1981; Pfenniger, 1984).

From the above discussion we see that photometric and kinematic studies of NGC 1381 are of great interest for a variety of reasons and in this paper we present measurements of its surface brightness distribution. In Sect. 2 we briefly review the data reduction techniques used in the present work. In Sect. 3 we first describe the general characteristics of the two-dimensional light distribution, examining the profiles parallel and perpendicular to the galactic plane. In this section we also show that the surface brightness distribution of NGC 1381 can be adequately modelled by the sum of a bulge, a disk, a bar and an outer ring. Finally, in Sect. 4 we discuss some possible implications of our results to the theories of galaxy formation.

2. Data reduction

The photographic material used in the present work consisted of a high-resolution plate in the B passband, taken at the 60-in. telescope of the Observatório Nacional (ON), to cover the central parts of the galaxy and the on-film copies of the ESO(B) and ESO/SRC(J) Sky Atlas to extend the measurements to faint light levels. This material was scanned on the PDS microdensitometer of the ON and 3 two-dimensional data arrays were generated as follows: an inner 200×200 array, each pixel 50μ ($=0''.65$), from the scan of the high-resolution ON plate; an intermediate 400×400 array measured on the ESO(B) copy, with a 20μ pixel ($=1''.35$); an outer 200×200 array measured on the ESO/SRC(J) copy, each pixel 50μ ($=3''.36$).

The techniques used to linearize the data and to determine the contribution of the sky background are essentially the same as those described in Paper I. The only exception is that we have adopted the analytical expression suggested by Llebaria and Figon (1981) to describe the characteristic curve of the ESO(B) and ESO/SRC(J) film copies, instead of using the more traditional form originally proposed by de Vaucouleurs (1968). The reason for this modification was to improve the density to intensity conversion at the high-density end, thereby increasing the brightness range covered by the ESO(B) and ESO/SRC(J) films. This improves the accuracy of the matching between the data points in the inner, intermediate and outer arrays, essential to produce smooth profiles covering the whole brightness range of the galaxy.

The zero-point of the magnitude scale was established separately for the ON and the ESO(B) data simulating annular apertures, as described in Paper I, and utilizing the photoelectric measurements of Sandage and Visvanathan (1978). We note that the same procedure could not be used for the ESO/SRC(J) film because the galaxy's image is saturated over the area covered by the available apertures. To overcome this problem the outer array was calibrated using, instead, the profiles along the principal axes of the galaxy as described below.

Light profiles along any given direction can be constructed by simply superimposing calibrated profiles obtained from the three distinct arrays, discarding the data points in saturated or noisy regions. Adopting this procedure to combine the profiles obtained from the inner and intermediate arrays, we found a small relative zero-point shift of $0.05\,\mu_B$. This value was used to correct the calibration of the inner raster, since more apertures were available in the area covered by the intermediate array. The outer array was calibrated by carefully shifting the profiles obtained along the principal axes of the galaxy onto the corresponding profiles derived from the intermediate raster. The final calibration constant for the outer array was taken to be the mean value of the shifts required in all four directions. As discussed in Paper I, the comparison of our data with those of other authors indicates that our measurements have an accuracy of about 0.2 mag arcsec^{-2}.

3. Data analysis

3.1. General description

The S0 galaxy NGC 1381 is located in the core of the Fornax cluster, assumed to be at a distance of 27.9 Mpc ($H_0 = 50$ km/s/Mpc) as determined from the cluster mean radial velocity given by Jones and Jones (1980). It has been frequently mentioned in the literature because of the box-shaped appearance of its bulge and overall light distribution, features that can easily be seen in the isophotal and contrast maps generated from the data obtained from the ON plate and ESO(B) and ESO/SRC(J) films (Fig. 1). These maps also indicate that the light distribution of NGC 1381 is

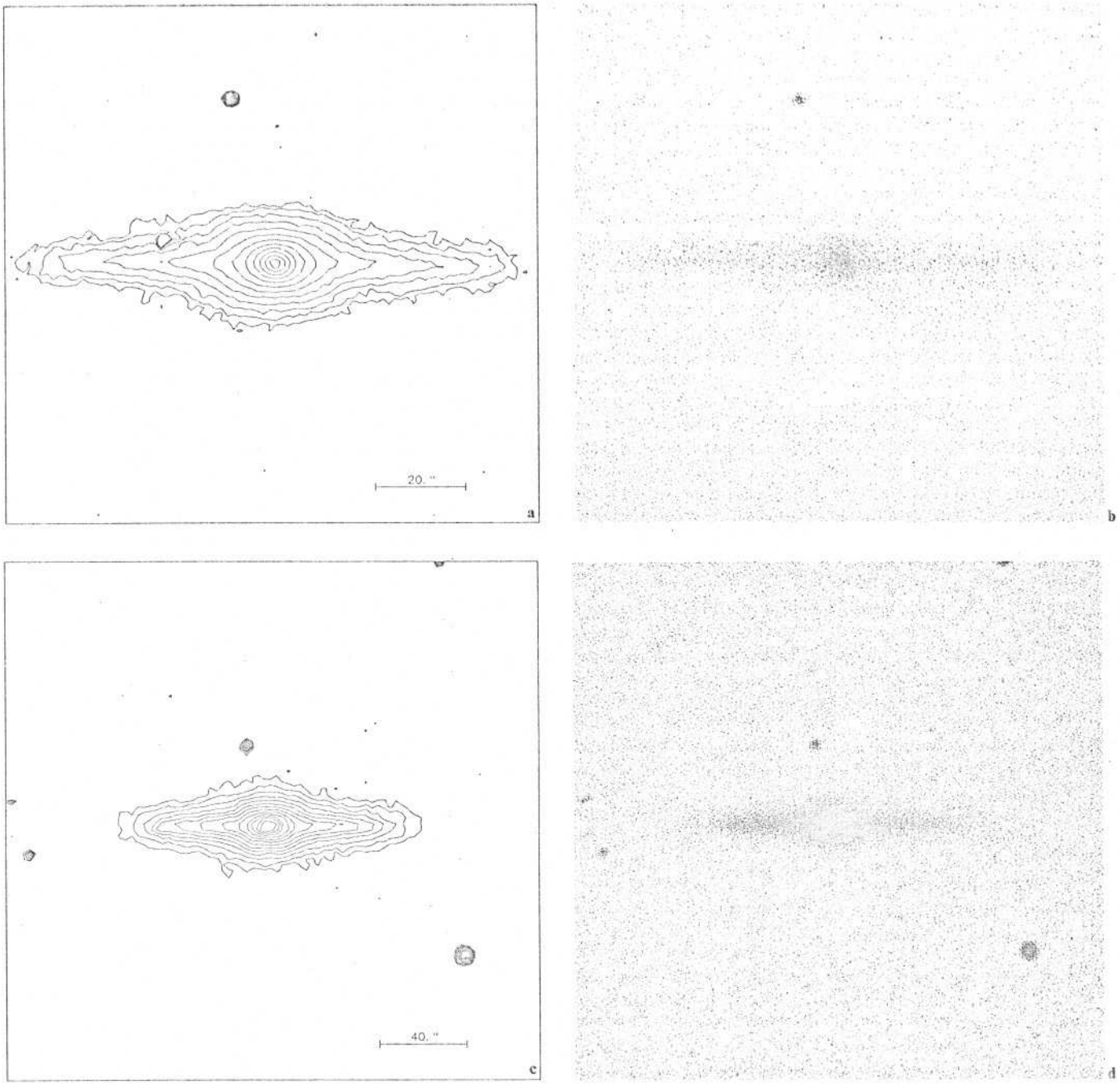

Fig. 1a–f. Isophotal and contrast maps of the nuclear (a, b), intermediate (c, d) and outer regions (e, f) generated from the data on the ON plate, ESO (*B*) and ESO/SRC (*J*) films, respectively. The blue isophotes are at 0.5 mag interval and are from: a $\mu_B = 17.5$ mag arcsec^{-2}; c $\mu_B = 18.5$ mag arcsec^{-2}; e $\mu_B = 24.5$ mag arcsec^{-2}

fairly symmetric about the major and minor axes, and all the profiles presented below were obtained from the average of corresponding data-points in each quadrant.

The major difficulty in the analysis of the light distribution of an edge-on galaxy is the fact that the observed intensity results from an integration along the line-of-sight, with the various galactic components contributing different amounts of light at each point. Furthermore, since all the azimuthal information is lost, it becomes quite difficult to make a clear identification of the individual components that make up the system. In the past, different techniques have been employed to analyse the light distribution of edge-on spiral and S0 galaxies (e.g. van der Kruit and Searle, 1981a; Hamabe, 1982) but, in general, they were used to study simple two-component systems with either dominant bulges or disks. The analysis becomes considerably more difficult for galaxies with secondary components such as bars, lenses and rings, especially when these are relatively prominent, as is the case of NGC 1381. In spite of the difficulties, attempts to study more complex systems have been made in the past (e.g. Tsikoudi, 1979, 1980; Wakamatsu and Hamabe, 1984, hereafter WH) and have

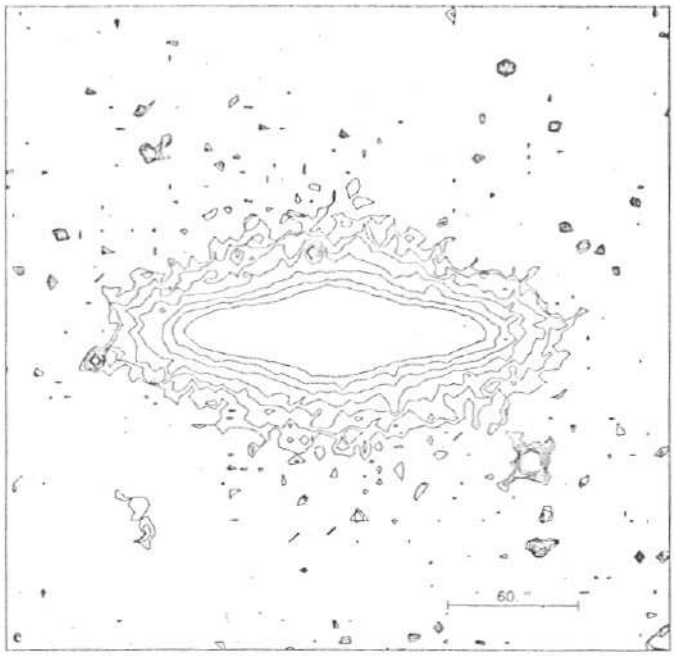

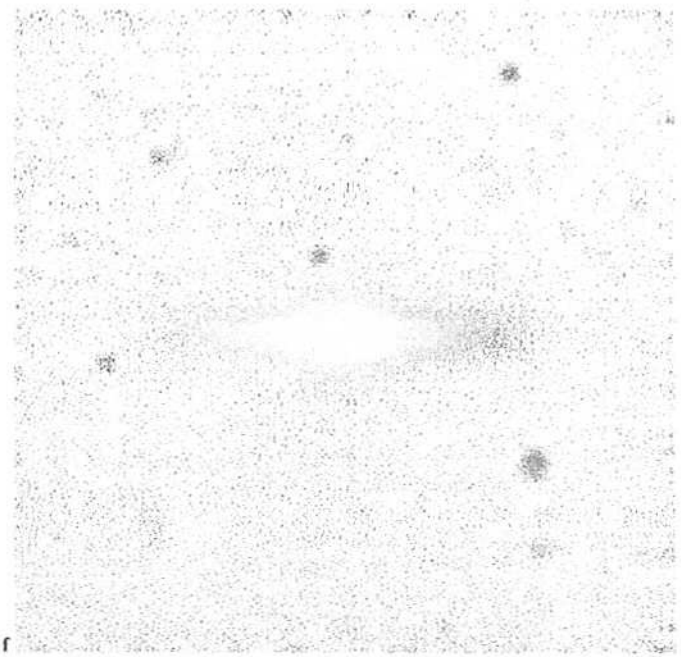

Fig. 1a–f (continued)

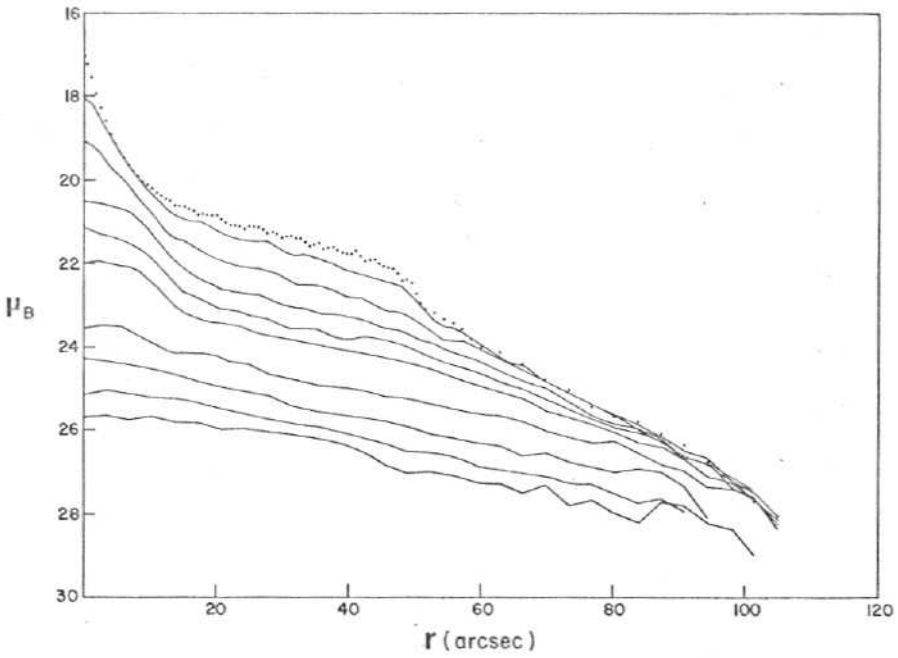

Fig. 2. Observed luminosity profiles parallel to the major-axis (r-profiles). For z between 0"–10" the profiles are plotted at 2" intervals, while in the domain $10'' < z < 30''$ the interval used is 5"

provided valuable information about the vertical structure of the different galactic components which are used in the present paper to verify our conclusions about the structure of NGC 1381.

Before attempting to decompose the light of NGC 1381 into separate components it is convenient to investigate the nature of its overall two-dimensional structure, using for this purpose the profiles parallel (r-profiles) and perpendicular (z-profiles) to the galactic plane plotted in Figs. 2 and 3, respectively. Inspection of the major-axis profile, for instance, reveals that it has apparently three important features which define four distinct regions along the equatorial plane. In each of these regions different galactic components probably make the dominant contribution to the light of the galaxy. Near the center the bulge light dominates both along the major ($r < 15''$) and minor axes ($z < 15''$). In particular, the minor-axis profile seem to follow a de Vaucouleurs law up to $z \sim 15''$ where it becomes exponential-like, indicating the presence of a thick component at large heights. On the other hand, examining the behavior of the parallel profiles we find that, between $5'' < z < 15''$, these are very flat near the center ($r < 10''$) manifesting the box-shaped appearance of the nuclear region.

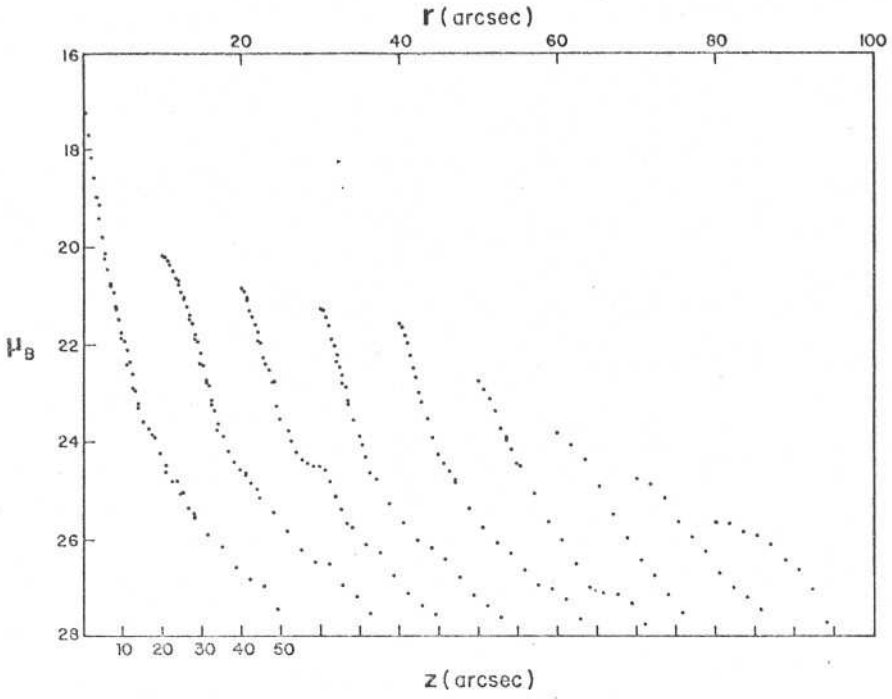

Fig. 3. Observed luminosity profiles perpendicular to the galactic plane (z-profiles) from $r = 0''$ to $r = 80''$ in $10''$ intervals.

For $15'' < r < 50''$ the profile along the major-axis has a shallow gradient probably due to the appearance of a second component. From the behavior of the parallel profiles (Fig. 2) we can infer that this component is thin since it virtually disappears for $z \sim 4''$ (~ 0.52 kpc). Examination of the z-profiles in this radial interval, shows that they are typically rounded near the galactic plane and are apparently the sum of at least two distinct components: near the center the profile resembles a $\mathrm{sech}^2(z)$ law, while at larger heights it has a shallower gradient. We note that this is a very general description and individual profiles show other significant features as can be seen in Fig. 3. In particular, the z-profile at $r = 20''$ displays a shoulder at $z \sim 20''$, associated with the box-shaped structure present near the center. In addition, most of the vertical profiles exhibit humps at faint light levels ($\sim 27\,\mu_B$), the nature of which is discussed below.

For $50'' < r < 80''$ the distribution of surface brightness along the galactic plane becomes steeper and apparently linear, revealing the possible presence of a third component. Note that in this region there is a significant change in the slope of the r-profiles for $z < 10''$. The vertical profiles are once again rounded near the plane and their overall shape indicates that two components contribute in this region.

Finally, for $r > 80''$ the major-axis profile shows a significant change in slope. Thereafter, it begins to fall steeply, indicating that the galaxy may have a sharp outer cutoff at $r \sim 110''$ (~ 14.30 kpc). In this region a single component seems to adequately describe the vertical profile. Examination of the r-profiles shows that the cutoff observed at the equatorial plane is also present at different heights. More significantly, for $z > 20''$ these profiles have a very shallow gradient. We interpret these observations as suggesting that the galaxy has a flat, truncated, thick component that dominates the light at large distances both along and above the galactic plane. We note that attempts to fit an exponential law to the r-profiles for $z > 20''$ yielded unreasonably large values for the radial scale-length, suggesting that this thick component might be annular. A clue on the nature of the three-dimensional structure of this component is provided by the work of WH who showed, using techniques to rectify the observed profile, that the shallow projected distribution observed along the major-axis of NGC 4762 was produced by an outer ring seen edge-on. By analogy, we argue that the shallowness of the surface brightness distribution produced by the thick component observed in NGC 1381 is indicative of an outer ring. Furthermore, as it will be shown in Sect. 3.2, the vertical scale of this component is also comparable to that obtained by WH for the outer ring identified in NGC 4762. An independent evidence in favor of this interpretation comes from the fact that the estimated diameter for the ring in NGC 1381, satisfies the correlation between ring diameters and magnitudes obtained by Kormendy (1979). The absolute magnitude of NGC 1381 was estimated to be $M_B = -19.9$, derived from the apparent magnitude listed in Sandage and Tammann (1981) and the assumed distance of Fornax cluster given above. The diameter of the ring was estimated to be ~ 26 kpc, corresponding to the point where the major-axis profile starts to drop.

3.2. *Modelling the light distribution*

From our previous discussion, we expect that the bulge and the suspected outer ring dominate the light distribution near the center and on the outskirts of the galaxy, respectively. In these regions the structural parameters of these components can be derived and used to define approximate models for their overall light distribution. A more detailed investigation of the other underlying components then becomes possible by subtracting these empirical models from the observed brightness distribution.

Examination of Figs. 1a and 3 shows that the isophotes near the center are round and that the minor-axis is well described by $z^{1/4}$ law up to $z \sim 15''$. Both of these characteristics indicate that the bulge is the major contributor to the light of the galaxy near the center and its parameters were determined by fitting a $z^{1/4}$ law to the data-points along the minor-axis (Fig. 5a), yielding a de Vaucouleurs radius $r_0 = 1''.49$ (0.19 kpc) and a surface brightness

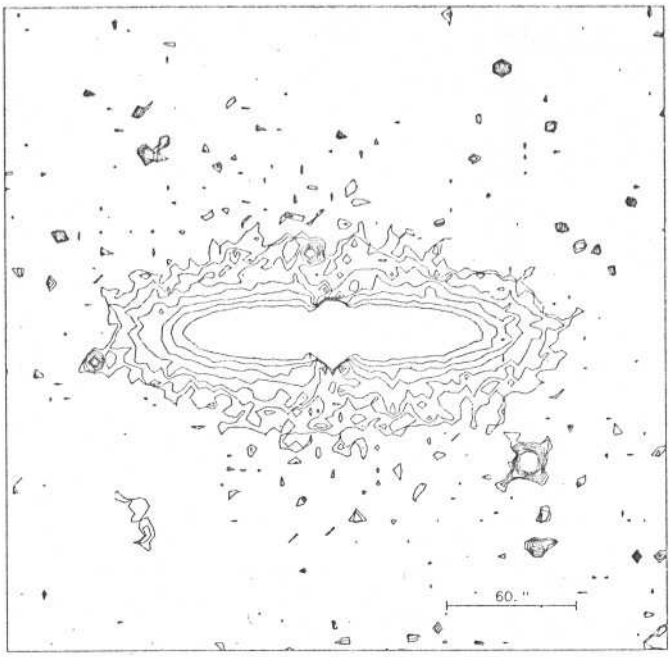

Fig. 4. Isophotal map of the residual light distribution after bulge model subtraction. Isophotes are at 0.5 mag interval and from $\mu_B = 24.5$ mag arcsec^{-2}

at that radius $B_0(V) = 16.8\,\mu_B$. In addition, we have fitted ellipses to the isophotes in the brightness range $17.5 - 19.0\,\mu_B$, which show that the bulge appears to be quite round, with an estimated axial ratio of 0.91. Following van der Kruit and Searle (1982b), in their study of a bulge-dominated galaxy, we assume that the bulge can be represented by an oblate spheroid with a constant axial ratio. This assumption may be questioned in view of the box-shaped character of the bulge which is believed to be associated with the presence of a bar. However, there is no evidence at present time whether this represents a global change in the structure of the bulge. Another possibility is that it reflects a local density enhancement produced by preferentially populating some stable three-dimensional orbits (Pfenniger, 1984) with stars originally in the disk and an undetermined fraction of bulge stars. If the fraction of bulge stars involved in creating the box-shaped pattern is small, a constant axial-ratio spheroid would still be a reasonable first order approximation of the structure of the bulge.

We have subtracted the above model for the bulge from the observed distribution and generated the isophotal map of the residual light, shown in Fig. 4. The overall box-shaped nature of the outermost galactic component becomes even more noticeable in this map, especially for isophotes fainter than $25.5\,\mu_B$. This fact strongly suggests that this component has indeed a sharp outer cutoff and a very flat projected light distribution, as would be expected for an outer ring. We note that the isophotes at brighter light levels become gradually more elliptical due to the contribution of other components. It is also interesting to notice that for radial distances less than 50", the outermost isophotes are somewhat distorted forming what appears to be a rectangular-shaped structure. These isophotes are associated with the observed humps in the z-profiles shown in Fig. 3.

The structure of the ring was investigated by analysing the perpendicular profile at $r = 80''$ and the parallel profile at $z = 30''$, both subtracted by the adopted bulge model. We find that the vertical profile is well fitted by a single sech$^2(z)$ law (Fig. 5b), with a characteristic scale-height of 20".54 (2.67 kpc) and an observed brightness at the galactic plane of $25.6\,\mu_B$. Based on the properties of the map shown in Fig. 4, we assume that the projected surface brightness distribution of the ring can be modelled, for $r < 80''$, by a plane parallel distribution with a constant scale-height. Furthermore, as a first approximation, we take the brightness of the ring at the galactic plane to be independent of r and given by the value derived at $r = 80''$, where this component starts

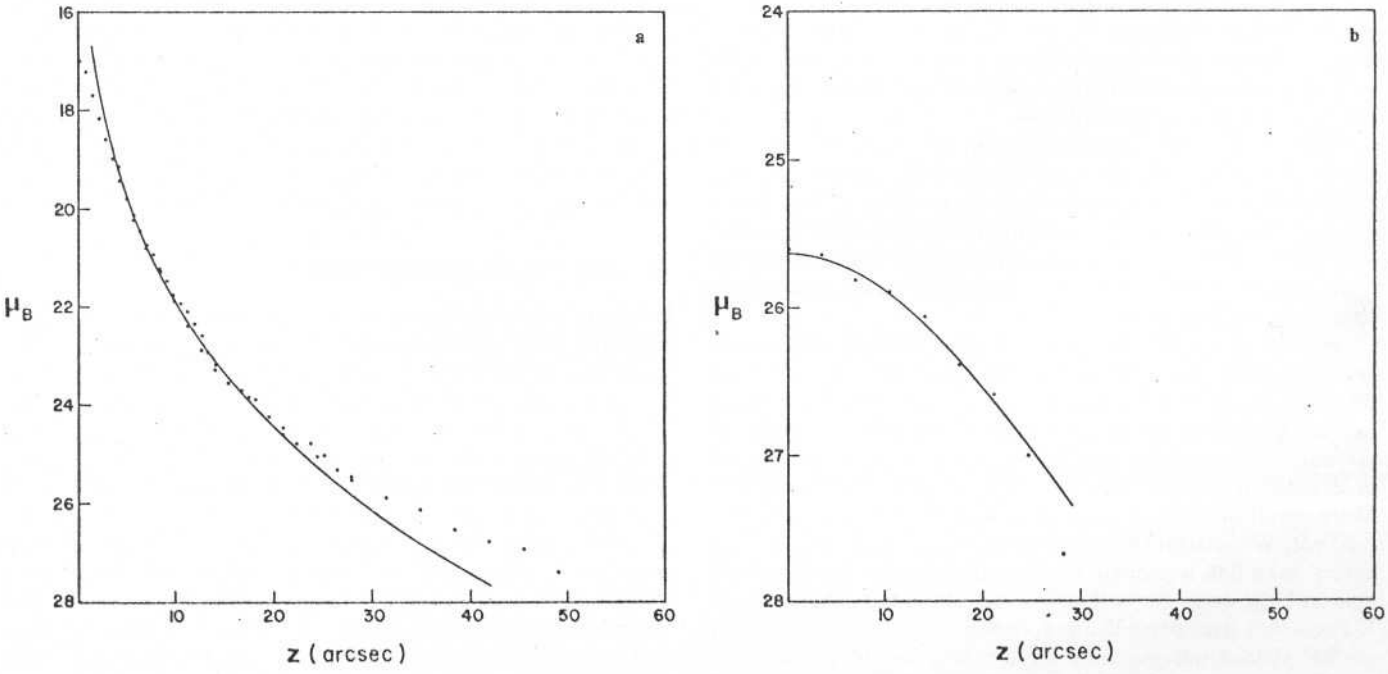

Fig. 5a and b. Observed perpendicular profiles at $r = 0''$ (a) and $r = 80''$ (b). The solid curves represent the bulge model ($z^{1/4}$ law) and the vertical model of the ring (sech$^2(z)$ law), respectively

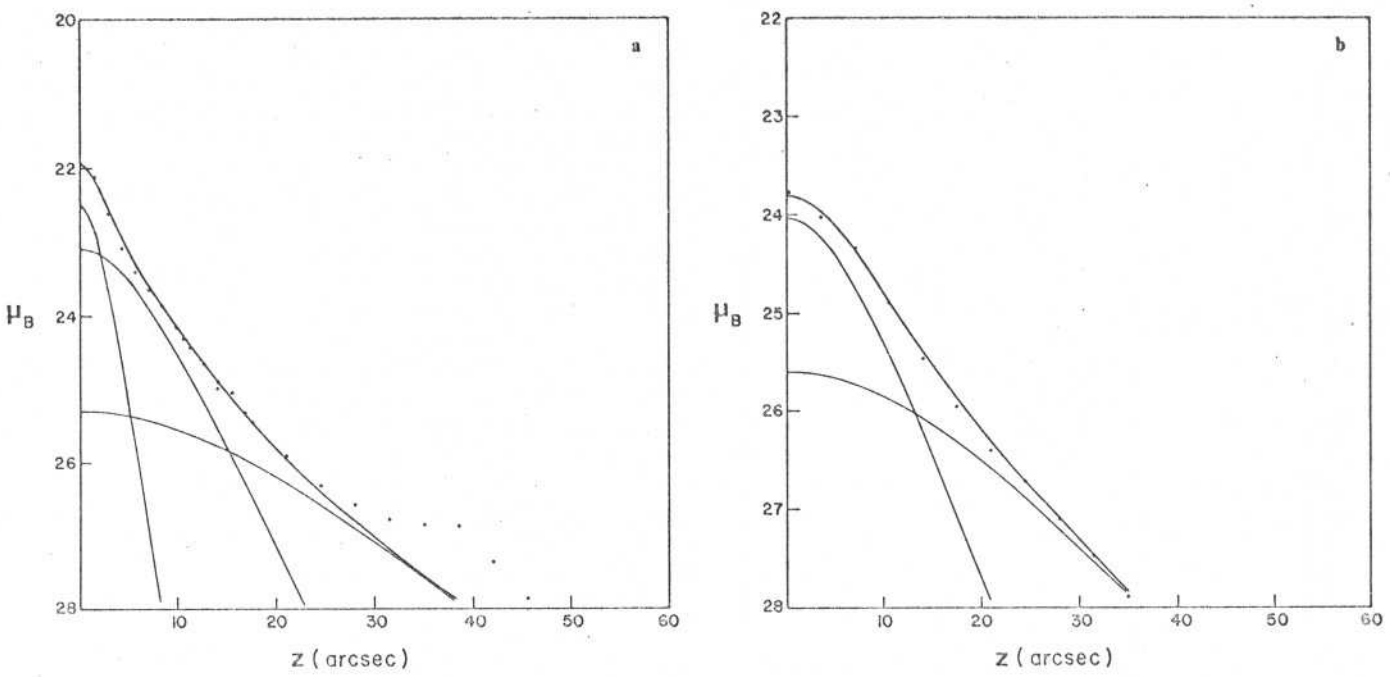

Fig. 6a and b. Observed z-profiles at $r = 45''$ (a) and $r = 60''$ (b). The solid curves represent the $\mathrm{sech}^2(z)$ law fits to the bar, disk and outer ring. We also show the total model obtained from the sum of these various components. Note the large light excess for $z > 25''$ which occurs over the radial extent of the bar. However, this excess disappears at large r, and at $r = 60''$ only the disk and outer ring contribute to the observed vertical profile

dominating the major-axis profile. Since, the ring is faint, this assumption should not significantly affect the radial structure of the other components, at least at the equatorial plane. We note that a similar assumption was made by WH in their analysis of NGC 4762. However, this is not true at large heights where the ring dominates the light of the galaxy. Therefore, in the vertical analysis, we have assumed that the ring is characterized by a constant scale-height but we have determined its brightness at the equatorial plane at each r so as to reproduce as close as possible the observed profiles at large z. This procedure allows for possible radial variations of the projected surface brightness of the ring due to geometrical effects and/or intrinsic assymmetries. In fact, we have found that these variations are small ($\sim 0.4\,\mu_B$) around a mean value of $25.3\,\mu_B$, close to the value determined at $r = 80''$.

In order to investigate the vertical structure of the remaining components we show in Fig. 6 the result of the decomposition of z-profiles at $r = 45''$ and $60''$. In this figure we also plot at each r the contribution from the outer ring, the $\mathrm{sech}^2(z)$ fits obtained for the other thin galactic components and the resulting total model. The contribution from the bulge was determined directly from the model but it is too small to appear in the figure. On the other hand, the contribution of the ring was calculated fitting a $\mathrm{sech}^2(z)$ law with a fixed scale-height, as discussed above. From this analysis we find that the major-axis light profile between $r = 50''$ to $80''$ is dominated by a thin component with an average scale-height of $8''.23$ (1.07 kpc), which we identify as the finite-thickness disk of NGC 1381. For $r < 50''$ (6.50 kpc) there is also a thinner component with a vertical scale-length of $2''.62$ (0.34 kpc), suggesting that it could be a lens, a bar or a superposition of both, since these components are believed to be rather thin (e.g. Kormendy 1982; WH). We note that we have found a small variation ($\sim 30\,\%$) in the scale-height of the disk in the radial domain of the bar/lens component.

The information obtained from the vertical analysis can now be used to derive the radial structure of the various components at the galactic plane. To derive the radial distribution of the disk we used the equatorial surface brightness determined from the vertical analysis at different radial distances, for $r < 70''$, and from the subtraction of the ring contribution along the fundamental plane for $r > 70''$. To these data points we fit an exponential disk model (Fig. 7), taking into account projection effects, and we find that the data are well described by a truncated disk with a radial scale-length $\alpha^{-1} = 14''$ (1.82 kpc) and an outer radius $r_{max} = 76''$ (9.88 kpc). Subtracting the contribution of the disk, we are left with the sum of the bulge and inner thin component also shown in Fig. 7. Note that this profile has an extremely shallow luminosity gradient in the radial interval $r = 20''$ to $45''$, in agreement with the expected behavior for a bar. Also note that there is a small feature along the major-axis between approximately $50''$ to $60''$, which becomes more prominent when the outer ring and disk are removed. This suggests that there may still exist another component superposed to the bar, which is not surprising since lenses and inner rings are commonly observed in barred systems (e.g. Kormendy, 1982). However, the presence and the unambigous identification of this possible additional component is not straightforward in the case of NGC 1381 since the region over which it is detectable is very small. We have attempted to investigate its vertical structure using the z-profile at $r = 55''$. Indeed, we find some evidence for the presence of another component, with a scale-height of the order of $5''.30$ (0.69 kpc), close to the value of 0.56 kpc derived by WH for the lens observed in NGC 4762. The reason why the lens is not clearly seen along the major-axis can be explained if the angle between the major-axis of the bar and the plane of the sky is small. Assuming the lens to be circular, we estimate from the ratio of the projected dimensions of the bar and the lens that this angle should be less than 40°. The

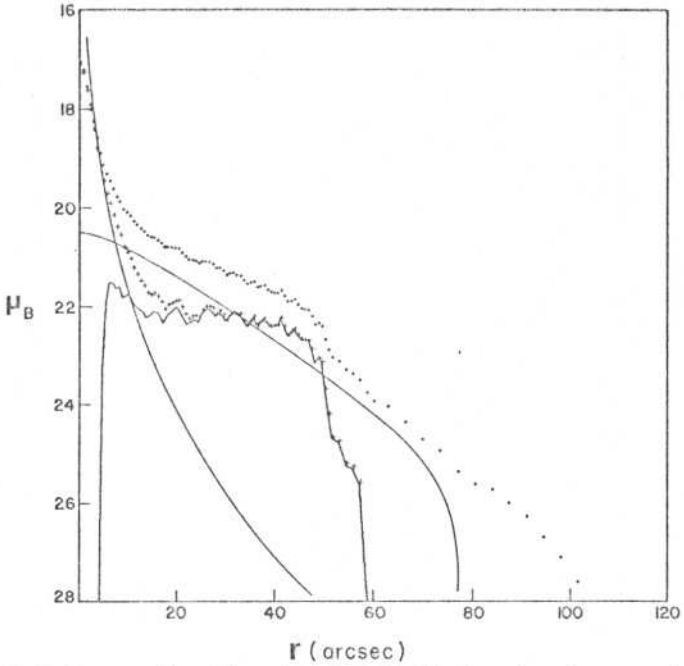

Fig. 7. Decomposition of the major-axis profile. The figure shows the truncated exponential disk model and the profile resulting from the disk subtraction. We also plot the bulge model and the residual light after its subtraction, exhibiting the contribution from the bar

suspected lens is also faint ($\sim 24.6\,\mu_B$ at the galactic plane) compared to the intensity of other components in the same region. This means that the lens should have little effect in the decomposition of the galaxy's light, and hence it is not considered in the subsequent analysis.

To investigate the structure of the bulge along the equatorial plane we have decomposed the light profile that results after the disk subtraction. This was done by fixing the value of the central brightness of the bulge, determined from the minor-axis analysis, and adjusting its effective radius in such a way as to produce a flat brightness profile for the bar all the way to the center (e.g. Kormendy, 1982; Duval and Athanassoula, 1983). The resulting total fit is shown in Fig. 7 together with the contributions from each individual component. As a check on the overall consistency of our model we remark that the bulge's effective radius, determined from the above procedure, yields an axial ratio of 0.92 in excellent agreement with our original assumption.

In Fig. 8 we plot once again the observed profiles perpendicular to the galactic plane. Also shown are the profiles of our galaxy model, confirming that it reproduces the major features of the two-dimensional light distribution of NGC 1381. However, as mentioned earlier there are localized departures associated with the box-shaped nucleus which we have not attempted to model. We also find significant light excesses at faint light levels for $r < 50''$. It is interesting that this effect is confined to the region of the bar suggesting that it may be associated to it. One possibility might be that this feature reflects the presence of an inner ring, which are know to have the same size of the bar. If this interpretation is correct the data suggest that the inner ring is faint and has a large scale-height, comparable to that of the outer ring.

3.3. *Characteristic parameters*

In Table 1 we summarize the parameters derived from the analysis of the light distribution of NGC 1381, listing the characteristics brightness, the radial and vertical scale-lengths, and estimated absolute magnitude of the various components of the system. From Table 1 we find that the bulge of NGC 1381 is small and not very luminous. Nevertheless, it still falls near the relationship found by Kormendy (1977) for normal ellipticals, although slightly more compact. We also find that the luminosity of the disk is small, yielding a disk-to-bulge luminosity ratio of approximately 0.4, consistent with the values obtained by de Carvalho et al. (1985) for other S0 galaxies near the center of the Fornax cluster. Moreover, the value derived for the disk luminosity of NGC 1381 confirms the trend observed in Paper I that the disks of

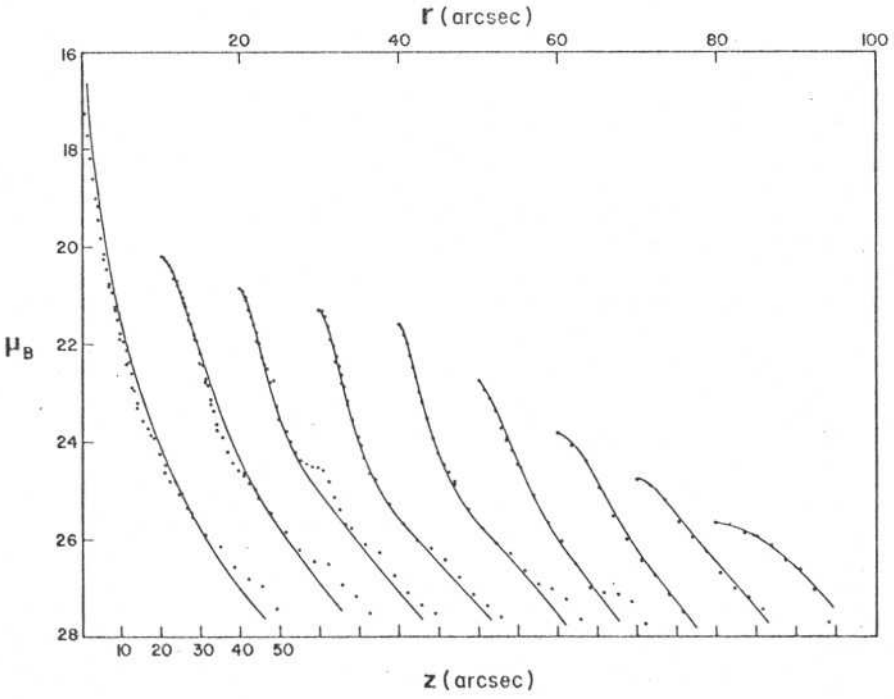

Fig. 8. Complete set of observed and model z-profiles. Note that the model, obtained from the detailed analysis of the two-dimensional surface brightness distribution, adequately describes the galaxy's structure as a whole. The light excesses above the model are discussed in the text

Table 1. Photometric parameters of the various components

Bulge	
Effective brightness	$B_0(V) = 16.7\,\mu_B$
Effective radius	$r_0 = 0.19$ kpc
Absolute magnitude	$M_B = -19.8$
Disk	
Face-on central brightness	$B_0(C) = 21.1\,\mu_B$
Radial scale-length	$\alpha^{-1} = 1.82$ kpc
Vertical length	$z_0^d = 1.07$ kpc
Cutoff radius	$r_{max} = 9.88$ kpc
Absolute magnitude	$M_B = -18.7$
Bar	
Face-on central brightness	$B_c^b = 24.0\,\mu_B$
Diameter	$D_b = 6.50$ kpc
Vertical scale-length	$z_0^b = 0.34$ kpc
Absolute magnitude	$M_B = -16.5$
Outer ring	
Observed surface brightness	$B_c^r = 25.6\ \mu_B$
Vertical scale-length	$z_0^r = 2.67$ kpc
Diameter	$D_r = 14.30$ kpc

S0's in dense regions usually have small luminosities. This is reassuring since the technique employed here for the derivation of the disk luminosity is completely different from our earlier work. On the other hand, the face-on central brightness of the disk ($20.9\,\mu_B$) is much brighter than those obtained in Paper I, suggesting that $B_c(0)$ does indeed span a large range of values ($\sim 3\,\mu_B$), as found in previous work on disk galaxies (e.g. Boroson, 1981).

From our analysis we find evidence that the disk has an outer cuttof at the radius $r_{max} = 5.5\,\alpha^{-1}$, in general agreement with the observations of spiral galaxies reported by van der Kruit and Searle (1981a, b, 1982a, b). At the observed cuttof, the corresponding face-on surface brightness is $\sim 26.1\,\mu_B$, implying that the detection of disk edges in less inclined systems may be difficult. Unfortunately, the reality of the disk edge may still be disputed since we cannot discard the possibility that it is an artifact of the procedure adopted in the analysis, which implicitly treats the ring as a separate component rather than as a perturbation of an underlying disk. It is possible that the disk extends beyond the outer ring at light levels fainter than those available from our photometry. In this case the existence of an outer edge would be artificial and due to the improper way of modelling the disk-ring system. We should emphasize that our results concerning the global properties of the disk are not very sensitive to the value of its outer radius.

The basic properties of the secondary galactic components are also listed in Table 1. The derived scale-height for the bar (~ 0.34 kpc) is slightly larger than that obtained in NGC 4762. This larger value can be partly caused by the probable presence of a superposed lens, with an estimated scale-height of 5".30 (0.69 kpc) which may affect the analysis of the vertical structure of the bar. As mentioned earlier, the existence of a lens is suspected but cannot be confirmed with the available data, although the tentative value derived for its vertical scale-length is consistent with previous determinations (WH). We note that the existence of a bar in NGC 1381 is consistent with our identification of an outer ring in the galaxy, since it is known that they are commonly associated (Schwarz, 1981; Kormendy, 1982; Athanassoula and Bosma, 1985). In particular, the ratio of the observed ring diameter to the bar diameter is approximately 2, comparable to the average value of 2.21 given by Kormendy (1979) and Athanassoula et al. (1982). We have estimated the face-on brightness of the bar assuming that it is aligned perpendicular to the line-of-sight and has an axial ratio of 0.2 (e.g. Kormendy, 1982). The value obtained is listed in Table 1 and is in good agreement with that derived by WH.

The structure of NGC 1381 presented above is similar in nature to that described by WH for the S0 galaxy NGC 4762. In both cases four distinct components were detected from features present on the major axis profile. There are, however, some important differences. First, WH clearly identify a bar and a lens in their analysis, deriving scale-heights of 0.16 kpc and 0.56 kpc, respectively. In the case of NGC 1381 we are sure that there is at least one thin component, identified by the sharp feature it produces at $r \sim 50''$, and possibly two as previously discussed. The derived vertical scales are slightly larger than, but consistent with, those encountered by WH. Second, the outer ring of NGC 4762 is relatively brighter than that observed in NGC 1381, producing an extended region over which the brightness distribution along the major-axis is very shallow. In our case the ring dominates the galaxy's light at the equatorial plane only over a small radial interval and at very faint light levels, and its detection was possible mainly because of its large scale-height.

4. Discussion

The study of the surface brightness distribution of NGC 1381 has shown that its overall structure can be adequately described by the superposition of galactic components commonly observed in less inclined systems. In particular, we find that the box-shaped form of the galaxy can be explained as a projection effect of an outer ring, with a relatively large vertical scale, and a compact bulge seen edge-on. Our description of NGC 1381 corroborates previous suggestions that Burstein's thick disks may not be a distinct galactic component and that the box-shaped appearance displayed by some edge-on S0 and spiral galaxies can, at least in some cases, be explained by different kinds of effects (e.g. van der Kruit and Searle, 1981a, b; Jensen and Thuan, 1982; WH). It is clear of importance, for theories of galaxy formation and evolution, to know whether thick disks really exist since several processes, which may lead to their formation either at early times or as a consequence of stellar dynamical evolution, have been investigated. This question alone should motivate further studies of edge-on galaxies.

The data presented here seems to confirm the trend found in Paper I that the disks of S0's in dense regions are less luminous than in the general field, an effect that is consistent with the scenario envisioned by Larson et al. (1980) for the formation of lenticular galaxies. The observation that the disk of NGC 1381 might have an outer cuttof also supports this picture since in the case of S0's the disk edge may be an imprint of the sudden removal of the galaxy's reservoir, unless viscous effects or stellar diffusion processes can alter the disk distribution after the gas accretion has stopped. Similar cutoffs were not detected in the galaxies studied in Paper I but this is not surprising since as shown here the cutoffs probably occur at faint light levels and may go undetected for less inclined systems. Another possibility, mentioned earlier, is that the observed edge is not real and the disk extends beyond the ring. The non-existence of an outer edge, if confirmed, is also significant

since it reveals basic differences between the overall mass distribution of S0's and spirals.

The observed structure of the disk is also in general agreement, if the edge is real, with the predictions of the slow infall model discussed by Gunn (1981). In this picture disks should have a constant scale-height and should remain exponential over about 4 scale-lengths throughout their growth, consistent with the present observations. An interesting result worth mentioning is our finding that the surface brightness at the edge of the disk of NGC 1381 may be significantly ($\sim 1\,\mu_B$) brighter than normally observed in spirals (e.g. Kormendy 1982). If this result is shown to be a general property of S0's disks, it may have important implications for disk formation models since if disks grow self-similarly, as proposed by Gunn (1981), the distribution of the characteristic brightness at the edge should be approximately the same for S0's and spirals. In this context, the study of the structure of edge-on disk galaxies may be helpful in understanding the time-dependent evolution disks and may help to discriminate between the models of disk formation.

From the detailed analysis of the light distribution of NGC 1381 we were also able to study the vertical structure of the bar and outer ring. Our results confirm some well-known general properties of bars, namely, that they are very thin structures, with sharp edges and a very shallow brightness distribution along its long axis. In particular, we find that the bar in NGC 1381 has a major-diameter of ~ 13 kpc, a vertical axial ratio of the order of 0.05 and contributes with approximately 4.5 % of the total light of the galaxy. As discussed in detail by Kormendy (1981), the presence of a bar drives secular evolution processes that can significantly alter the structure of a galaxy. The observed structure of NGC 1381 illustrates well some of the possible consequences of this dynamical evolution, as evidenced by the presence of components like the outer ring, the box-shaped structure near the center and the possible lens, all believed to be associated with the bar phenomenon. In particular, we note that according to Schwarz (1981) the formation of an outer ring is a natural endpoint in the evolution of a barred galaxy without gas replenishment, giving further support to the description given in this paper for NGC 1381. In agreement with previous theoretical and observational results (e.g. Schwarz, 1981; Athanassoula et al., 1982) we find that the derived diameters for the outer ring and the bar are consistent with the interpretation that the bar ends near the corotation radius and that the outer ring is formed close to the outer Lindblad resonance. We also find that the vertical scale of the outer ring is comparable with the value obtained by WH in NGC 4762.

Another feature associated with the stellar dynamical evolution driven by the bar is the box-shaped structure observed near the center. Although is difficult to define the edges of this box precisely, we estimate from the figure 1d that it has an observed axial ratio of ~ 1.4, comparable to the theoretical value given by Pfenniger (1984). The diameter of the box is estimated from the behavior of the vertical profiles to be < 8 kpc (Sect. 3.1). The connection between box-shaped structures and bars has been demonstrated by the results of N-body simulations (e.g. Combes and Sanders, 1981) where box and peanut-shape morphologies are often observed during the evolution of a barred system. The experiments of Combes and Sanders (1981) are particularly interesting since they show that box-shaped structure can be formed exclusively by stars originally in the disk and the bar, partly justifying the argument given in Sect. 3.2. The origin of box-shaped features has also been investigated by numerical studies of the shape and stability properties of possible three-dimensional stellar orbits in barred galaxy models. These studies have shown the existences of a family of orbits that can give rise to structure with a rectangular aspect (e.g. Pfenniger, 1984) and with kinematic properties compatible with the cylindrical rotation observed in galaxies with box-shaped nucleus (e.g. Illingworth, 1983).

The structure of NGC 1381 described in this paper, reveals that this galaxy has a number of structural properties related to the bar phenomenon, being ideally suited for comparison with the results of theoretical investigations on the evolution of barred galaxies. It is therefore of great interest to complement, in the near future, the photometric data presented here with kinematic observations of this galaxy.

Acknowledgements. We would like to thank P.S. Pellegrini for several discussions, C. Willmer for his careful reading of the manuscript and C. Rite for his assistance.

References

Athanassoula, E., Bosma, A., Crézé, M., Schwarz, M.P.: 1982, *Astron. Astrophys.* **107**, 101

Athanassoula, E., Bosma, A.: 1985, *Ann. Rev. Astron. Astrophys.* **23**, 169

Barnes, J., White, S.D.M.: 1984, *Monthly Notices Roy. Astron. Soc.* **211**, 253

Binney, J.: 1981, *Monthly Notices Roy. Astron. Soc.* **196**, 455

Burstein, D.: 1979a, *Astrophys. J.* **234**, 435

Burstein, D.: 1979b, *Astrophys. J.* **234**, 829

Burstein, D.: 1979c, Photometry, Kinematics and Dynamics of Galaxies, Ed. D.S. Evans p. 81

Combes, F., Sanders, R.H.: 1981, *Astron. Astrophys.* **164**, 173

de Vaucouleurs, G.: 1968, *Appl. Optics* **7**, 1513

de Vaucouleurs, G., Buta, R.: 1980, *Astron. J.* **85**, 637

de Carvalho, R.R., da Costa, L.N., Pellegrini, P.S.: 1985, *Astron. Astrophys.* **149**, 449

Dressler, A.: 1980, *Astrophys. J.* **236**, 351

Freeman, K.C.: 1979, Photometry, Kinematic and Dynamics of Galaxies, Ed. D.S. Evans, p. 85

Gunn, J.E.: 1981, Proc. Study Week on Cosmology and Fundamental Physics, Pont. Acad. Scient., Scripta Varia 48, 233

Hamabe, M.: 1982, *Publ. Astron. Soc. Japan* **34**, 423

Illingworth, G.: 1983, in *Internal Kinematic and Dynamics of Galaxies, IAU Symp*, **100**, Reidel, Dordrecht, p. 266

Jensen, E.B., Thuan, T.X.: 1982, *Astrophys. J. Suppl.* **50**, 421

Jones, J.E., Jones, B.J.T.: 1980, *Monthly Notices Roy. Astron. Soc.* **191**, 685

Jones, B.J.T., Wise, R.F.G.: 1983, *Astron. Astrophys.* **120**, 165

Kent, S.M.: 1985, *Astrophys. J. Suppl.* **59**, 115

Kormendy, J.: 1977, *Astrophys. J.* **218**, 333

Kormendy, J.: 1979, *Astrophys. J.* **227**, 714

Kormendy, J.: 1981, The Structure and Evolution of Normal Galaxies, eds. S.M. Fall, Lynden-Bell, p. 85

Kormendy, J.: 1982, Morphology and Dynamics of Galaxies, 10th Advanced Course Swiss Society of Astronomy and Astrophysics, eds. L. Martinet, M. Mayor, p. 113

Kruit, P.C. van der, Searle, L.: 1981a, *Astron. Astrophys.* **95**, 105

Kruit, P.C. van der, Searle, L.: 1981b, *Astron. Astrophys.* **95**, 116

Kruit, P.C. van der, Searle, L.: 1982a, *Astron. Astrophys.* **110**, 61

Kruit, P.C. van der, Searle, L.: 1982b, *Astron. Astrophys.* **110**, 79

Larson, R.B., Tinsley, B.M., Caldwell, C.N.: 1980, *Astrophys. J.* **237**, 692

Llebaria, A., Figon, P.: 1981, Astronomical Photography 1981 Meeting of the IAU Working Group on Photographic Problems, eds. M.E. Sim, J.L. Heudier, p. 25

Monet, D.G., Richstone, D.O., Schechter, P.L.: 1981, *Astrophys. J.* **245**, 454

Pfenniger, D.: 1984, *Astron. Astrophys.* **134**, 373

Pfenniger, D.: 1985, *Astron. Astrophys.* **150**, 112

Sandage, A., Visvanathan, N.: 1978, *Astrophys. J.* **223**, 707

Sandage, A., Tammann, G.: 1981, A Revised Shapley-Ames Catalog of Bright Galaxies, Carnegie Institution of Washington (RSA)

Schwarz, M.P.: 1981, *Astrophys. J.* **247**, 77

Spitzer, L., Schwarzschild, M.: 1953, *Astrophys. J.* **118**, 106

Tsikoudi, V.: 1979, *Astrophys. J.* **234**, 842

Tsikoudi, V.: 1980, *Astrophys. J. Suppl.* **43**, 365

Wakamatsu, K., Hamabe, M.: 1984, *Astrophys. J. Suppl.* **56**, 283

IV- Fotometria Superficial de Galáxias Elípticas no Hemisfério Sul

As galáxias elípticas têm sido objeto de vários estudos cinemáticos e dinâmicos não só devido a sua importância para as teorias de formação de galáxias como também por serem os sistemas mais simples na sequência de Hubble. Recentemente, vários programas de fotometria foram realizados (e.g. Watanabe et al. 1982, Djorgovski 1985, Schombert 1986) acumulando uma quantidade apreciável de informação sobre estas galáxias. Complementando estes trabalhos, neste capítulo são apresentados os resultados de um levantamento fotométrico para 131 galáxias elípticas no hemisfério sul. Este levantamento foi feito utilizando o Atlas ESO (B) que, como visto no capítulo II, apresenta uma qualidade fotométrica adequada para a determinação dos principais parâmetros estruturais de galáxias. No caso específico de galáxias elípticas, alguns problemas foram verificados na região central relacionado aos problemas de não linearidade do material fotográfico. Mesmo assim, os dados fotométricos são confiáveis num domínio de aproximadamente 5 mag arcsec^{-2} e neste domínio sendo comparável às observações CCD. Comparações feitas com fotometria CCD mostram que os dados apresentados neste capítulo são adequados para uma descrição paramétrica das galáxias elípticas. Em particular, as magnitudes totais derivadas a partir dos ajustes de uma lei $r^{1/4}$ aos perfís ao longo do eixo-maior estão em acordo com medidas fotométricas publicadas por Burstein et al. (1987).

Neste capítulo são apresentados os perfís de brilho e os mapas isofotais das galáxias analisadas. Os perfís foram utilizados para determinar os parâmetros característicos de tamanho e brilho, ajustando a lei empírica

de de Vaucouleurs ao perfil de brilho ao longo do eixo-maior. Estes parâmetros são utilizados para determinar a magnitude total do objeto e várias correlações entre estas quantidades são examinadas. Da análise da distribuição de brilho bidimensional podem ser obtidas outras informações importantes, como a variação da elipticidade e do ângulo de posição em função do brilho isofotal. Estas informações serão usadas futuramente para investigar possíveis relações entre os parâmetros estruturais, parâmetros da forma, perfís de elipticidade, perfís de ângulo de posição e a densidade galáctica. Estas correlações representam uma ferramenta importante para a compreenssão da estrutura interna das galáxias elípticas e a possível influência que o meio ambiente pode exercer sobre a sua evolução.

Finalmente, os dados fotométricos obtidos, em conjunção com os dados espectroscópicos (vide capítulo V) são essenciais para a análise do "plano fundamental" e do campo de velocidade peculiar local feita mais adiante no capítulo VI.

SURFACE PHOTOMETRY OF SOUTHERN ELLIPTICAL GALAXIES

R. R. de Carvalho and L. N. da Costa

Departamento de Astronomia, CNPq/Observatorio Nacional

Rua General Bruce 586, Rio de Janeiro, Brasil

ABSTRACT

We present the results of a surface photometry survey for 131 elliptical galaxies in the southern hemisphere. In this paper we show isophotal maps and major-axis profiles, deriving for each galaxy in the sample structural parameters using the de Vaucouleurs law as an useful parametric descriptor of the light distribution of elliptical galaxies.

I. INTRODUCTION

The understanding of the structural and dynamical properties of elliptical galaxies is of fundamental importance for theories of galaxy formation, since these systems are structurally the simplest along the Hubble sequence. Unfortunately, despite considerable progress in the observations of the photometric and kinematic properties of these galaxies, some fundamental questions concerning their intrinsic shapes and origin remain unanswered and motivate further studies of these objects.

Over the years, several surface photometry programs of elliptical galaxies have been carried out and have provided a large body of information (e.g. Watanabe et al. 1982, Djorgovski 1985, Schombert 1986). These studies have revealed that although the brightness distribution of elliptical galaxies can approximately be described by the well-known $r^{1/4}$ law of de Vaucouleurs, in reality they exhibit a large variety of profile shapes. As mentioned by previous authors the light profiles show departures from the empirical law both at large and intermediate radial distances. Systematic studies of moderate samples have also revealed that isophotal twists are common, and have been interpreted as evidence for the triaxiality of elliptical galaxies (e. g. Williams and Schwarzschild 1979a, b; di Tullio 1979). Several statistical studies have attempted to find further clues about the intrinsic shape of ellipticals based, for instance, on correlations between isophotal twisting, ellipticity and characteristic surface brightness (e.g. Marchant and Olson 1979, Galleta 1980, Merrit 1982). However, as pointed out by Kormendy (1982) several

problems affect the interpretation of these observed correlations and larger samples are necessary to improve the statistics.

Considerable progress has also been achieved in dynamical studies of elliptical galaxies. Kinematic observations have shown that these systems are in general slow rotators and much of their flatness may be due to the anisotropy of their velocity distribution, giving further support to the idea that ellipticals may be triaxial. Measurements of the central velocity dispersion for a large sample of galaxies have also confirmed the original correlation between luminosity and velocity dispersion found by Faber and Jackson (1976). Attempts have also been made to explain the observed scatter in this relation in terms of a hidden parameter (Terlevich et al. 1981, Tonry and Davis 1981). Such an explanation has been recently found concurrently by Djorgovski and Davis (1987) and Burstein et al. (1987) showing that ellipticals form a two-parameter family. The scatter in the relations found by these authors is small, comparable to that of the Tully-Fisher relation for spirals, and has become an essential tool as a distance-scale indicator and as a probe of streaming motions (Dressler et al. 1987, Djorgovski and Davis 1987). However, several points should be examined, such as the uncertainties in the zero-points and the possible effects associated with the environment, before one can confidently use this relation as a reliable secondary-distance indicator to map out the nearby velocity field.

In the present paper we present the data of a surface photometry survey for 131 elliptical galaxies in the southern hemisphere. The main goal of

this project was to determine the necessary photometric parameters to supplement the kinematic measurements obtained as part of the Southern Sky Redshift Survey (SSRS, da Costa et al. 1987). In section II we describe the sample and present the details of the data reduction. In section III we show and discuss the characteristics of the surface brightness distribution and major-axis profiles. In this section we also derive the photometric parameters, obtained from $r^{1/4}$ law fits to the data, and compare them with previous determinations. Finally, in section IV we briefly review the main results of the present survey.

II. DATA REDUCTION

a) Measurements

The present surface photometry survey used the on-film copies of the ESO Quick Blue Survey, the photometric quality of which has been discussed previously by Sim (1981), de Carvalho et al. (1985) and de Carvalho and da Costa (1987). A total of 85 fields were used to cover all objects in our sample as well as calibrating galaxies used to establish the magnitude zero-point. Our galaxy list consists of two overlapping samples. Sample I consists of 86 galaxies classified by Lauberts (1982) as E and E-S0, south of $\delta = -17.5°$ and galactic latitude $|b| \geq 30°$. This sample includes galaxies with a diameter greater than the cutoff value adopted in the SSRS sample (da Costa et al. 1987). Sample II covers the same region but consists of galaxies with estimated B(0) magnitudes brighter than 14.5. The magnitudes were calculated on the basis of mean relations between diameters and magnitudes, derived for different morphological type groups (Pellegrini 1987). The basic information about the sample is presented in table I where we give: in column (1) the entry number; in column (2) the ESO identification number and the corresponding NGC or IC name, whenever available; in columns (3) and (4) 1950.0 coordinates; in column (5) the morphological type, as given by Lauberts (1982); in column (6) the estimated magnitude; in column (7) the heliocentric radial velocity; in column (8) the reference for the velocities; in column (9) the galaxies which are only in the magnitude-limited sample, indicated by the letter m. In the rest of the paper the velocities

were corrected to the centroid of the Local Group (Yahil et al. 1977) and for a dipole Virgocentric infall model (Huchra and Geller 1982). A Hubble constant of 50 km/s/Mpc is used throughout.

The raster scans were made utilizing the Observatorio Nacional (ON) microdensitometer PDS. 1010A, using an aperture of 20 x 20 microns (1.4"). For each object we have digitized a square area with a side four times the diameter of the galaxy as estimated from the visual inspection of the object, comparable to the values for the major-diameter given by Lauberts (1982). The area of the scans were sufficiently large to allow an adequate background sky determination. Typical scan sizes were 200 x 200 pixels, the largest being 500 x 500 pixels. For the smallest galaxies we adopted a fix scan size of 100 x 100 pixels.

In order to linearize the specular density measurements we have used a mean characteristic curve derived from all the available sensitometric spots in different fields, following the procedure described by de Carvalho et al (1985). The analytical function adopted for the characteristic curve was that proposed by the Llebaria and Figon (1981). However, the value used for the saturation density was set to a high value because its measurement is very uncertain, due to adjacency effects (c.f. Barrows and Wolfe 1971), and could severely affect the intensity distribution in the central regions of galaxies saturated or near saturation. On the other hand, it is important to have an objective indicator where in the galaxy the non-linear effects at high-density may become important and for that purpose we have defined for every galaxy

a characteristic radius r_{sat}. This quantity was defined to be the radius at which the measured density reaches the value where the appropriate Llebaria and Figon fit departs from the quasi-linear approximation described above. The former is a fit of the characteristic curve obtained using the saturation density actually measured on the film. As will be discussed below, we discard all points within r_{sat}.

The determination of the sky contribution was made analyzing the density distribution of pixels within a strip near the outer edge of the scan area, with a width of 10% of the scan size. To eliminate bright sources we have adopted an asymmetric clipping algorithm similar to that of Ratnatunga and Newell (1984) and used the mean value of the resulting distribution as the sky level. Several tests were made to evaluate the systematic variations of the sky over areas similar to those used in the object scans. These tests showed that the maximum variation was smaller than the rms value associated with the fluctuations in the sky density, justifying our assumption of a constant sky contribution. The standard deviation of the final sky density distribution was used to compute for each galaxy the limiting isophotal level not significantly affected by the sky subtraction, which corresponds to $\mu_B \approx$ 25.2 mag arcsec^{-2}.

b) Calibration

The calibration of our data were made utilizing all the photoelectric

measurements available in the compilation made by Lauberts and Sadler (1984) and Lauberts (1987). We have also used the new measurements of Burstein et al. (1987) to calibrate six additional galaxies (see discussion below). In order to avoid saturation problems our calibration was made simulating annular apertures. Thus only galaxies having photoelectric measurements for more than two apertures and located in an adequate radial interval, were used for this purpose. A total of 80 fields had galaxies satisfying this condition, implying that most galaxies could be adequately calibrated. For the remaining 5 galaxies, in 5 distinct fields, a tentative calibration was made using the mean value of $\mu_B = 22.96$ quoted as the typical value of the sky brightness at the La Silla site (ESO Users Manual 1983). This value is very close to the mean value of $\mu_B = 22.98$ determined from the distribution of sky brightness for all the fields with calibrating galaxies. Although this calibration should be verified in the future they can be used as a first approximation. We note that the standard deviation of the sky brightness distribution is of the order of 0.21 mag arcsec^{-2}, which gives an idea of the error in the zero-point in this kind of calibration.

The accuracy of the calibration based on annular apertures was established using two fields containing several galaxies, of different morphological types, that had photoelectric data available. These fields are 358 and 443 which have 10 and 6 galaxies, respectively. Comparison of the calibration constant derived for each galaxy in the same field indicates that our zero-point is accurate to about 0.15 mag. The accuracy of the overall zero-point was estimated from the standard

deviation of the differences in the calibration constants computed for all the fields with calibration galaxies, which yields a value of 0.19 mag, comparable to the value determined from galaxies in the same field (0.15 mag).

A good test of the accuracy of our zero-point determination is to compare the magnitudes within annular apertures obtained from the Burstein et al. (1987) data to those computed here for the galaxies calibrated using the various sources compiled by Lauberts and Sadler (1984) and Lauberts (1987). This comparison is interesting because we have found 67 galaxies in common with Burstein et al.'s homogeneous sample that can be used for this purpose, allowing us to compare a total of 87 independent measurements. In this procedure we selected only annular apertures in the brightness domain where our data is reliable and discarded those with superimposed stars. In figure 1 we show the histogram of the resulting magnitude differences, which yields a mean shift of 0.09 mag and a standard deviation of 0.27 mag, which are probably the best estimates of our systematic and random errors.

c) Comparison with other authors

The accuracy of our photometry can be best evaluated from a direct comparison between the brightness profiles obtained in the present work, as discussed in section III, with those available in the literature. From

those, the most reliable are the CCD observations and we have found fourteen galaxies for which these comparisons could be made. Figure 2 shows surface brightness profiles obtained subtracting from our major-axis profiles those listed by the different authors indicated in the figure caption. In comparing these profiles we have rebinned the data to match the different resolutions and shifted the profiles, to account for different color bands and possible zero-point differences. The shift was computed from the mean raw difference between the two brightness profiles beyond the radius r_{sat} defined above. We note that in the case of the galaxy IC 3370, the only object observed in the same color band as the one used here, the mean shift was of 0.11 mag, again indicating the accuracy of our magnitude zero-point. In general, the surface brightness difference profiles do not show any strong systematic departures like those presented by Djorgovski (1985) from the comparison of his CCD data and Watanabe's (1983) photographic profiles. There is, nevertheless, a trend for negative values near the center, which may be due to errors in the high-density part of the characteristic curve, although we only show points beyond r_{sat}. The worst case is the galaxy NGC 1426 which presents the largest deviation reaching 0.6 mag arcsec^{-2} near the center. It is important to note, however, that this galaxy exhibits the largest isophotal twisting in the comparison sample. Moreover, the methods used to derive the profiles are different; while ours is obtained along the major-axis, as determined at the isophotal level of μ_B = 25.0, Djorgovski's (1985) profile is determined using the method described, for instance, by Kent (1983). In general, we also observe positive differences at large radii which may be caused by systematic differences in the determination

of the sky level between the photographic and CCD data. This trend is particularly noticeable in the comparison between our profiles and those of Jedrzejewski (1987) with all showing this behavior in the brightness domain from 23 to 25 mag arcsec^{-2}.

Some galaxies show a very good agreement over the radial range of interest, especially the galaxies IC 3370, NGC 1407, NGC 1521, NGC 1549 and NGC 6909. In the case of IC 3370, the only problem is the large scatter observed in the outer parts of the galaxy. We point out that the brightness profile differences presented here are similar to the large variety observed by Djorgovski (1985) not only from his comparison with photographic data but also with other CCD measurements.

Finally, in order to determine the intrinsic error of our photometry we have fitted and subtracted low-order polynomials to the brightness difference profiles and computed the rms of the scatter, which with the exception of IC 3370 yields values smaller than 0.14 mag arcsec^{-2}, which is an estimate of the mean random error of our photometry.

All the above comparisons demonstrate that our photographic data is reliable, except in the central regions of the galaxies where difficulties associated to the photographic material become important. In section IIIb, we give further evidence of the quality of the data.

III. RESULTS

a) Brightness Distributions

The calibrated isophotal maps for all galaxies in our sample are shown in figure 3, ordered by their ESO identification number. In each panel we give the ESO name, the entry number of the galaxy in table I and the scale corresponding to 30 arcsec. In all maps we show isophotes in the range 19-25 mag arcsec^{-2}, in intervals of 0.5 mag arcsec^{-2}. There are several fields that present some sort of difficulty which can, at least in some cases, impair the analysis of the surface brightness distribution. The most frequent problems are contamination due to bright stars, background/foreground confusion and interacting galaxies. Some examples are: 107 G 4, 152 IG 32, 507 G 66, 510 G 54 and 577 G 9. Plate defects are also noticeable in the fields of the galaxies 233 G 32, 253 G 4, 341 G 15 and 471 G 26, but in most cases they can be circumvented to derive a brightness profile.

A preliminary inspection of these maps already suggests that our sample shows an enourmous variety of morphologies. For instance, several galaxies exhibit visible asymmetries in their outer parts like 342 G 39, 440 G 17 and 482 G 25. Others show considerable isophotal twists such as 148 G 16, 157 G 16, 343 G 4, 358 G 45 and 482 G 19. In fact, over 11% of the galaxies in our sample have twists larger than 20°. Significant variations of the ellipticity as a function of the isophotal

level are also detectable, with the ellipticity profiles showing the various forms previously discussed by di Tullio (1979). Also interesting are the galaxies with outer isophotes having a box-like shape, similar to the galaxy IC 3370 recently studied in detail by Jarvis (1987). Possible candidates of this class of objects are: 148 G 16, 235 G 72, 237 G 37, 286 G 49, 418 G 5, 445 G 46, 482 G 19, 508 G 38 and 576 G 35.

Although a quantitative analysis of the structural properties of these galaxies will be postponed to a future paper, we can already make some preliminary comments based on the isophotal maps. An interesting question that one can consider is whether isophotal twists have intrinsic causes, possibly associated with the triaxial shape of ellipticals, or is due to galaxy-galaxy encounters in pairs or dense regions. We can tentatively address this question considering the subset of galaxies in sample I with $b \leq -30^{\circ}$ and velocities less than 12000 km/s, which have been assigned to groups (Maia, da Costa and Latham 1987), for different density contrasts, following the prescription of Huchra and Geller (1982). Examining galaxies both "isolated" and in groups we find no dependence between the amount of observed twist and the environment, with galaxies having equal chance of showing large twists in low- and high-density regimes. This is not too surprising since tidal effects probably occur at fainter light levels than those reached with the present photometry. This preliminary result does nevertheless suggest that isophotal twists may reflect the nature of the internal structure of elliptical galaxies.

Another information that can be extracted from the isophotal maps is

the identification of interacting galaxies. There are at least 21 galaxies with superimposed images or with companions of comparable size in the same field of view. In five of these, the distortions present in the two-dimensional light distribution are in the form of tails that can be interpreted as resulting from the tidal interactions of physical pairs. These have been confirmed to form pairs since radial velocities are available for both galaxies in each system. These pairs are: 444 G45-444 G44 (not in this sample) with velocities 4317 km/s and 4376 km/s; 466 G 39 - 466 G 41 with velocities 2696 km/s and 2596 km/s; 533 G 20-533 G 21 with velocities 11612 km/s and 11620 km/s. Note that 466 G 39 has an enormous twist visible in the isophotal map.

Brightness profiles for the program galaxies were obtained along the major axis, defined at the isophotal level $\mu_B = 25.0$, by averaging the intensity of the two semi-major axes light profiles, except in cases where features occured in only one of the sides. Since one of the main purposes of the present survey was to derive photometric parameters (size and characteristic brightness) that could describe the structural properties of elliptical galaxies, we have fitted an $r^{1/4}$ law to the resulting major-axis profiles. We note that here we do not attach any special meaning to this law but use it simply to derive a characteristic length scale and surface brightness. In figure 4 we show, side by side, the observed profiles and corresponding fits (left panel), plotted as a function of $r^{1/4}$, and the residual brightness profile, obtained subtracting the fit from the observed profile. Once again the plots are ordered according to their ESO identification number. In these plots we show

only the data points beyond the radius r_{sat} calculated for each individual galaxy. We do not show a profile for 466 G 41 because it was not possible to define for this galaxy a major-axis profile due to its extremely peculiar shape. The profiles for all the other galaxies, in tabular form, are available upon request.

The parameters derived from these fits are listed in table II, which gives: in column 1 the identification of the galaxy; in column 2 the number of the galaxy in the sample; in columns 3 and 4 the surface brightness $B_o(V)$ and its formal error; in columns 5 and 6 the de Vaucouleurs radius r_o and the estimated error in arcsec; in column 7 the ellipticity, ε_o, derived by ellipse fitting at the isophotal level corresponding to $B_o(V)$; in column 8 the total apparent magnitude, calculated using the appropriate values of $B_o(V)$, r_o and ε_o; in column 9 the corresponding absolute magnitude, assuming their Hubble distances; in column 10 are indicated peculiar systems (13 galaxies), for which the deduced parameters are uncertain, galaxies without accurate zero-point determination (5 galaxies), galaxies with $r_o < r_{sat}$ (33 galaxies) and galaxies without measured velocities (4 galaxies), all in the Hydra-Centaurus region. In the table we do not include the galaxy 466 G 41 for which, as mentioned above, it was not possible to derive a light profile.

Examination of the profiles show that a large fraction of galaxies have brightness distributions which seem to be well represented by the de Vaucouleurs law over the entire brightness range considered. This can

best be seen by looking at the brightness profile differences which suggest that about 52% of the profiles fall into this class. In addition, there are apparently two other general categories of profiles: about 24% of them exhibit light excesses at large radii either localized (e.g. 107 G 4), or have profiles that deviate systematically above the fitting law (e.g. 467 G 54); about 12% show some indication of having truncated profiles which lie below the $r^{1/4}$ law for brightnesses fainter than approximately $\mu_B = 24.0$ (e.g. 480 G 28); the rest of the profiles are poorly described by the $r^{1/4}$ law either because of its overall curvature (e.g. 356 G 17) or because of relatively prominent features in the middle parts of the profiles (e.g. 286 G 57). We emphasize that the profiles shown here were obtained averaging the semi-major axis light distributions and any feature detected in the final profile should be real since they can only occur if they are recognized on both sides of the major-axis.

The great variety of forms observed in the light profiles make any attempt of classification extremely difficult and sometimes a very subjective task. However, this variety seems to confirm the complexity of ellipticals since profiles similar to ours have been observed in previous studies including the recent surveys of Djorgovski (1985), Schombert (1986) and Jedrzejewski (1987). Although it is difficult to look for any systematic behavior, several trends have emerged and are worth mentioning, even though on a preliminary basis.

In general, galaxies classified as E-S0 have profiles which lie above the fitting law starting at about $\mu_B = 23.0$-24.0. A rough estimate indicates

that approximately 60% of the E-S0 show this behavior, which is not surprising since it probably reflects the feature that led to their classification as E-S0 in the first place. An obvious interpretation is that the light excess may be associated to the presence of a disk component in these systems. In order to explore this possibility we have also examined all the profiles in μ x log(r) plots, since in this representation the profile should become linear at large radial distances, easing the task of identifying disks. The galaxies with suspected disks are: 235 G 21, 244 G 45, 298 G20, 440 G 37, 464 G 17, 467 G 37, 467 G 54, 509 G 20, 574 G 12 and 575 G13. Unfortunately, even examining the profiles as a function of log(r), it is not easy to find convincing evidence for a disk, probably because of our relative bright isophote limit, especially if the disks are faint. This might be expected since if the E-S0 class have disks they probably represent extreme cases of large bulge to disk light ratios, and at μ_B = 25.0 the disk would probably still not make the dominant contribution.

Another possible evidence for the inclusion of S0 galaxies in the E-S0 class comes from a more detailed inspection of the behavior of the light profiles, which in some cases are very similar to the major-axis profiles of S0's with underlying components like 244 G 45, 286 G 57 and 298 G 20 (see for instance Tsikoudi 1979, de Carvalho et al. 1985). They also show variations in the ellipticity and position angle profiles which give mild support to this interpretation.

There are also galaxies classified as E, which show light excesses in the

outer parts, reminiscent of the profiles first discussed by Kormendy (1977), who interpreted them as tidal distensions. In contrast to Kormendy we find no obvious relation between the galaxy profile and its environs, with light excesses occuring in "isolated" galaxies as well as in galaxies in high galactic density regions. However, we cannot make any conclusive statement due to the small number statistics. It may also be the case that true S0 galaxies could have been misclassified as ellipticals. Moreover, at the present time it is not known whether a clear distinction between these types can actually be made, i. e., they may very well form a continuous family.

As mentioned earlier, several E galaxies and curiously some E-S0, exhibit truncated profiles which drop sharply for brightnesses fainter than μ_B = 24.0. They apparently occur in all density regimes, thus showing no indication that they reflect tidal interaction. This result is not surprising since N-body experiments of Aguillar and White (1987) suggest that the effects associated with tidal forces can be detected only at very faint light levels.

b) Comments on the Photometric Parameters

In figure 5 we compare the photometric parameters obtained from our fits with those of previous studies, showing the distribution of points in the $B_o(V)$-$\log(r_e)$ plane, where r_e is the equivalent radius. In this figure we show 83 galaxies, excluding all objects marked in column 10 of table

II. In order to compare our points with the relation of Kormendy (1980), we have converted our parameter r_o to $r_e = r_o(1-\varepsilon_o)^{1/2}$ and $B_o(V)$ was corrected for galactic extinction (0.2 cosec(b)). A linear-square fit of our points gives

$$B_o(V) = 3.15\ (+/-0.27)\ \log\ (r_e)\ + 19.29\ (+/-\ 0.18)$$

in close agreement with the expression found by Kormendy (1980)

$$B_o(V) = 3.28\ \log\ (r_e) + 19.45$$

and reexamined by several authors for different types of ellipticals including cD's (e.g. Morbey and Morris 1983, Thomsen and Frandsen 1983, Malumuth and Kirshner 1985, Schombert 1986). Our points cover the entire range of sizes (1-40 kpc) and surface brightnesses (19-25 mag arcsec^{-2}), typical of normal ellipticals. Small galaxies, $r_e < 3$ Kpc, show a small departure from the mean relation, tending to be slightly brighter than expected. A similar trend seems to be also present in Schombert's data, although not as well-defined as observed here. At this point it is unclear whether this is real or reflect problems with our photographic data at high density. The scatter about the relation is large (0.72 mag arcsec^{-2}) but comparable for instance with that inferred from the figure presented by Schombert (1986). This value is considerably larger than 0.38 mag arcsec^{-2} cited by Kormendy (1977), but this may due to the size and the type of sample considered by him, which only includes normal ellipticals previously studied by King (1978). The scatter about the mean

relation can be significantly reduced discarding points 2σ away, which after two iterations and throwing out 8 galaxies becomes 0.44 mag arcsec^{-2}. We have also investigated the sensitivity of this relation to several factors like making separate fits for E and E-S0, applying K-dimming correction and using, for galaxies in groups, the centroid velocity of the group to estimate their distance. The resulting fits were always very similar and no improvement of the dispersion was achieved in these various cases.

Using the present data we have also examined the M_B-log(r_e) relation, shown in figure 6. We also plot our best fit line given by

$$-M_B = 1.85\ (+/-\ 0.27)\ \log\ (r_e) + 20.66\ (+/-\ 0.18)$$

with a dispersion of 0.74 mag. This relation corresponds to a luminosity-effective radius relation $L \propto r_e^{0.72}$, reproducing quite well previous determinations (e.g. Kormendy 1980, Romanishin 1986) for bright elliptical galaxies. As pointed out, for instance, by Schombert (1986), intrinsically faint galaxies such as those studied by Strom and Strom (1978 a,b,c) may not obey the same law. However, as can be seen by examining the luminosity function shown in figure 7 the galaxies in our sample are typically brighter than M_B= -20.0, showing that the sample considered here is consistent with those of Kormendy (1980) and Romanishin (1986).

These results show that the photometric parameters derived here

represent well the structural properties of ellipticals and can be used to describe the global properties of these galaxies. As mentioned earlier we consider the radius r_o (r_e) only as a characteristic scale length of the galaxy.

Another way of evaluating our results is to compare the total magnitudes calculated using the photometric parameters derived here with those published in previous work. This comparison has been done with the B_T magnitudes derived from photoelectric measurements of Sadler (1984) and Burstein et al. (1987). In our sample there are 27 galaxies in common with Sadler's data set, but 4 are excluded from the comparison because, as indicated in table II they do not have reliable parameters. In figure 8 we compare our magnitudes with the remaining 23 galaxies, showing in figure 8a a plot of B_T (present work) x B_T (Sadler) and in figure 8b the histogram of the magnitude differences. In figure 9 we show the same plots for 56 galaxies in common with Burstein et al. (1987) sample. Our total overlap is of 95 galaxies but 39 were eliminated because: some do not have B_T magnitudes available in Burstein et al.; some were used in the calibration of our galaxies; and others have $r_o < r_{sat}$. The galaxies common to both catalogs have magnitudes that cover fairly uniformly a range of approximately five magnitudes between B_T = 10.0 to 15.0. Examination of the figures shows that despite the scatter, in both cases there are no systematic departures in zero-point or as a function of magnitude. In order to estimate the zero-point shift we eliminate galaxies that deviate more than 2σ from the mean of the raw distribution. In this case we find from the comparison with the Sadler sample that the

mean of the magnitude diferences is -0.08 mag and the rms magnitude difference is of 0.28 mag. This implies that our error is roughly 0.24 mag, since the quoted error for Sadler's B_T magnitudes is 0.15 mag. Adopting the same procedure to estimate the mean magnitude shift between our data and the Burstein et al. sample yields a mean shift of 0.09 mag and an rms of 0.17 mag, comparable to the error quoted by these authors for the accuracy of their measurements.

The results obtained above demonstrate two important points. First, it reinforces the quality of our photometry showing that there is no significant zero-point shift and that the random errors are comparable to those obtained in photoelectric work. Second, it shows that the structural parameters derived from the photographic data and based on $r^{1/4}$ law fits do, in fact, describe fairly well the global properties of the galaxies in our sample. The agreement is particularly impressive considering the problems asssociated with the high density regions near to the center of the images which prevents the direct calculation of the total magnitude that must, instead, be estimated from extrapolations of the $r^{1/4}$ law fits.

The present data set can also be used to calibrate the eye-measured diameters of the ESO catalog (Lauberts 1982). This question is important because of recent attempts to define a standard diameter system and appropriate conversion relations for the various galaxy catalogs like the ESO, UGC and MCG (e.g. Fouque and Paturel 1985). In view of the paucity of photometric data in the south, the use of

diameter-limited samples may be the only short-term possibility for creating a uniform whole-sky catalog (Sharp 1986). Three different methods were used to measure diameters: the first is based on the simple interpolation of the data points along the major-axis profile to determine the radial distance at which $\mu_B = 25.0$; the second determines the semi-major axis from an eye-fitted ellipse to the data points at the isophotal level $\mu_B = 25.0$; the third is a more accurate version of the second method using a more sophisticated ellipse-fitting routine (e.g. Cawson 1983). Comparison of the measurements made by the different methods show that they yield virtually identical results. Thus, in table III we give the values for the major diameter and axial ratio obtained using the eye-fitted ellipse method, which is less time consuming and sufficiently accurate for our purposes. In the table we present these quantities for 99 galaxies of our sample, avoiding those without accurate zero-point, disturbed and/or with very noisy outer isophotes. In figures 10 and 11 we compare our diameters and axial ratios with those listed by Lauberts (1982). In figure 10a we plot the logarithm of our diameter D_{our} versus the logarithm of the diameter D_{ESO}. In this figure we also show the least-square fit to the data points giving the relation

$$\log D_{our} = 0.998\ (+/-0.050)\ \log D_{ESO} - 0.117\ (+/-0.017)$$

for 99 points with a scatter of 0.22. This relation indicates that the ESO diameters are measured at a surface brightness fainter than $\mu_B = 25.0$, consistent with the conclusion reached by Lauberts (1982) from a comparison with diameters listed in the RC2 (de Vaucouleurs et al. 1976).

It also shows that there are no apparent systematic trends in Lauberts' measurements with his diameters following a linear relation with respect to the photometric diameters for galaxies with sizes in the range 1'-10'. This can best be seen in figure 10b where we plot $\Delta\log(D) = \log(D_{ESO}) - \log(D_{our})$ versus $\log(D_{our})$, which yields a mean shift of 0.12 and a dispersion of 0.10.

The fit obtained above is different from the conversion formula given by Fouque and Paturel (1985), in particular there seems to be no need to add a constant to the visual diameters as proposed by these authors to convert them to a photometric system. It is important to recall that they derived the conversion law for early-type galaxies in the ESO catalog from a very small number of objects.

In figure 11 we compare the axial ratios obtained here with those calculated from the ratio of the diameters given by Lauberts (1982).

The best least-square fit is

$$\log R_{our} = 0.619\ (+/-\ 0.045)\ \log R_{ESO} - 0.056\ (+/-\ 0.008)$$

with a dispersion of 0.048. The fit is shown as the solid line in figure 11a. The difference in the logarithm of R_{ESO} and R_{our} as a function of $\log R_{our}$ is shown in figure 11b, where we find no systematic trends and a dispersion of 0.06.

IV. CONCLUSIONS

In the present paper we have presented the data from a photographic surface photometry survey of nearby bright southern elliptical galaxies. Although the use of photographic material is inadequate to measure the light profiles near the center of the galaxies it provides, nevertheless, reliable data over a range of 4 to 5 mag arcsec^{-2} in brightness. Moreover, the larger field obtained with photographic material allows for better sky corrections, thus providing more reliable light profiles at faint light levels. In this sense the present survey may be useful even after CCD observations become available for the galaxies in the sample and should also be supplemented with data from the ESO/SRC (J) plates.

The present survey complements that recently completed in the northern hemisphere by Djorgovski (1985) and a comparison between the few objects in common provides evidence that it produces a fairly good parametric description of ellipticals. In particular, our parameters obey fairly well relations determined in earlier works, yielding total magnitudes in good agreement with published measurements. Here we have only presented a very sketchy discussion of the observed properties of the galaxies which will be used in forthcoming papers to investigate possible correlations between structural parameters, shape parameters, ellipticity profiles, position angle profiles, and galactic density. This kind of investigation may eventually lead to a better understanding of the internal structure of elliptical galaxies and the possible influence of the

environment in their evolution and present-day morphology. We also intend to use the present database, in conjunction with spectroscopic data available from the ongoing redshift survey of the southern sky, to determine the fundamental plane described by the ellipticals in our sample. Using this plane as a distance-scale indicator we intend to investigate the peculiar motions of the large scale structures observed in the southern hemisphere and the actual size of the large voids detected.

ACKNOWLEDGMENTS

We would like to thank C. Willmer for his careful reading of the manuscript and S. Djorgovski for useful discussions and for sending us a tape with his data for comparison.

Table I. Galaxy Sample

#	Name	Id	α_{1950}	δ_{1950}	Type	m	V (km/s)	ref	Notes
1	409 G 12		00 02 09	-30 45 42	E	13.80	7985	1	
2	409 G 25		00 08 49	-29 08 00	E	13.60	18475	2	
3	540 G 7	N 179	00 35 16	-18 07 30	E	14.00	6027	1	
4	151 G 6	N 312	00 54 04	-53 03 12	E	13.80	8026	1	
5	151 G 9	N 323	00 54 29	-53 14 48	E	14.20	7763	3	m
6	541 G 7		00 57 35	-21 45 30	E-S0	13.90	16805	1	
7	541 G 13		01 00 15	-22 09 00	E-S0	13.30	17073	1	
8	243 G 33	I 1625	01 05 29	-47 10 24	E-S0	13.40	6714	1	
9	412 G 18	N 439	01 11 27	-32 00 42	E-S0	13.10	5803	1	
10	542 G 13		01 24 45	-18 54 48	E-S0	14.20	9744	1	m
11	244 G 42	N 641	01 36 31	-42 46 48	E	13.10	6397	1	
12	244 G 45		01 36 54	-46 49 42	E-S0	14.10	6633	3	m
13	477 G 4	I 1729	01 45 37	-27 08 24	E-S0	13.00	1495	2	
14	152 IG 32	N 745	01 52 24	-56 56 06	E+E	14.30	6079	3	m
15	298 G 9	N 822	02 04 36	-41 23 42	E	14.30	5395	1	m
16	298 G 20	N 862	02 11 02	-42 16 00	E-S0	14.30	5337	1	m
17	416 G 19	N 1097A	02 44 02	-30 26 18	E	14.10	1327	1	m
18	416 G 31	I 1860	02 47 28	-31 23 48	E	13.00	6959	1	
19	356 G 17	I 1864	02 51 37	-34 24 00	E	14.10	4465	1	m
20	480 G 28	N 1201	03 01 58	-26 15 42	E	12.00	1671	1	
21	417 G 21		03 11 13	-31 50 18	E-S0	14.30	4121	1	m
22	358 G 6		03 25 20	-34 42 00	E	14.50	1237	4	m
23	418 G 4	N 1339	03 26 06	-32 27 30	E	12.80	1380	1	
24	418 G 5	N 1340	03 26 17	-31 14 24	E	11.70	1126	5	
25	358 G 27	N 1379	03 34 08	-35 36 18	E	12.50	1352	2	
26	482 G 19	N 1395	03 36 19	-23 11 24	E	11.60	1702	6	
27	358 G 45	N 1399	03 36 34	-35 36 42	E	11.30	1464	2	
28	358 G 46	N 1404	03 36 57	-35 45 18	E	11.60	1942	2	
29	482 G 25	N 1403	03 37 00	-22 33 00	E	12.90	4310	1	
30	548 G 62	N 1400	03 37 16	-18 51 00	E-S0	12.50	562	1	
31	548 G 67	N 1407	03 37 57	-18 44 30	E-S0:	11.20	1784	1	
32	301 G 23	N 1419	03 38 51	-37 40 18	E	14.50	1566	3	m
33	549 G 1	N 1426	03 40 38	-22 16 06	E	12.70	1443	1	
34	549 G 9	N 1439	03 42 39	-22 04 42	E	13.00	1670	6	
35	359 G 59		03 43 10	-36 07 42	E	14.30	1020	4	m

Table I- Continued

#	Name	Id	α_{1950}	δ_{1950}	Type	m	V (km/s)	ref	Notes
36	359 G 7	I 2006	03 52 36	-36 06 48	E-S0	12.70	1340	1	
37	83 G 11	N 1490	03 53 09	-66 09 48	E	14.50	5397	4	m
38	550 G 11	N 1521	04 06 08	-21 11 00	E	12.80	4232	1	
39	250 G 7	I 2035	04 07 28	-45 38 54	E	12.60	1503	1	m
40	420 G 12	N 1537	04 11 44	-31 46 18	E	12.00	1371	1	
41	157 G 16	N 1549	04 14 39	-55 42 54	E-S0	11.30	1238	3	
42	202 G 25	N 1595	04 26 56	-47 55 30	E	13.80	4723	3	m
43	484 G 28		04 27 57	-26 56 36	E-S0	14.50	4030	7	m
44	552 G 20		04 52 39	-18 11 36	E-S0	12.30	9415	1	
45	552 G 21	N 1692	04 53 14	-20 39 00	E	14.10	10602	6	m
46	552 G 52		04 59 52	-21 12 30	E-S0	13.70	4600	1	
47	253 G 4	N 1930	05 24 33	-46 46 18	E	13.30	4224	1	
48	16 G 5	N 2012	05 26 10	-79 53 42	E-S0	14.40	4770	7	m
49	569 G 33	I 2623	11 01 23	-19 49 24	E	14.50	3754	7	m
50	502 G 25	N 3585	11 10 50	-26 29 00	E	11.40	1373	2	
51	440 G 13	N 3904	11 46 41	-28 59 54	E	12.40	1496	8	
52	440 G 17	N 3923	11 48 30	-28 31 42	E	11.50	1788	6	
53	440 G 37		11 56 44	-28 37 36	E-S0	14.30	2080	1	m
54	440 IG 54	N 4105	12 04 06	-29 29 00	E-S0	11.80	1900	6	m
55	442 G 3		12 30 46	-31 05 06	E-S0	14.10	15572	1	m
56	574 G 12		12 33 47	-19 07 12	E-S0	14.50	6546	7	m
57	575 G 13		12 49 29	-21 35 42	E-S0	13.60	6955	2	
58	575 G 37	N 4830	12 54 48	-19 25 18	E	12.90	3353	2	
59	507 G 58	I 3927	12 55 30	-22 36 24	E	14.20			m
60	575 G 43		12 57 05	-21 54 24	E	12.80	6990	2	
61	443 G 24		12 58 17	-32 10 12	E	13.50	5104	1	
62	443 G 32	I 3986?	12 58 48	-32 01 12	E	13.50	4605	1	
63	507 G 66		12 58 58	-23 43 12	E	14.50			m
64	443 G 47	N 4936	13 01 32	-30 15 24	E	12.80	3269	6	
65	443 G 62	N 4955	13 03 21	-29 29 12	E-S0	12.90	3489	1	
66	508 G 13	I 4197	13 05 22	-23 31 48	E	13.40	2998	1	
67	508 G 18	N 4993	13 07 05	-23 07 06	E-S0	14.20	2944	1	m
68	443 G 87	N 5048	13 13 23	-28 08 48	E-S0	13.30	4434	1	
69	508 G 38	N 5061	13 15 20	-26 34 24	E	11.80	2041	2	
70	576 G 35	N 5087	13 17 43	-20 20 54	E	12.40	1832	6	

Table I- Continued

#	Name	Id	α_{1950}	δ_{1950}	Type	m	V (km/s)	ref	Notes
71	444 G 45	N 5153	13 25 07	-29 21 36	E	14.00	4317	1	
72	509 G 20	I 4255	13 25 14	-27 05 42	E-S0	14.20	10164	1	m
73	577 G 9		13 30 23	-22 20 36	E	13.90			
74	509 G 77	I 4293	13 33 15	-25 37 36	E-S0	13.10	4563	1	
75	445 G 4	N 5253	13 37 05	-31 23 30	E-S0	11.40	395	6	
76	445 G 46	I 4329	13 46 14	-30 02 54	E-S0	13.00	4487	9	
77	445 G 59		13 48 48	-30 14 30	E	14.50			m
78	445 G 67	N 5328	13 50 03	-28 14 30	E-S0	13.00	4776	10	
79	510 G 54		14 01 13	-25 58 30	E-S0	14.20	6094	1	m
80	511 G 21		14 15 21	-27 11 06	E	14.40	7746	1	m
81	580 G 39	N 5761	14 46 18	-20 10 12	E	13.60	4106	1	
82	339 G 32	N 6849	20 02 54	-40 20 30	E	13.90	6063	1	
83	233 G 32	N 6861	20 03 41	-48 30 54	E	12.50	2769	1	
84	233 G 39	N 6868	20 06 16	-48 31 36	E	12.20	2876	1	
85	462 G 15		20 20 11	-27 52 30	E	13.00	5827	7	
86	285 G 12	N 6909	20 24 07	-47 11 30	E	13.20	2753	1	
87	341 G 15	N 6958	20 45 30	-38 10 54	E	12.60	2627	1	
88	235 G 21	N 6987	20 54 42	-48 49 24	E-S0	14.50	5319	4	m
89	107 G 4		20 59 03	-67 22 42	E	13.20	3099	1	
90	464 G 17		20 59 58	-31 10 36	E-S0	14.30	11648	1	m
91	235 G 43	N 7002	21 00 17	-49 13 42	E	13.90	7520	1	
92	235 G 49		21 01 15	-48 23 18	E	13.80	4812	6	
93	286 G 49		21 03 24	-47 23 13	E	13.80	5163	6	
94	286 G 50		21 03 25	-42 45 24	E	13.90	2635	1	
95	286 G 57	N 7014	21 04 29	-47 22 48	E-S0	13.70	4860	1	
96	286 G 59		21 05 22	-43 41 18	E	14.40	9413	1	m
97	235 G 72	N 7029	21 08 26	-49 29 18	E	13.10	2795	3	
98	342 G 39	I 5105	21 21 12	-40 45 06	E-S0	13.00	5437	1	
99	599 G 16	I 1386	21 26 48	-21 24 54	E	13.60	10682	1	
100	343 G 4	N 7075	21 28 26	-38 50 18	E-S0	14.00	5487	1	
101	287 G 48	N 7097	21 37 04	-42 46 00	E	12.90	2682	1	
102	531 G 18		21 37 13	-22 39 06	E-S0	14.50	9648	1	m
103	236 G 40	N 7117	21 42 31	-48 39 06	E-S0	14.10	5689	3	m
104	236 G 45	N 7118	21 42 54	-48 35 06	E-S0	13.90	5168	1	
105	466 G 26		21 55 51	-28 42 24	E	13.90	6192	2	

Table I- Continued

#	Name	Id	α_{1950}	δ_{1950}	Type	m	V (km/s)	ref	Notes
106	237 G 26	N 7168	21 58 51	-51 59 00	E-S0	13.30	2760	4	
107	466 G 39	N 7173	21 59 09	-32 12 54	E	13.50	2696	1	
108	466 G 41	N 7176	21 59 14	-32 13 54	E	13.30	2596	1	m
109	601 G 6	N 7180	21 59 32	-20 47 18	E	13.80	1238	6	
110	404 G 26	I 5157	22 00 30	-35 11 00	E-S0	13.40	4443	1	
111	237 G 36	N 7196	22 02 42	-50 21 48	E	13.00	2900	3	
112	108 G 12	N 7192	22 03 09	-64 33 36	E	12.60	2952	3	
113	237 G 37	N 7200	22 03 57	-50 14 24	E-S0	14.10	2897	6	m
114	76 G 3	N 7216	22 08 44	-68 54 30	E	14.40	3459	1	m
115	467 G 37		22 13 25	-27 39 06	E-S0	14.00	5568	2	
116	533 G 20		22 19 46	-23 46 36	E-S0	14.10	11612	1	m
117	533 G 21		22 19 47	-23 46 06	E-S0	14.10	11620	1	m
118	467 G 54		22 22 00	-31 34 48	E-S0	14.00	8288	1	
119	534 G 2		22 33 43	-24 36 06	E	14.40	10215	1	m
120	603 G 10	N 7365	22 42 28	-20 12 54	E	13.00	3050	1	
121	346 G 10	N 7404	22 51 29	-39 34 54	E-S0	13.20	1899	1	
122	406 G 30	I 1459	22 54 23	-36 43 48	E	11.40	1628	1	
123	469 G 19	N 7507	23 09 26	-28 48 48	E-S0	11.70	1548	1	
124	148 G 16	N 7676	23 26 12	-59 59 36	E	14.30	3398	1	m
125	291 G 29	I 5328	23 30 35	-45 17 36	E	12.40	3136	1	
126	471 G 14	I 5350	23 44 39	-28 14 06	E	14.40	8424	7	m
127	471 G 17	I 5353	23 44 53	-28 23 12	E-S0	14.50	8218	2	
128	408 G 37		23 47 21	-35 45 24	E-S0	13.90	12782	1	
129	471 G 26	I 5362	23 49 01	-28 38 30	E-S0	14.10	8221	1	m
130	471 G 45		23 53 49	-31 37 54	E	14.10	8563	1	m
131	149 G 7	N 7796	23 56 25	-55 44 06	E	12.70	3252	1	

Notes to table I

1 - da Costa et al. (1987)
2 - Menzies et al. (1987)
3 - Davis (1987)
4 - Sadler (1984)
5 - Richter and Sadler (1985)
6 - Lauberts (1982)
7 - Burstein et al. (1987)
8 - Huchtmeier and Richter (1986)
9 - Richter (1984)
10- Huchra (1984)

Table II. Photometric Parameters for Galaxies in the present sample

Name	#	$B_o(V)$	+/-	r_o (arcsec)	+/-	ε_o	m	$-M_B$	Notes
16 G 5	48	21.99	.38	9.70	1.48	.50	14.43	20.35	
76 G 3	114	22.33	.18	11.44	.92	.31	14.07	20.05	2
83 G 11	37	21.93	.18	10.70	.79	.16	13.60	21.46	2
107 G 4	89	20.12	.24	6.09	.57	.07	12.90	20.93	
108 G 12	112	21.57	.25	14.36	1.48	.06	12.48	21.23	
148 G 16	124	20.91	.22	8.52	.70	.42	13.47	20.54	
149 G 7	131	22.24	.16	18.77	1.41	.16	12.69	21.23	
151 G 6	4	20.46	.27	5.41	.57	.24	13.72	22.23	
151 G 9	5	19.29	.30	3.29	.35	.14	13.49	22.46	3
152 IG 32	14	20.33	.25	5.37	.50	.29	13.68	21.65	1
157 G 16	41	23.18	.14	62.08	4.84	.14	11.00	20.64	
202 G 25	42	18.93	.32	3.72	.41	.10	12.82	21.95	3
233 G 32	83	19.73	.15	10.68	.61	.48	11.92	21.71	
233 G 39	84	21.95	.20	26.23	2.48	.20	11.72	21.99	
235 G 21	88	21.57	.14	8.48	.54	.05	13.61	21.45	
235 G 43	91	22.35	.22	12.38	1.18	.17	13.71	22.12	
235 G 49	92	19.84	.21	4.69	.34	.23	13.39	21.45	3
235 G 72	97	20.22	.25	10.59	.97	.42	12.31	21.31	
236 G 40	103	21.14	.26	7.55	.76	.34	13.83	21.38	
236 G 45	104	22.78	.21	15.57	1.49	.15	13.62	21.37	
237 G 26	106	20.26	.35	8.02	1.17	.23	12.65	20.93	
237 G 36	111	19.78	.20	8.06	.56	.30	12.26	21.43	
237 G 37	113	18.60	.21	3.11	.20	.40	13.32	20.37	3
243 G 33	8	23.17	.22	19.17	2.13	.30	13.77	21.78	
244 G 42	11	20.96	.17	7.44	.52	.05	13.28	22.16	
244 G 45	12	21.86	.24	9.86	1.01	.20	13.76	21.77	
250 G 7	39	13.67	.55	1.16	.14	.30	10.36	21.78	3
253 G 4	47	21.89	.33	13.89	2.13	.22	13.07	21.45	
285 G 12	86	21.47	.19	15.19	1.18	.50	12.94	20.68	
286 G 49	93	20.17	.26	5.71	.57	.18	13.23	21.77	
286 G 50	94	20.02	.24	7.08	.60	.46	13.06	20.53	
286 G 57	95	20.04	.38	5.79	.78	.34	13.30	21.56	
286 G 59	96	20.56	.21	5.94	.48	.52	14.11	22.22	
287 G 48	101	20.69	.19	11.22	.87	.34	12.52	21.03	
291 G 29	125	22.04	.19	23.42	2.20	.22	12.09	21.76	

Table II- Continued

Name	#	B_o(V)	+/-	r_o (arcsec)	+/-	ε_o	m	$-M_B$	Notes
298 G 9	14	20.54	.35	5.35	.67	.32	13.94	21.12	
298 G 20	16	19.80	.43	3.57	.51	.02	13.68	21.35	3
301 G 23	32	16.86	.32	1.64	.15	.02	12.43	19.82	3
339 G 32	82	22.34	.18	14.72	1.23	.34	13.58	21.80	1
341 G 15	87	19.88	.15	8.05	.44	.22	12.25	21.29	
342 G 39	98	21.65	.30	15.95	2.13	.30	12.65	22.47	
343 G 4	100	22.27	.25	10.37	1.15	.11	13.94	21.20	
346 G 10	121	23.54	.24	28.30	3.52	.50	13.66	19.09	
356 G 17	19	18.94	.31	4.03	.41	.20	12.78	21.86	3
358 G 6	22	16.01	.43	1.98	.22	.64	12.26	19.46	3
358 G 27	25	21.14	.15	15.37	.89	.02	11.85	20.16	
358 G 45	27	22.02	.12	40.48	2.25	.08	10.70	21.34	
358 G 46	28	19.93	.18	14.09	.95	.11	10.94	21.80	
358 G 59	35	18.14	.27	2.31	.20	.58	13.89	17.38	3
359 G 7	36	23.55	.18	26.98	2.52	.13	13.17	18.73	
404 G 26	110	20.99	.23	7.63	.64	.03	13.23	21.44	
406 G 30	122	20.30	.16	22.31	1.39	.33	10.62	21.95	
408 G 37	128	19.89	.25	2.91	.25	.22	14.46	22.53	
409 G 12	1	18.76	.30	2.68	.26	.32	13.66	22.30	3
409 G 25	2	24.53	.28	19.96	3.25	.33	15.09	22.72	1
412 G 18	9	23.12	.13	28.74	2.01	.28	12.81	22.43	
416 G 19	17	14.65	.79	1.03	.19	.48	11.92	19.98	3
416 G 31	18	22.90	.22	17.93	1.95	.27	13.60	22.05	
417 G 21	21	17.61	.56	1.86	.31	.41	13.46	21.01	3
418 G 4	23	21.87	.18	17.99	1.45	.34	12.67	19.39	
418 G 5	24	21.22	.21	27.50	2.38	.35	11.12	20.41	
420 G 12	40	21.72	.14	22.85	1.41	.50	12.30	19.68	1
440 G 13	51	20.49	.17	16.56	1.09	.29	11.39	21.36	
440 G 17	52	21.84	.11	50.34	2.68	.41	10.53	22.43	
440 G 37	53	19.42	.27	3.04	.29	.03	13.66	19.58	
440 IG 54	54	21.35	.14	23.37	1.50	.27	11.47	21.60	1
442 G 3	55	19.20	.33	1.74	.18	.31	15.02	22.44	3
443 G 24	61	19.56	.21	7.06	.56	.32	12.36	22.70	
443 G 32	62	17.35	.44	3.10	.44	.29	11.89	22.95	3
443 G 47	64	20.67	.14	19.01	1.10	.15	11.08	23.09	

Table II- Continued

Name	#	$B_o(V)$	+/-	r_o (arcsec)	+/-	ε_o	m	$-M_B$	Notes
443 G 62	65	20.45	.34	9.63	1.35	.20	12.40	21.88	
443 G 87	68	17.16	.30	2.76	.25	.34	12.03	22.74	3
444 G 45	71	21.07	.22	7.69	.70	.19	13.49	21.22	1
445 G 4	75	20.20	.12	25.35	1.18	.61	10.83	16.62	
445 G 46	76	22.83	.21	27.35	3.00	.35	12.74	22.00	
445 G 59	77	20.75	.30	6.17	.70	.16	13.61		4
445 G 67	78	19.82	.25	7.14	.68	.41	12.75	22.20	
462 G 15	85	22.90	.19	22.86	1.96	.34	13.18	22.12	
464 G 17	90	22.69	.35	10.30	1.73	.41	14.82	21.99	
466 G 26	105	19.60	.24	4.62	.40	.19	13.13	22.29	1 3
466 G 39	107	18.60	.33	3.43	.40	.11	12.67	20.90	1 3
467 G 37	115	18.98	.36	3.90	.45	.40	13.20	21.98	3
467 G 54	118	20.02	.37	3.60	.47	.33	14.30	21.75	
469 G 19	123	20.59	.15	14.47	.82	.07	11.49	20.92	
471 G 14	126	18.60	.22	1.91	.14	.19	14.05	22.03	3
471 G 17	127	22.89	.30	14.02	1.95	.06	13.85	22.18	
471 G 26	129	20.87	.23	5.88	.55	.04	13.69	22.34	
471 G 45	130	20.18	.27	4.00	.39	.11	13.92	22.19	
477 G 4	13	20.95	.19	8.87	.68	.46	13.50	18.69	
480 G 28	20	23.53	.13	71.72	5.17	.50	11.63	20.82	
482 G 19	26	18.16	.18	12.24	.70	.25	9.66	22.85	1 3
482 G 25	29	15.46	.49	1.67	.22	.22	11.24	23.35	1 3
484 G 28	43	18.97	.35	2.79	.31	.25	13.68	20.76	3
502 G 25	50	21.44	.14	34.33	2.09	.30	10.77	21.62	
507 G 58	59	21.26	.20	7.06	.56	.20	13.88		4
507 G 66	63	23.70	.33	13.43	2.03	.40	15.24		4
508 G 13	66	21.00	.25	9.22	.87	.27	13.14	20.85	
508 G 18	67	20.26	.16	6.13	.35	.11	13.07	20.89	
508 G 38	69	21.19	.19	20.28	1.58	.16	11.47	21.78	
509 G 20	72	20.33	.35	3.88	.48	.36	14.49	22.05	
509 G 77	74	22.22	.24	11.14	1.23	.26	13.94	20.91	
510 G 54	79	20.10	.32	4.31	.46	.26	13.88	21.57	3
511 G 21	80	19.88	.34	3.37	.39	.20	14.11	21.85	2 3
531 G 18	102	19.58	1.25	2.07	.82	.12	14.76	21.64	2 3
533 G 20	116	18.37	.69	1.09	.22	.23	15.09	21.71	3

Table II- Continued

Name	#	$B_o(V)$	+/-	r_o (arcsec)	+/-	ε_o	m	$-M_B$	Notes
533 G 21	117	16.56	.61	.83	.14	.06	13.66	23.15	1 3
534 G 2	119	20.69	.32	3.68	.46	.25	14.80	21.72	1 3
540 G 7	3	20.12	.36	3.69	.44	.40	14.46	20.88	3
541 G 7	6	22.11	.26	6.46	.68	.14	14.85	22.76	
541 G 13	7	23.76	.26	15.55	1.81	.35	14.89	22.75	1
542 G 13	10	22.12	.22	7.97	.82	.18	14.45	21.95	2
548 G 62	30	21.86	.16	21.81	1.65	.24	12.09	18.00	
548 G 67	31	22.57	.14	47.83	3.50	.03	10.83	21.81	
549 G 1	33	20.15	.21	10.70	.80	.39	12.16	20.01	
549 G 9	34	22.18	.19	22.18	1.93	.08	12.17	20.31	
550 G 11	38	22.58	.14	27.75	1.78	.34	12.44	22.12	
552 G 20	44	24.98	.15	59.82	5.59	.44	13.35	22.98	
552 G 21	45	23.63	.28	15.55	2.20	.10	14.41	22.18	
552 G 52	46	20.67	.29	4.80	.52	.07	13.97	20.78	
569 G 33	49	15.71	.97	.94	.25	.37	12.97	21.46	3
574 G 12	56	21.75	.39	6.66	1.08	.05	14.31	21.30	
575 G 13	57	22.05	.16	9.19	.68	.17	14.06	21.68	
575 G 37	58	20.96	.20	11.32	.88	.30	12.70	21.54	
575 G 43	60	21.63	.24	8.89	.88	.44	14.14	21.61	
576 G 35	70	18.57	.24	6.44	.48	.38	11.67	21.44	3
577 G 9	73	22.31	.25	9.07	.99	.26	14.47		4
580 G 39	81	21.71	.22	8.85	.78	.09	13.70	20.94	
599 G 16	99	21.85	.37	8.15	1.19	.23	14.20	22.42	
601 G 6	109	17.14	.49	2.98	.44	.58	16.49	15.48	3
603 G 10	120	22.41	.29	13.68	1.79	.21	13.61	20.26	

1- Peculiar objects

2- No aperture photometry available

3- $r_o < r_{sat}$

4- No radial velocity available

Table III. Diameters and Axial Ratios for E Galaxies

Name	log D_{25}	log R_{25}	Name	log D_{25}	log R_{25}	Name	log D_{25}	log R_{25}
16 G 5	.01	-.23	342 G 39	.33	-.24	471 G 14	-.16	-.10
107 G 4	.16	-.08	343 G 4	.01	-.13	471 G 45	-.09	-.11
108 G 12	.21	-.02	346 G 10	.13	-.23	477 G 4	.14	-.26
148 G 16	.14	-.23	356 G 17	.05	-.22	480 G 28	.45	-.23
149 G 7	.28	-.06	358 G 6	.06	-.28	484 G 28	-.12	-.18
151 G 6	.09	-.13	358 G 27	.34	-.03	502 G 25	.62	-.23
151 G 9	-.05	-.02	358 G 45	.62	-.04	507 G 58	.01	-.09
157 G 16	.52	-.05	358 G 46	.45	-.05	507 G 66	-.12	-.14
202 G 25	.10	-.18	358 G 59	-.10	-.07	508 G 13	.12	-.22
233 G 32	.49	-.15	359 G 7	.15	-.07	508 G 18	.07	-.06
233 G 39	.54	-.08	404 G 26	.07	-.06	508 G 38	.41	-.09
235 G 21	.11	-.09	406 G 30	.63	-.14	509 G 20	-.11	-.15
235 G 43	.11	-.10	412 G 18	.36	-.20	509 G 77	.12	-.21
235 G 49	.04	-.16	416 G 19	-.11	-.26	540 G 7	-.14	-.06
235 G 72	.35	-.26	416 G 31	.16	-.16	541 G 7	-.17	-.09
236 G 40	.04	-.19	417 G 21	-.10	-.20	548 G 62	.35	-.09
236 G 45	.06	-.09	418 G 4	.21	-.15	548 G 67	.60	-.04
237 G 26	.23	-.11	418 G 5	.57	-.22	549 G 1	.34	-.18
237 G 36	.34	-.15	440 G 13	.43	-.14	549 G 9	.33	-.02
243 G 33	.14	-.15	440 G 17	.74	-.19	550 G 11	.38	-.21
244 G 42	.11	-.04	443 G 24	.22	-.08	552 G 20	.23	-.26
244 G 45	.01	-.07	443 G 32	.18	-.12	552 G 52	-.06	-.15
250 G 7	.05	-.09	443 G 47	.53	-.09	569 G 33	-.13	-.18
285 G 12	.28	-.31	443 G 62	.26	-.15	574 G 12	-.08	-.09
286 G 49	.04	-.33	443 G 87	.18	-.24	575 G 13	-.03	-.06
286 G 50	.13	-.31	445 G 4	.65	-.37	575 G 37	.22	-.17
286 G 57	.13	-.07	445 G 46	.38	-.23	575 G 43	.12	-.15
286 G 59	.05	-.25	445 G 59	.04	-.20	576 G 35	.33	-.10
287 G 48	.23	-.15	445 G 67	.22	-.14	577 G 9	-.10	-.16
291 G 29	.35	-.19	462 G 15	.21	-.09	580 G 39	.02	-.10
298 G 20	-.09	-.03	464 G 17	-.07	-.22	599 G 16	-.02	-.10
301 G 23	-.03	-.03	467 G 54	-.03	-.22	601 G 6	.08	-.32
341 G 15	.27	-.12	469 G 19	.37	-.01	603 G 10	.10	-.22

REFERENCES

Aguilar, L. A., and White, S. D. M. 1986, Ap. J. 307, 97

Barrows, R. S., and Wolfe, R. N. 1971, Photogr. Sci. Eng. 15, 472

Burstein, D., Davies, R. L., Dressler, A., Faber, S. M., Stone, R. P. S., Lynden-Bell, D., Terlevich, R. J., and Wegner, G. 1987, Ap. J. Suppl., 64, 601

Cawson, M. 1983, Ocass. Rep. Royal Obs. Edinburgh 10, 175

da Costa, L. N., Pellegrini, P. S., Sargent, W. L. W., Tonry, J., Davis, M., Meiksin, A., and Latham, D. 1987, Ap. J. in press

da Costa, L. N., Pellegrini, P. S., Willmer, C., de Carvalho, R., Maia, M., Latham, D., and Geary, J. 1988, in preparation

Davis, M. 1987, private communication

de Carvalho, R. R., da Costa, L. N., and Pellegrini, P. S. 1985, Astr. Ap. 149, 449

de Carvalho, R. R., and da Costa, L. N. 1987, Astr. Ap. 171, 66

de Vaucouleurs, G., de Vaucouleurs, A., and Corwin, H. C. 1976, Second Reference Catalogue of Bright Galaxies, University of Texas Press (RC2)

di Tullio, G. A. 1979, Astr. Ap. Suppl. 37, 591

Djorgovski, S. 1985, Ph.D. Thesis, University of California, Berkeley.

Djorgovski, S., and Davis, M. 1987, Ap. J. 313, 59

Dressler, A., Faber, S. M., Burstein, D., Davies, R. L., Lynden-Bell, D., Terlevich, R. J., and Wegner, G. 1987, Ap. J. (Letters) 313, 37

Faber, S. M., and Jackson, R. E. 1976, Ap. J. 204, 668

Fouque, P., and Paturel, G. 1985, Astr. Ap. 150, 192

Galleta, G. 1980, Astr. Ap. 81, 179

Huchra, J. P., and Geller, M. J. 1982, Ap. J. 257, 423

Huchra, J. P. 1984, private communication

Huchtmeier, W. K., and Richter, O. G. 1986, Astr. Ap. Suppl. 64, 111

Jarvis, B. 1987, Preprint

Jedrzejewski, R. I. 1987, Mon. Not. R. Astr. Soc. 226, 747

Kent, S. 1983, Ap. J. 266, 562

King, I. R. 1978, Ap. J. 222, 1

Kormendy, J. 1977, Ap. J. 218, 333

Kormendy, J. 1980, Proc. ESO Workshop on Two-dimensional Photometry, eds. P. Crane and K. Kjar (Leiden: Sterrenacht Leiden), p. 191

Kormendy, J. 1982, Morphology and Dynamics of Galaxies, 10th Advanced Course Swiss Society of Astronomy and Astrophyssics, eds. L. Martinet, M. Mayor, p. 113

Lauberts, A. 1982, The ESO/Uppsala Survey of the ESO(B) Atlas, European Southern Observatory

Lauberts, A., and Sadler, E. 1984, ESO-Scientific Report, 3

Lauberts, A. 1987, Astr. Ap. Suppl. 68, 215

Llebaria, A., and Figon, P. 1981, Astronomical Photography 1981 Meeting of the IAU Working Group on Photographic Problems, eds. M. E. Sim and J. L. Heudier, p. 25

Maia, M., da Costa, L. N., and Latham, D. 1987, in preparation

Malumuth, E. M., and Kirshner, R. P. 1985, Ap. J. 291, 8

Marchant, A. B., and Olson, D. W. 1979, Ap. J. (Letters), 230, 157

Menzies, J. W., Coulson, I. M., and Sargent, W. L. W. 1987, preprint

Merrit, D. 1982, A. J. 87, 1279

Morbey, C., and Morris, S. 1983, Ap. J. 274, 502

Oemler, A. 1976, Ap. J. 209, 693

Pellegrini, P. S. 1987, private communication

Ratnatunga, K. U., and Newell, E. B. 1984, A. J. 89, 176

Richter, O. G. 1984, Astr. Ap. Suppl. 58, 131

Richter, O. G., and Sadler, E. M. 1985, Astr. Ap. Suppl. 59, 433

Romanishin, W. 1986, A. J. 91, 76

Sadler, E. M. 1984, A. J. 89, 23

Sadler, E. M. 1984, A. J., 89, 34

Schombert, J. M. 1986, Ap. J. 60, 603

Sharp, N. A. 1986, Publ. Astron. Soc. Pacific 98, 740

Sim, M. E. 1981, Astronomical Photography 1981 Meeting of the IAU Working Group on Photographic Problems, eds. M. E. Sim and J. L. Heudier, p. 179

Strom, K. M., and Strom, S. E. 1978a, A. J. 83, 73

Strom, S. E., and Strom, K. M. 1978b, A. J. 83, 732

Strom, K. M., and Strom, S. E. 1978c, A. J. 83, 1293

Thomsen, B., and Frandsen, S. 1983, A. J. 88, 789

Terlevich, R., Davies, R. L., Faber, S. M., and Burstein, D. 1981, Mon. Not. R. Astr. Soc. 196, 381

Tonry, J., and Davis, M. 1981, Ap. J. 246, 680

Tsikoudi, V. 1979, Ap. J. 234, 842

Watanabe, M., Kodaira, K., and Okamura, S. 1982, Ap. J. Suppl. 50, 1

Watanabe, M. 1983, Ann. Tokyo Astron. Obs. 19, 121

Williams, T. B., and Scwarzschild, M. 1979a, Ap. J. 227, 56

Williams, T. B., and Scwarzschild, M. 1979b, Ap. J. Suppl. 41, 209

Yahil, A., Tammann, G. A., and Sandage, A. 1977, Ap. J. 217, 903

Figure Captions

Figure 1 - Histogram of the differences in annular aperture magnitudes between our photographic data and the Burstein et al. (1987) photometric measurements.

Figure 2 - Surface brightness difference profiles obtained subtracting from our major-axis light distributions those obtained by other authors (Williams and Schwarzschild 1979a, Djorgovski 1985, Jarvis 1987, Jedrzejewski 1987). A mean value is also subtracted to account for possible overall zero-point differences and different color bands used by the various authors.

Figure 3 - Calibrated isophotal maps for the program galaxies from 19 to 25 mag arcsec^{-2}, in intervals of 0.5 mag arcsec^{-2}. The maps have north down and east at the left. In each panel we give the ESO identification number, the entry number in table I and in the upper-left corner the scale corresponding to 30 arcsec.

Figure 4 - Major-axis light profile and the corresponding de Vaucouleurs fit (left panel). Also shown (right panel) is the residual light distribution resulting from the subtraction of the observed profile from the $r^{1/4}$ law. The identification of the galaxies is given as in figure 3.

Figure 5 - Structural parameters derived from the $r^{1/4}$ law fits presented in the $B_o(V)$ x log r_e plane. The solid line represents the least-square fit to our data points (full square), as discussed in the text. For comparison we also show the points for the compact elliptical galaxies (open circle) and the cD galaxies (open triangle) investigated by Kormendy (1977) and Oemler (1976), respectively.

Figure 6 - The $-M_B$ x log re relation for the program galaxies. Also shown is the best fit line for our data points.

Figure 7 - The luminosity function in the B band for the galaxies in our sample.

Figure 8 - Comparison of our total magnitudes with those of Sadler (1984) showing in panel (a) the B_T (Sadler) x B_T (our) plot and in panel (b) the histogram of the magnitude differences.

Figure 9 - Same as in figure 8 for galaxies in common with the Burstein et al. (1987) sample.

Figure 10 - Comparison of the visual diameters given by Lauberts (1982) with the isophotal diameters measured here at μ_B = 25.0. In panel (a) we show the comparison of the logarithm of the diameters, with the solid line representing the best fit

line to the data points. In panel (b) we plot the difference between the logarithm of the visual and isophotal diameters versus the logarithm of the isophotal diameter.

Figure 11 - Same as figure 10 for the comparison of the visual and isophotal axial ratios.

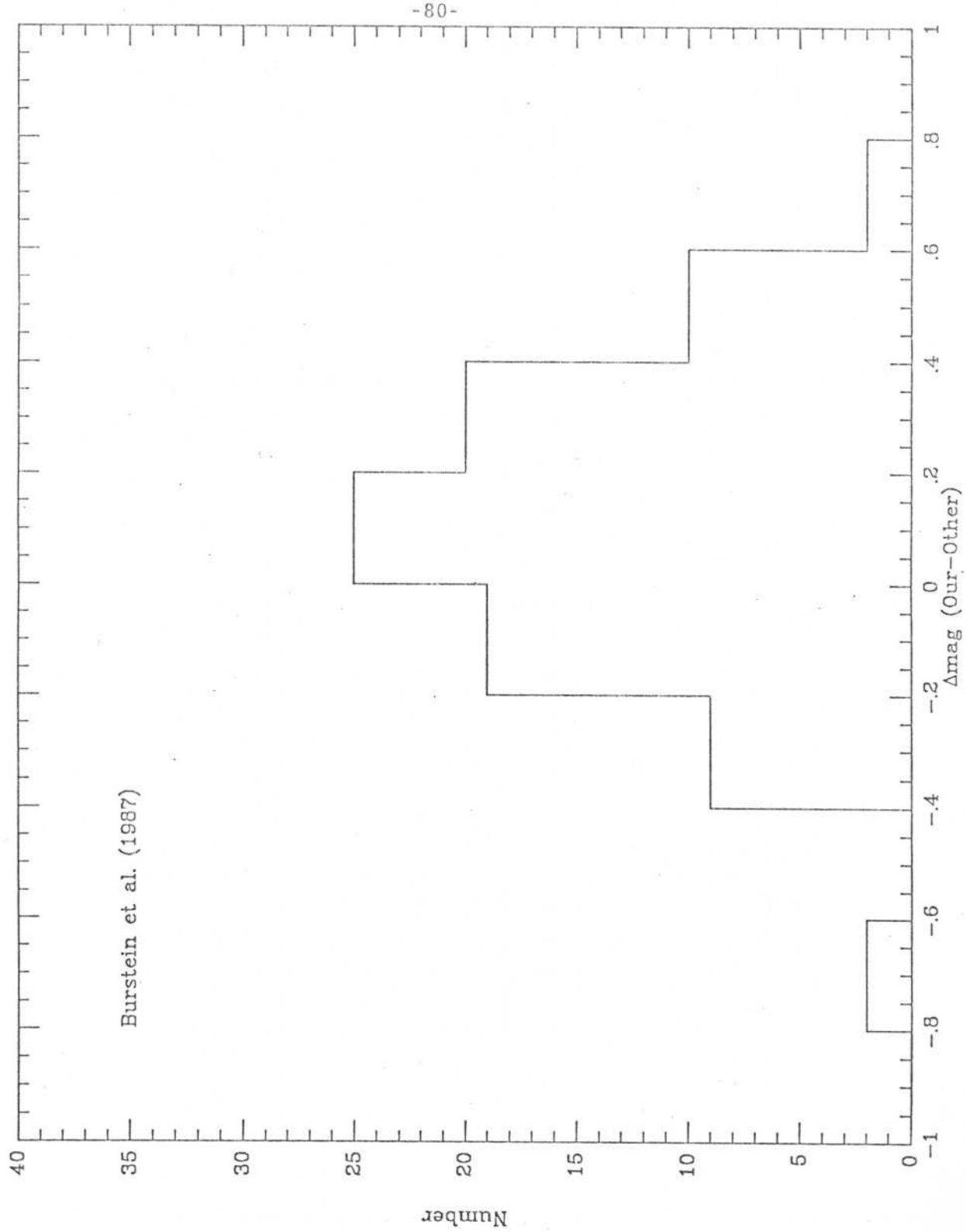
Burstein et al. (1987)
Number
40
35
30
25
20
15
10
5
0
-1
-.8
-.6
-.4
-.2
0
.2
.4
.6
.8
1
Δmag (Our-Other)

Fig.1

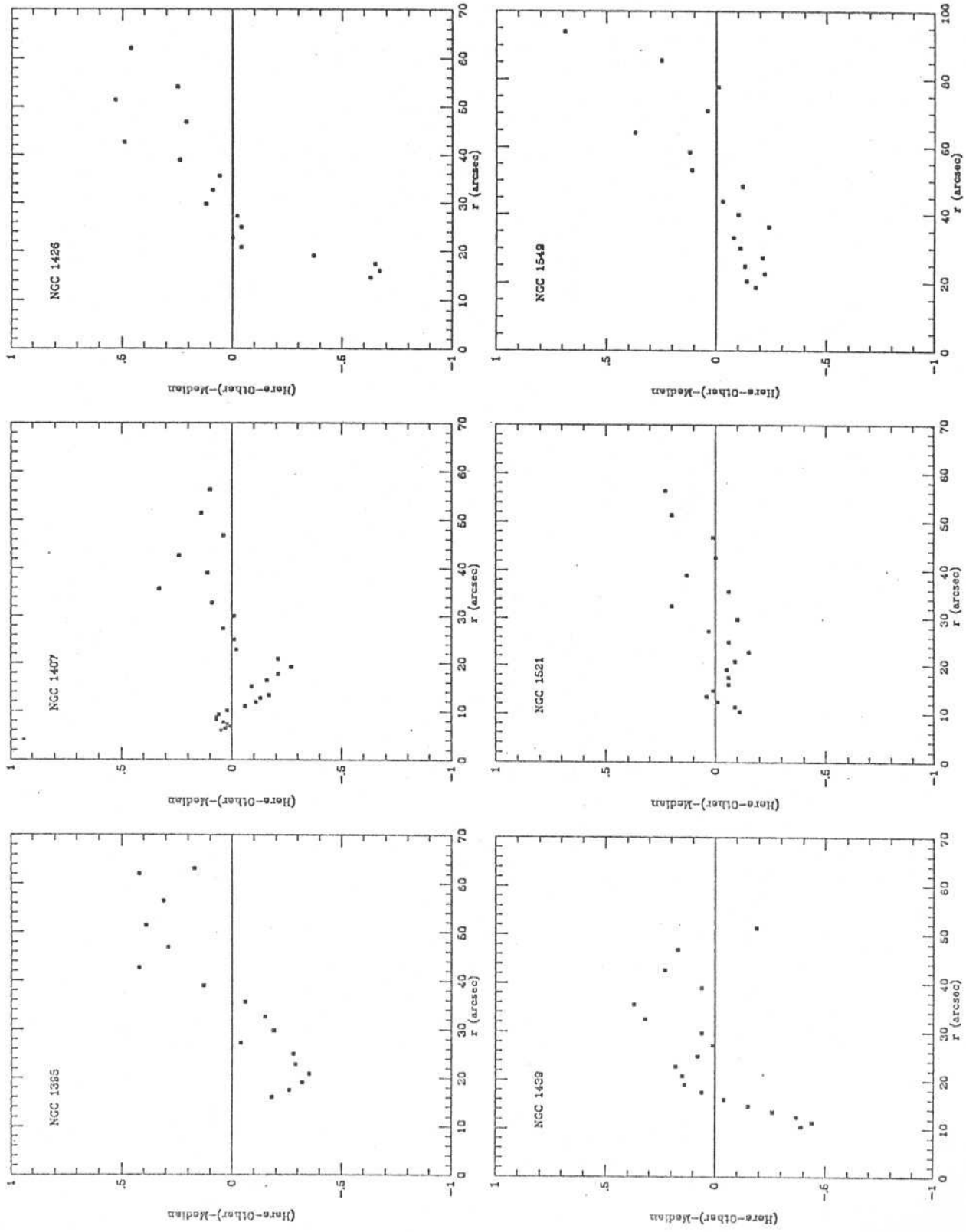
NGC 1426
NGC 1549
NGC 1407
NGC 1521
NGC 1365
NGC 1439
(Hera-Other)-Medlan
r (arcsec)

Fig.2

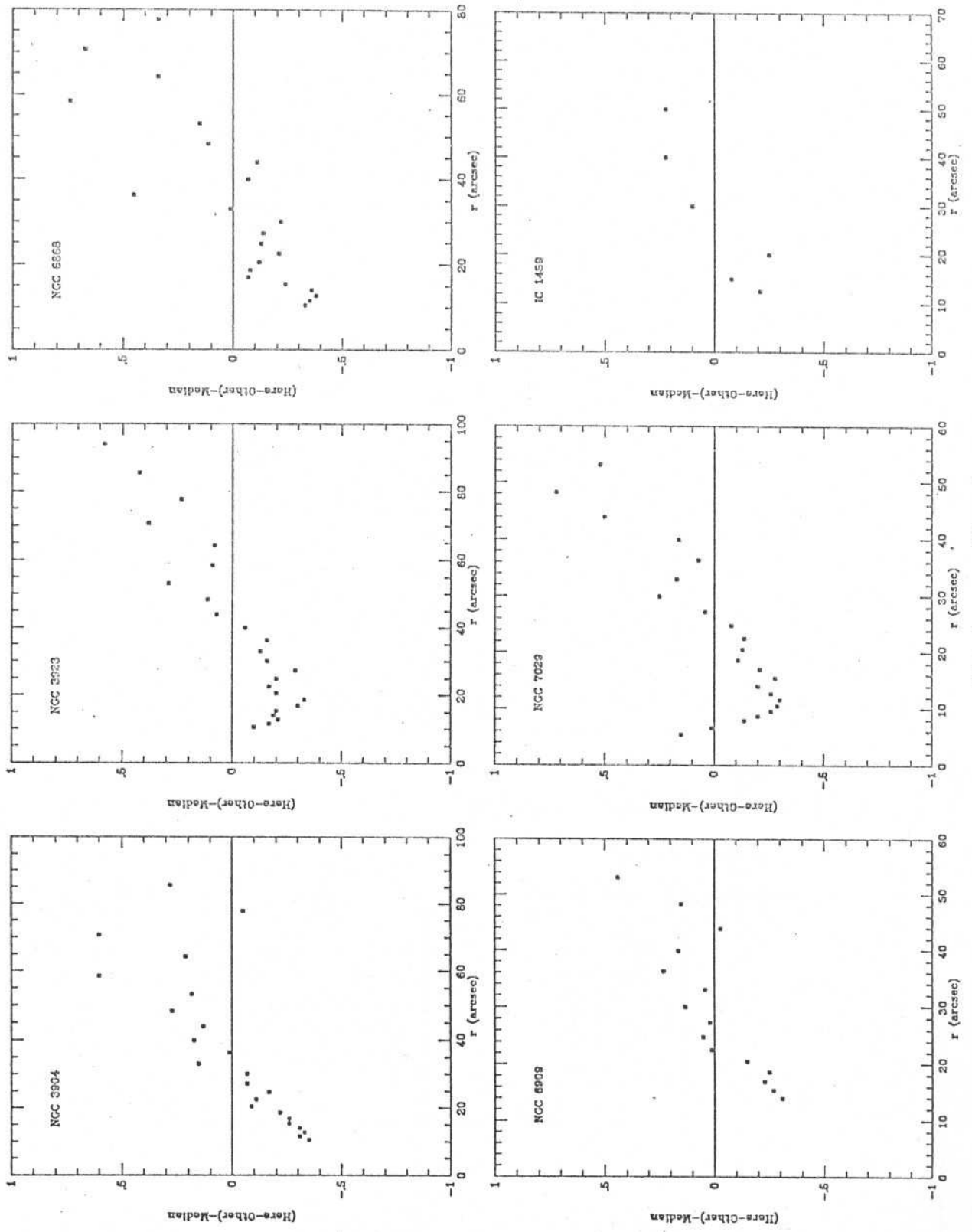

Fig.2 - continued

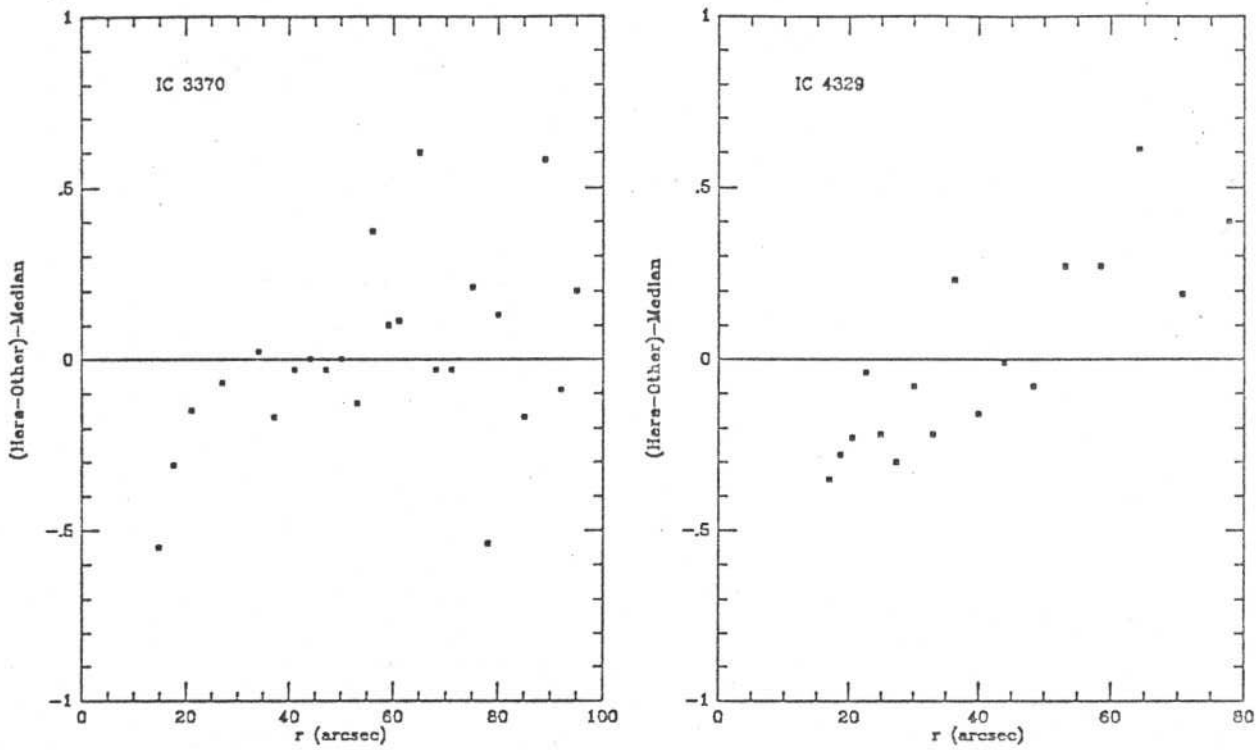

Fig.2 - continued

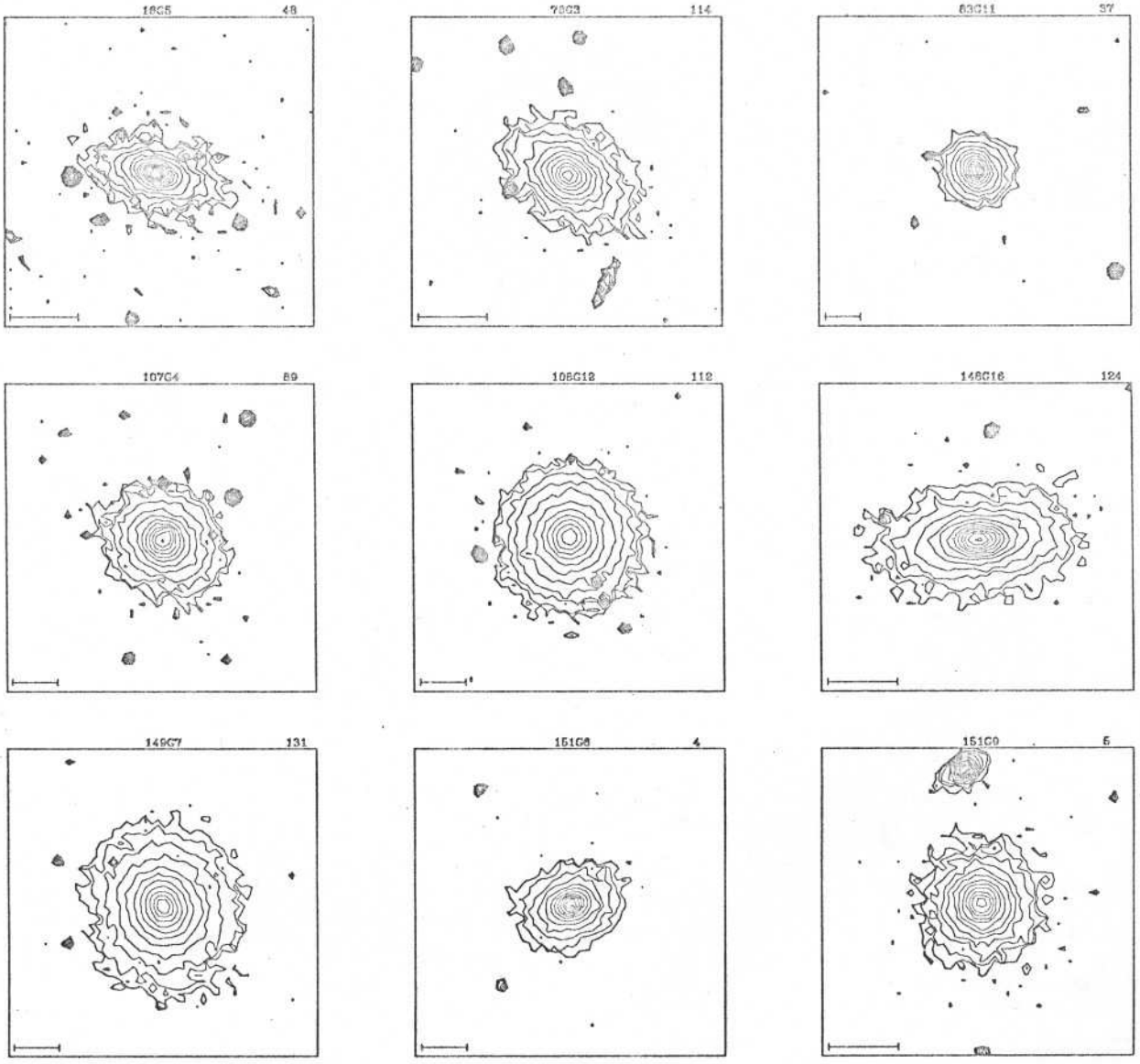
18G5
48
70G3
114
83G11
37
107G4
89
108G12
112
148G16
124
149G7
131
151G8
4
151G9
5

Fig. 3

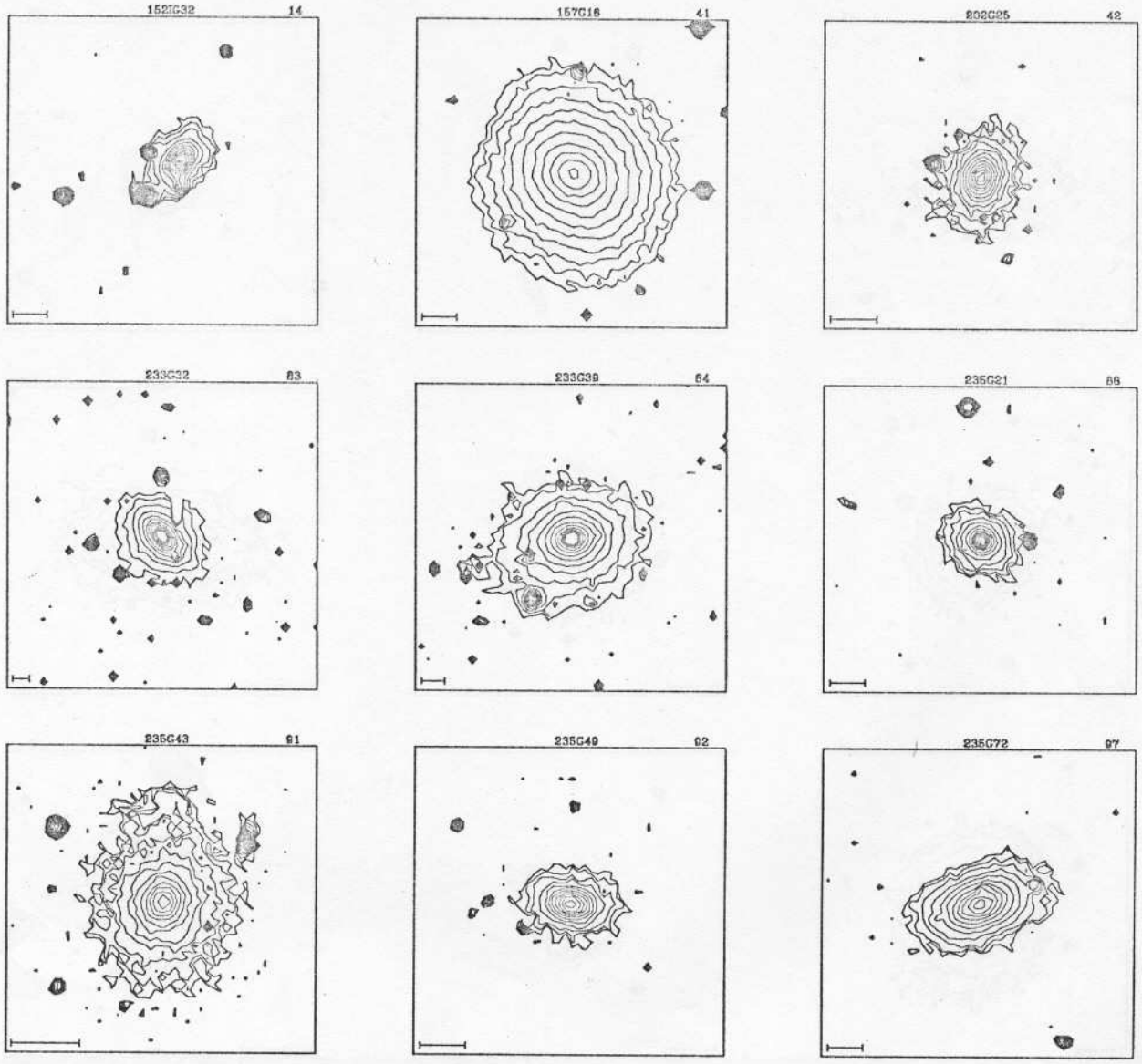

Fig.3 - continued

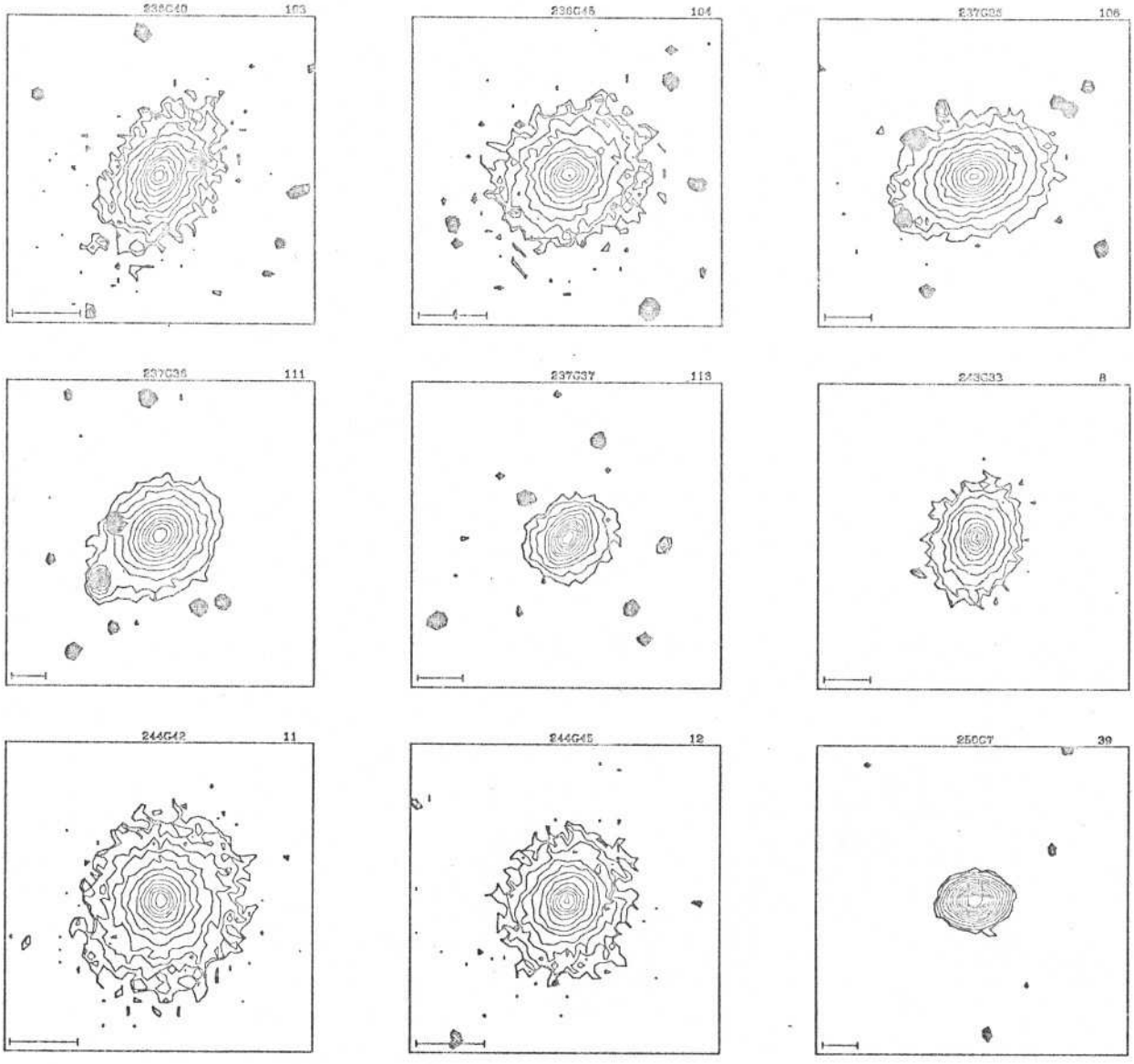

Fig.3 - continued

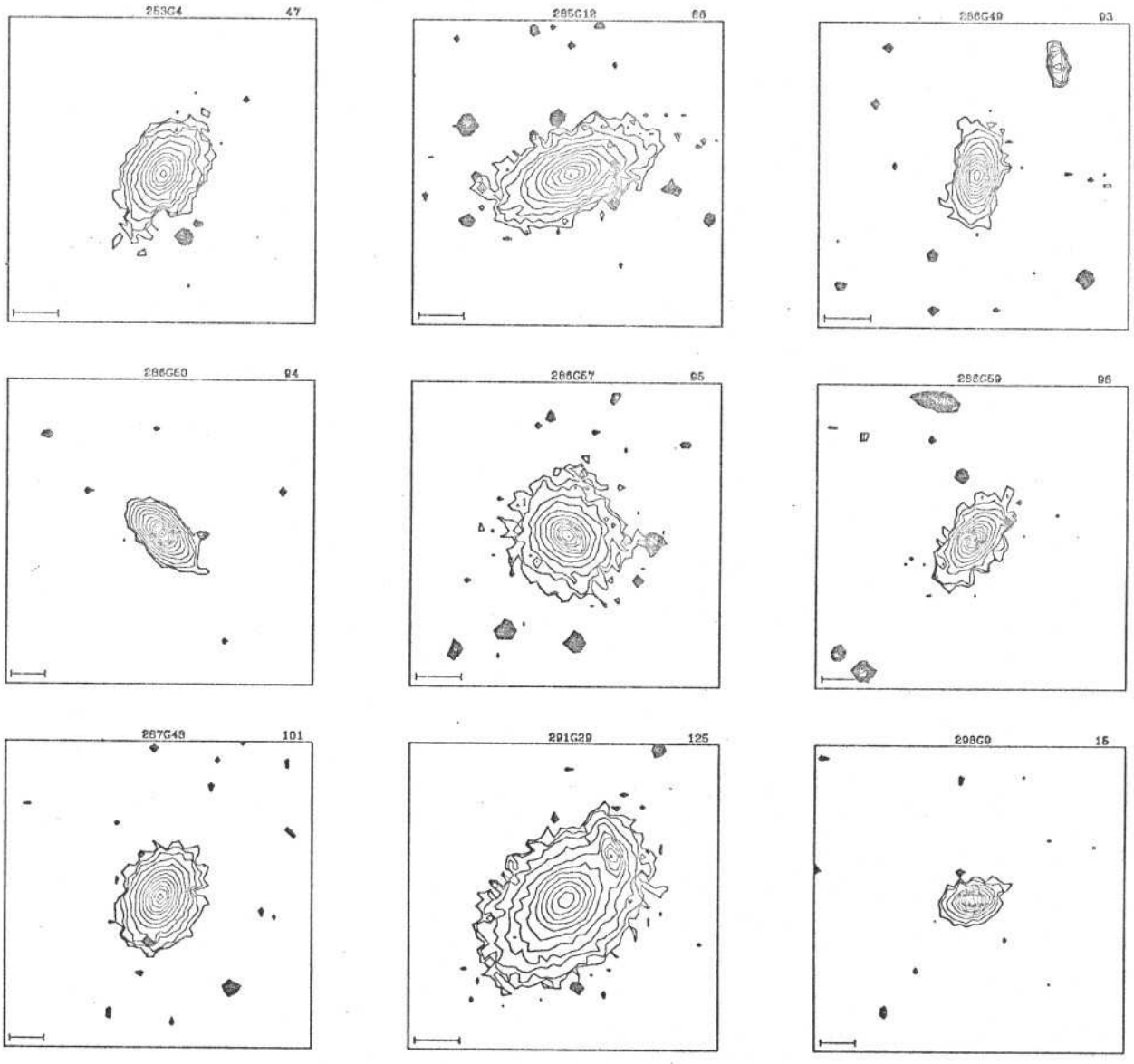

Fig.3 - continued

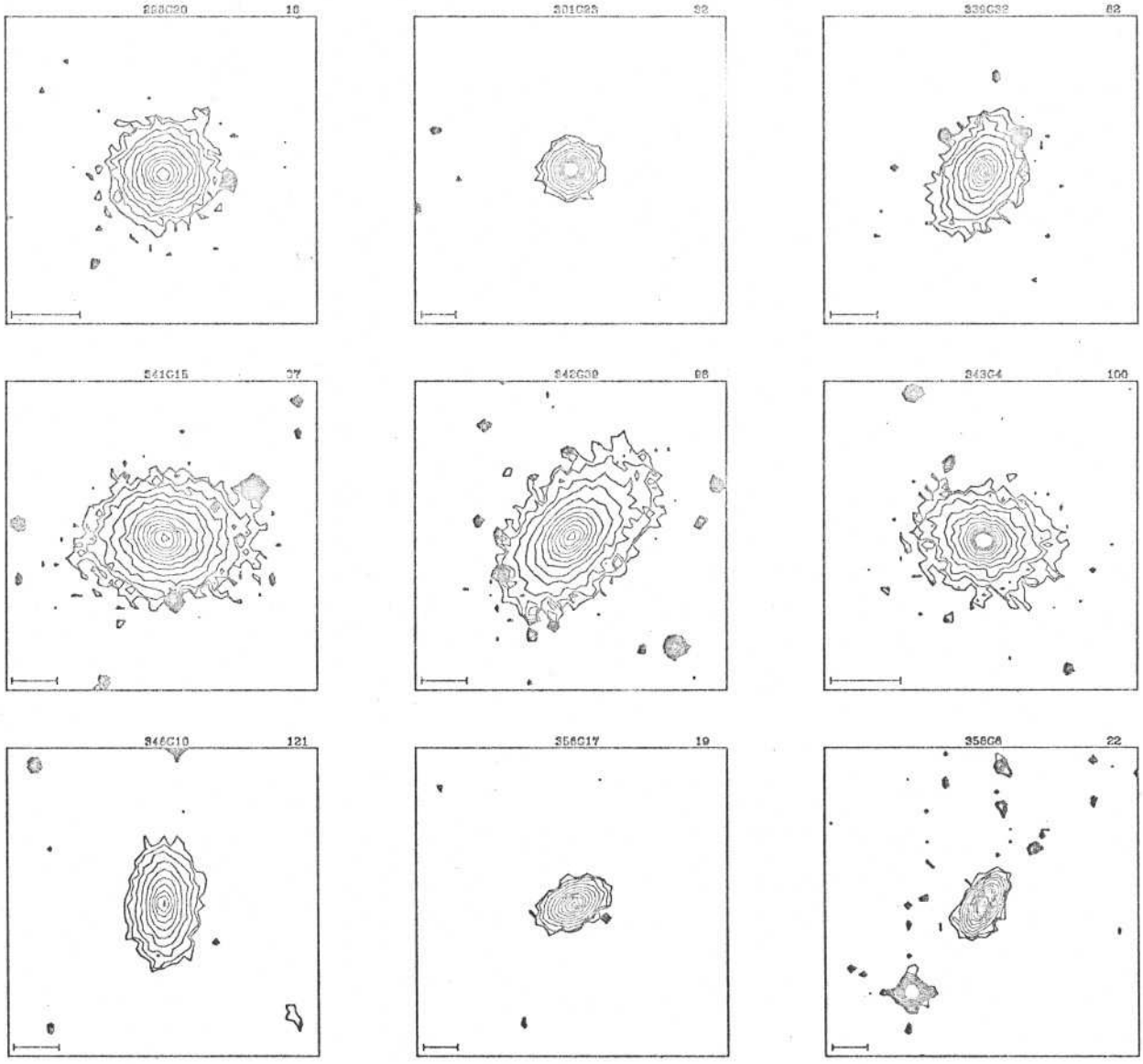

Fig.3 - continued

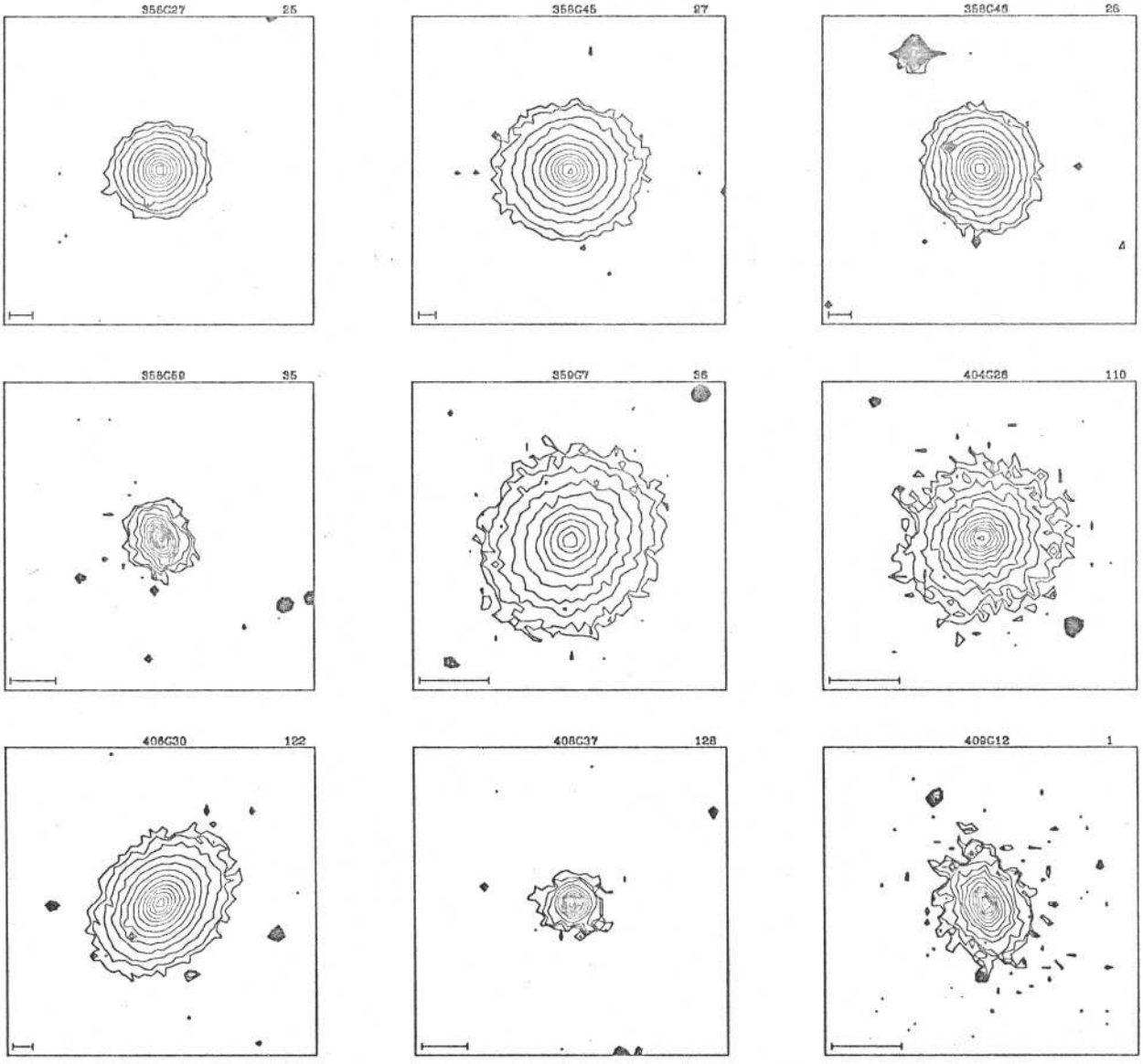

Fig.3 - continued

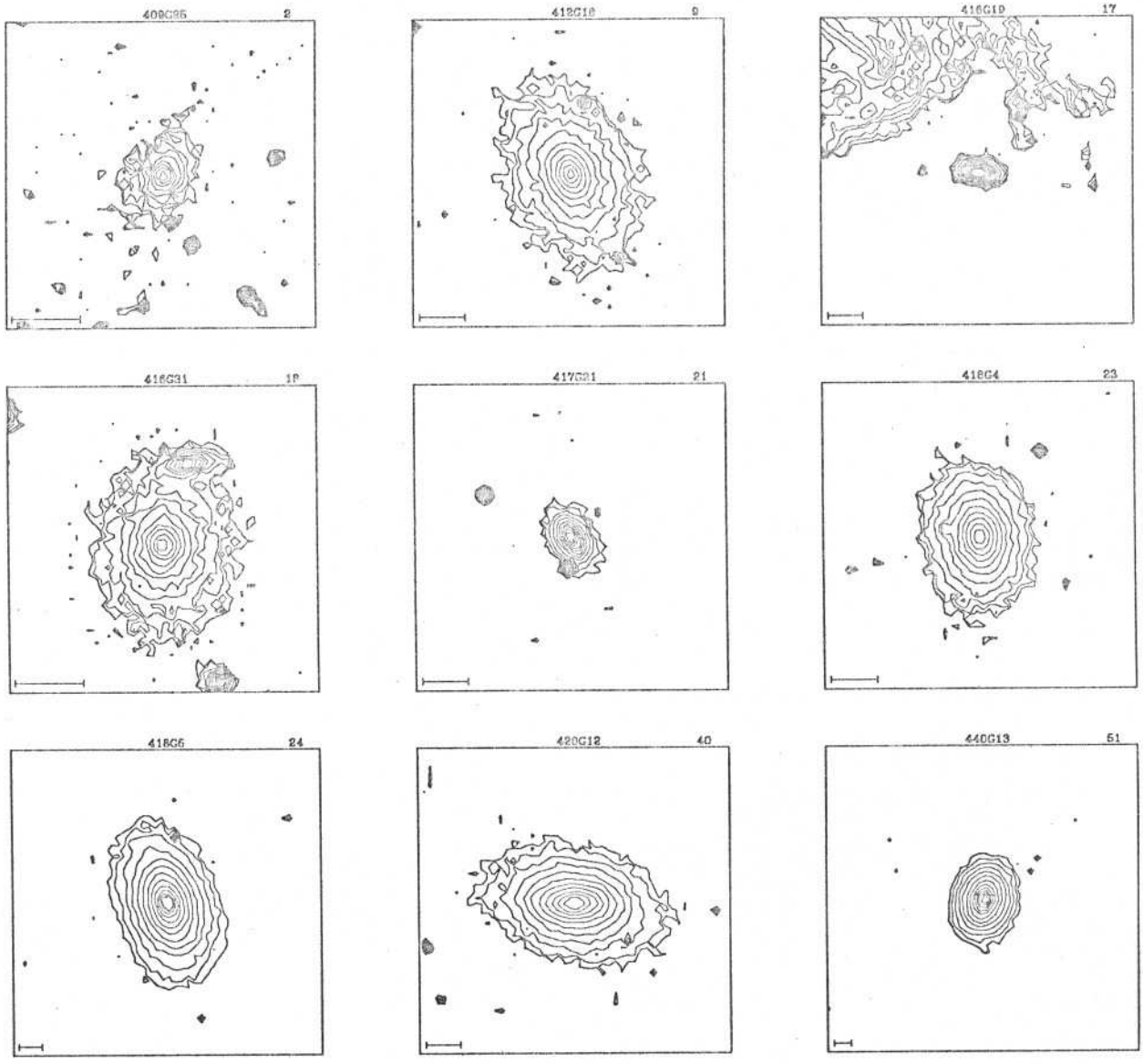

Fig.3 - continued

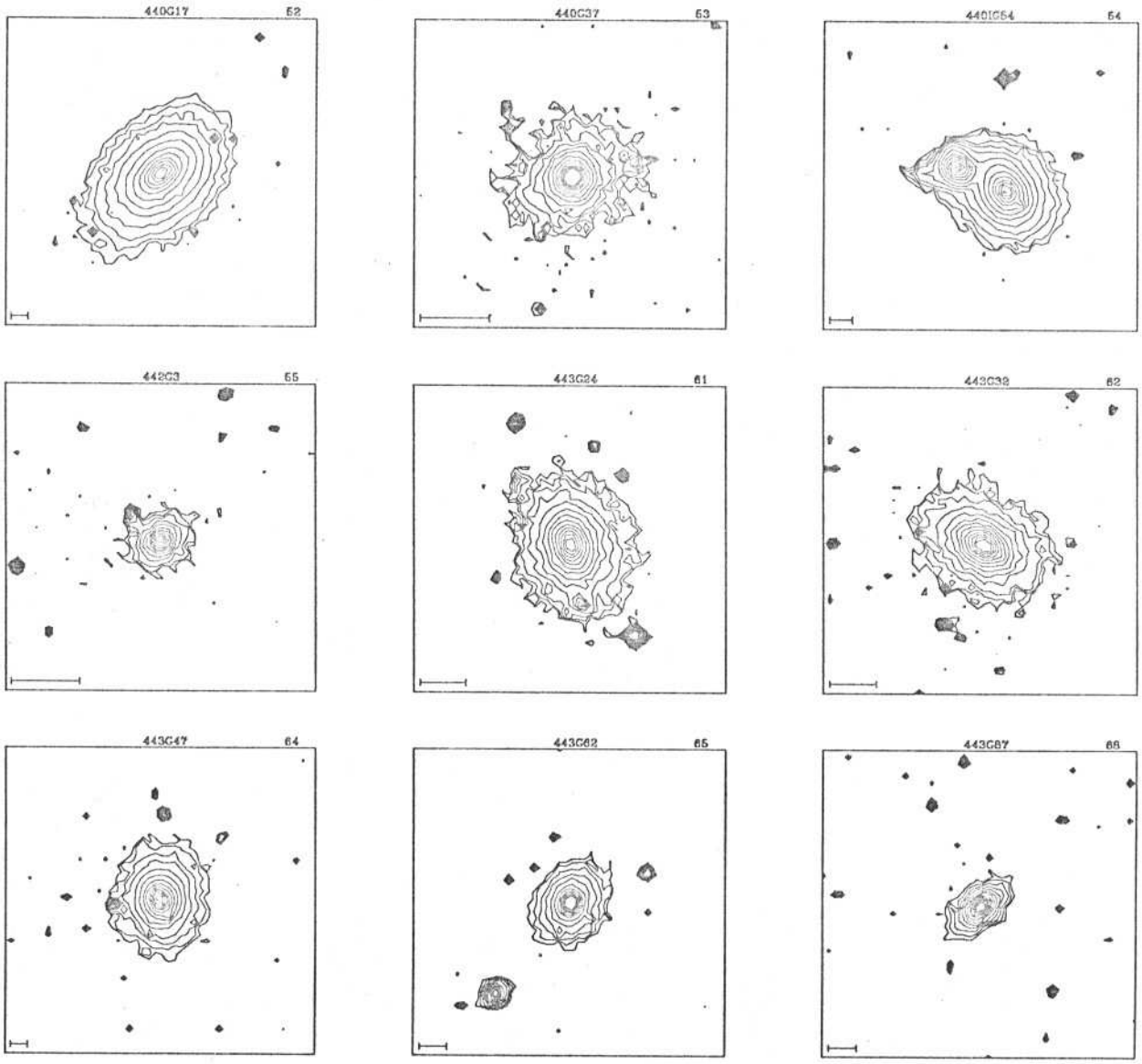

Fig.3 - continued

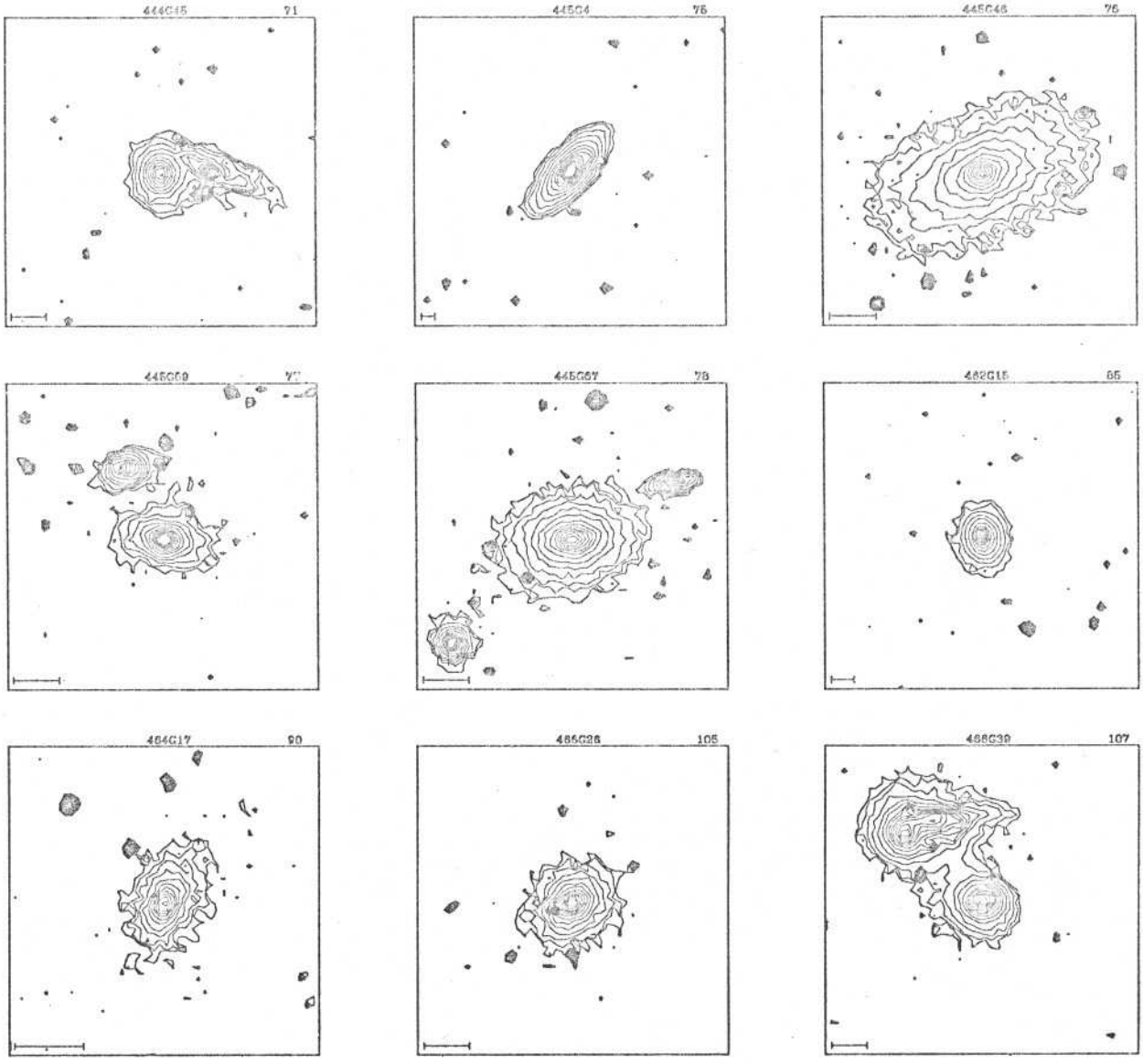

Fig.3 - continued

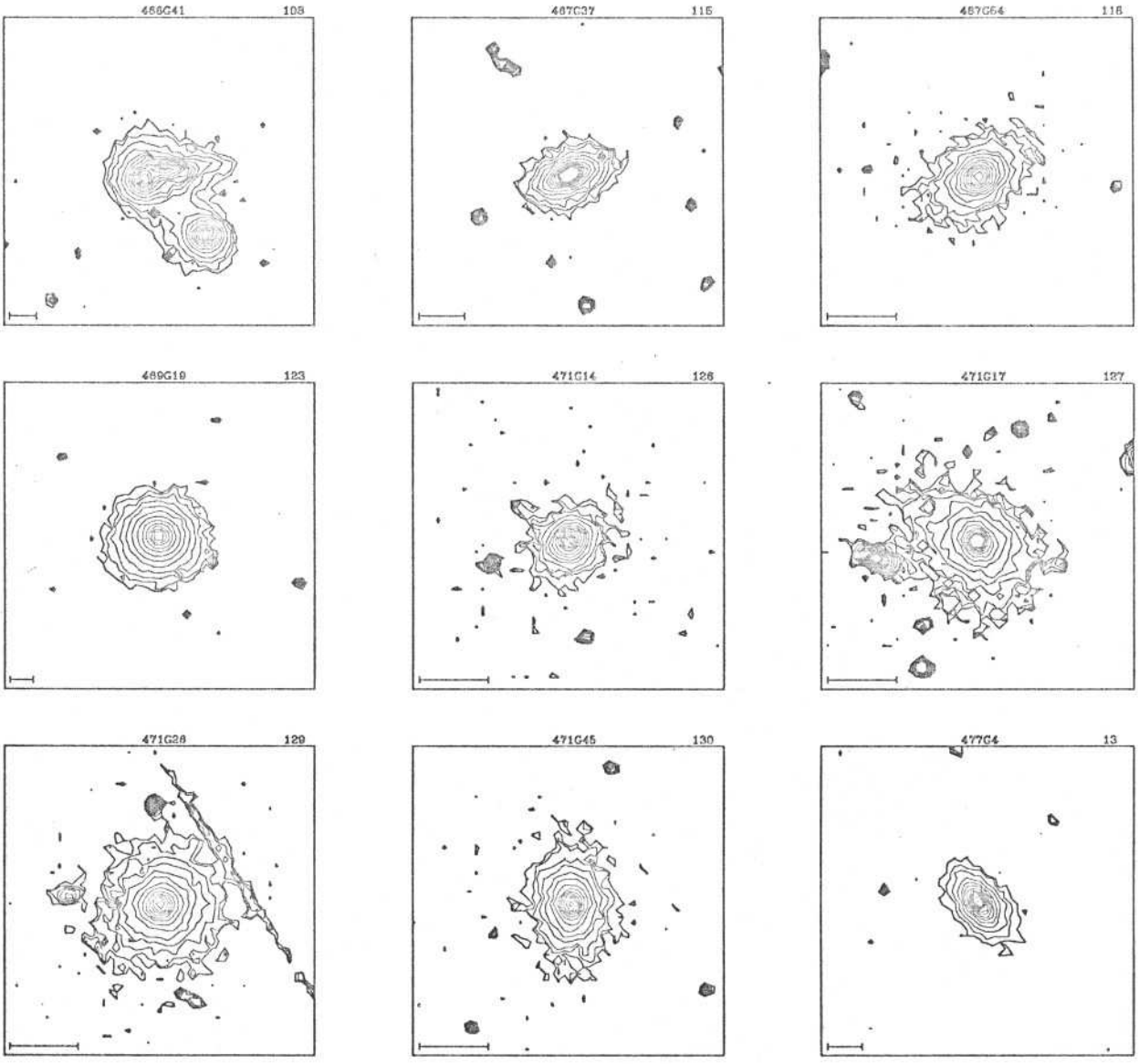

Fig.3 - continued

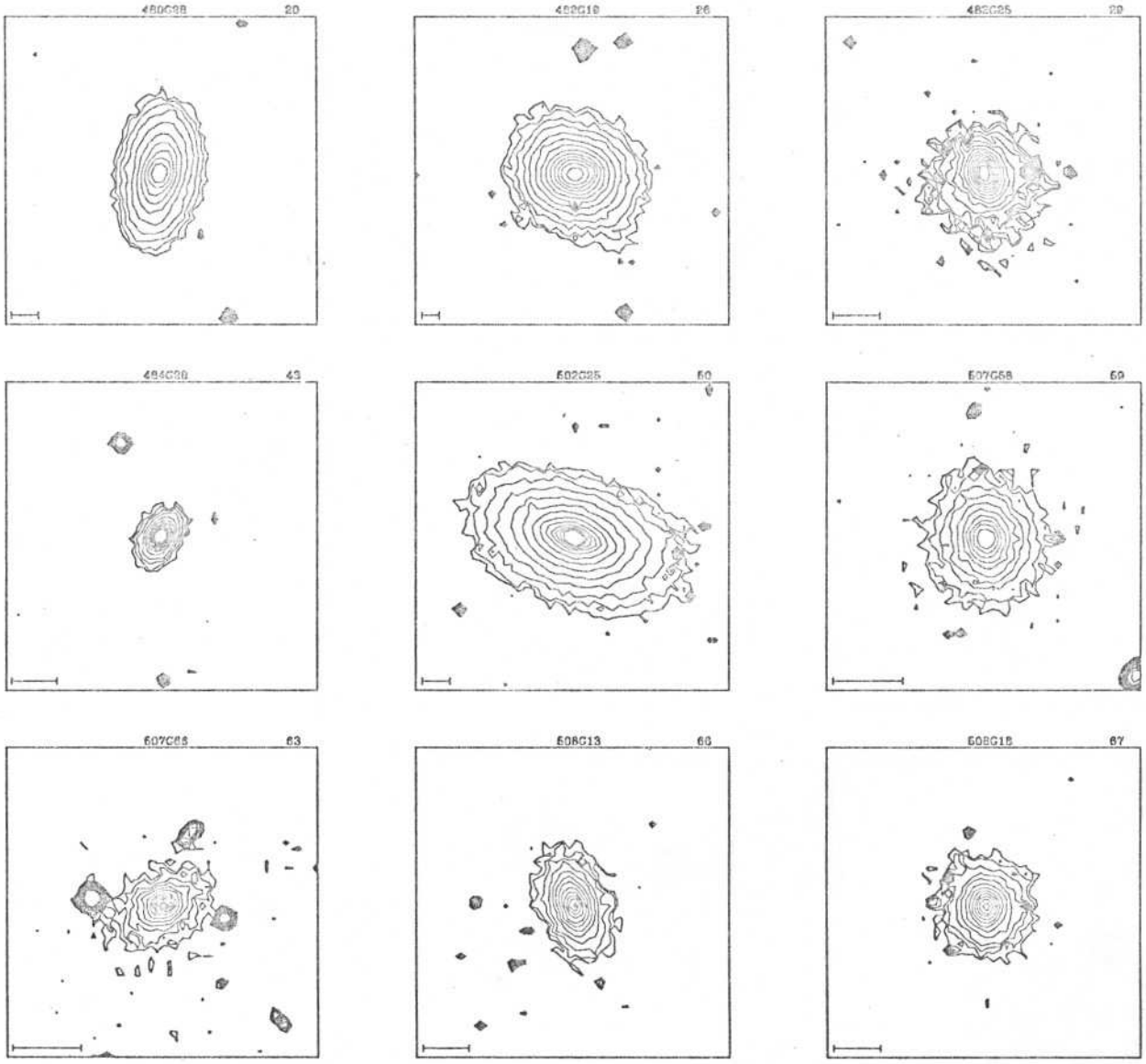

Fig.3 - continued

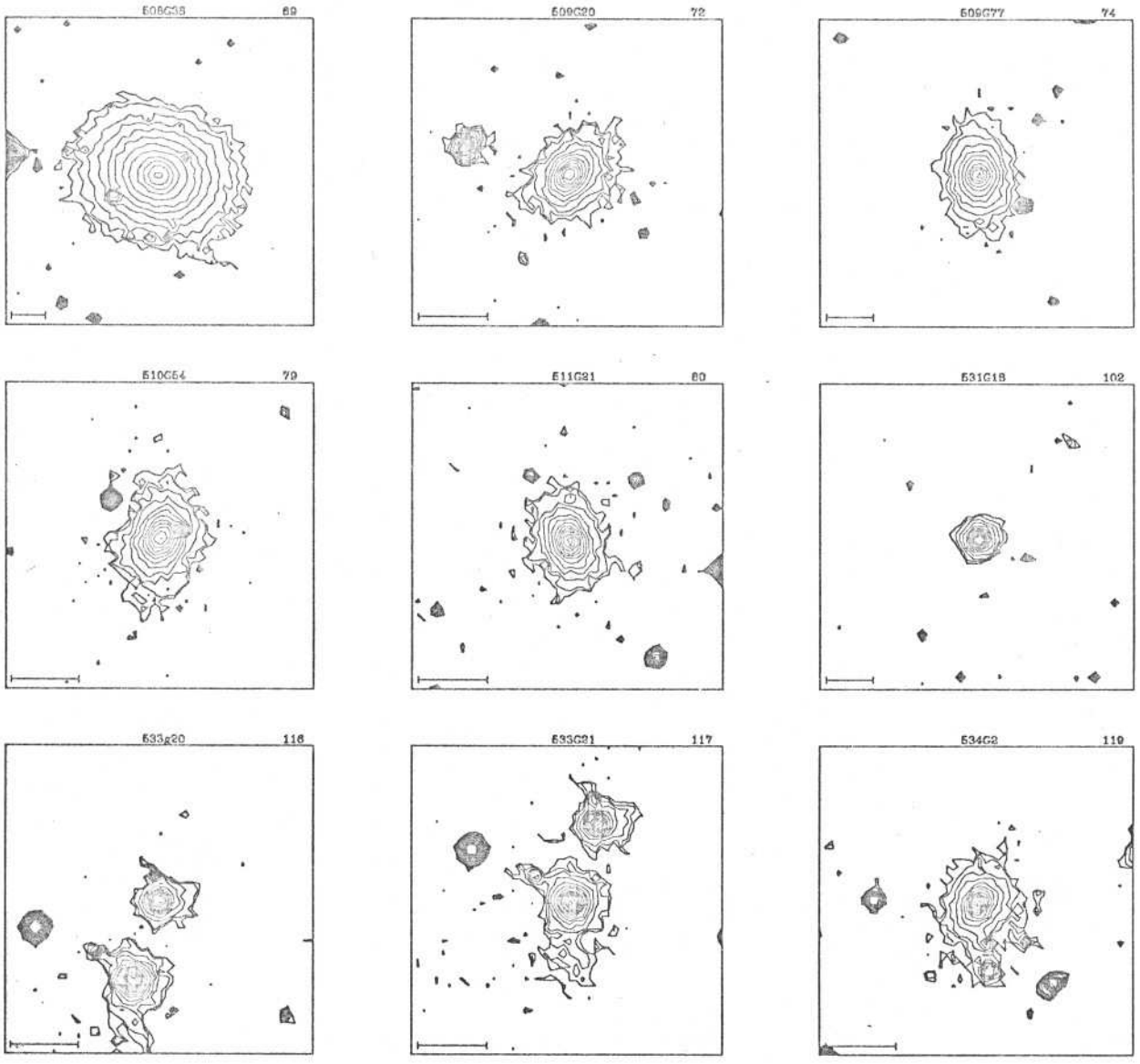

Fig.3 - continued

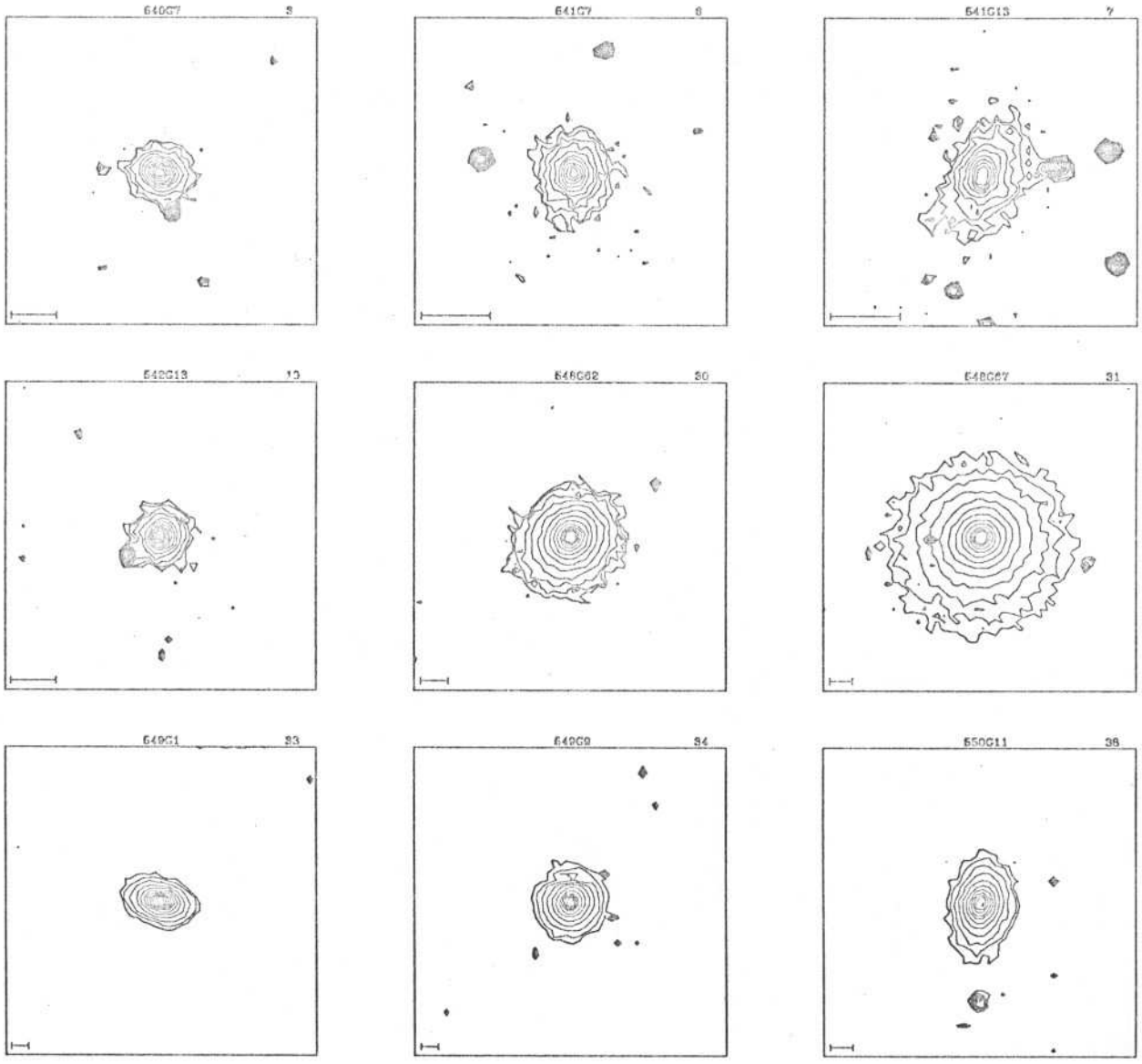

Fig.3 - continued

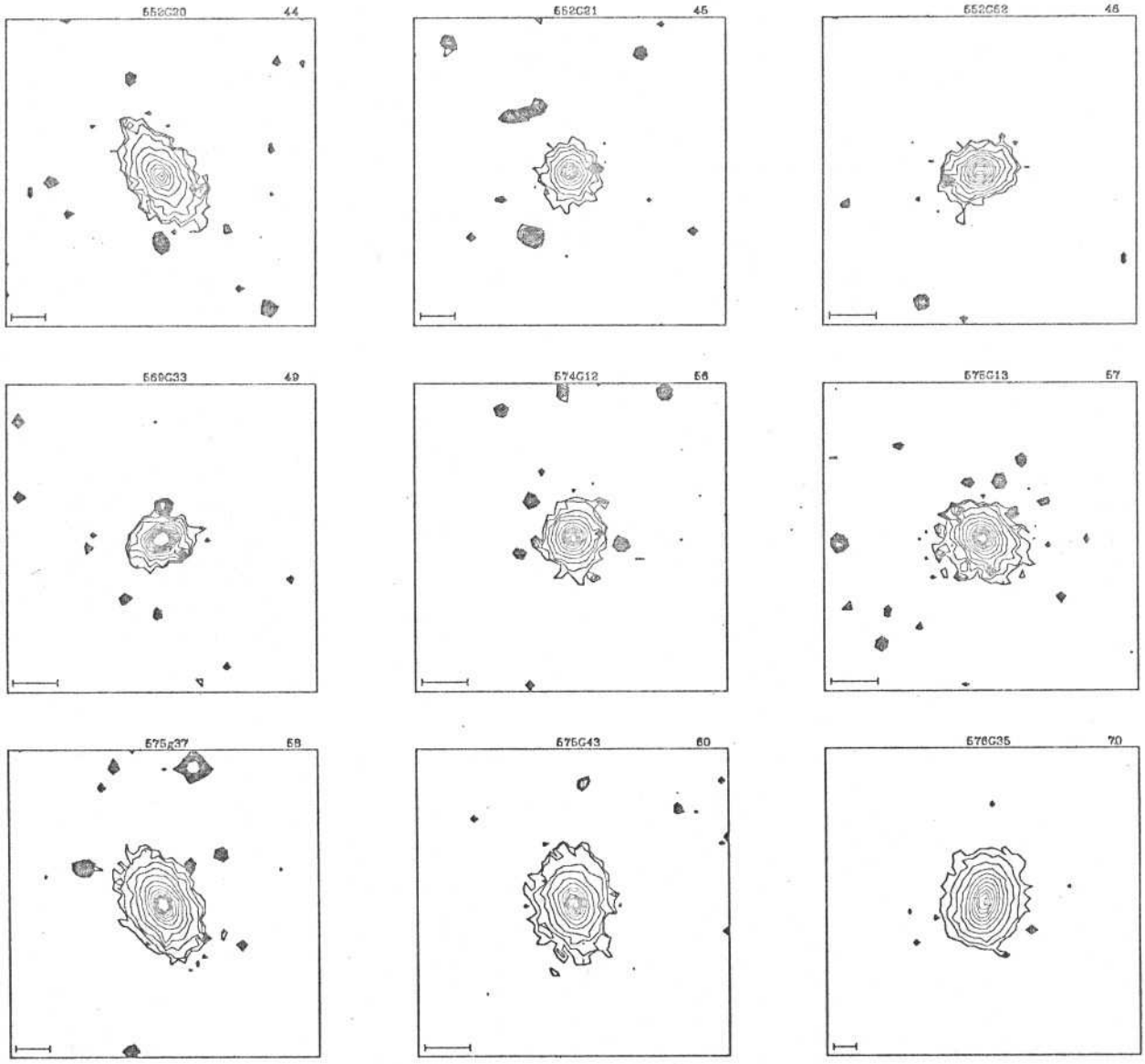

Fig.3 - continued

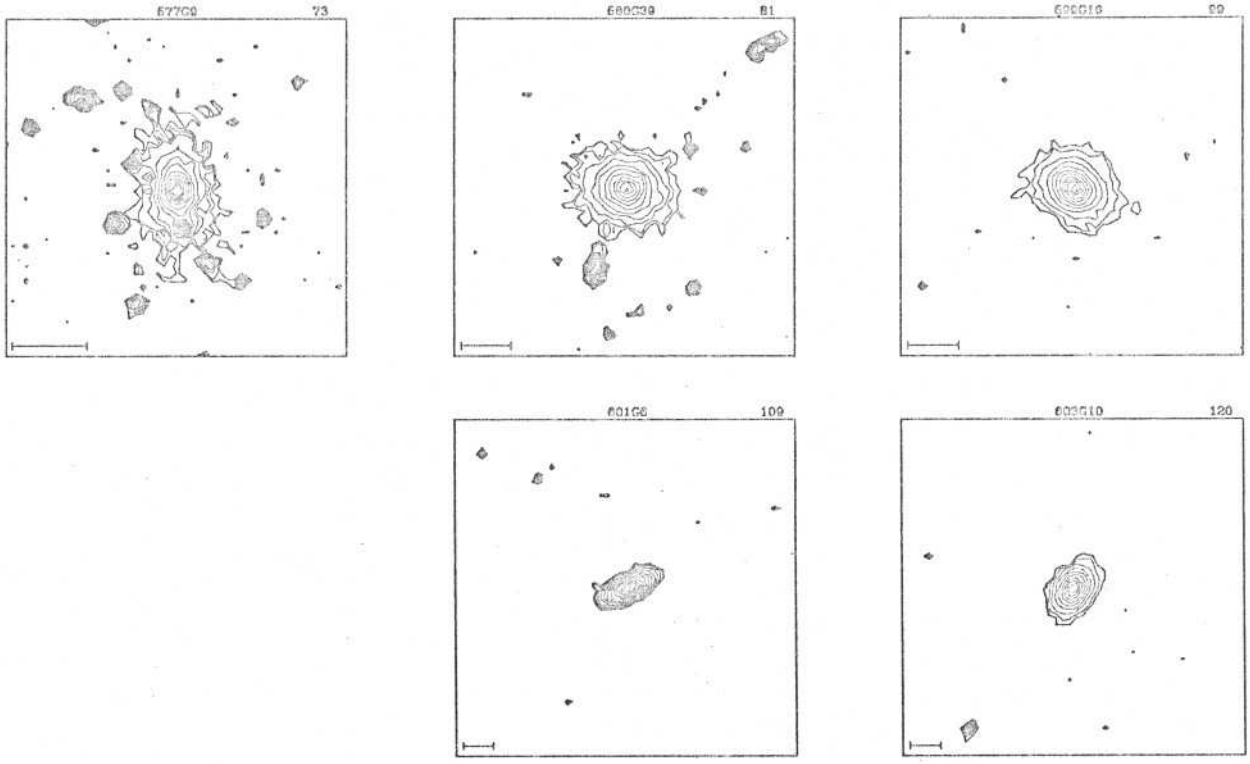

Fig.3 - continued

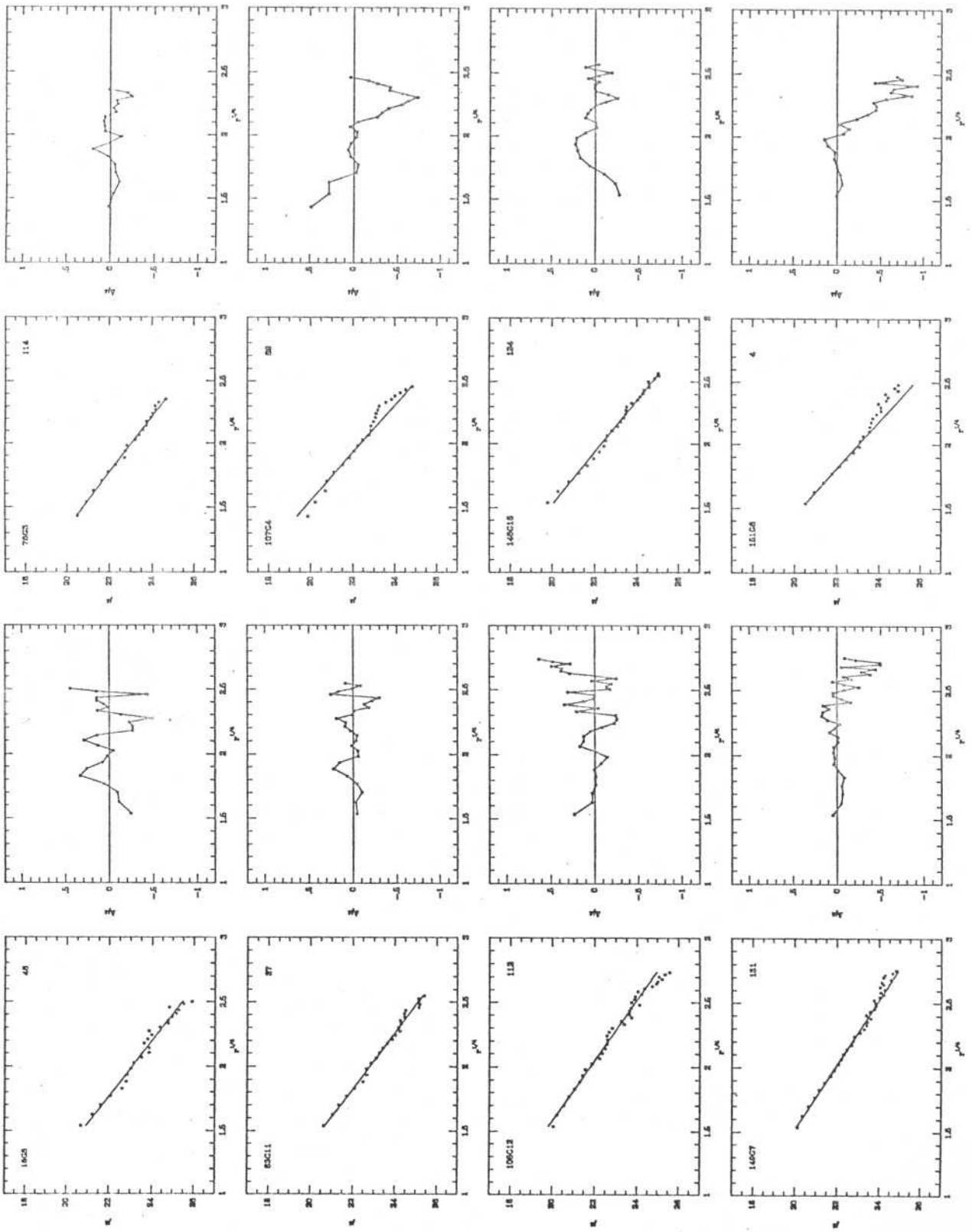

Fig.4

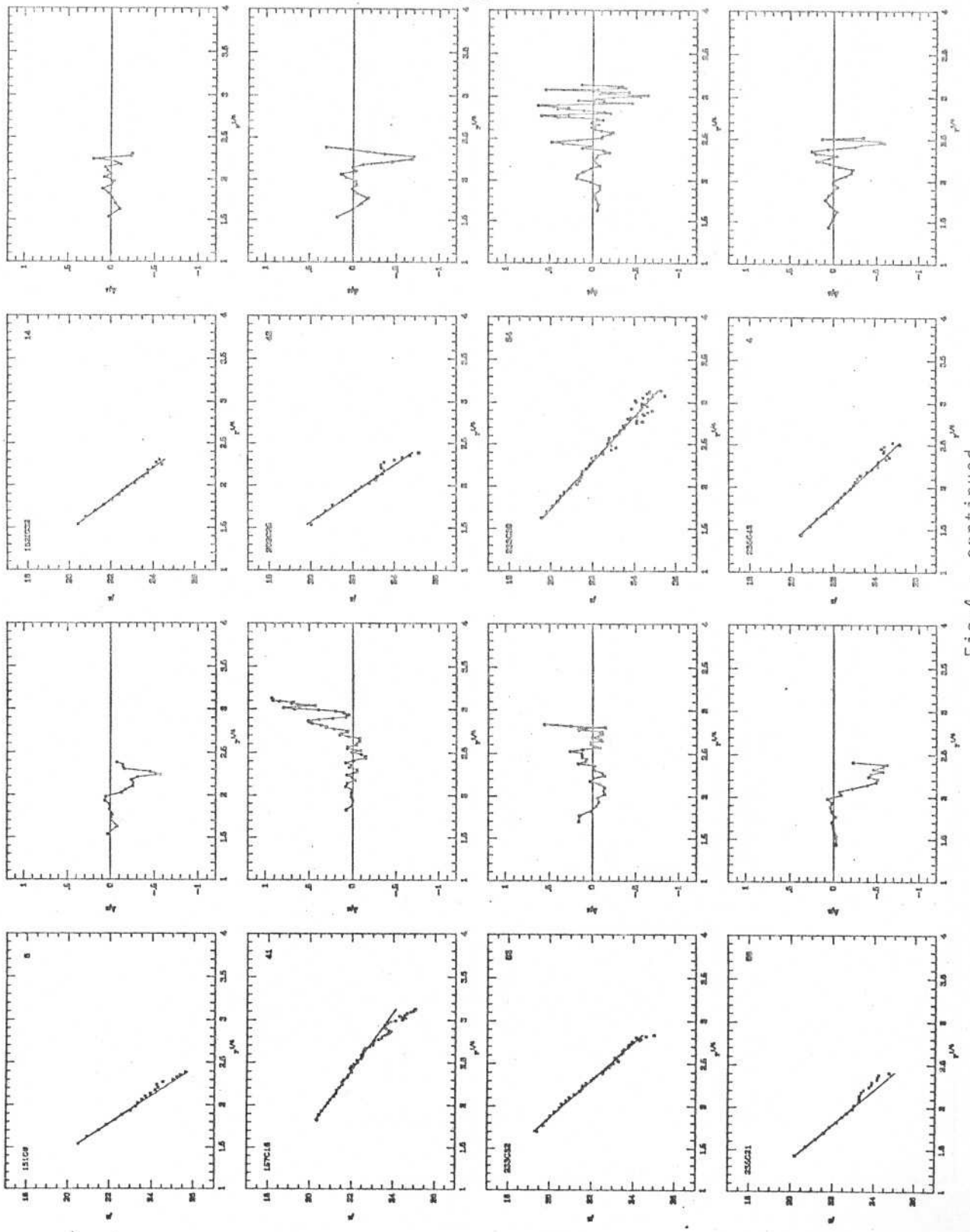

Fig.4 - continued

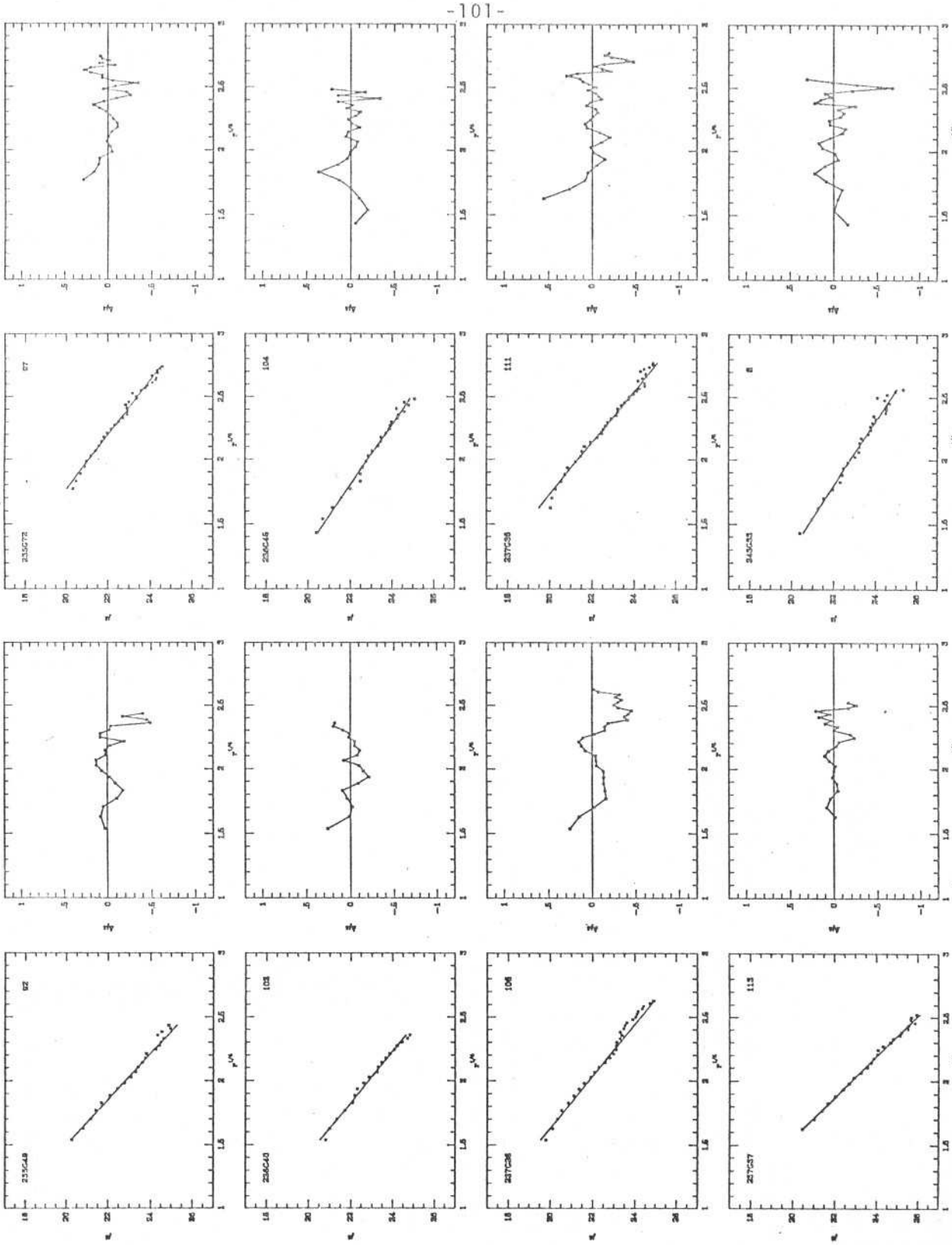

Fig.4 - continued

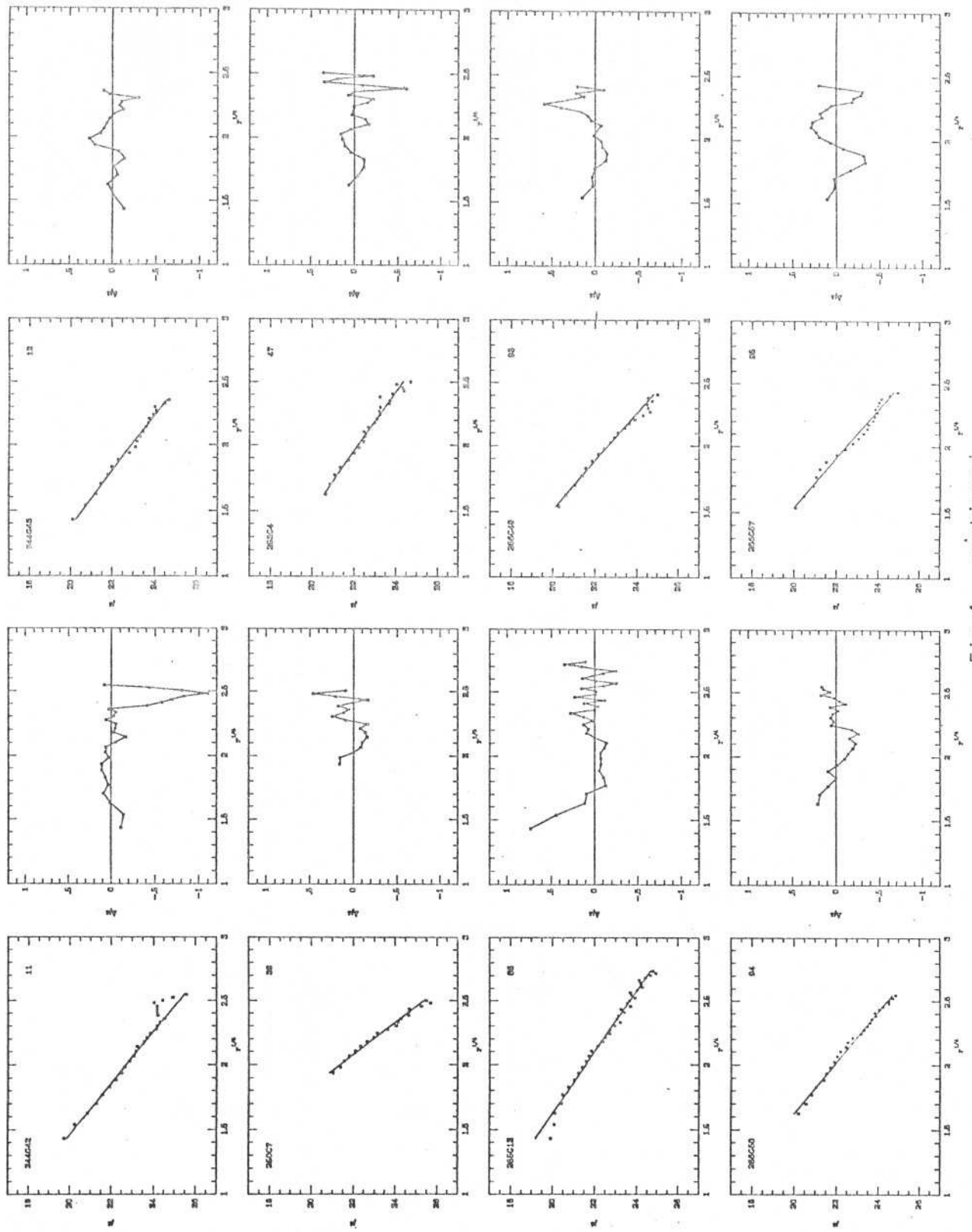

Fig.4 - continued

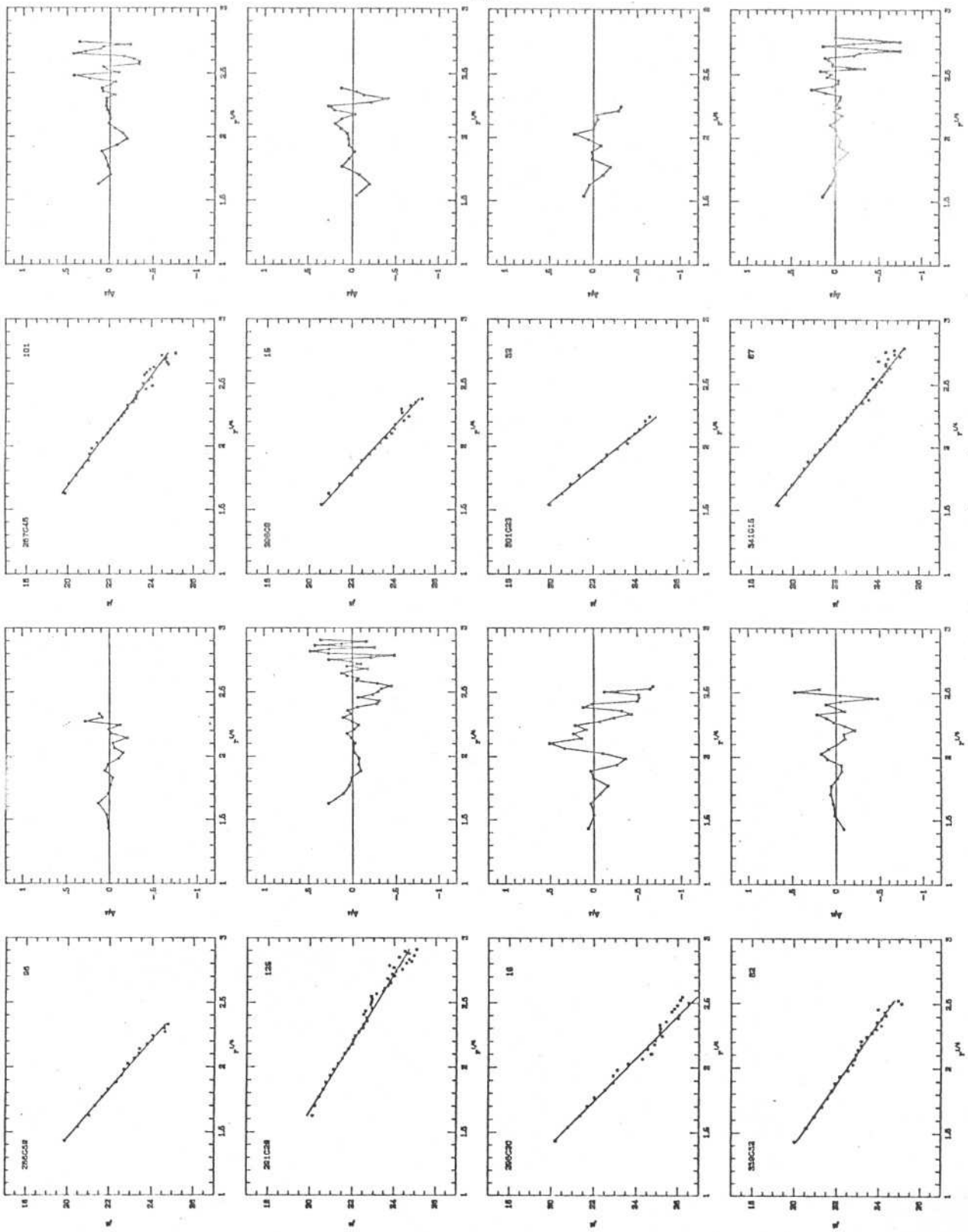

Fig.4 - continued

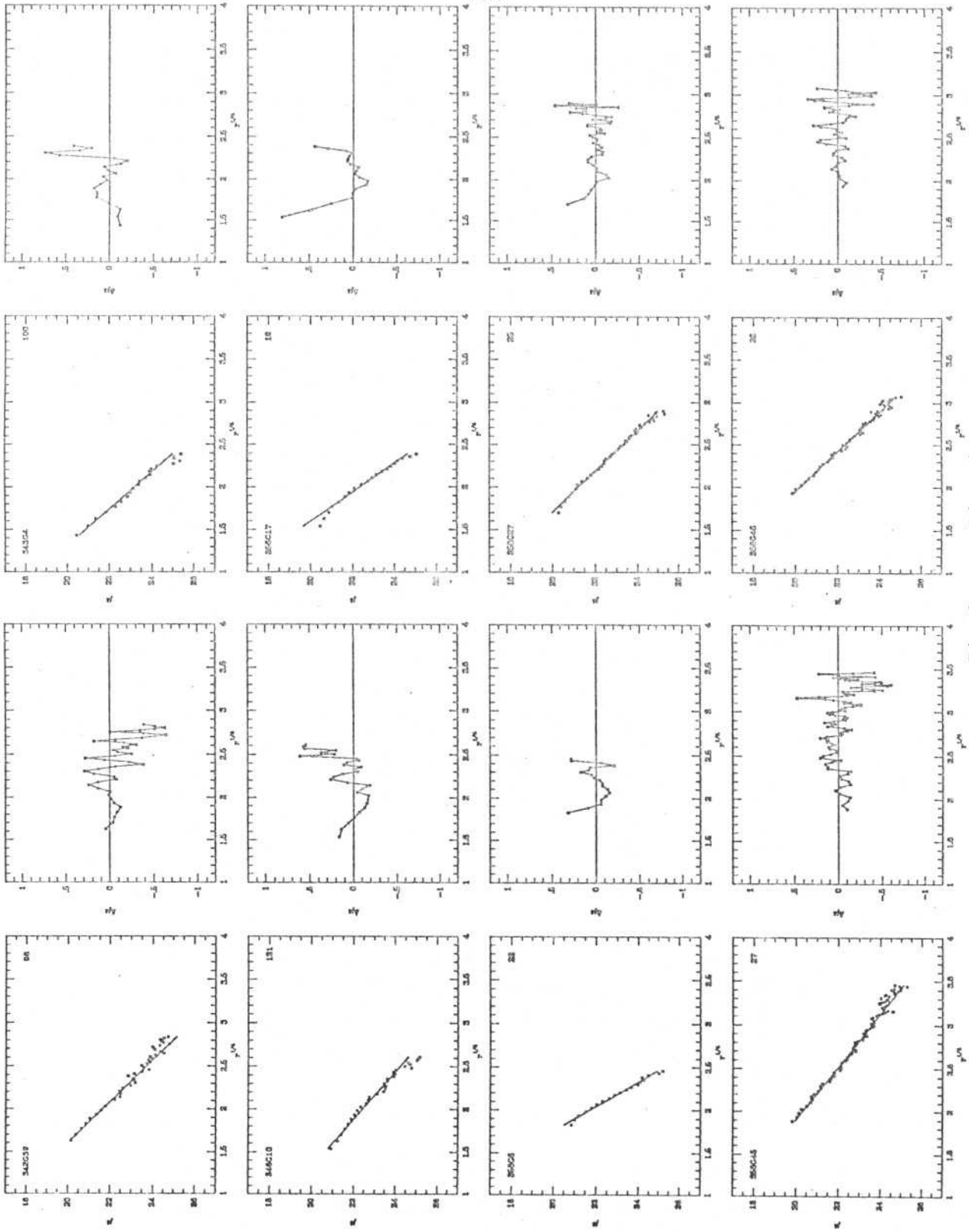

Fig.4 - continued

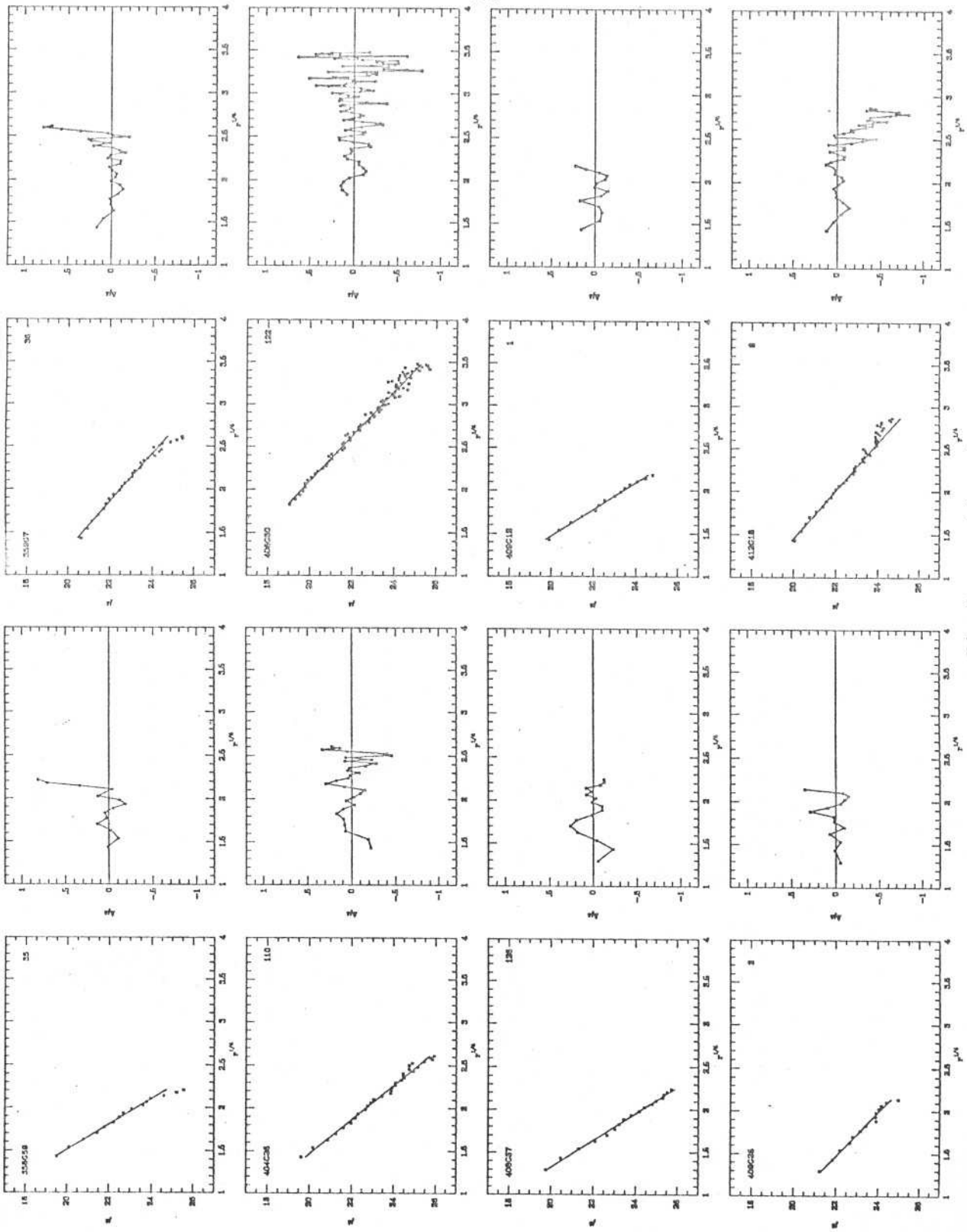

Fig.4 - continued

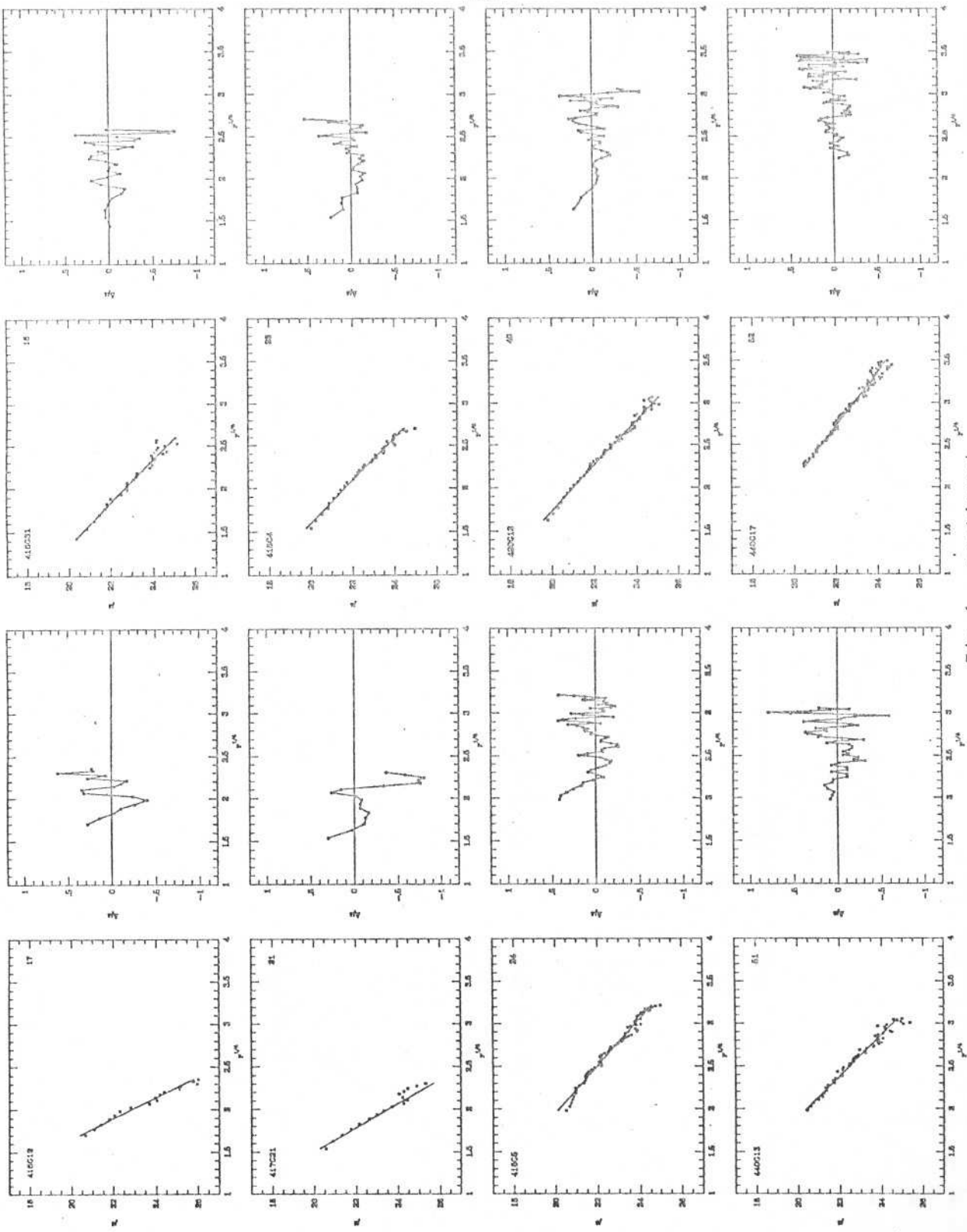

Fig.4 - continued

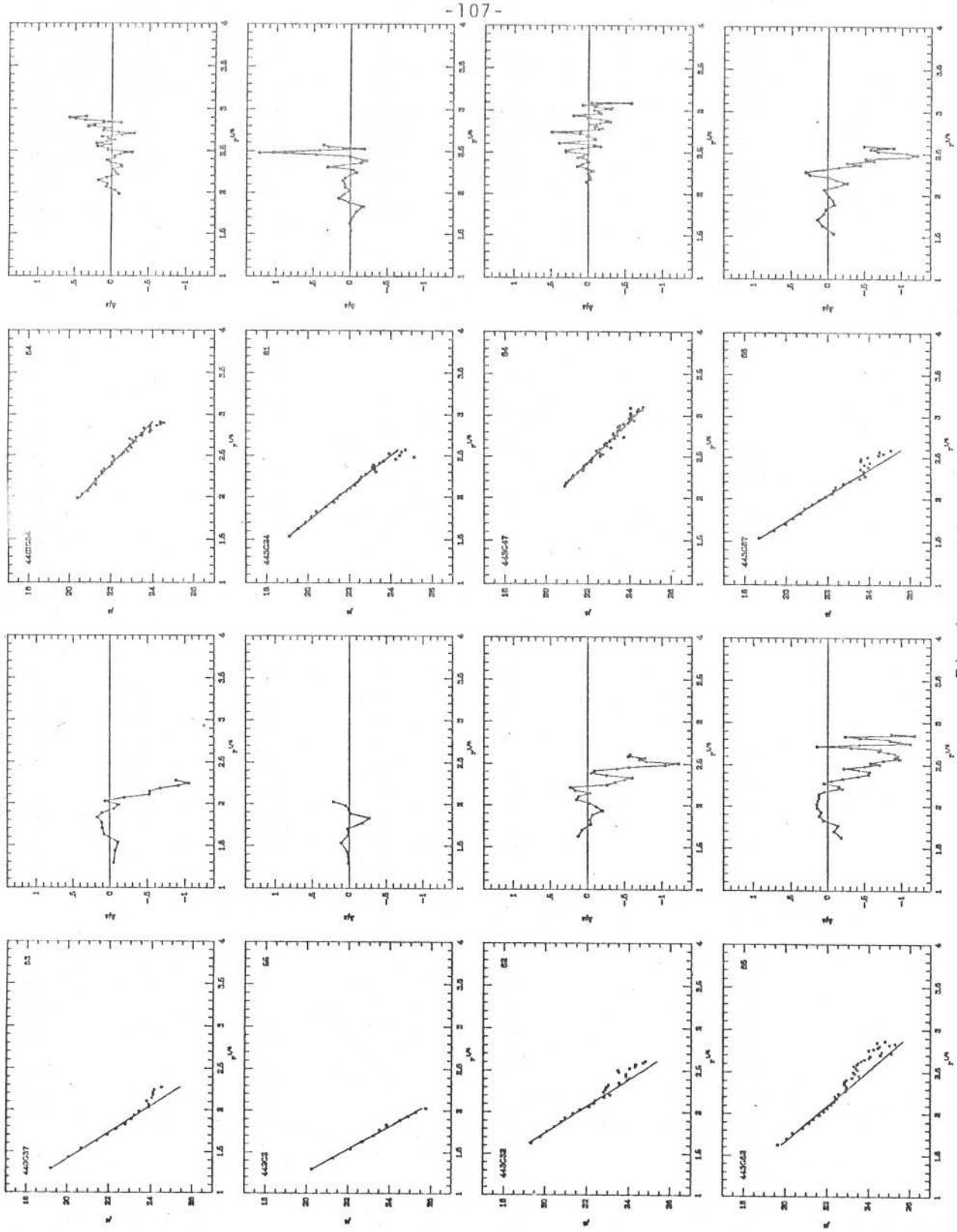

Fig.4 - continued

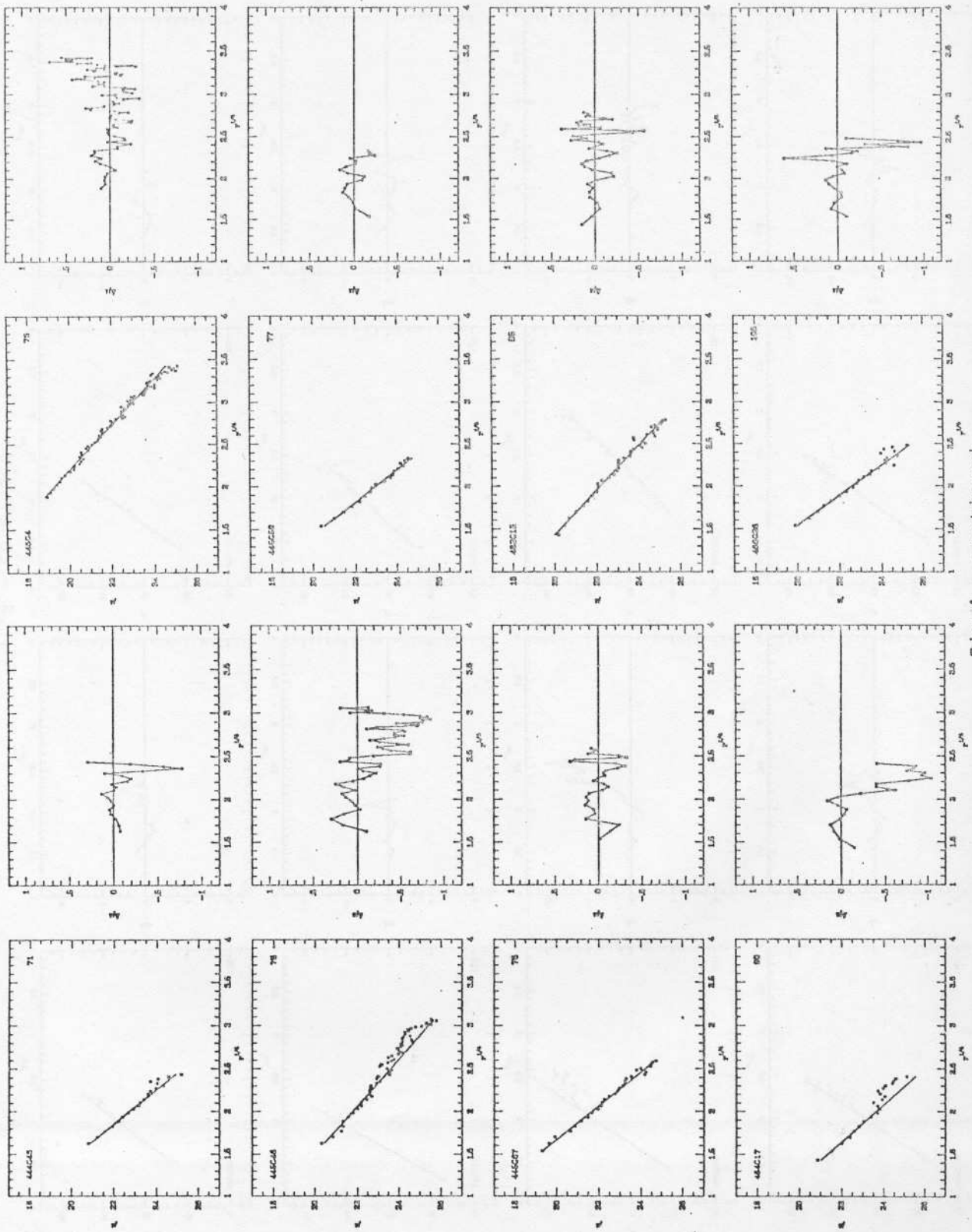

Fig.4 - continued

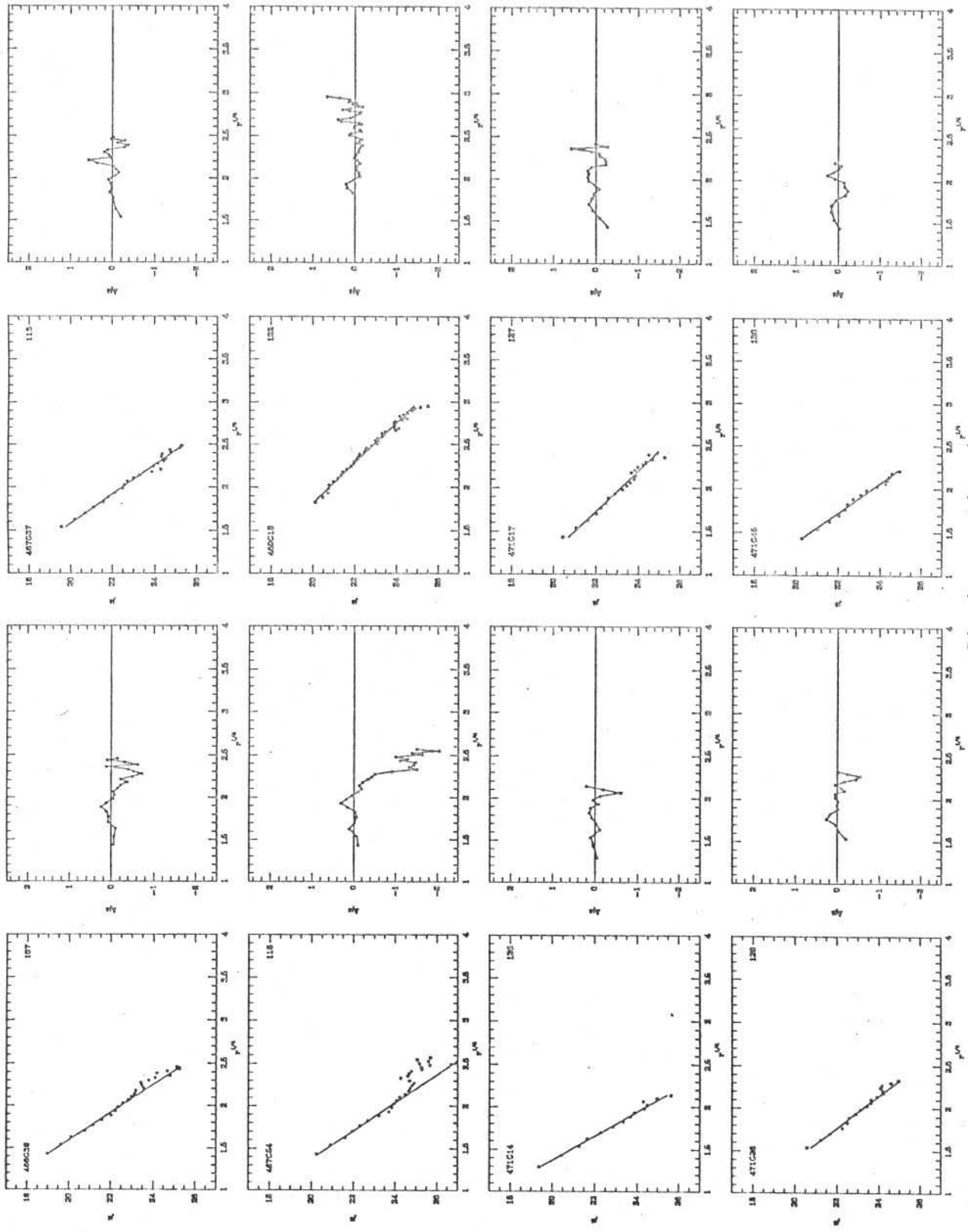

Fig.4 - continued

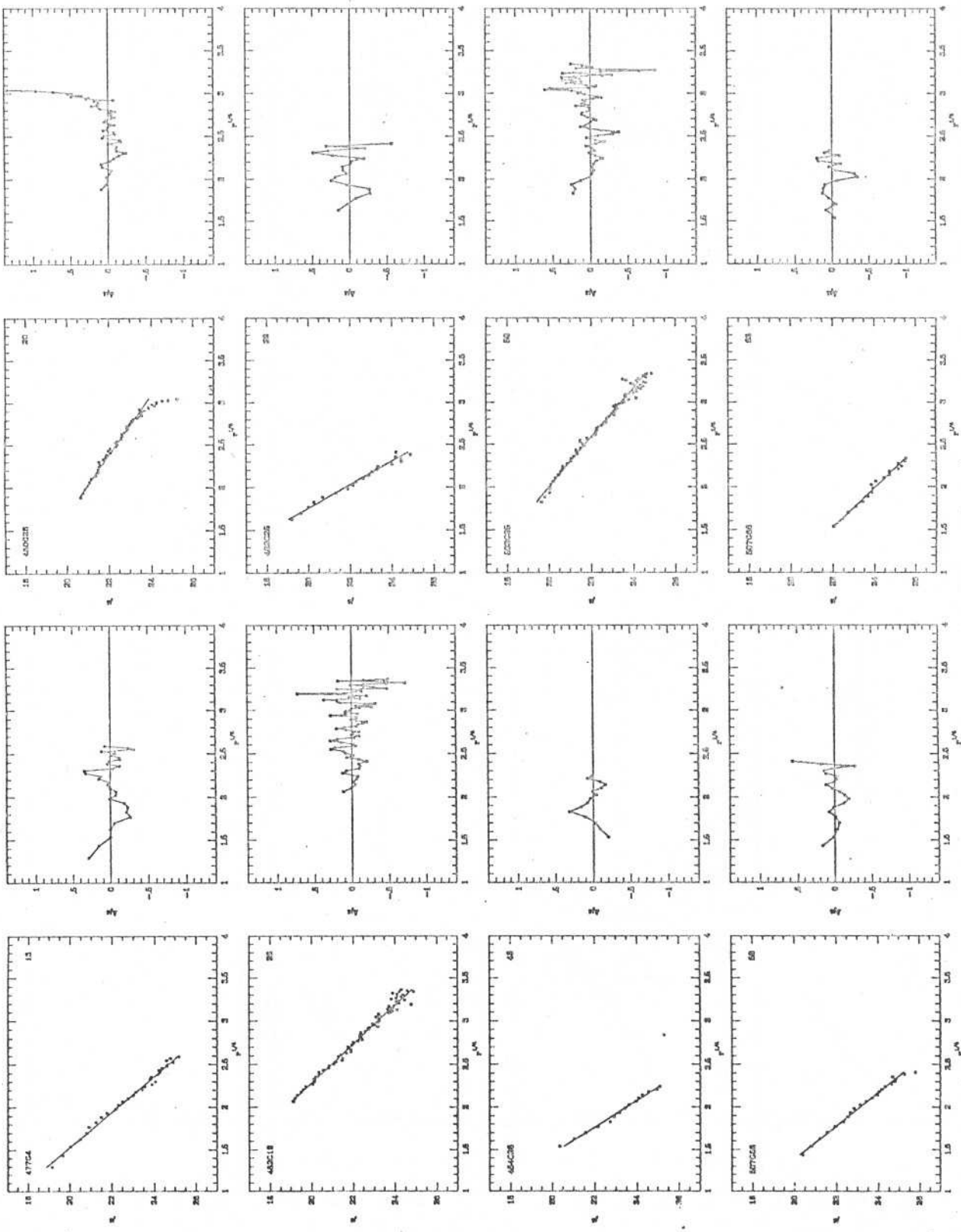

Fig.4 - continued

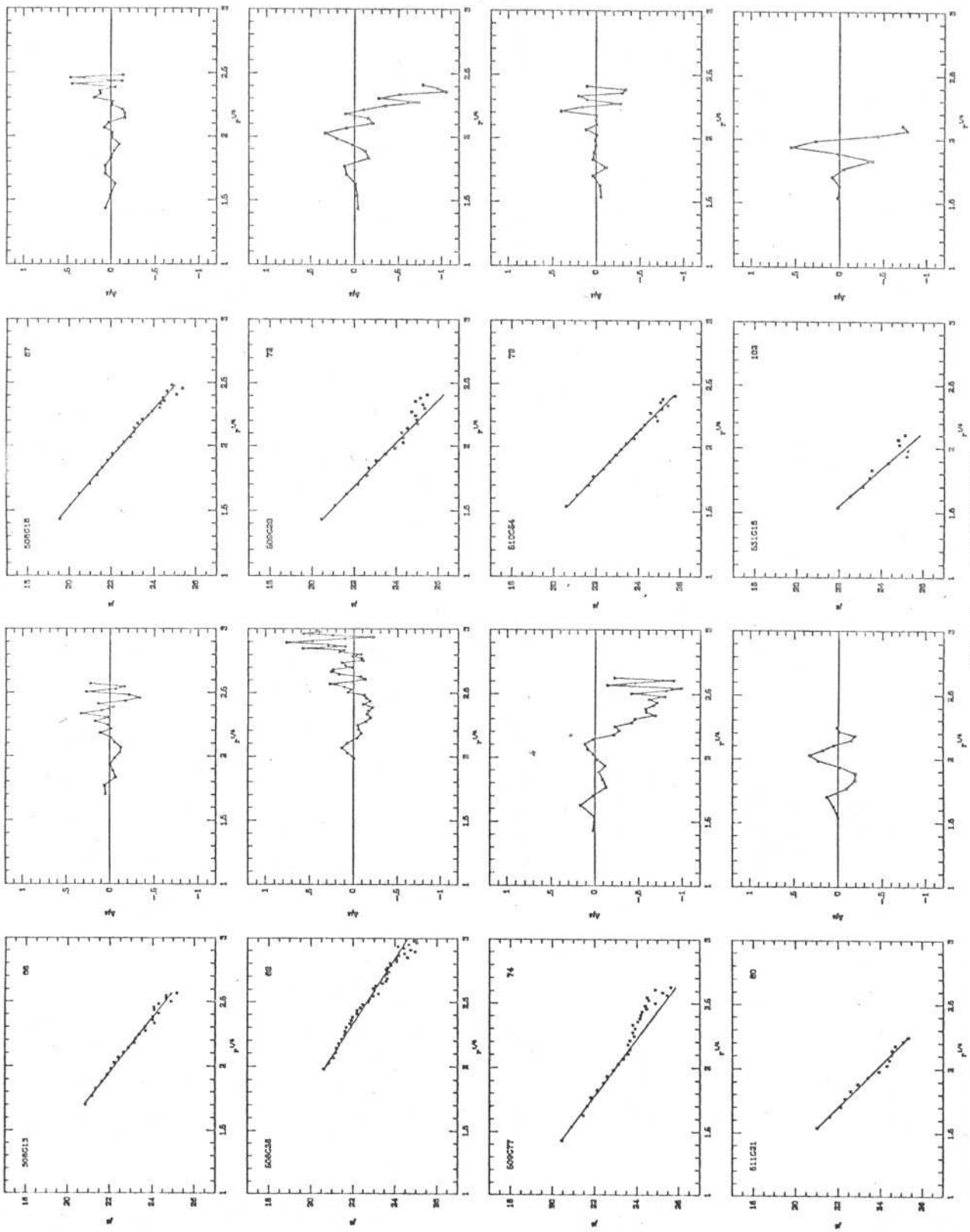

Fig.4 - continued

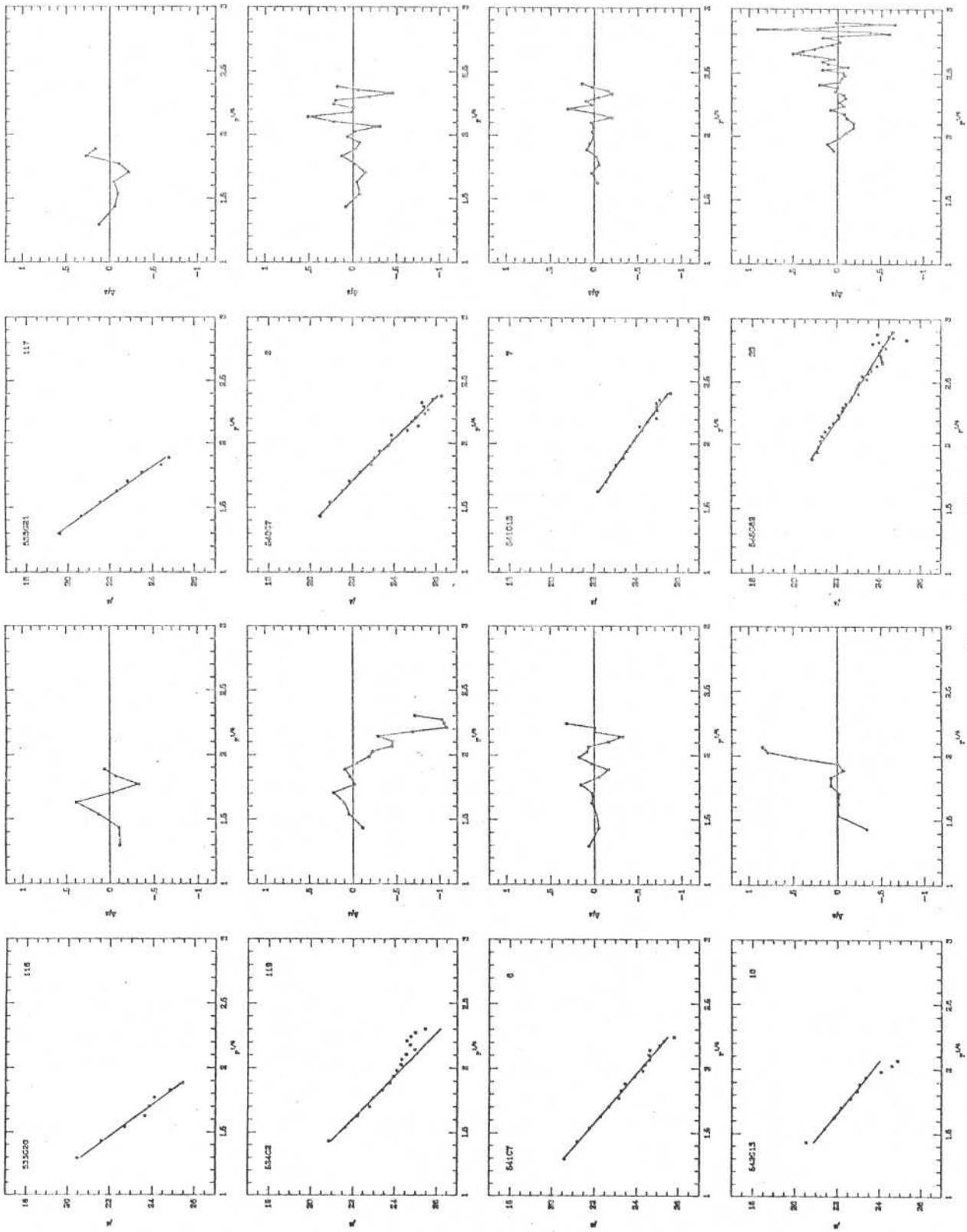

Fig.4 - continued

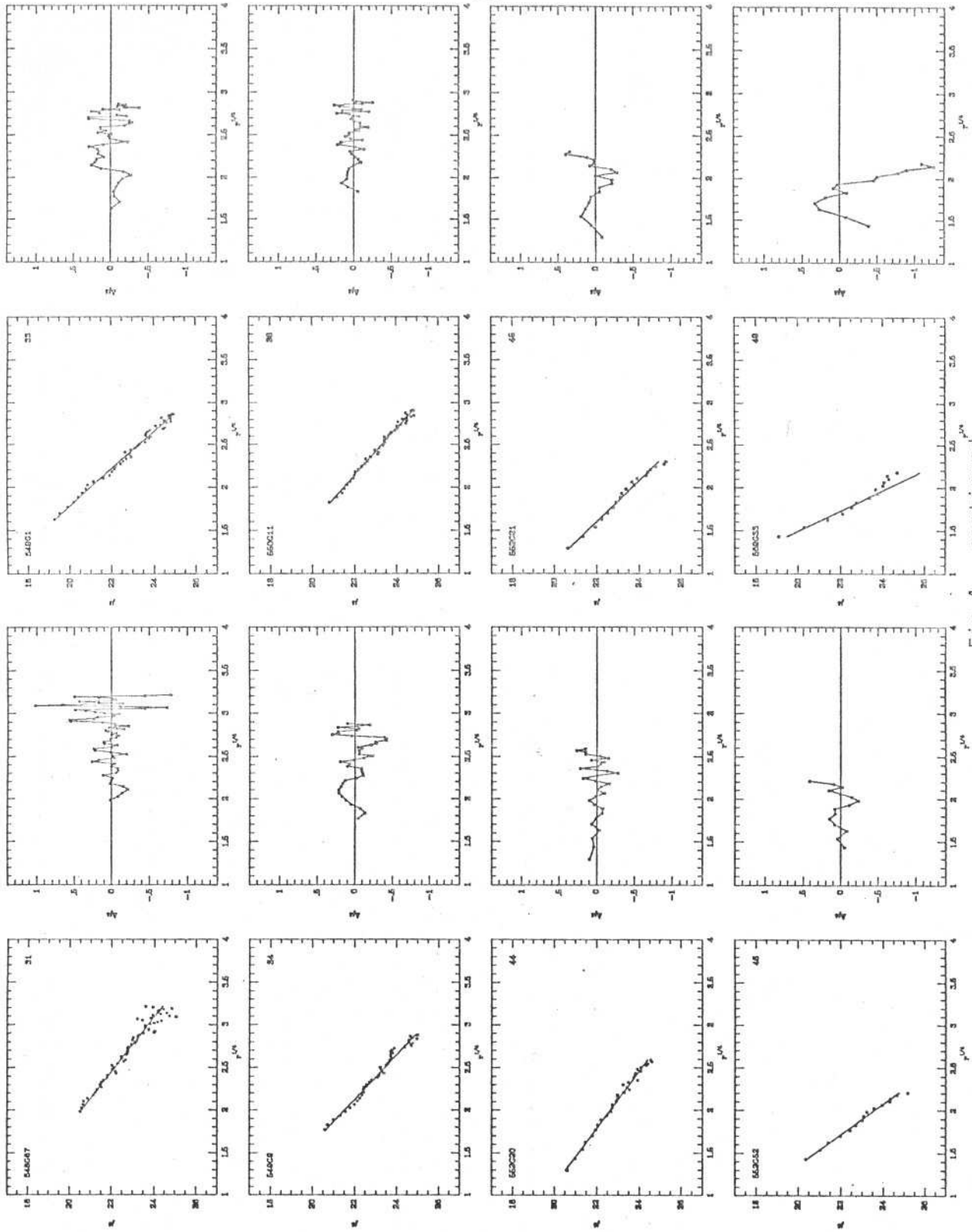

Fig.4 - continued

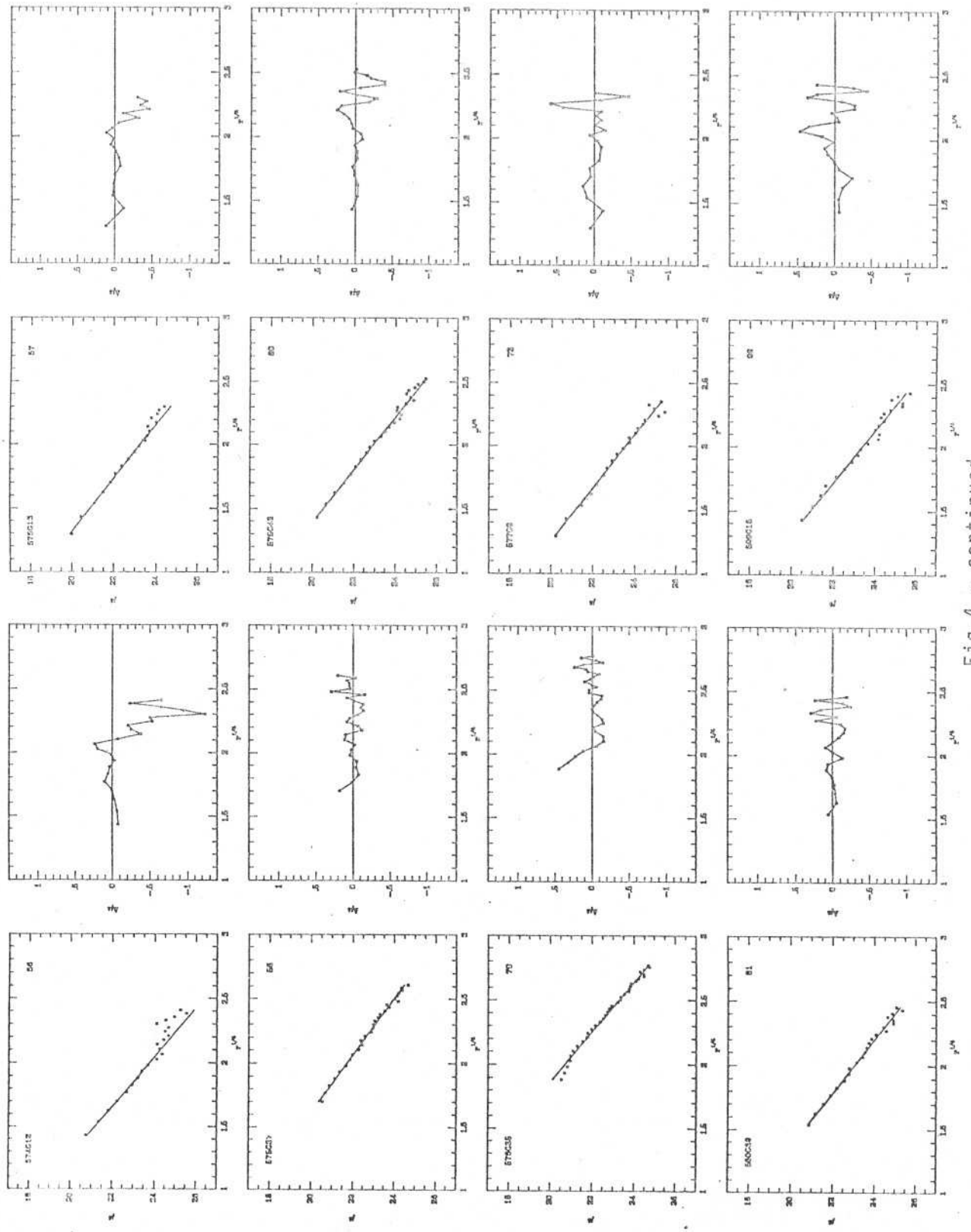

Fig.4 - continued

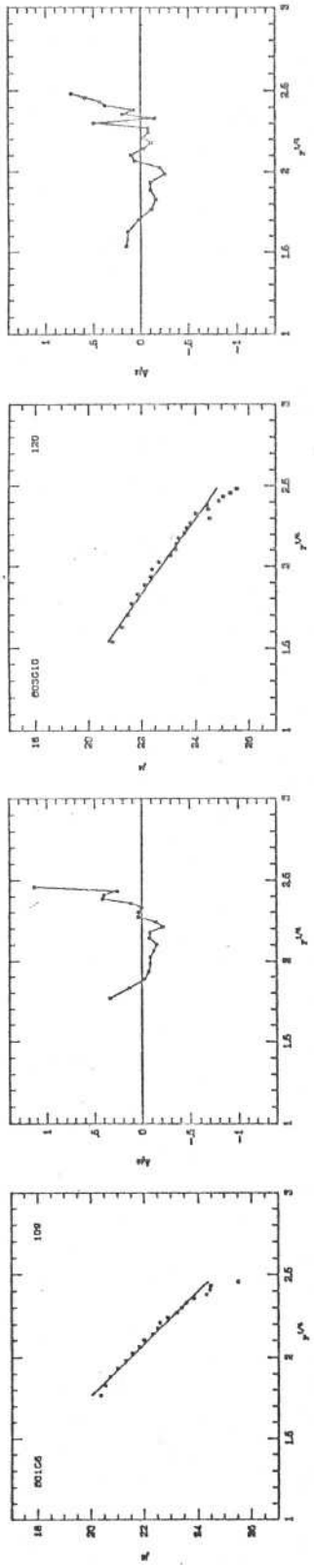

Fig.4 - continued

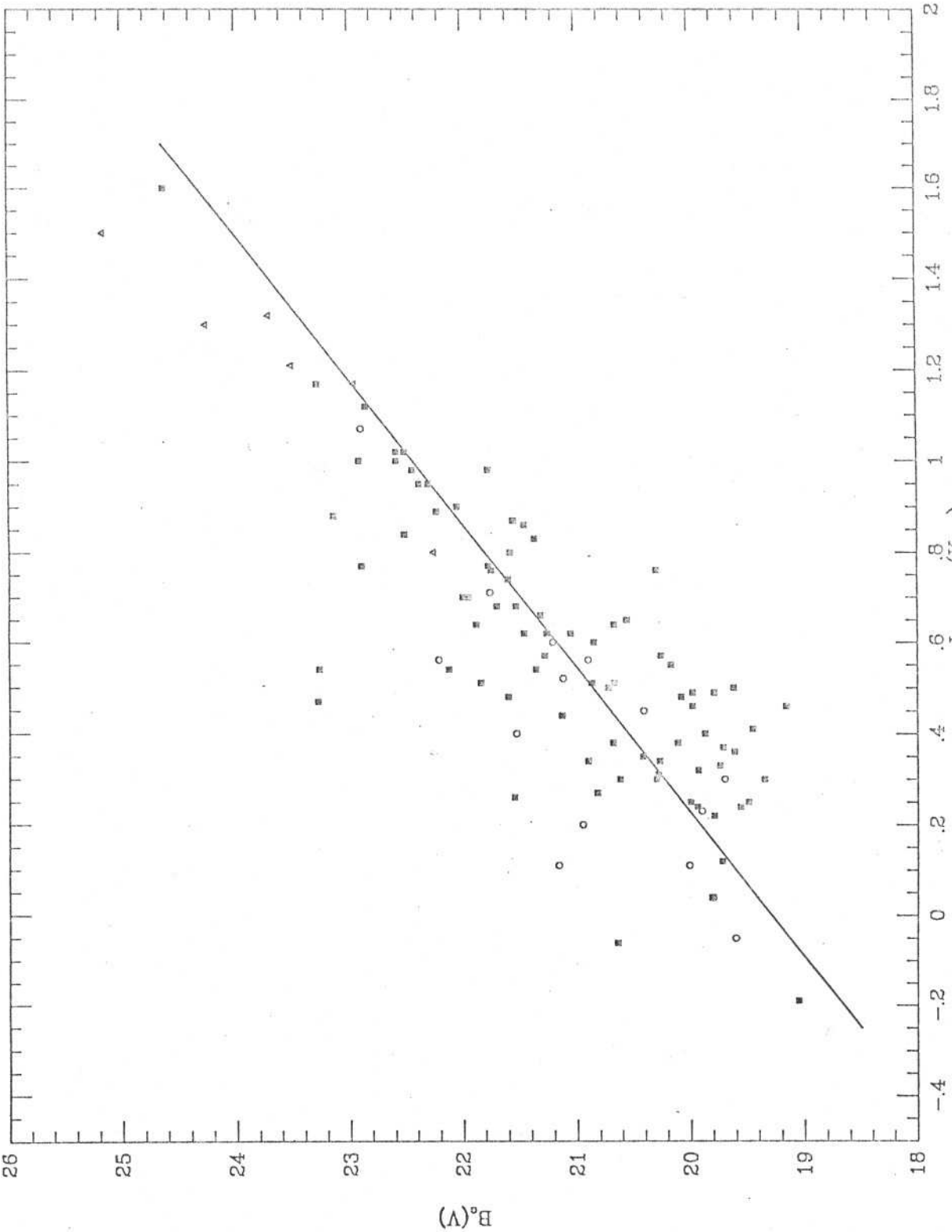

Fig.5

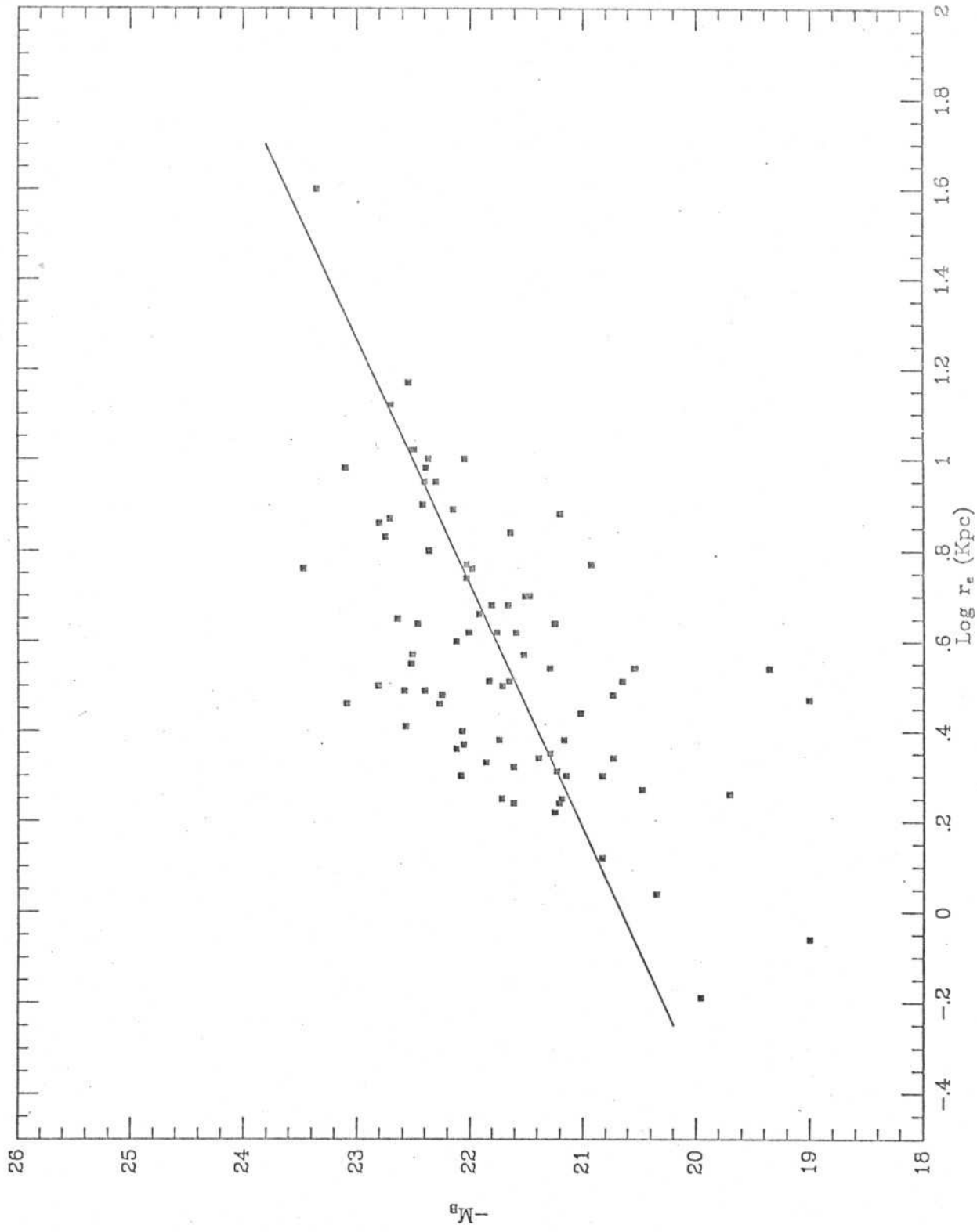

Fig.6

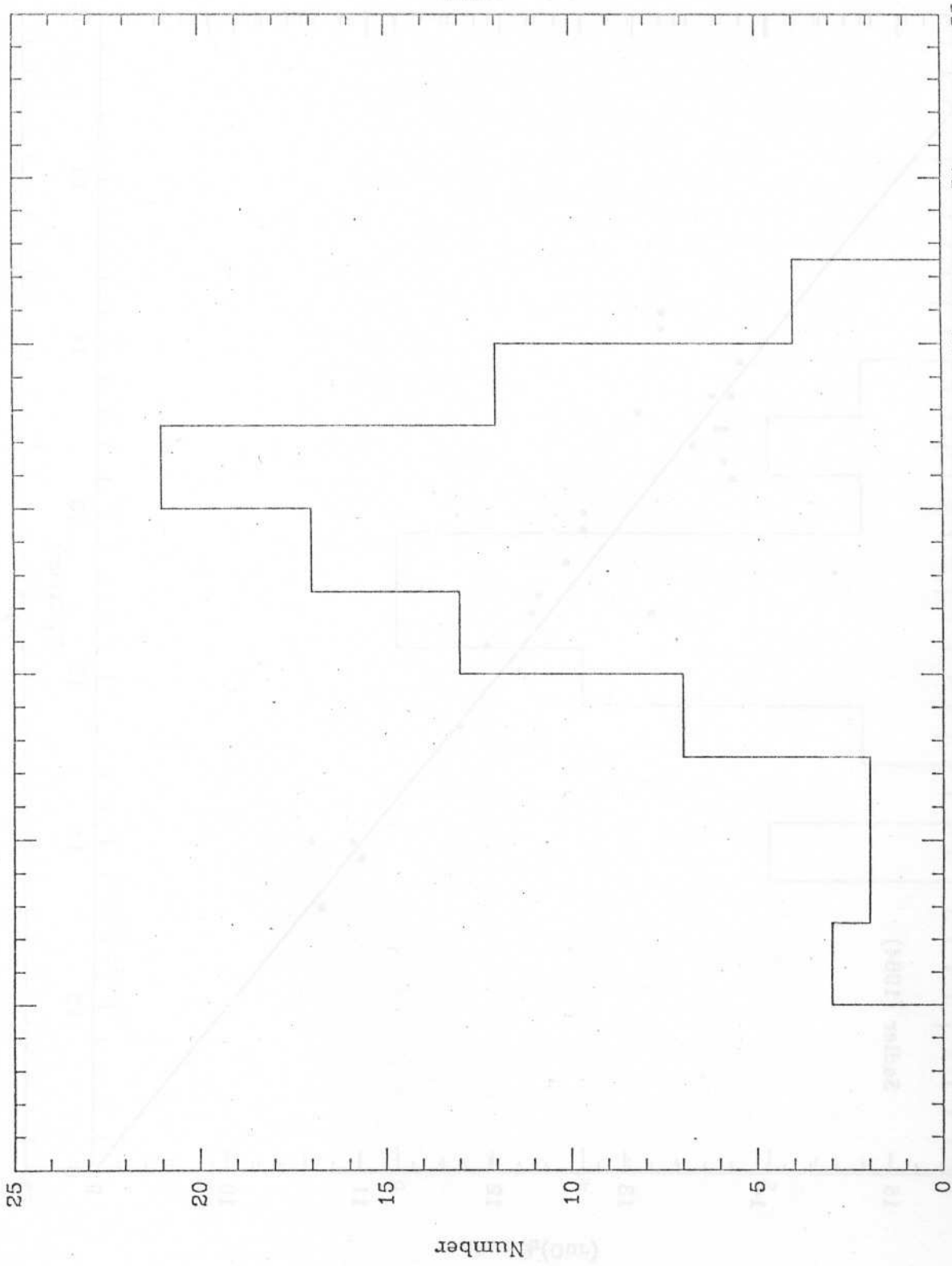

Fig.7

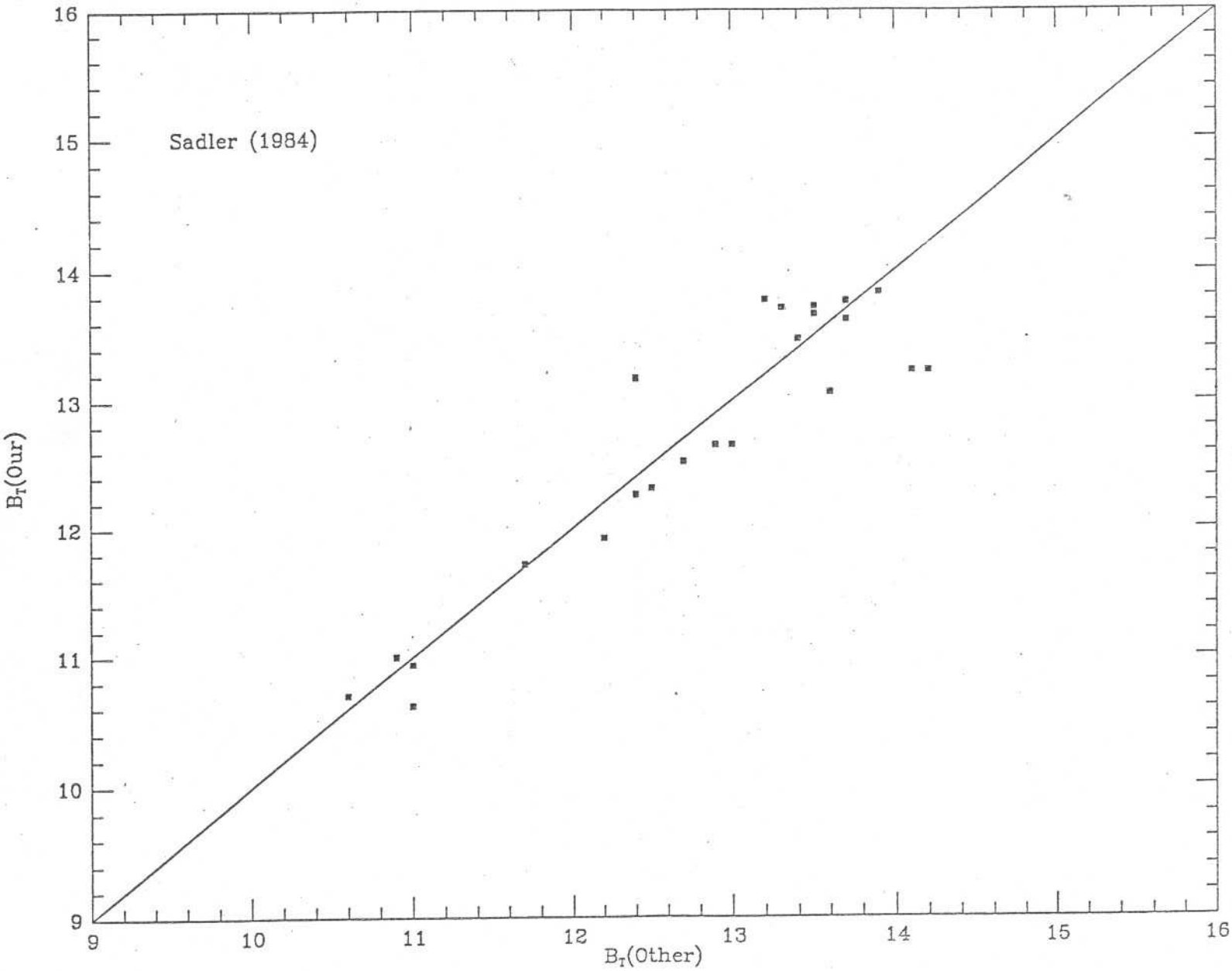
Sadler (1984)
B_T(Our)
B_T(Other)
16
15
14
13
12
11
10
9
9
10
11
12
13
14
15
16

Fig.8a

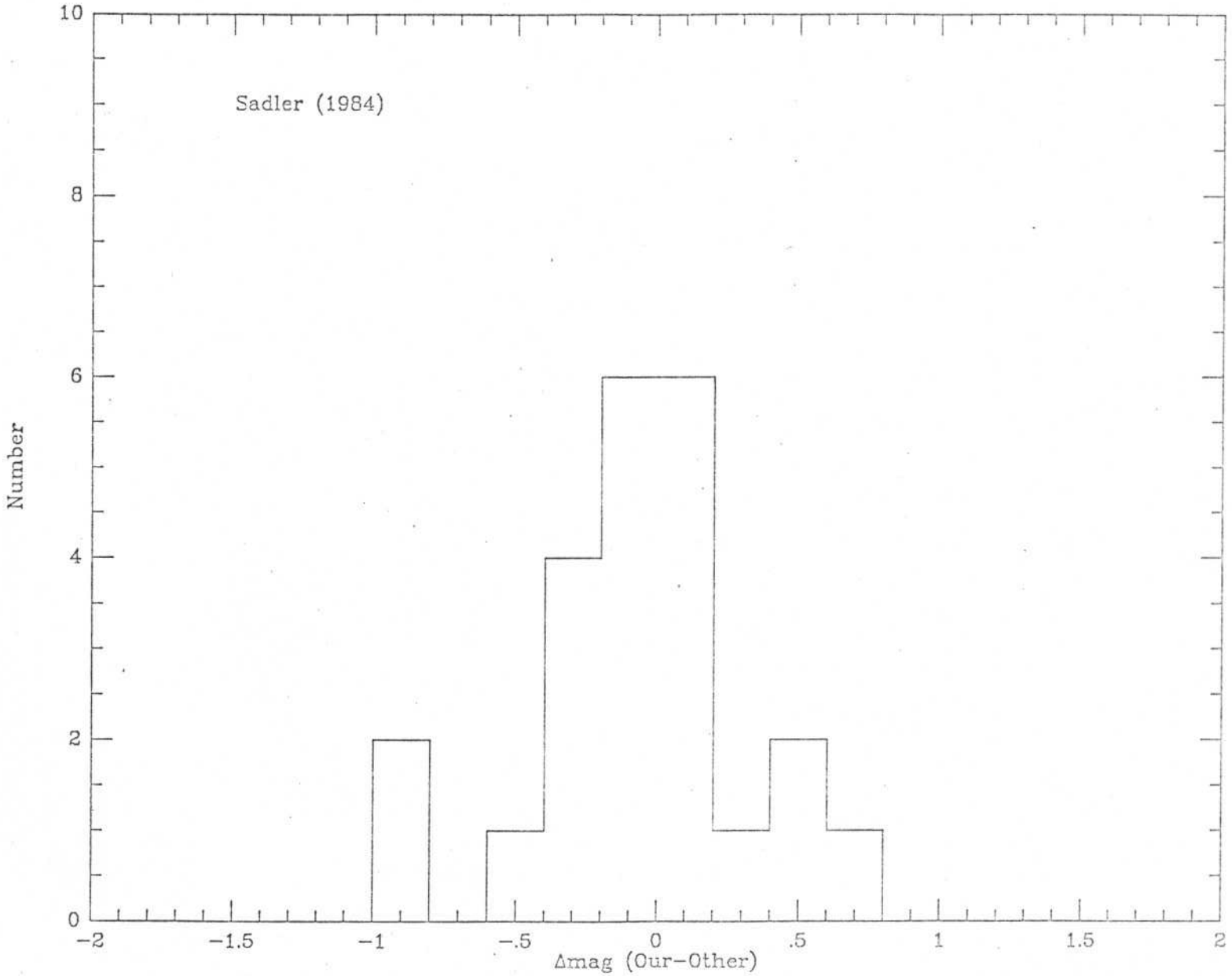

Fig.8b

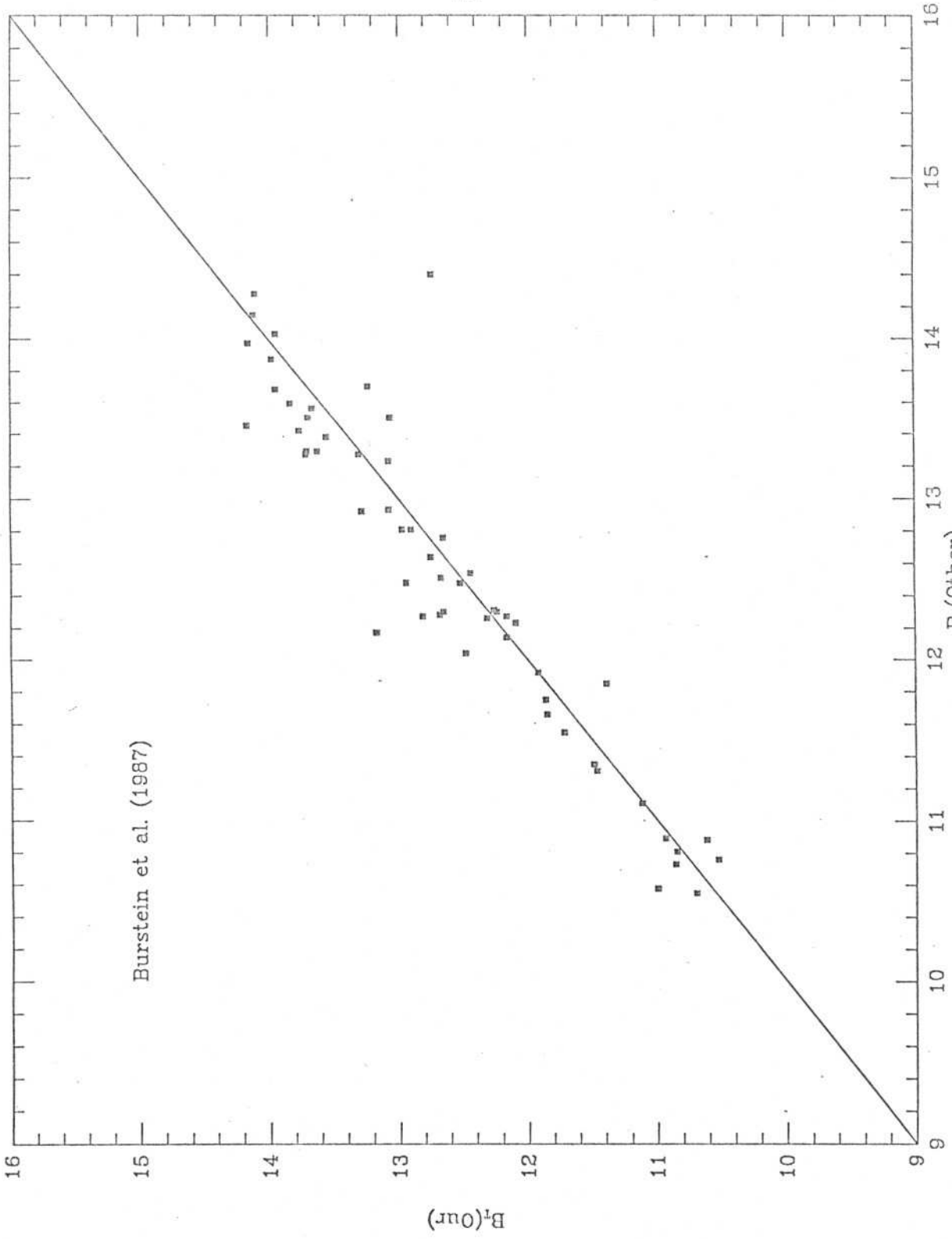

Fig.9a

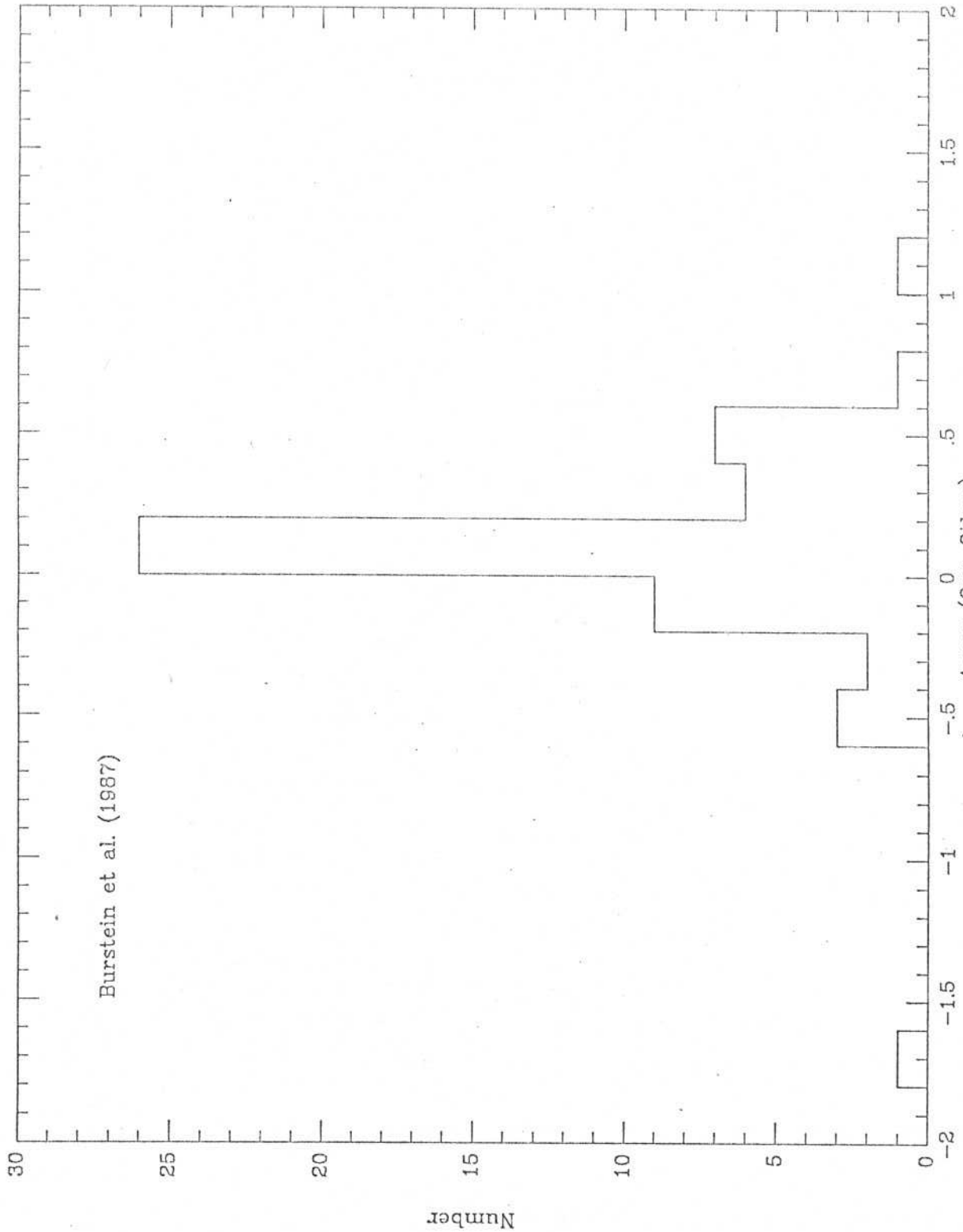
Burstein et al. (1987)
Number
30
25
20
15
10
5
0
-2
-1.5
-1
-.5
0
.5
1
1.5
2
Δmag (Our-Other)

Fig.9b

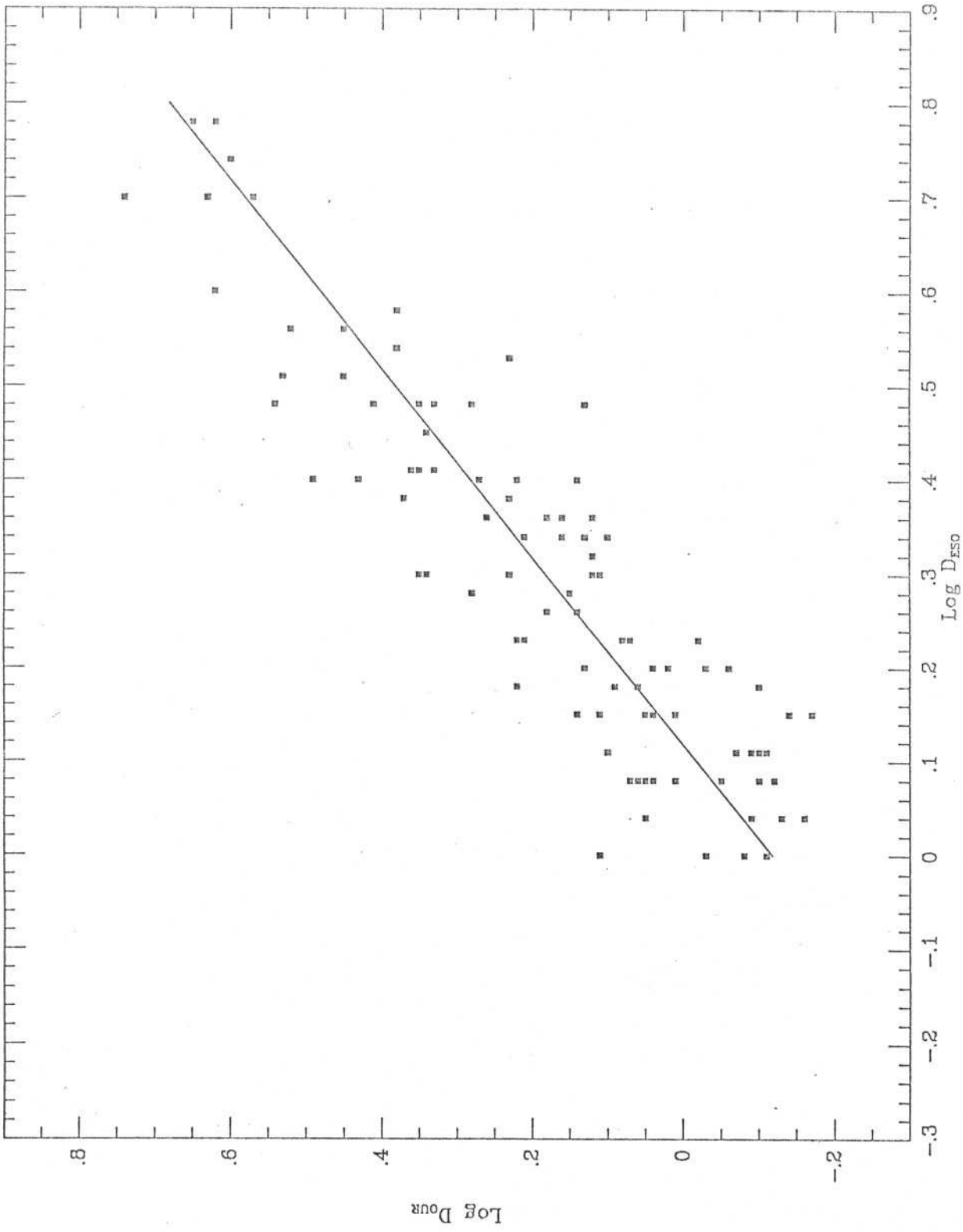

Fig.10a

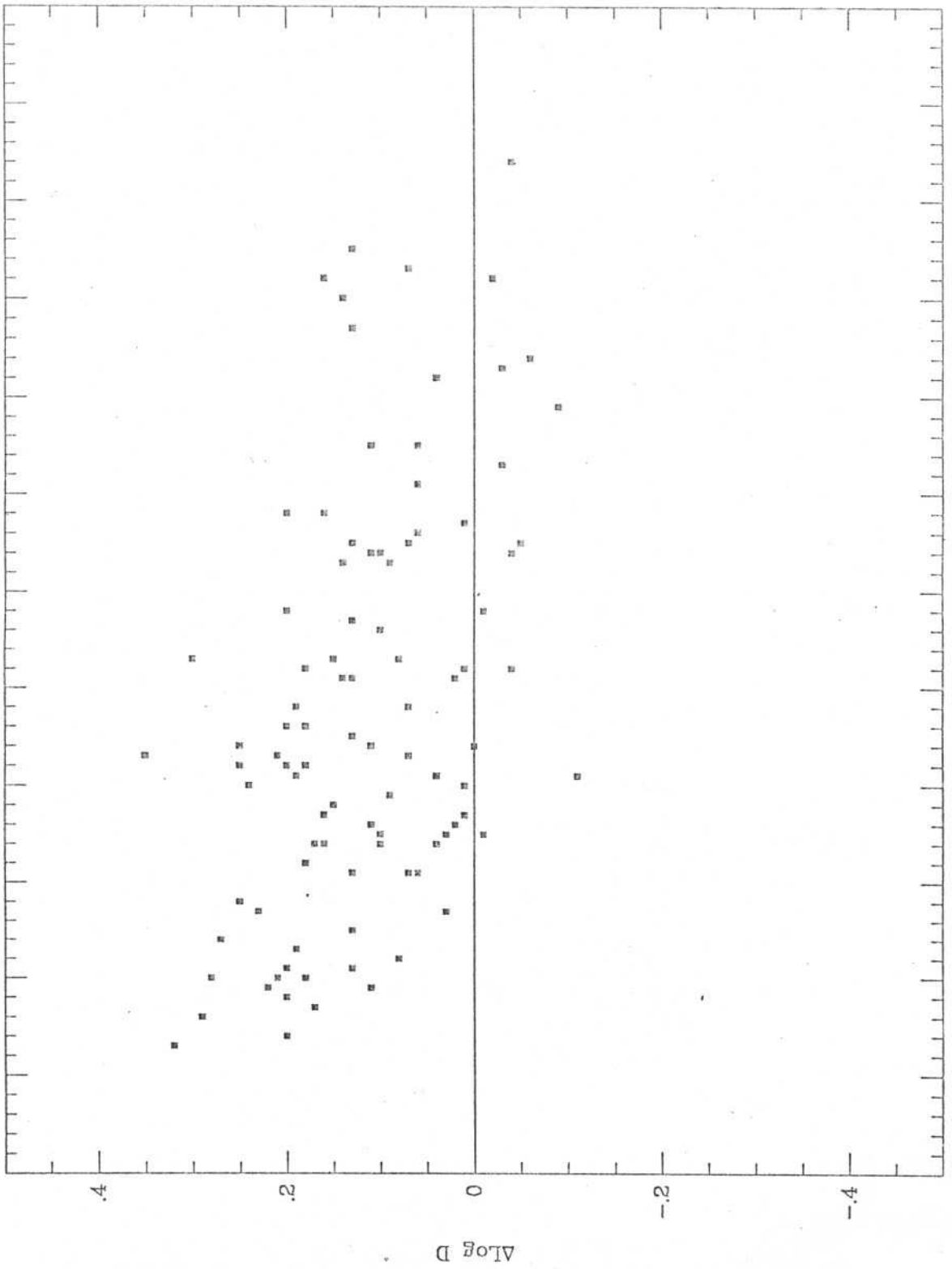

Fig.10b

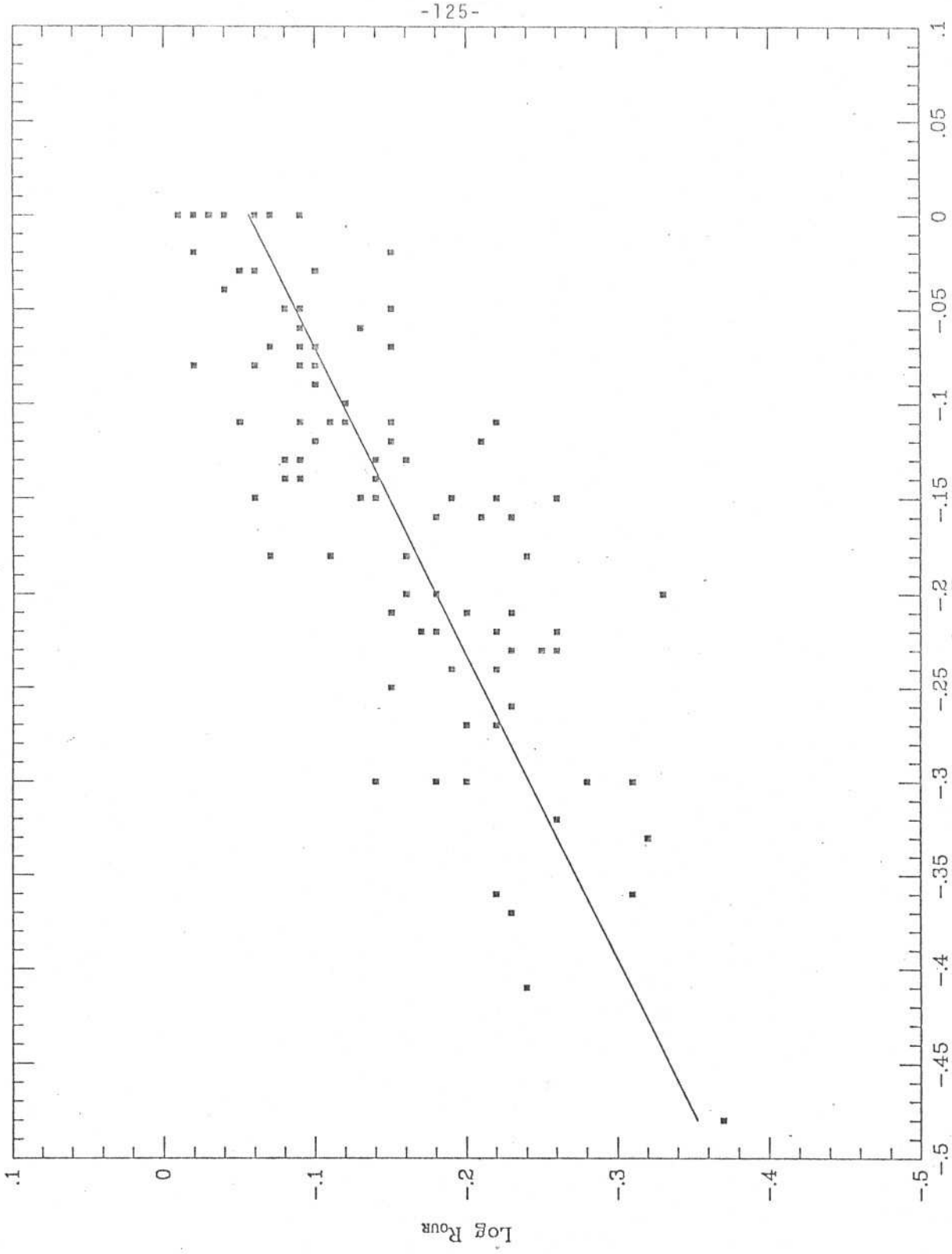

Fig.11a

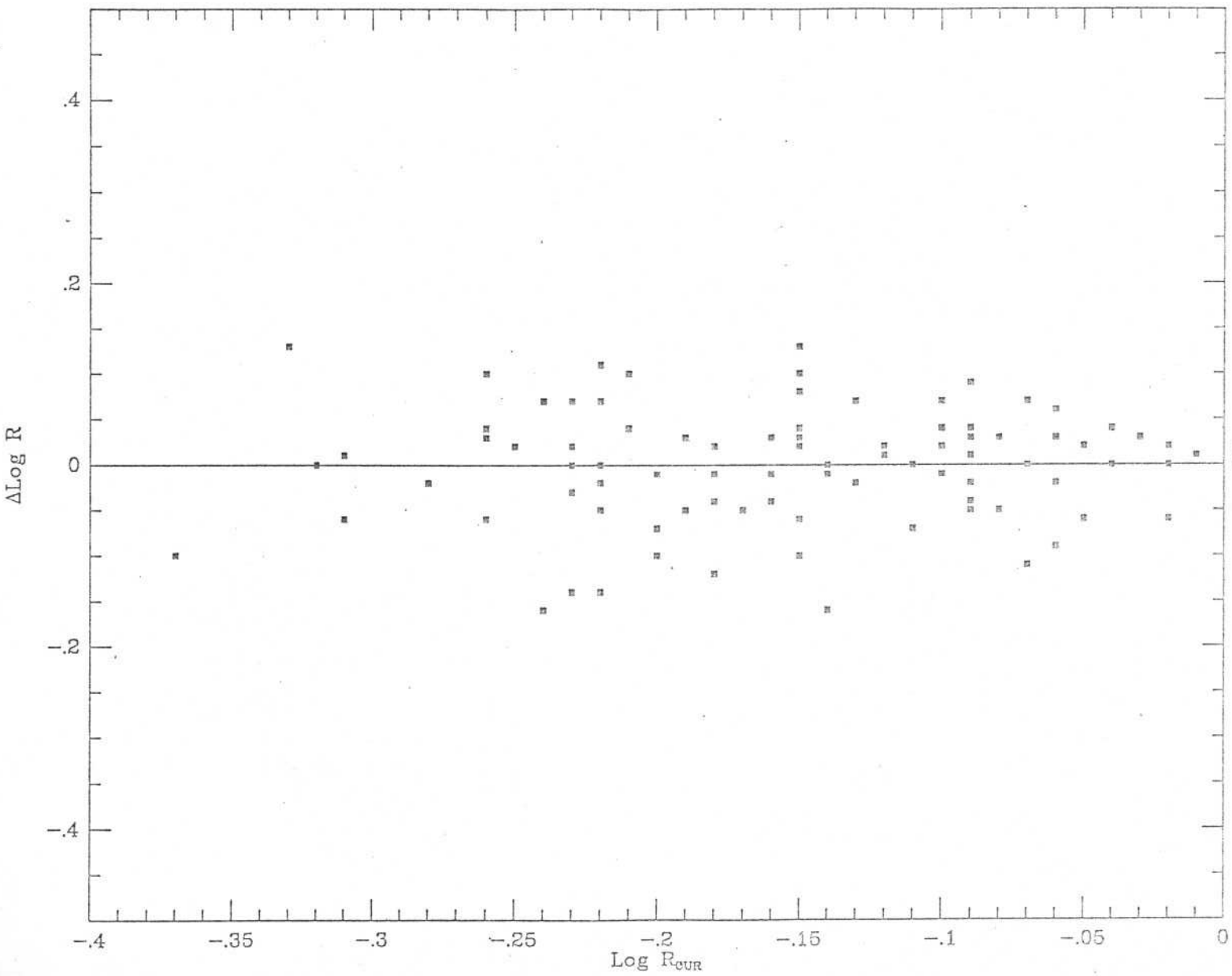

Fig.11b

V-Medidas de Velocidade de Dispersão de Galáxias Elípticas no Hemisfério Sul

Recentemente, Dressler et al. (1987) e Djorgovski e Davis (1987) mostraram que as galáxias elípticas formam uma família que descreve um plano no espaço dos parâmetros raio característico (ou luminosidade), brilho superficial e velocidade de dispersão. Esta relação entre quantidades dependentes e independentes da distância pode ser usado como um indicador de distância de galáxias elípticas tão preciso quanto a relação Tully-Fisher para espirais. Este indicador foi utilizado por Dressler et al. (1987) que em sua análise do campo de velocidades peculiares encontrou evidências de que a matéria dentro de 6000 km s^{-1} possui um movimento uniforme de $\approx$ 600 km s^{-1} com relação ao sistema de referência da radiação de fundo. Lynden-Bell et al. (1988), analisando o mesmo conjunto de dados também constatou a existência de um fluxo direcionado. No entanto, propos que uma melhor descrição do campo de velocidades é obtida quando se considera a existência de uma concentração de massa na posição de l=307° e b=9°. Uma vez que a existência de movimentos peculiares desta magnitude tem importantes implicações para as teorias sobre a origem de estruturas em grande escala, torna-se fundamental a confirmação destes resultados utilizando-se uma base de dados independente.

Com este objetivo, os espectros de 193 galáxias "early-type" foram obtidos como parte do levantamento de velocidades radiais realizado no Observatório Nacional por da Costa et al. (1988). Embora o objetivo principal deste levantamento tenha sido a obtenção de velocidades radiais

das galáxias, os espectros para as galáxias "early-type" são, em geral, de boa qualidade permitindo medidas de velocidade de dispersão bastante precisas.

Neste capítulo é apresentada uma análise da qualidade destes dados comparando-os com medidas feitas com outros autores (Tonry e Davis 1981, Whitmore et al. 1985, Davies et al. 1987, Davis et al. 1988). Esta comparação confirma que as nossas medidas de dispersão são precisas com um êrro externo da ordem de 30 km/s e uma êrro de ponto-zero menor do que 25 km s^{-1}.

Os dados obtidos neste capítulo são usados em conjunto com os dados fotométricos do capítulo IV para investigar as propriedades das galáxias elípticas e para investigar o campo de velocidades peculiares na região da calota polar do hemisfério sul coberta pelo SSRS.

I. INTRODUCTION

We have recently completed the Southern Sky Redshift Survey (SSRS), a wide-angle redshift survey of a diameter-limited sample in the southern galactic cap (da Costa et al. 1988). Since the primary goal of this survey was to measure redshifts, we generally integrated only long enough so as to accumulate low signal to noise spectra, except for early-type galaxies for which we were also interested in determining central velocity dispersions. For these, we have obtained better quality spectra making it possible to derive accurate dispersions. These velocity dispersion measurements, in conjuction with photometric data, are essential for the study of the intrinsic properties of early-type galaxies. Moreover, as recently demonstrated by Dressler et al. (1987) and Djorgovski and Davis (1987), these data can also be used to establish a distance indicator for elliptical galaxies which has an accuracy comparable to the IR Tully-Fisher relation for spirals.

Previous studies of the local large-scale velocity field using ellipticals, were based primarily on the well-know $L \propto \sigma^4$ relation, established by Faber and Jackson (1976), to determine their relative distances (e.g. Tonry and Davis 1981). However, as pointed out by several authors in the past (e.g. Terlevich et al. 1981, Tonry and Davis 1981) the scatter in this relation is larger than would be expected from the individual measurement errors and several attempts were made to identify the presence of "hidden parameters" that could account for the residual scatter. Recently, Dressler et al. (1987) and Djorgovski and Davis (1987) showed that the extra scatter was related to the surface brightness,

demonstrating that the family of ellipticals describe a plane in the parameter space of radius (luminosity), surface brightness and velocity dispersion. More important, these authors also showed that the resulting relationship between distance-dependent and independent observables had considerably less scatter than the Faber-Jackson relation, thus providing a much more reliable distance indicator, and consequently an important tool to investigate the velocity field.

Although the parametrization of the fundamental plane of the ellipticals obtained by Dressler et al. (1987) and Djorgovski and Davis (1987) agree quite well (e.g. Dressler et al. 1987), the use of this distance indicator has led to quite striking results concerning the peculiar velocity field. In particular, a preliminary analysis of the data from an all-sky survey of elliptical galaxies led Dressler et al. (1987) to the interpretation that matter within a radius of 6000 km/s would have a uniform bulk motion of about 600 km/s with respect to the microwave background. More recently, Lynden-Bell et al. (1988) have argued that a better fit to the data can be obtained by postulating the existence of a large mass concentration hidden by the galactic plane at l=307°, b=9°. Since these results can impose severe constraints on the theoretical models for the origin of large-scale structures, it is of interest to confirm these findings using an independent database.

As a first step toward this end, in this paper we present the results of spectroscopic observations of a subset of early-type galaxies drawn from the SSRS sample, as well as galaxies used for comparison of our observations with those of other observers. In section II, we briefly

describe the galaxy sample, the observations and the reduction procedure. In section III, we compare our velocity dispersion measurements with those of other authors, while in section IV we summarize our main results and outline future work.

II. OBSERVATIONS AND REDUCTION

In our survey we have measured velocity dispersions for 193 elliptical and SO galaxies, with morphological T types in the range $-5 \leq T \leq -2$, according to the notation adopted by Lauberts (1982). These objects form a subset of the early-type galaxies in the diameter-limited sample utilized in the SSRS. The SSRS sample contains a total of 68 E and 275 S0 galaxies, south of declination -17.5° and below galactic latitude -30°. During the survey, at the Observatorio Nacional (ON) we measured 43 E and 150 SO, but for some of these ellipticals velocity dispersions have recently become available from the work of Davies et al. (1987). Additional velocity dispersions for elliptical and S0 galaxies were also obtained from observations conducted at the Las Campanas Observatory as part of the SSRS effort and some of those are in common with our subset. A cross-comparison between these different data sets is presented in the next section.

The observations were made using a Cassegrain spectrograph and an intensified photon-counting Reticon detector mounted on the 1.60 m telescope operated by the ON. The observations were carried out through a pair of 3x12 arcsec entrance apertures, separated by 30 arcsec on the sky for simultaneous object and sky exposures. We have used a 900 line/mm grating, giving a dispersion of about 100 Å and a typical resolution of 5.0 Å (≈270 km s^{-1}). The wavelength coverage was from about 4700 Å to 7100 Å. For early-type galaxies we typically accumulated over 10^5 net counts, with most observations being comparable in quality to those obtained by Tonry and Davis (1981, hereafter TD)

using a similar system.

The determination of the velocity dispersion was based on the technique developed by Tonry and Davis (1979), which uses the correlation function's peak width obtained from the cross-correlation of a galaxy spectrum against a stellar template. The calibration of the relation velocity dispersion-correlation peak width is obtained using two sets of stellar templates. One of them is convolved with Gaussians of known width, and the resulting peak width, obtained by cross-correlation with the other stellar template, is used to derive the curve that relates it to the known dispersion. Each template was generated by shifting to zero redshift and adding together 11 high signal-to-noise spectra of K giant stars. A detailed discussion of the method and error analysis can be found in Tonry and Davis (1979).

III. RESULTS

In this section we discuss the quality of our data by comparing our central velocity dispersion measurements with those available in the literature. For that purpose we have compared our measurements with those of TD, the compilation made by Whitmore et al. (1985, hereafter WMT) and the recent measurements of Davies et al. (1987). We have also compared our velocity dispersions with unpublished results of observations carried out at the LCO (Davis et al. 1988). Galaxies used in these comparisons are listed in table I, including those from the SSRS sample for which there are published measurements. In this table we give: in column (1) the galaxy's name, ordered by their NGC, IC or ESO number; in column (2) our velocity dispersion, and in columns (3)-(5) the values listed by TD, WMT and Davies et al. (1987), respectively. A table containing our new observations will be presented elsewhere.

In figure 1 we examine how our estimated internal errors compare with those obtained by TD, showing the histograms of the errors associated with our measurements and those of TD for the 31 ellipticals in common. From this figure we see that the distributions of error are similar, with comparable median errors of the order of 25 km s^{-1}. In addition, examining our internal errors as a function of the velocity dispersion we find that they increase dramatically for dispersion values less than 100 km s^{-1}, leading to unreliable measurements.

We show in figures 2 and 3 the cross-comparison between the different

data sets mentioned above, considering first only the elliptical galaxies. In figure 2 we plot σ_{other} x σ_{our}, indicating in each panel the source of the data being compared; error bars are also shown, whenever available. In panel (b) the data points with error bars correspond to the subset of galaxies which WMT recommend to be used as standards. In figure 3 we show the same data by plotting the quantity $\Delta\log\sigma = (\log\sigma_{other} - \log\sigma_{our})$ versus $\log\sigma_{our}$. Examining these figures we find that there is a fairly good agreement between our measurements and those of TD and WMT. We note that the latter two are not completely independent samples since the WMT catalog includes the TD data. Nevertheless, we show them separately because WMT give, whenever available, the weighted average of dispersion measurements of different observers, corrected to a standard aperture. The comparison is particularly good with the standards of WMT, over the entire velocity dispersion domain, showing no systematic deviations. Note that the errors of the individual measurements are also comparable, indicating the good quality of our data (figure 2).

In contrast, the comparison with Davies et al. (1987) shows a significant departure from the 45° line, with our velocities being systematically larger than those measured by Davies et al., especially for $\sigma > 250$ km s^{-1}. We note that in the plots we have used our raw values while the dispersions of Davies et al. were corrected for distance effects. However, this correction is small and cannot account for the observed trend, since the use of a fixed aperture would tend to lower the velocity dispersions for the bright distant galaxies, which are expected to have the highest velocity dispersions. Finally, since the number of ellipticals

in common with the LCO sample is too small, we cannot draw any firm conclusion from the comparison with our measurements, except that there are no significant discrepancies.

In figures 4 and 5 we compare our velocity dispersion measurements for the S0 galaxies with those of other observers, except Davies et al. (1987) who only give dispersion values for elliptical galaxies. From these comparisons we find that the measurements of different observers show good agreement and no indication of systematic deviations. This is also true for the S0 galaxies in common with LCO, with which we have a much larger overlap than in the case of the ellipticals. There is, however, in all comparisons a noticeable increase in the scatter as compared to that observed for the elliptical galaxies.

The results of these comparisons are summarized in table II, where we list the median zero-point shift and the rms of $\Delta\log\sigma$, and the number of objects used in each comparison. When computing these quantities, we have discarded galaxies with $\sigma < 100$ km s^{-1}. From table II, we find that the offsets between the different data sets of ellipticals are, in general, comparable to those obtained by Davies et al. (1987) in their comparison of the observations made at different telescopes. We calculate that the error in the zero-point for the ellipticals is less than 25 km s^{-1}; while we compare quite well with the WMT standards (3 km s^{-1}), the comparison with Davies et al. yields the largest offset. The rms scatter derived from the different comparisons varies from 35 to 60 km s^{-1}, consistent with what would be expected from the comparison of data sets with similar internal errors and in the range of 25 to 40 km s^{-1}. Cross-

comparison of the S0 galaxies yields similar values for the zero-point offset and rms dispersion, except the LCO data with which we find a median shift of about -53 km s^{-1}, with respect to our measurements.

IV SUMMARY

We have measured velocity dispersions for 43 elliptical and 150 S0 galaxies. Comparison with published results indicates that our dispersion measurements are accurate and that the overall error established from these external comparisons is consistent with our internal error estimates. Our data is particularly good when compared to the standards of WMT. On the other hand, comparison with the data of Davies et al. (1987) shows some evidence for systematic discrepancies at the high-velocity end. As pointed out above, the observed behavior is not related to distance effects, since it goes in the opposite sense from what would be expected. The possible implications of this effect in estimating distances of galaxies, and consequently in deriving peculiar velocities, should be examined in more detail.

With the present data we intend to analyze the intrinsic properties of ellipticals and S0's. Toward this end, we have recently completed a photometric survey of the elliptical galaxies in the region of the SSRS and we are currently finishing a similar survey of the S0 galaxies. These new photometric and spectroscopic data will be used: 1) to reexamine the fundamental plane of ellipticals using independent data and a sample of galaxies in the southern hemisphere which is probably less affected by the uncertainties associated to the flow model adopted for Virgo; 2) to examine the fundamental plane of S0 galaxies from an enlarged database and outside the cores of rich clusters, complementing the recent work of Dressler (1987); 3) to probe the dynamics of the large-scale structures observed in the volume of space surveyed by the SSRS, using the early-

type galaxies of the sample.

ACKNOWLEDGMENTS

We thank all the people involved in the our redshift survey effort which provided the data presented here. We would also like to thank the assistance of J. Tonry in helping us utilize some of his analysis routines. We would also like to thank C. Willmer for reading the manuscript.

Table I - Published Velocity Dispersions

Name	Our	TD	WMT	Davies et al.
NGC 179	378			241
312	230			255
430	383	320	314	
545	241	255	307	226
547	255	295	322	173
641	257			252
686	210			159
822	219			157
936	249	233	193	
1016	312	306	301	
1132	321	253	248	
1201	226	170	167	
1209	318	250	258	219
1289	174	80	78	
1298	351	181	178	
1316	230		252	
1339	147			169
1351	183			151
1381	189		169	
1400	214	270	269	262
1403	182			167
1407	298	285	274	299
1426	166	177	157	151
1521	210	216	212	229
1537	243			167
1700	310	241	234	
3115	303		247	
3309	274			274
3379	201	214	218	212
3412	144	126	107	
3557	340		220	302
4374	317	319	296	
4406	221	267	256	
4472	354	316	315	
4486	365	348	335	

Table I- Cont.

Name	Our	TD	WMT	Davies et al.
4782	338	392	385	
5576	177	196	192	
5761	301			186
5770	120	127	124	
5791	289			200
5813	211	210	231	249
5831	180	211	171	
5839	219	138	135	
5845	233	203	244	
5846	278	246	250	
5865	203	248	244	
5903	326			245
6721	313			253
6851	229			187
6868	320			296
6909	147			153
6958	247			227
7002	370			247
7014	371			267
7075	450			256
7173	160			220
7176	305			228
7236	198	257	252	
7237	270	225	221	
7377	213	169	166	
7391	265	308	303	282
7458	225	150	147	
7506	178	154	151	
7507	234	220	205	250
7562	230	333	288	
7612	152	203	199	
7619	255	285	330	
7626	255	222	270	
7711	195	188	184	
7778	325	214	210	

Table I- Cont.

Name		Our	TD	WMT	Davies et al.
	7785	306	240	241	299
IC	1625	346			257
	2006	146			129
	4296	353			332
	5362	320			217
ESO	185G27	185			175
	286G59	341			252
	384G49	255			176
	409G12	283			189
	467G54	275			249
	552G52	157			179

Table II- Comparison of the measurements of σ

Source	median	r.m.s.	Number
	Ellipticals		
WMT	-0.033	0.098	31
Davies et al	-0.047	0.091	46
TD	-0.019	0.107	31
WMT (Standard)	0.004	0.057	11
LCO	-0.003	0.113	9
	S0's		
TD	-0.022	0.122	15
WMT	-0.060	0.121	18
LCO	-0.080	0.124	19

REFERENCES

da Costa, L.N., Pellegrini, P.S., Sargent, W.L.W., Tonry, J., Davis, M., Meiksin, A., and Latham, D. 1988, Ap. J. in press

Davis, M. et al. 1988, private communication.

Davies, R.L., Burstein, D., Dressler, A., Faber, S.M., Lynden-Bell, D., Terlevich, R., and Wegner, G. 1987, Ap. J. Suppl., 64, 581.

Djorgovski, S., and Davis, M. 1987, Ap. J., 313, 59.

Dressler, A., Lynden-Bell, D., Burstein, D., Davies, R.L., Faber, S.M., Terlevich, R., and Wegner, G. 1987, Ap. J., 313, 42.

Faber, S.M., and Jackson, R.E. 1976, Ap. J., 204, 668.

Lauberts, A. 1982, The ESO/Uppsala Survey of the ESO (B) Atlas, European Southern Observatory.

Lynden-Bell, D., Faber, S.M., Burstein, D., Davies, R.L., Dressler, A., Terlevich, R., and Wegner, G. 1987, preprint.

Tonry, J.L., and Davis, M. 1979, A. J., 84, 1511.

Tonry, J.L., and Davis, M. 1981, Ap. J., 246, 666.

Whitmore, B., McElroy, D., and Tonry, J.L. 1985, Ap. J. Suppl., 59, 1.

Figure Captions

Figure 1- Comparison of the distributions of errors of our measurements (dashed line) and those of TD (solid line) for the 31 elliptical galaxies in common.

Figure 2- Comparison of our measured central velocity dispersions of elliptical galaxies and those of the other authors, as indicated in each panel. Whenever available, we also show the error bar associated with each measurement. In panel (b) those objects with error bars form a subset of standards of WMT.

Figure 3- The differences between the logarithms of our velocity dispersions and those of other authors, plotted against our value of the velocity dispersion. The objects are the same as those plotted in figure 2.

Figure 4- Same as figure 2 for S0 galaxies.

Figure 5- Same as figure 3 for S0 galaxies.

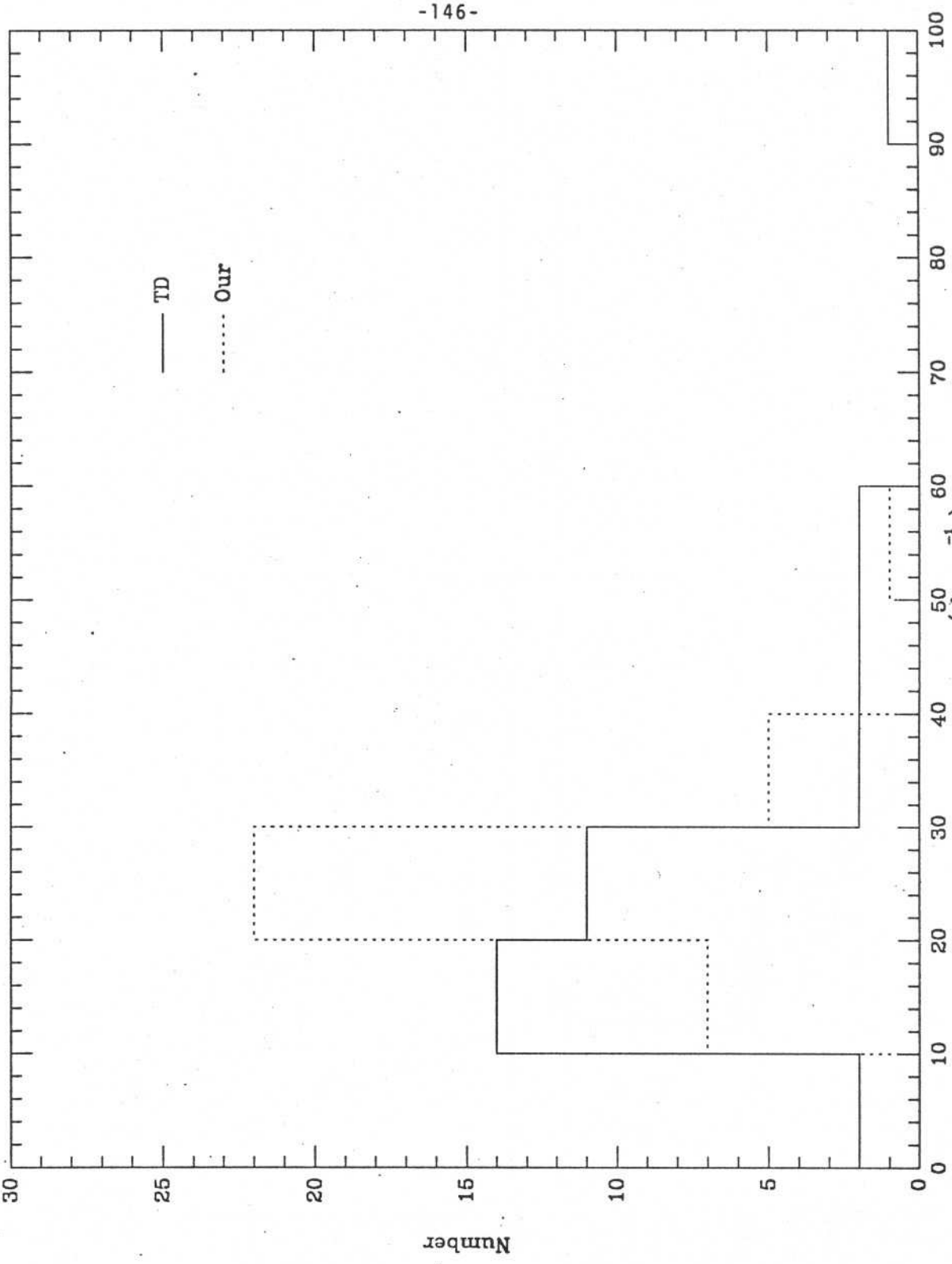
TD
Our
Number
error (km s^{-1})
0
5
10
15
20
25
30
0
10
20
30
40
50
60
70
80
90
100

Fig.1

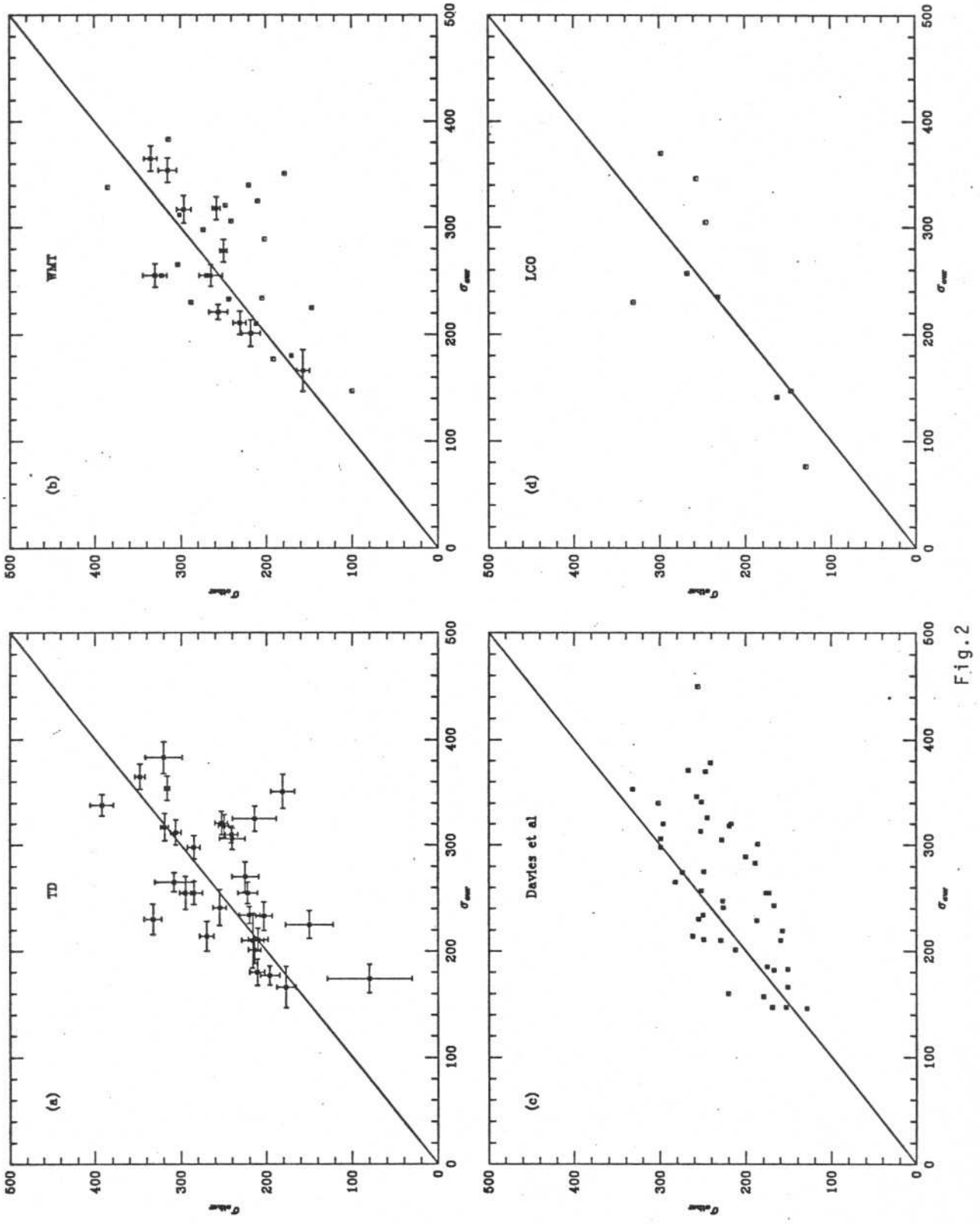

Fig.2

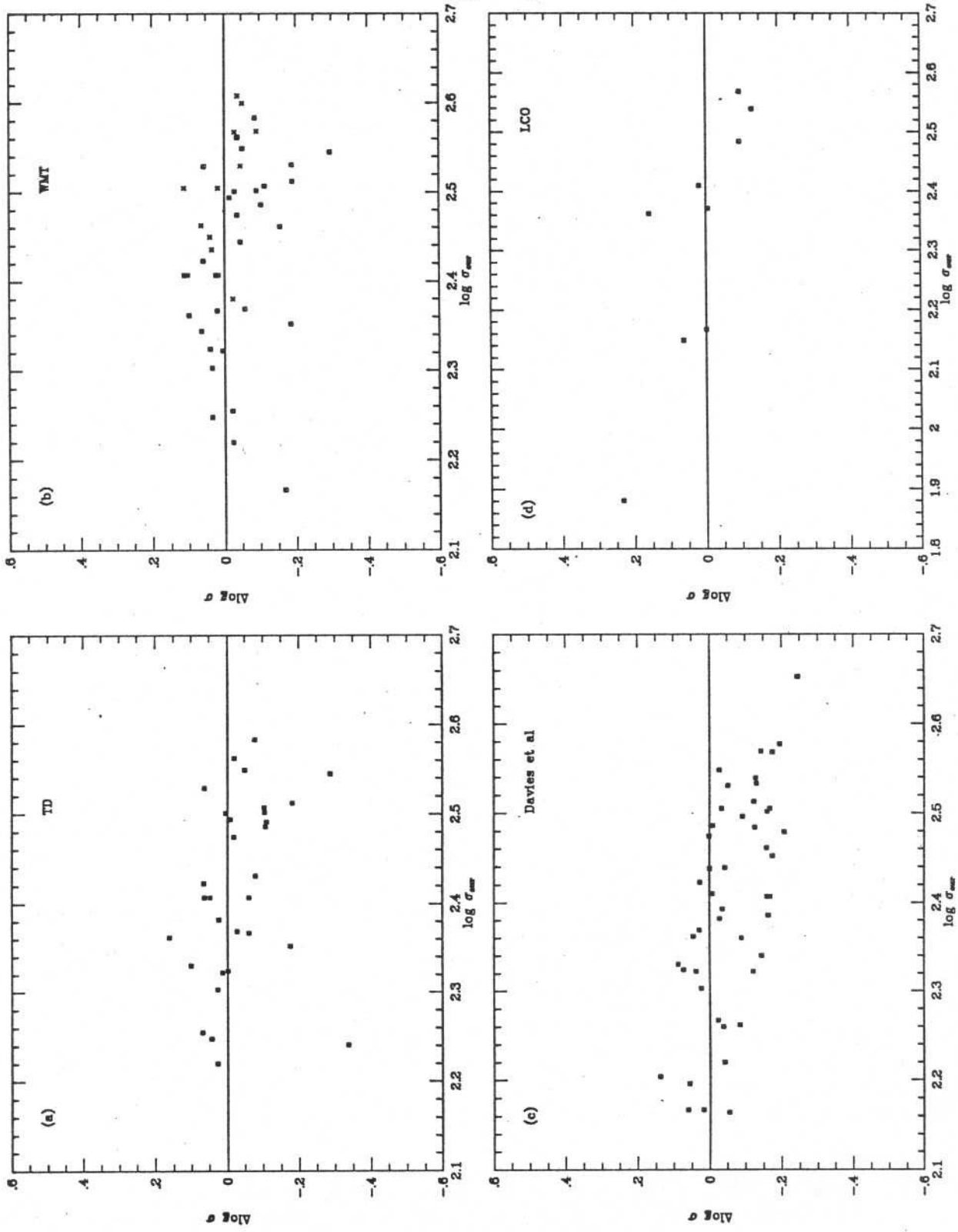

Fig.3

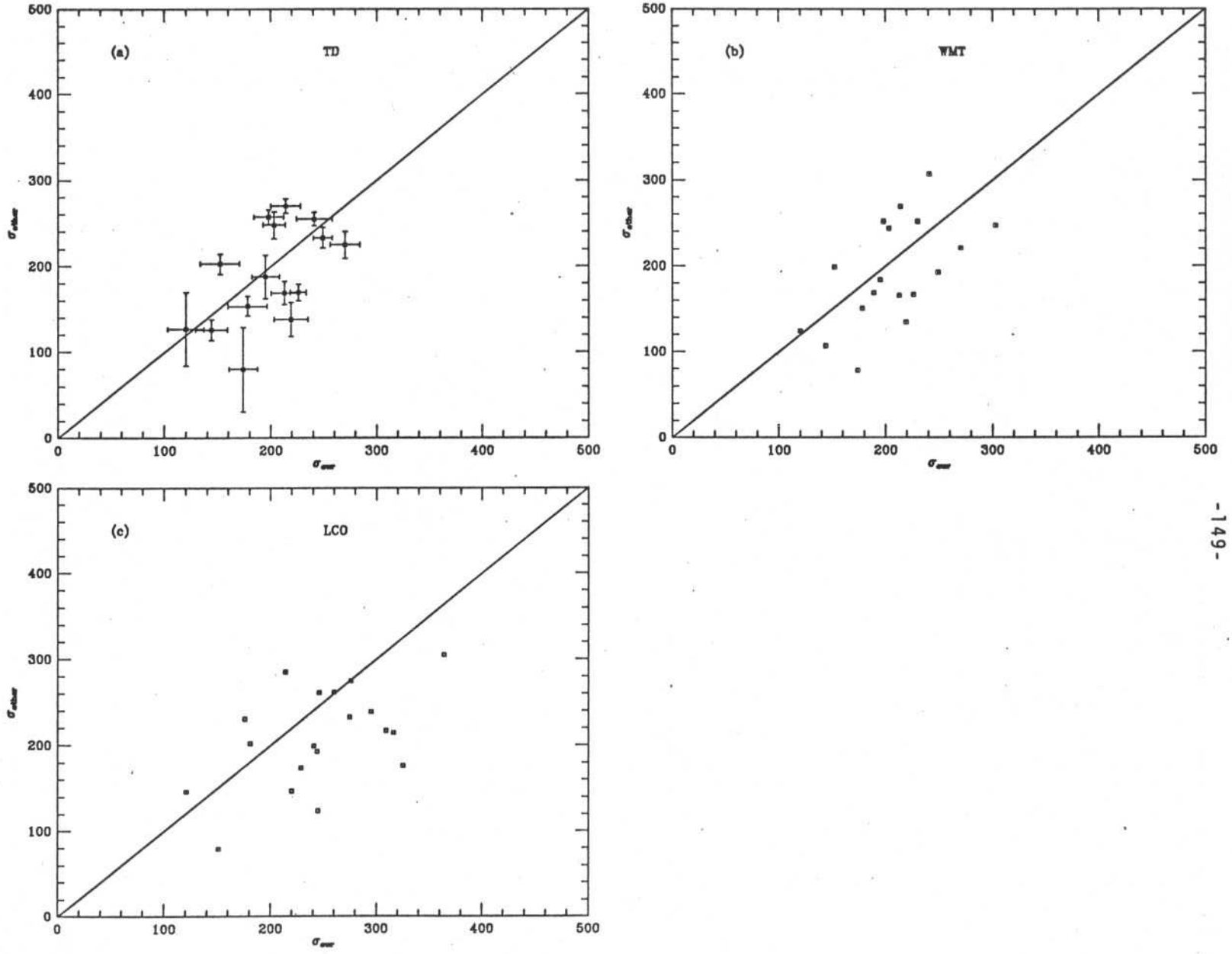

Fig.4

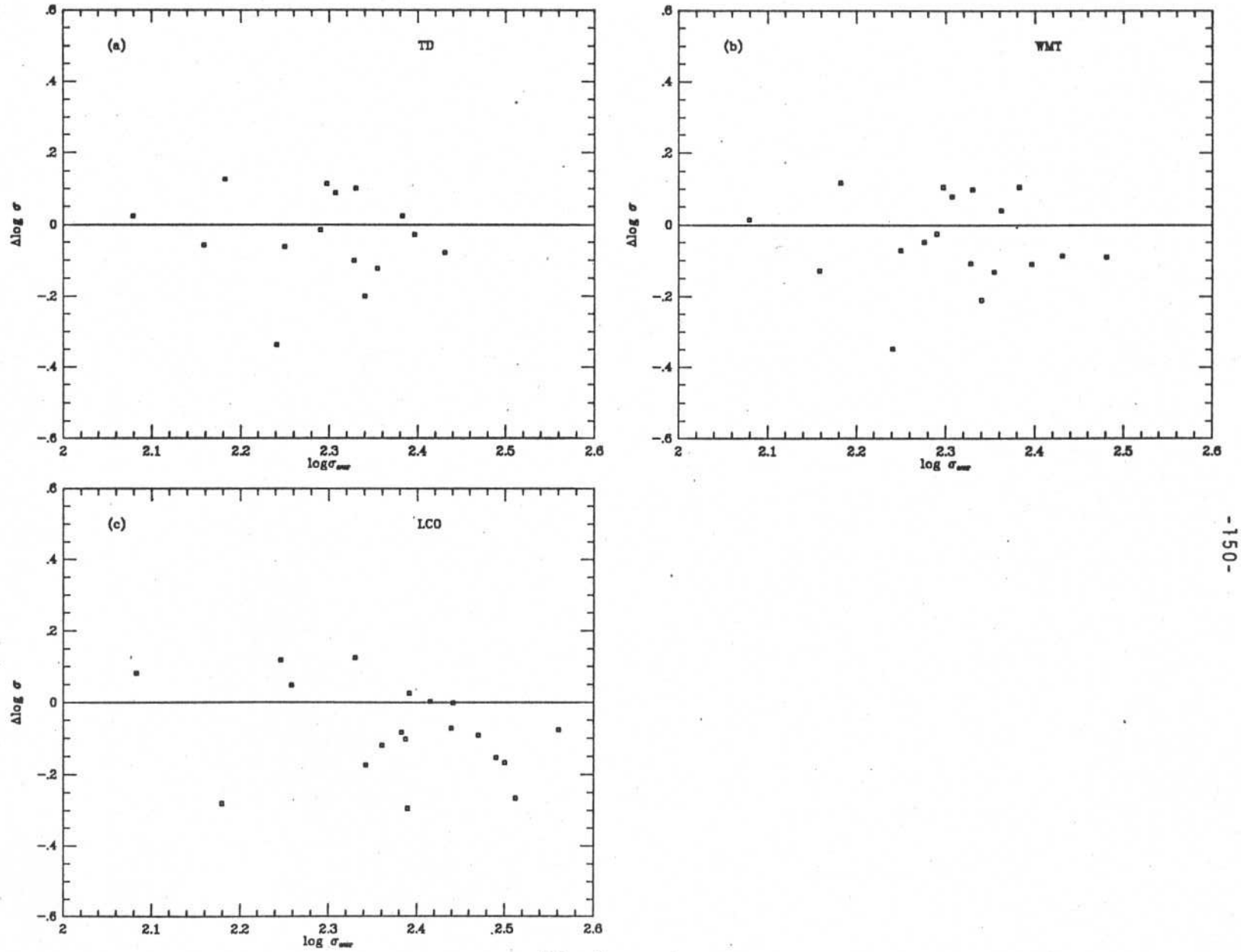

Fig.5

VI- Estudo do Campo de Velocidade Peculiar

O estudo das propriedades estruturais das galáxias elípticas tem tido um grande desenvolvimento, nos últimos anos, com o acúmulo de observações espectrocópicas e fotométricas de boa qualidade. Em particular, Dressler et al. (1987) e Djorgovski e Davis (1987) mostraram que as galáxias elípticas formam uma família de dois parâmetros e que o espalhamento em torno da relação entre raio, brilho superficial e velocidade de dispersão e pequeno, sendo completamente explicado pelos erros de medida dos parâmetros envolvidos. No entanto, o uso desta relação como indicador de distância tem levado a resultados surpreendentes no que se refere ao campo de velocidade peculiar e revela a necessidade de uma confirmação independente destes resultados.

No capítulo VI, a equação que define o plano fundamental das galáxias elípticas é examinada, usando os novos dados fotométricos e espectroscópicos apresentados nos capítulos IV e V, respectivamente. A extensão deste estudo para o hemisfério sul é importante devido a pequena influência que as contribuições de Virgo e do grande atrator, proposto por Lynden-Bell et al. (1988), exercem sobre as galáxias nesta região. O campo de velocidade peculiar na região do hemisfério sul é examinado, sendo dada uma atenção especial às velocidade residuais obtidas após a subtração do movimento produzido por Virgo e o grande atrator.

I. INTRODUCTION

Recent work by Dressler et al. (1987a) and by Djorgovski and Davis (1987) on the properties of elliptical galaxies have shown that these objects form a two-parameter family which describes a plane in the parameter space defined by the size (luminosity), central velocity dispersion and surface brightness. These works have thus resolved the long-standing problem of identifying the "hidden parameter" that could explain the residual scatter in the relation $L \propto \sigma^4$ not accountable by the measurement errors. These authors have also demonstrated that by considering the surface brightness, one obtains a very tight relation between the distance-dependent variable and a linear combination of distance-independent quantities, thus providing a distance indicator, much superior to the traditional Faber-Jackson relation (Faber and Jackson 1976). These new developments have not only provided a better understanding of the internal structure of ellipticals but also an important tool for investigating the large-scale peculiar velocity field.

Dressler et al. (1987a) have determined the "fundamental plane" of ellipticals based on a sample of galaxies in clusters, which avoids the need of specifying a particular model of the local velocity field. On the other hand, Djorgovski and Davis (1987) have used a sample of galaxies in the general field, solving simultaneously for the parameters of the fundamental plane and the Local Group infall velocity toward the Virgo cluster. In spite of differences in the data and in the method of analysis, these studies derived very similar relations between the characteristic radius of the galaxy and its velocity dispersion and surface

brightness.

The use of this relation as a distance indicator has led Dressler et al. (1987b) and Lynden-Bell et al. (1988) to striking results concerning the large-scale motions of our surroundings which either indicate a uniform bulk motion of matter within at least 6000 km/s or the presence of a large concentration of mass at l=307° and b=9° at a distance of 4350 km/s. Since these results can impose severe constraints on the theories for the origin of structures in the Universe, it is important to confirm them using not only additional independent data but also examining the behavior of the distance-indicator relation in different environments and directions of the sky.

In this paper we derive the fundamental plane of elliptical galaxies using new photometric and spectroscopic data reported by de Carvalho and da Costa (1988, paper I) and da Costa et al. (1988b, paper II), respectively, for a subset of ellipticals from the diameter-limited sample used in the Southern Sky Redshift Survey (SSRS, da Costa et al. 1988a). In section II, we describe the sample used in this study and the method of analysis, while in section III we present the solutions obtained under different assumptions. In section IV, we discuss in detail the application of these relations to estime relative distances to ellipticals, comparing them to those obtained by Lynden-Bell et al. (1988). Using our best distance indicator, we calculate the peculiar radial velocity of ellipticals and investigate the nature of the velocity field. A discussion of our main results is presented in section V.

II. DATA SET AND METHOD

The SSRS sample consists of 68 elliptical galaxies south of declination -17.5° and below galactic latitude of -30°, for 52 of which we have derived reliable photometric parameters in paper I. Measurements of central velocity dispersions are available for 56 galaxies: 43 observed at the Observatorio Nacional (ON) and 41 available in the literature (e.g. Davies et al. 1987). In the region covered by the SSRS, 16 are new velocity dispersions reported in paper II, while 26 galaxies are in common with Davies et al. (1987) data set.

Cconsidering our velocity dispersion measurements alone, we are left with 36 galaxies for which we have reliable photometry and spectroscopic data, 16 of which are the new measurements mentioned above. The sample is further reduced when we discard from the analysis galaxies with velocity dispersions less than 100 km/s (3 galaxies), for which the measurement errors are large (paper II), and those with recessional velocities greater than 8000 km/s (5 galaxies). We are thus left with 28 galaxies with a median radial velocity of 3075 km/s. In order to allow us to map the velocity field slightly better, we have added to our sample 10 galaxies, for which velocity dispersions are available from Davies et al. (1987). As discussed in paper II, cross-comparison of the overlapping sample indicates that there may be some systematic differences between the two data sets, especially at the high-velocity end. However, the inclusion of these 10 galaxies has essentially no effect in our results, probably because 9 of these galaxies have $\sigma < 250$ km/s. Therefore, in the analysis below we consider a total of 38 galaxies.

For each elliptical galaxy in our final sample, we correct the characteristic surface brightness $B_0(V)$, derived in paper I, for galactic extinction and K-dimming. The radial velocities were taken from the SSRS catalog and corrected to the rest frame of the local group (Yahil et al. 1977). Whenever a galaxy is in a group, we take its velocity to be the mean group velocity. The assignment of our ellipticals to groups were made utilizing the group catalog given by Maia et al. (1988), which identifies groups out to 10000 km/s based on the redshifts for the essentially complete diameter-limited sample of the SSRS.

The method employed here to determine the fundamental plane is the same as that used by Djorgovski and Davis (1987, hereafter DD). Here we only consider the relation between the characteristic radius, velocity dispersion and surface brightness, since as pointed out by DD, it is less affected by zero-point errors in the magnitude scale. We search for the linear combination of distance-independent parameters (surface brightness and velocity dispersion) which best correlates with the radius of the galaxy, as measured by the χ^2 value of the least-squares fit of the two quantities. We note that other statistics could be used to indicate the quality of the fit, such as the linear regression coefficient and the size of the predicted errors in galaxy distances (see below). Like DD, the least-squares routine we have used allows for errors in both coordinates which, as argued by these authors, minimizes the effects of a possible Malmquist bias.

III. INTERNAL PROPERTIES OF ELLIPTICALS

In this section we examine the parametrization of the fundamental plane, considering different Local Group infall velocities toward Virgo and the effects of including a mass concentration as advocated by Lynden-Bell et al. (1988). The results are given in table I where we list: in column (1) the solution number; in columns (2)-(4) the coefficients of the expression

$$\log r_e = a\,(\log\sigma + bB_0(V)) + c;$$

in column (5) the reduced χ^2 of the best fit; in column (6) the rms of log r_e residuals, which expresses the error in distance; in column (7) the final number of points used in the fit. In the above expression r_e is the de Vaucouleurs' radius, measured in parsecs, $B_0(V)$ is the surface brightness at this radius, and σ is the central velocity dispersion. Hereafter, we adopt $H_0 = 50$ km/s/Mpc.

Solutions for the fundamental plane were obtained considering the following cases: (1) no infall toward Virgo; (2) an infall velocity of 430 km/s of the Local Group toward Virgo (DD); (3) an infall velocity of 570 k/s of the Local Group toward a mass concentration at l=307°, b=9°, at a distance of 4350 km/s, and an infall velocity of 100 km/s toward Virgo (see Lynden-Bell et al. 1988). In contrast to Lynden-Bell et al., we adopt a Virgocentric flow model with the infall velocity varying as 1/r, but this should not affect our conclusions significantly since the contribution of Virgo is small. All the solutions were obtained by least-squares fitting the data, discarding points two standard deviations away

from the mean relation and repeating the fit for the remaining points. In all solutions the galaxies NGC 439 and NGC 7075 were discarded, the former probably due to errors in the determination of $B_0(V)$, and the latter because of errors in σ. We note that for NGC 7075 there is a large discrepancy between the dispersion values given in paper II and by Davies et al. (1987). The other galaxies discarded were: 107 G 4 in solution (2) and IC 5105 in solution (3).

The errors listed in table I indicate that the uncertainty in distance, using our distance-indicator relations is of about 30% per galaxy, slightly larger than that obtained by Dressler et al. (1987a). The amplitude of the scatter of log (r_e), denoted hereafter by Δ, is, nevertheless, consistent with that expected considering the mean errors of the variables used in the determination of the fundamental plane. The predicted errors in galaxy distances are larger, probably because of the larger uncertainties in our photometric parameters. We recall that in paper I we calculate these parameters by analyzing major-axis profiles, rather than integrating over the galaxy as done by Dressler et al. (1987a) and DD, and consequently are more uncertain. In figure 1 we show our data points and the best fits for the different cases considered above.

The following points are worth mentioning about the solutions presented in table I. First, the solutions are not very sensitive to the value adopted for the Local Group infall velocity toward Virgo, which could introduce errors in the distance-dependent quantities. As can be seen in table I, there is no improvement in either the χ^2 or Δ, over the plausible range of values of the Local Group infall velocity. Furthermore, the

coefficients of solutions (1) and (2) are similar and within the estimated errors. Second, the same holds true if we take into account the flow generated by the great attractor proposed by Lynden-Bell et al. (1988). These results indicate that the location of our sample is not adequate to investigate the Local Group motion; it has a limited sky coverage and lies in the direction opposite to Virgo, and roughly perpendicular to the direction of the great attractor. Conversely, a possible advantage of our sample is that it yields solutions for the fundamental plane that may be less sensitive to the assumed flow model and thus may better describe the properties of "field" ellipticals.

The errors of the coefficients of the equation for the fundamental plane are assumed to be the 1σ-uncertainty associated with the χ^2 statistics and are typically of the order of 10%. The parameters listed in table I indicate that the characteristic size of ellipticals varies with velocity dispersion and surface brightness according to the power-law $R \propto \sigma^{0.99-1.24}\ SB^{-(0.40-0.44)}$, where SB is the characteristic surface brightness in linear flux units. We note that the power coefficient of the velocity dispersion, although not exactly the same, is comparable to that determined by Dressler et al. (1987a) and DD. On the other hand, the dependence on surface brightness is quite different and cannot be ascribed only to errors in its determination (10%). Moreover, this effect is present regardless of the statistics used to define the quality of the fit since besides the reduced χ^2, we have also examined the behavior of the solutions using the dispersion of log radius residuals and the linear-regression coefficient. All these methods yield parameters which do not reproduce the power-law coefficient of the surface brightness term. One

possible explanation for this discrepancy could be that the quantity used here to measure the characteristic brightness is a local measure that is proportional to the mean surface brightness only if the luminosity profiles of ellipticals obey a pure $r^{1/4}$ law. Another possibility is that it could reflect real differences in the large-scale environment of the galaxies considered in these studies.

We note that, despite the incompleteness of the present sample, the domain in velocity dispersion and surface brightness covered by our data is comparable to those of DD, as shown in figure 2. As expected, there is no relation between these two distance-independent parameters and the errors for each variable are comparable to those of DD. Furthermore, the sampling of the parameter space is reasonably uniform, indicating that our photometric and spectroscopic data are adequate for the present study.

IV. THE FUNDAMENTAL PLANE AS A DISTANCE INDICATOR

a) Distance Estimates

The significant reduction of scatter in the relation betweeen distance-dependent and independent quantities, obtained with the introduction of the surface brightness, allows one to use the equation of the fundamental plane to estimate distances of elliptical galaxies and to compute deviations from a pure Hubble flow. Here we use the different solutions listed in table I, to calculate distances to the elliptical galaxies in our sample. In order to evaluate the accuracy of our distance estimates we compare them with those calculated by Lynden-Bell et al. for the subset of galaxies in common with the Burstein et al. (1987) sample. For the latter distances were computed using equation 3.1 of Lynden-Bell et al. and the photometric and spectroscopic data given by Burstein et al. (1987) and Davies et al. (1987), respectively. In this comparison our distances were determined using the solutions listed in table I. For each solution we show the raw differences $\Delta D = D_{LB}-D_{our}$ (upper panels) and the fractional difference $\Delta D/D_{our}$ (lower panels), before the application of the Malmquist bias correction discussed below. Two points are noteworthy: first, for all solutions there is no signicant zero-point difference in the distance estimates, with the median value of ΔD, in velocity units, being less than 400 km/s. Note that the inclusion of the great attractor in solution (3) leads to a striking improvement in the zero-point, which in this case is essentially zero; second, the behavior of the scatter plot of the quantity $\Delta D/D_{our}$ is consistent with errors that are proportional to the distance of the objects. These results indicate

that despite the differences in the equation of the fundamental plane, our solution yields distances which are consistent with those obtained by Lynden-Bell et al. within the expected errors. This in turn justifies the application of our data set to derive the equation of the fundamental plane and to study the peculiar motions of the ellipticals in our sample. Based on the previous results hereafter we adopt solution (3) as our distance indicator, since it is the most consistent with the recent results of Lynden-Bell et al..

Finally, we should point out that the good agreement between our distance estimates and those of Lynden-Bell et al., suggests that there are no real differences in the properties of the galaxies considered in both studies and that the expression derived here for the fundamental plane is different only because of the way we have defined the characteristic surface brightness.

b) Velocity Field

We can now use the above distance-indicator relation to investigate the peculiar velocity field. As mentioned earlier the limited sky coverage of our sample precludes any attempt to find a global solution. Instead, we use our data to investigate in more detail the nature of the velocity field after subtracting the flow generated by the mass concentration from the peculiar velocity . In particular, we make a preliminary attempt to investigate the dynamics of the large-scale structures observed in the spatial volume sampled by the SSRS. However, since the number of ellipticals is relatively small, especially after trimming the sample, the

results of the present work should be considered as tentative.

In figure 4a we plot the peculiar velocity $v_{pec} = v - v_{pred}$ versus v, where v is the observed radial velocity in the Local Group reference frame and v_{pred} is the predicted Hubble velocity calculated from the distance estimated using our equation for the fundamental plane. In this figure we show all the galaxies used in the determination of solution (3) of table I, but represent those in the same group as a single point. In our sample there is one group with 6 ellipticals (Fornax), one group with 4 (Eridanus) and one group with 2 (Telescopium). In these cases we take the observed velocity to be the mean velocity of the group, as given by Maia et al. (1988), and the distance to be the mean value of the estimated distances of the ellipticals in that group. It can be easily seen in figure 4a that there is a clear trend of the mean peculiar velocity to lie above zero, an effect that increases with distance. The same effect is present in Lynden-Bell et al.'s data and, as discussed by these authors, it reflects the tendency of the distance indicator to underestimate the true distance of the galaxy. Following the prescription of Lynden-Bell et al., we correct this effect by multiplying the estimated distances by the factor $\exp(18.56\Delta^2/N)$, where Δ once again represents the dispersion of $\log(r_e)$, and N is the number of elliptical galaxies in the same group. The corrected peculiar velocities are shown in figure 4b. Although necessary, we must emphasize that there are several potentially serious effects associated with the Malmquist correction that should be kept in mind while interpreting the resulting peculiar velocity field. First, we should emphasize that the correction proposed by Lynden-Bell et al. is only valid for a uniform distribution of galaxies, which is certainly not the case in

the region of our survey. Second, it may lead to spurious peculiar velocities, depending on its assumed value. Third, it assumes that the correction is uniform over the entire sample, in particular, that it is distance-independent. Regarding the second point, we should mention that at least within 4000 km/s it does not produce a qualitative change in the peculiar velocities which were predominantly negative even before the Malmquist correction, as can be seen comparing figures 4a and 4b. We have also verified that the value of Δ does not change significantly for galaxies with recessional velocities less or greater than 4000 km/s.

In figure 5a we project onto the Supergalactic plane the peculiar velocities of ellipticals within 45° of the plane. We note that in this figure the velocities are with respect to the reference frame of the microwave background radiation (MWB), obtained by adding the radial component of the Local Group's motion relative to the MWB. We assume that this motion is of 614 km/s toward l=268°, b=29° (Fixsen et al. 1983). The x-axis is chosen to point in the direction l=317°, b=0°, in order to make the graph similar to those presented by Dressler et al. (1987b) and Lynden-Bell et al.. A visual inspection of this plot immediately shows why the region surveyed is not adequate for detecting motions in the direction l=307°, b=9°; it covers roughly a cone 40° wide around a direction some 80° from this direction. Therefore, our sample is not expected to be very sensitive to streaming or induced motions in that direction. This can be seen in figure 5b, where we show the residual velocity field, after subtracting the flow generated by Virgo and the great attractor. As expected, in the region covered by our sample the contribution of these two concentrations to the peculiar velocities is

small. Detailed examination of figure 5b further indicates that the galaxies within the surveyed volume do not show a random scatter about zero but are predominantly approaching the Local Group. In spite of differences in the sample, the same overall trend can also be seen in figure 6c of Lynden-Bell et al., with the residual velocities for some galaxies being as large as those derived here. These motions may be possibly reflecting the inadequacies of the flow models adopted for Virgo and the great attractor or residual Malmquist errors. Another possibility, that we explore below, is that the residual velocities do indeed reflect real coherent motions of the structures observed in the galaxy distribution in that region of space.

In order to investigate the latter possibility, the peculiar velocity field is represented in a cartesian coordinate system in figure 6. In this figure we plot projections of the radial peculiar velocities, relative to the MWB, onto the x-y (figure 6a) and x-z (figure 6b) planes, after subtracting the contribution of Virgo and the great attractor. The coordinate system is defined with the x and y axis in the equatorial plane and pointing in the directions $\alpha=18^h$ and $\alpha=0^h$, respectively, and the z axis pointing towards the south celestial pole. In this coordinate system the great attractor proposed by Lynden-Bell et al. would lie at a position given by the coordinates (17, -49, 70). In order to investigate in more detail the nature of the residual motions and their relation to the observed distribution of galaxies, we plot separately in figure 7 different cuts of the velocity field. The projections of the radial component of the residual velocities are superposed to the distribution of galaxies in slices 20 Mpc thick, in the interval $0 < z < 80$ Mpc. In order to unravel

any possible relationship between the velocity field and the structures in the galaxy distribution, in figure 7 we take the origin of the velocity vectors to be at the position given by their heliocentric velocities. In some cases the origin does not coincide with the position of the galaxy because the observed velocity corresponds to the mean velocity of the group.

Examining this sequence of plots we find evidence for some degree of spatial coherence in the motion, especially up to 60 Mpc, for ellipticals in the general direction of the Telescopium-Pavo-Indus (TPI) system of galaxies. This region, as described by da Costa et al. (1988a), is rather complex; it is formed by a number of small groups and seems to be the intersection of two large, thin structures, one of which extends out of the boundary of the survey volume in the direction of the Hydra-Centaurus region.

The interpretation of the data is definitely hampered by the small number of points available and the fact that the ellipticals delineate the large scale structures rather poorly. For z between 40 and 60 Mpc we have the impression that the motion of the galaxies may be reflecting a large streaming motion of the structure that cuts across the survey volume. On the other hand, for the slice between 20 and 40 Mpc the motion seems to be along one of the sheets. The only thing that we can say for sure is that the TPI complex exhibts evidence of coherent peculiar motions with an amplitude of about 1200 km/s, much larger than the dispersion expected from small scale motions (<300 km/s). However, at this time it is premature to say whether these motions are actually

reflecting the peculiar motion of the structures themselves. This will only be possible when more data become available, allowing us to sample the structures more densely.

V. DISCUSSION

In this paper we have used independent photometric and spectroscopic data to derive the equation of the two-dimensional surface that describes the family of ellipticals. In particular, we have shown that although the coefficients are slightly different from those obtained in earlier works (Dressler et al. 1987a, DD), the elliptical galaxies in our sample describe essentially the same surface. This has been demonstrated from the comparison between our estimated distances and those obtained by Lynden-Bell et al.. This result also indicates that despite the use of photographic material we can still determine good photometric parameters that can be used to define a reliable distance indicator.

The previous conclusion is important because it justifies the use of the same techniques employed here to study the properties of the S0 galaxies in the SSRS sample. This work would complement that of Dressler (1987) for S0 galaxies in the core of rich clusters. This extension would also be of interest in the mapping of the peculiar velocity field since the S0 galaxies delineate the structures more densely than ellipticals. The extension to the southern hemisphere is particularly important because in this region the influence of both Virgo and the great attractor are relatively small, thus allowing a better determination of the fundamental plane of S0 galaxies in the general field.

The more general question of uniform bulk motions, the existence of the great attractor and the influence of the environment on the fundamental plane should be pursued utilizing a larger number of groups and clusters

of galaxies, for which the distance estimates are much more reliable, extending the observations to fainter members.

In the present work we have found some marginal evidence for systematic, coherent motions in the surveyed volume which may be associated to the observed structures in the galaxy distribution. Despite the large uncertainties, the peculiar motions detected exhibit a systematic trend and a certain degree of spatial coherence. Furthermore, the amplitudes of these residual velocities are also significantly larger than the expected velocity dispersion of field galaxies (Lynden-Bell et al. 1988). All of this may indicate that we have detected motions of, or within, the large-scale structures, but the confirmation of this result will have to await until more data on groups, S0's and late-type galaxies become available. We are presently taking the first steps in those directions.

Finally, we emphasize that the detection of bulk motions of the large-scale structures, if confirmed, would be an important feature of the distribution of matter in the Universe that could help discriminating amongst competing models for formation and evolution of large-scale structures.

ACKNOWLEDGEMENTS

We would like to thank the entire Redshift Survey team for their help in obtaining the data used in this paper. We would also like to thank S. Djorgovski for inumerous suggestions and for making available some of

the analysis routines.

Table I- Parameters for the Fundamental Plane

Solution	a	b	c	χ^2	Δ	Number
1	0.99	0.18	-2.60	1.34	0.11	36
2	1.24	0.14	-3.08	1.36	0.11	35
3	1.16	0.14	-2.56	1.35	0.12	35

REFERENCES

Burstein, D., Davies, R.L., Dressler, A., Faber, S.M., Stone, P.S., Lynden-Bell, D., Terlevich, R.J., and Wegner, G. 1987, Ap. J. Suppl., 64, 601.

da Costa, L.N., Pellegrini, P.S., Sargent, W.L.W., Tonry, J., Davis, M., Meiksin, A., and Latham, D. 1988a, Ap. J. in press.

da Costa, L.N., de Carvalho, R.R., Rite, C., and Latham, D. 1988b, in preparation (paper II).

Davies, R.L., Burstein, D., Dressler, A., Faber, S.M., Lynden-Bell, D., Terlevich, R., and Wegner, G. 1987, Ap. J. Suppl., 64, 581.

de Carvalho, R.R., and da Costa, L.N. 1988, to appear in Ap. J. Suppl. (paper I).

Djorgovski, S., and Davis, M. 1987, Ap. J., 313, 59.

Dressler, A. 1987, Ap. J., 317, 1.

Dressler, A., Lynden-Bell, D., Burstein, D., Davies, R.L., Faber, S.M., Terlevich, R., and Wegner, G. 1987a, Ap. J., 313, 42.

Dressler, A., Faber, S.M., Burstein, D., Davies, R.L., Lynden-Bell, D., Terlevich, R., and Wegner, G. 1987b, Ap. J. (Letters), 313, L37.

Faber, S.M., and Jackson, R.E. 1976, Ap. J., 204, 668.

Fixsen, D.J., Cheng, E.S., and Wilkinson, D.T. 1983, Phys. Rev. Letts., 50, 620.

Lynden-Bell, D., Faber, S.M., Burstein, D., Davies, R.L., Dressler, A., Terlevich, R., and Wegner, G. 1988, preprint.

Maia, M., da Costa, L.N., and Latham, D. 1988, in preparation.

Yahil, A., Tammann, G.A., and Sandage, A. 1977, Ap. J., 217, 903.

Figure Captions

Figure 1- The best fits for the three solutions of the fundamental plane described in the text.

Figure 2- Plot of $\log\sigma$ x $B_0(V)$ for the 38 galaxies used in the determination of the fundamental plane of ellipticals.

Figure 3- Comparison between the estimated distances using our different solutions and those obtained using the expression given by Lynden-Bell et al. (1988) and the data of Burstein et al. (1987) and Davies et al. (1987). In the upper panels we plot the quantity $\Delta D=D_{LB}-D_{our}$ and in the lower panels $\Delta D/D_{our}$.

Figure 4- Plot of the peculiar velocity, $v_{pec}=v-v_{pred}$, versus the recessional velocity v, in the Local Group rest frame, before (a) and after (b) the Malmquist correction defined in the text.

Figure 5- Projection of the peculiar radial velocities onto the supergalactic plane, for galaxies within 45° of the plane. In panel (a) the velocities are in the MWB rest-frame, while in (b) we show the peculiar velocities after subtracting the flow generated by Virgo and the great attractor.

Figure 6- Projection of the peculiar velocities onto the x-y (a) and x-z (b) planes of the cartesian coordinate system defined in the text. We plot the peculiar velocities in the MWB rest-frame,

after subtracting the flow generated by Virgo and great attractor.

Figure 7- Same as figure 6 for slices 20 Mpc thick, projected onto the x-y plane of the coordinate system of figure 6. The z-intervals shown are indicated in the figures. The different symbols denote: (full squares) elliptical galaxies; (full triangles) S0's; (open circles) galaxies of later morphological types. All galaxies are from the SSRS sample. The tip of the velocity vectors are represented by small full squares.

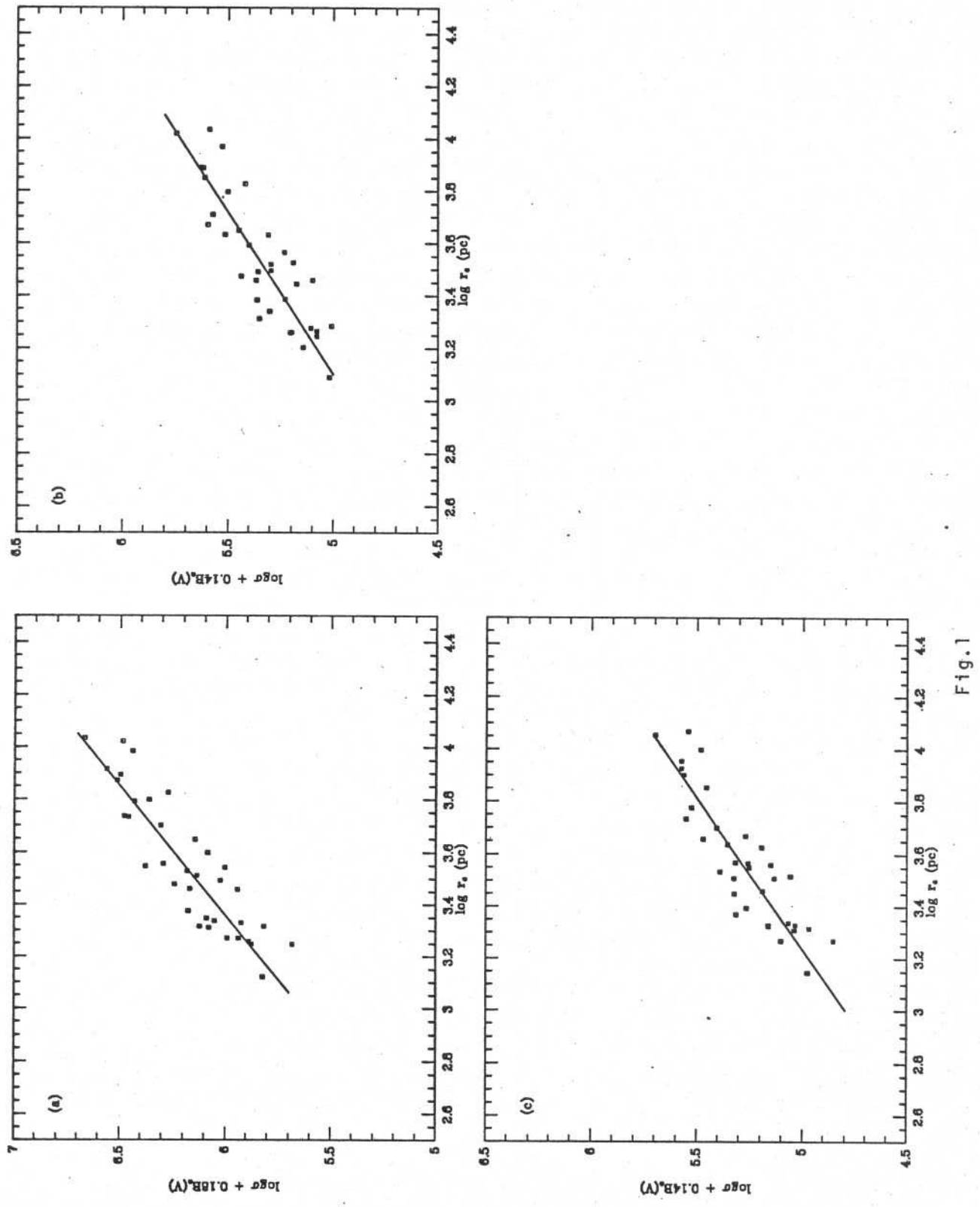

Fig.1

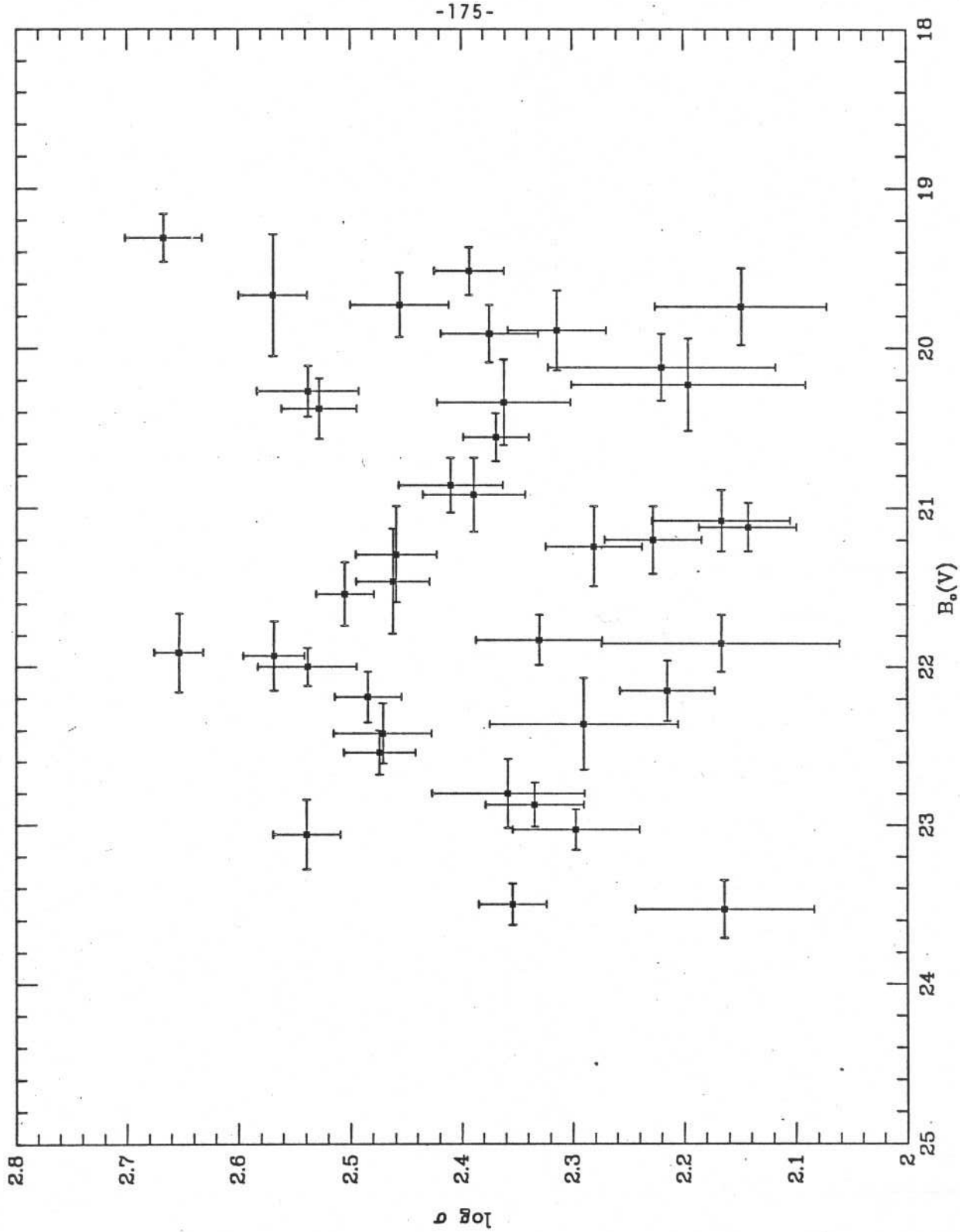

Fig.2

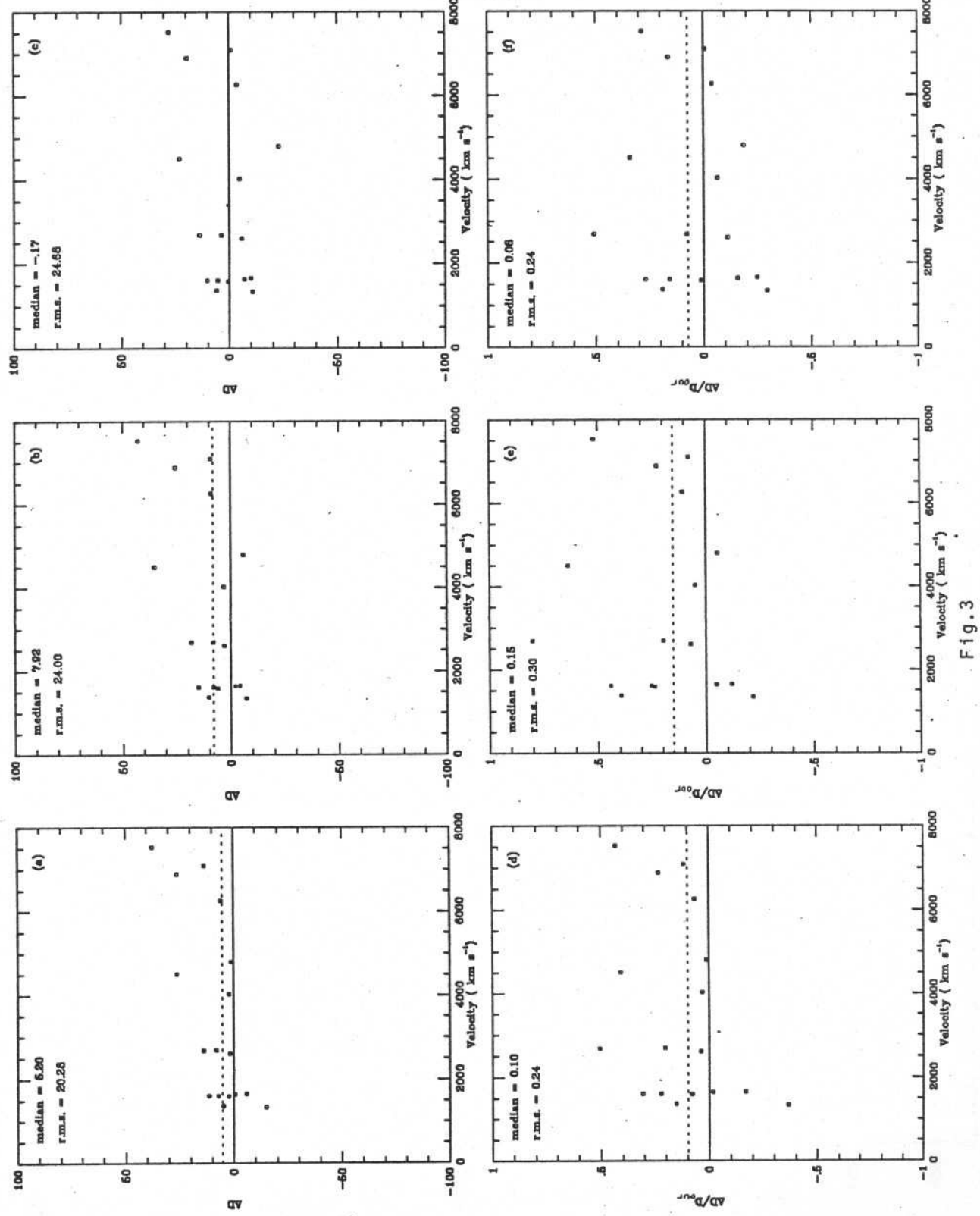
(a)
median = 6.20
r.m.s. = 20.26
(b)
median = 7.92
r.m.s. = 24.00
(c)
median = -.17
r.m.s. = 24.68
(d)
median = 0.10
r.m.s. = 0.24
(e)
median = 0.15
r.m.s. = 0.30
(f)
median = 0.06
r.m.s. = 0.24
ΔD
ΔD/D_our
Velocity (km s⁻¹)

Fig.3

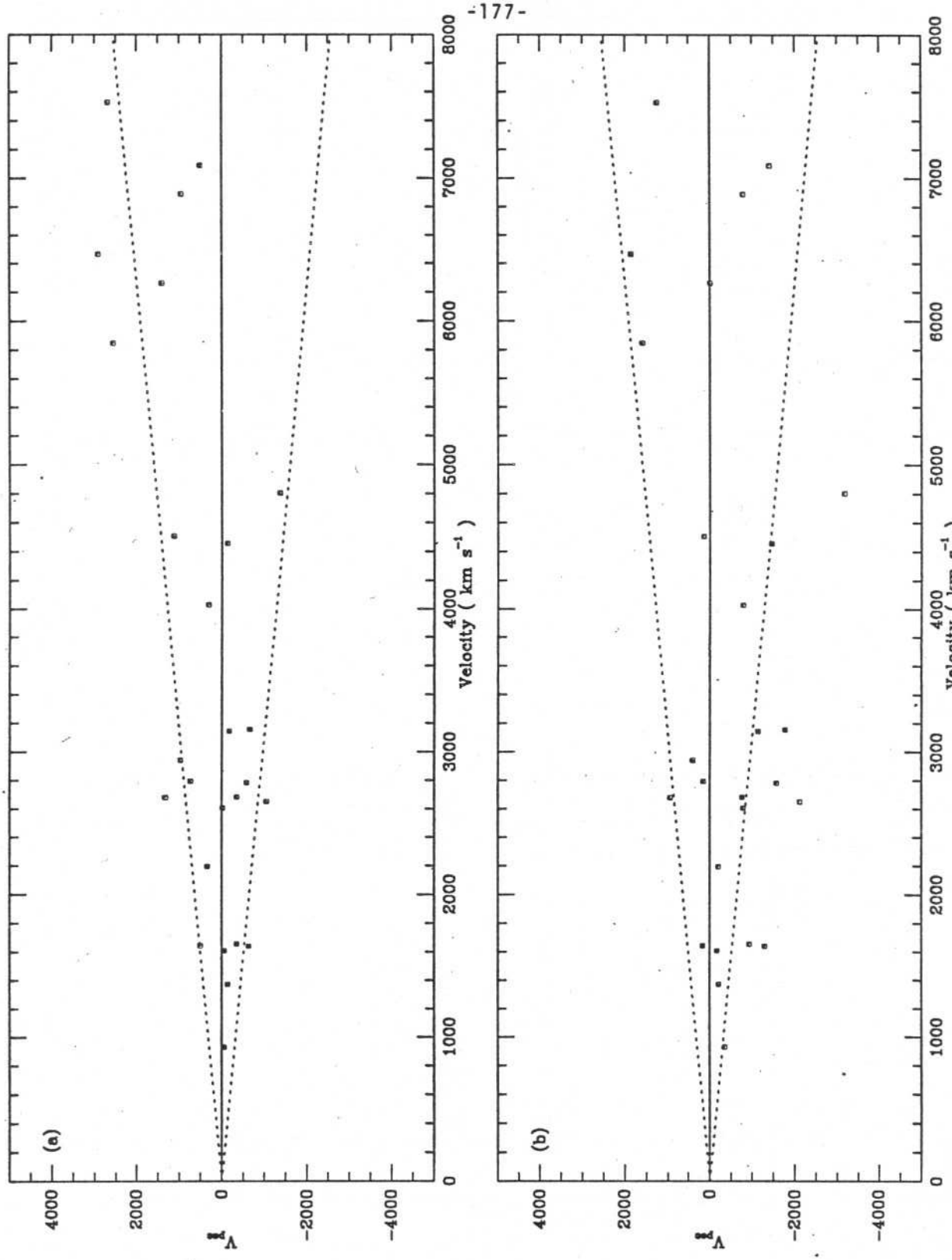
(a)
(b)
V_{pe}
4000
2000
0
−2000
−4000
0
1000
2000
3000
4000
5000
6000
7000
8000
Velocity (km s^{-1})

Fig.4

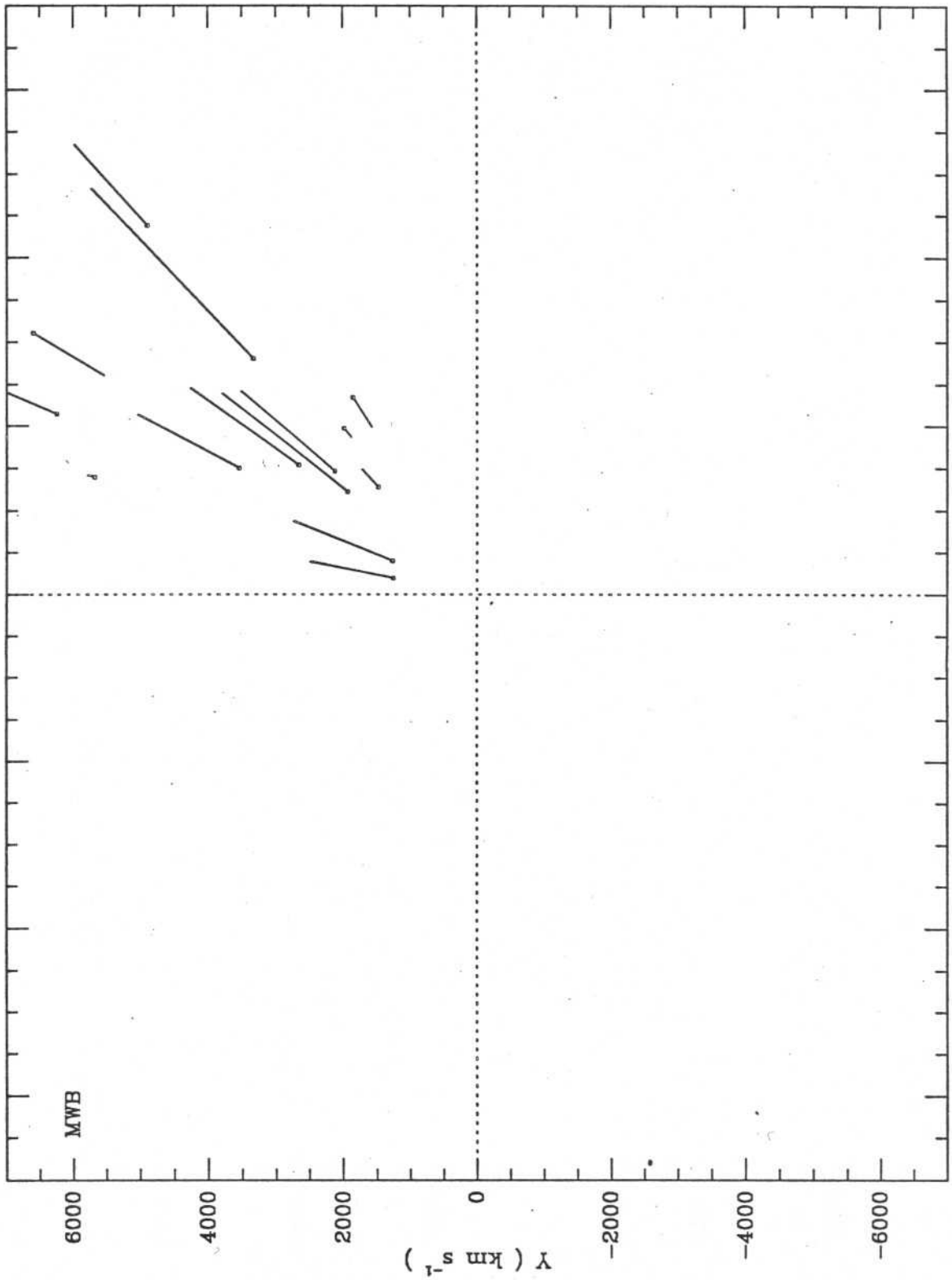
MWB
6000
4000
2000
0
-2000
-4000
-6000
Y (km s^{-1})
-6000
-4000
-2000
0
2000
4000
6000
X (km s^{-1})

Fig.5a

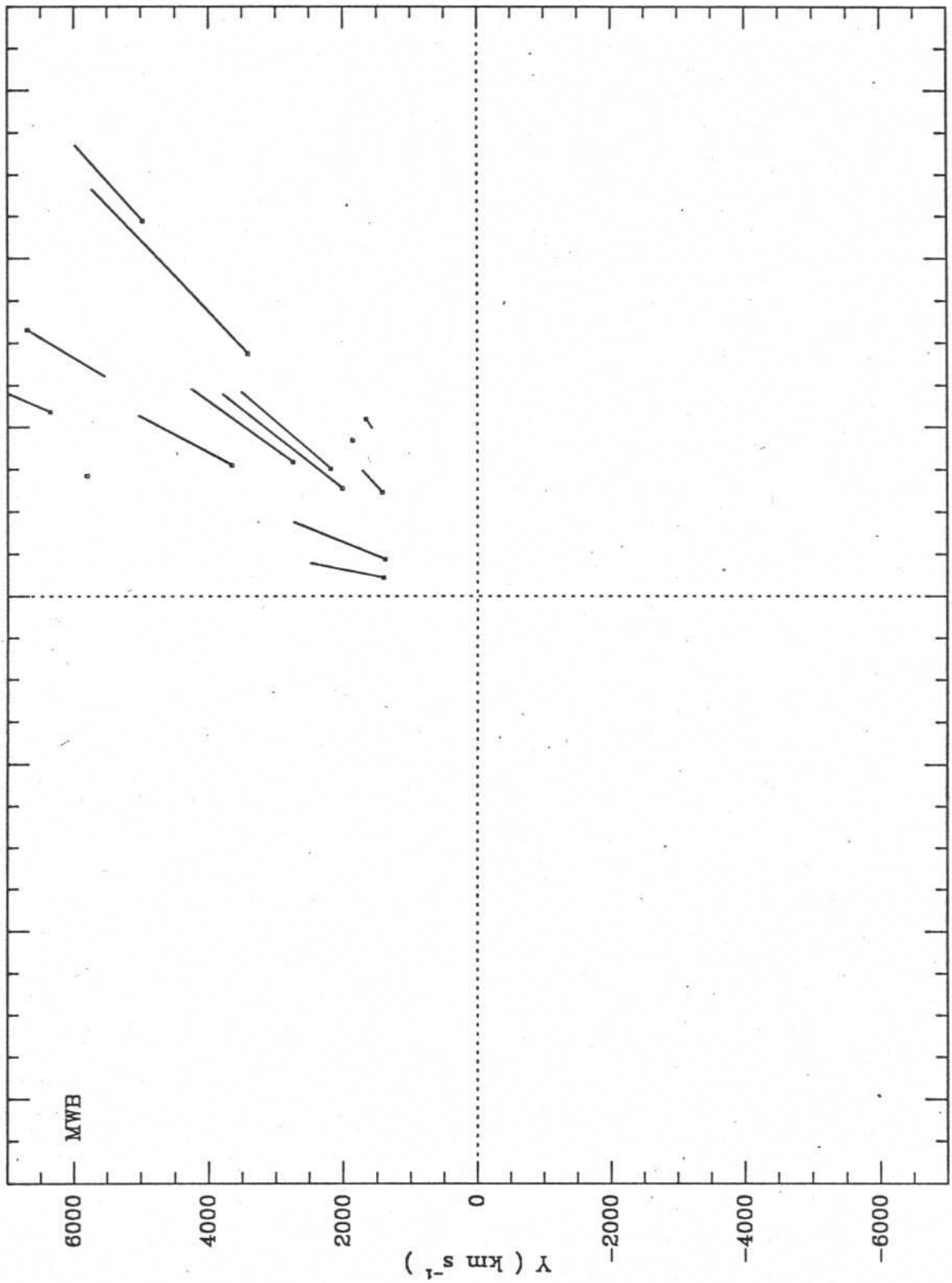

Fig.5b

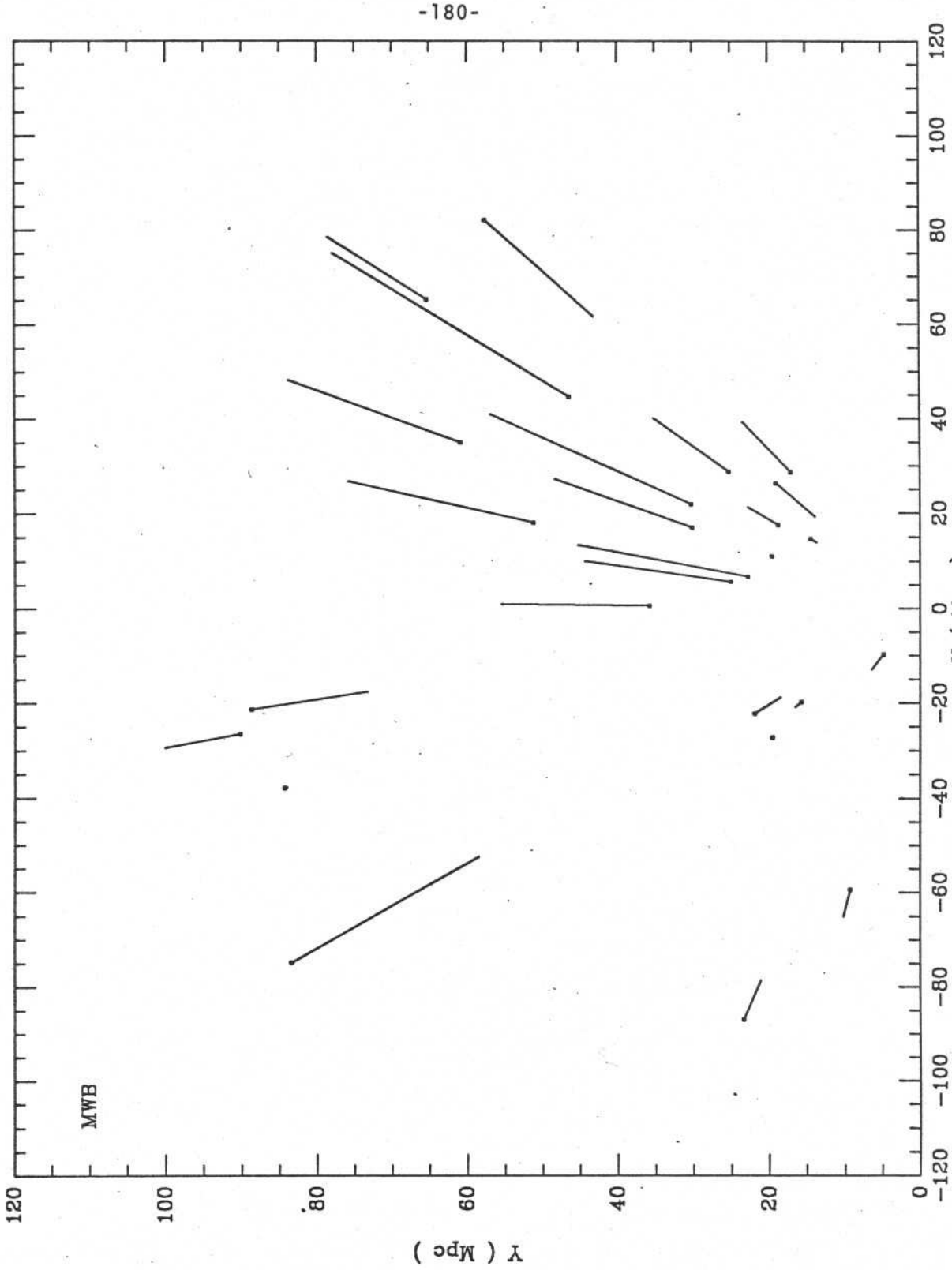
MWB
Y (Mpc)
X (Mpc)
120
100
80
60
40
20
0
-120
-100
-80
-60
-40
-20
0
20
40
60
80
100
120

Fig.6a

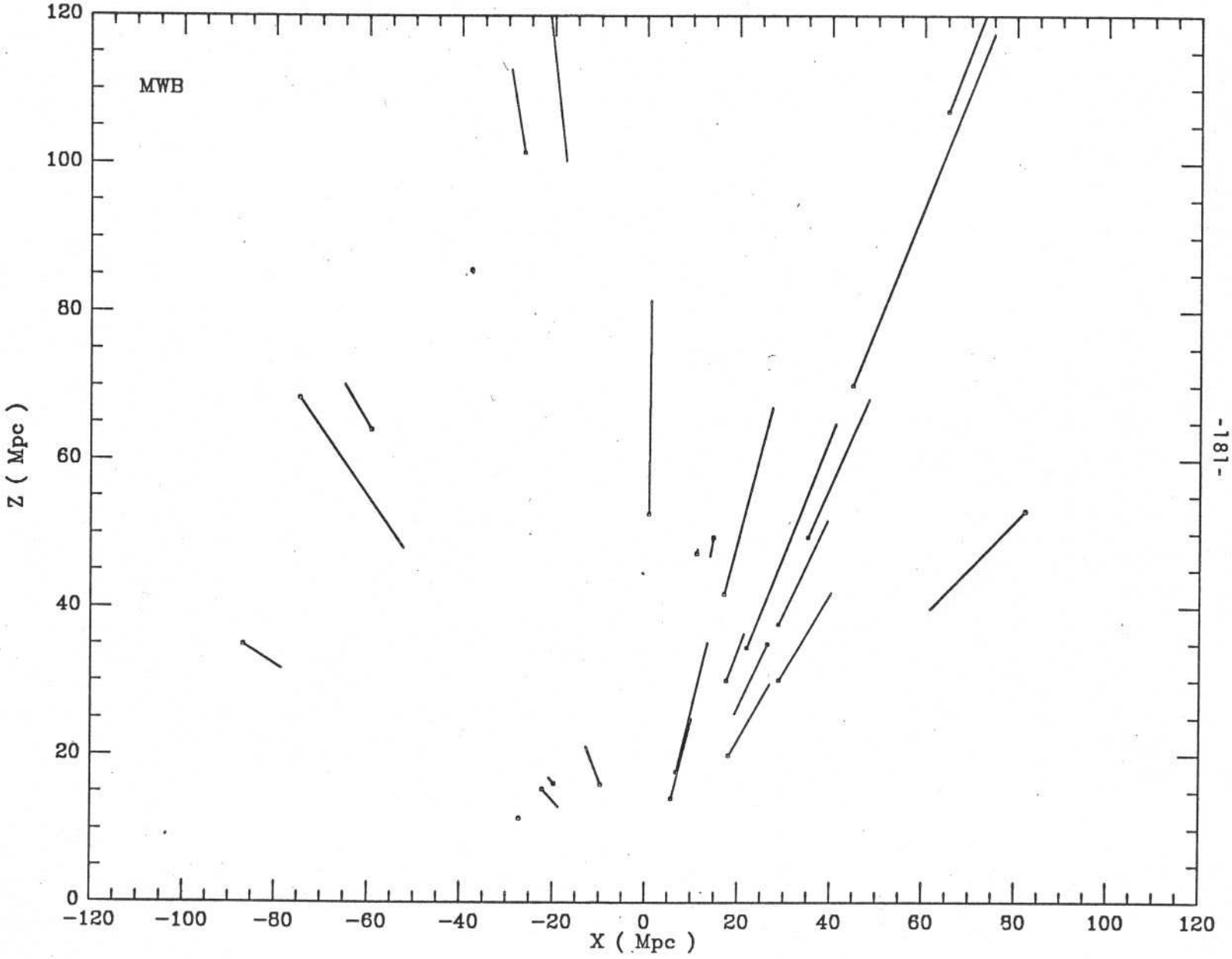
MWB
120
100
80
60
40
20
0
Z (Mpc)
-120
-100
-80
-60
-40
-20
0
20
40
60
80
100
120
X (Mpc)

Fig.6b

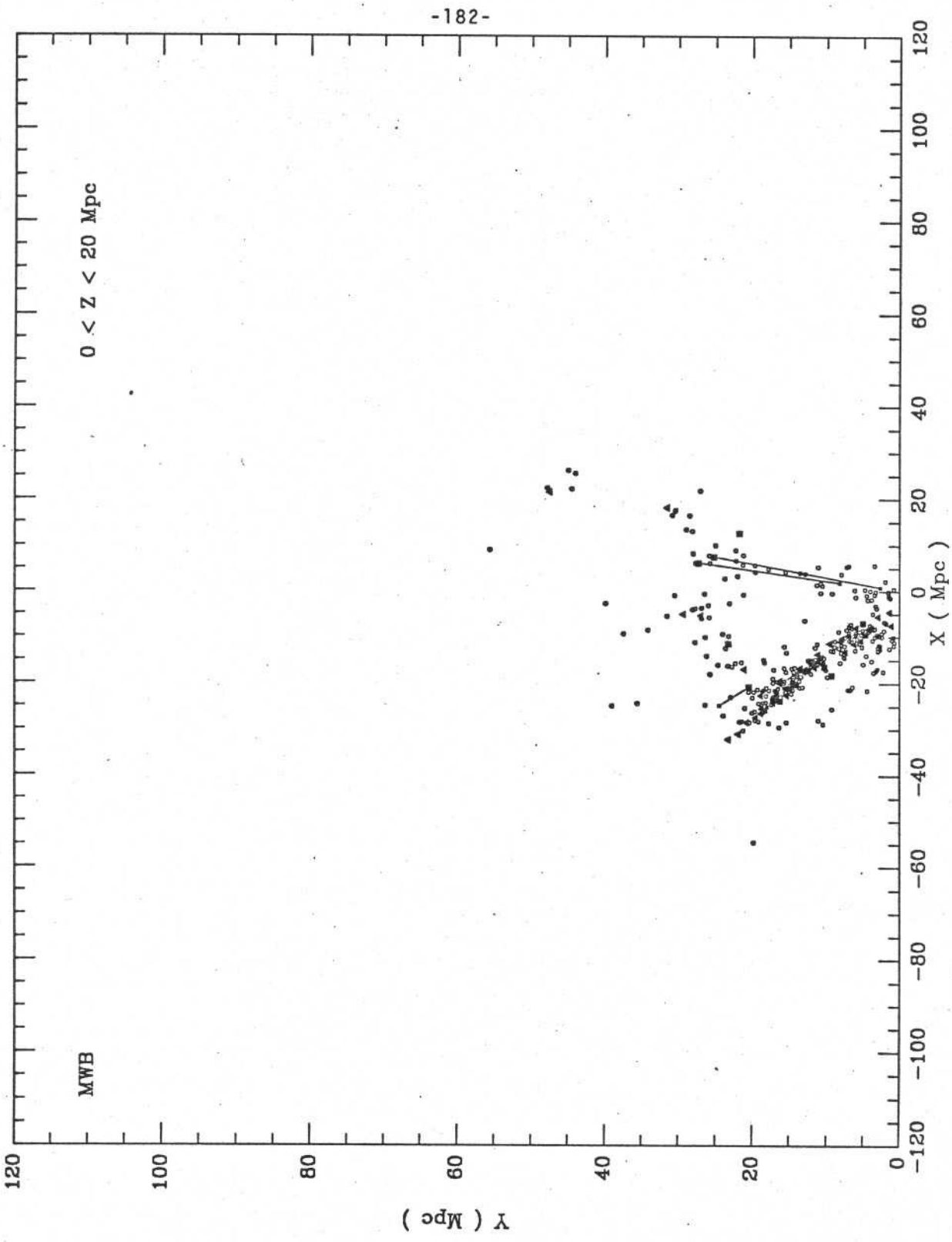
0 < Z < 20 Mpc
MWB
Y (Mpc)
X (Mpc)
120
100
80
60
40
20
0
-120
-100
-80
-60
-40
-20
0
20
40
60
80
100
120

Fig.7

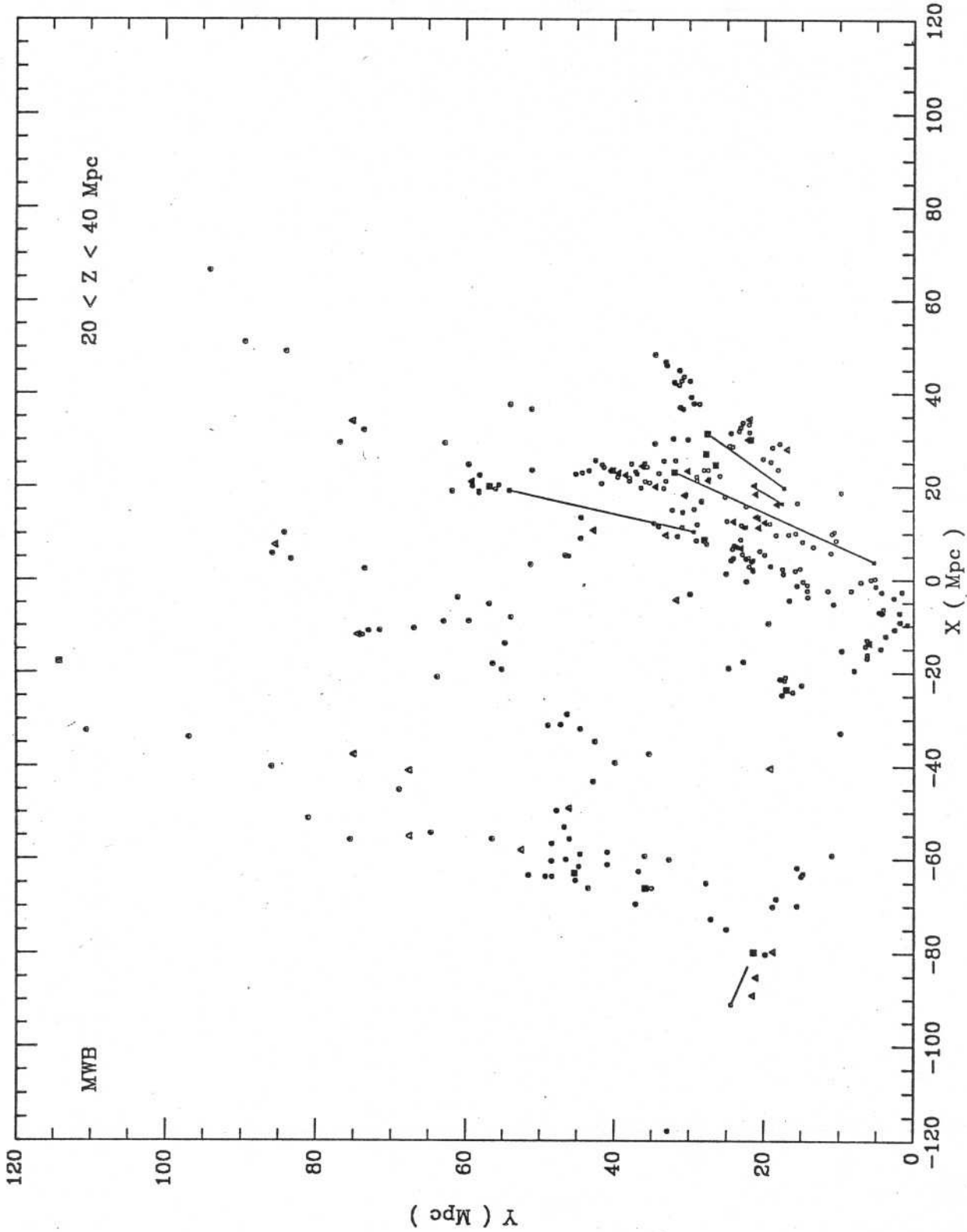

Fig.7 - continued

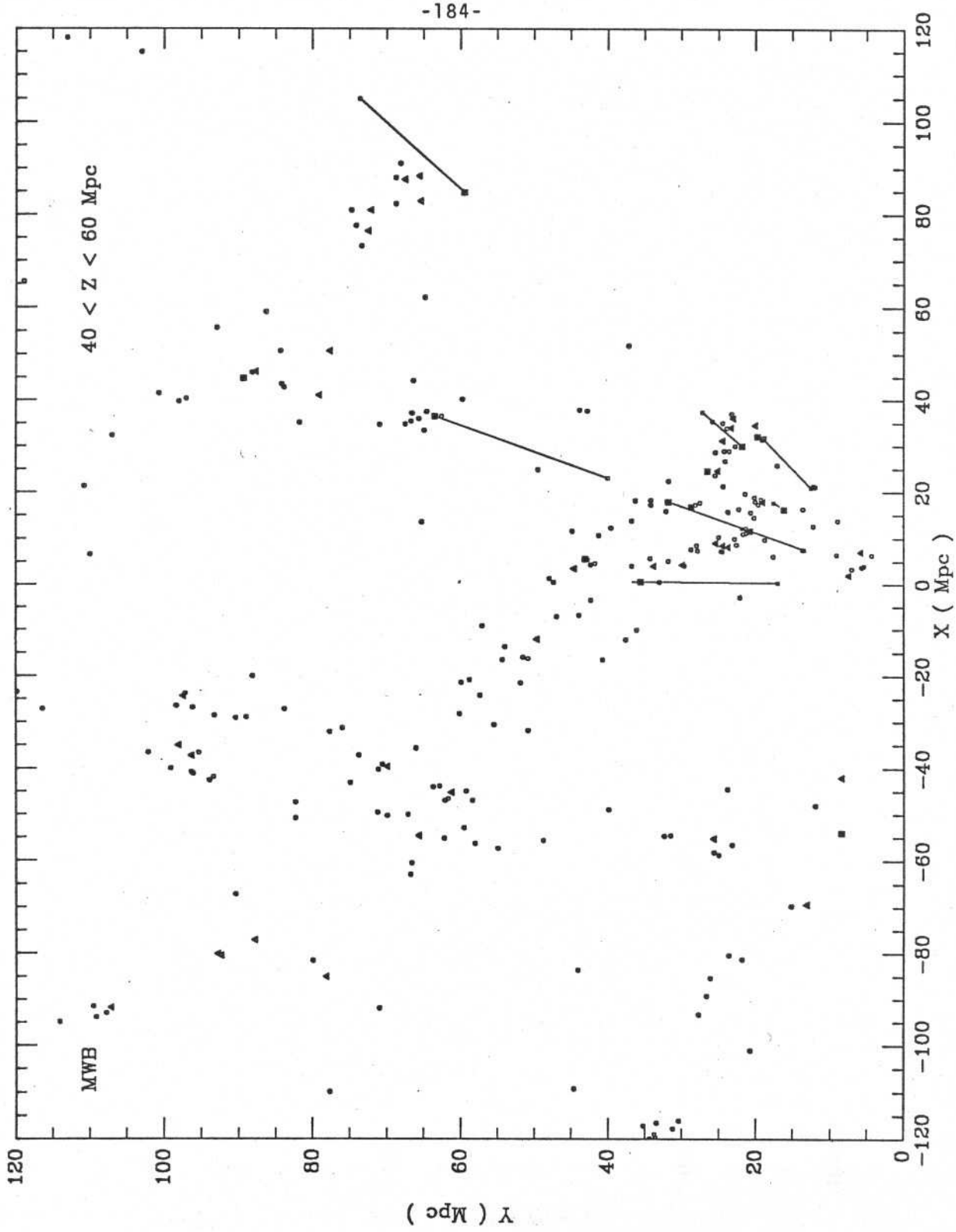

Fig.7 - continued

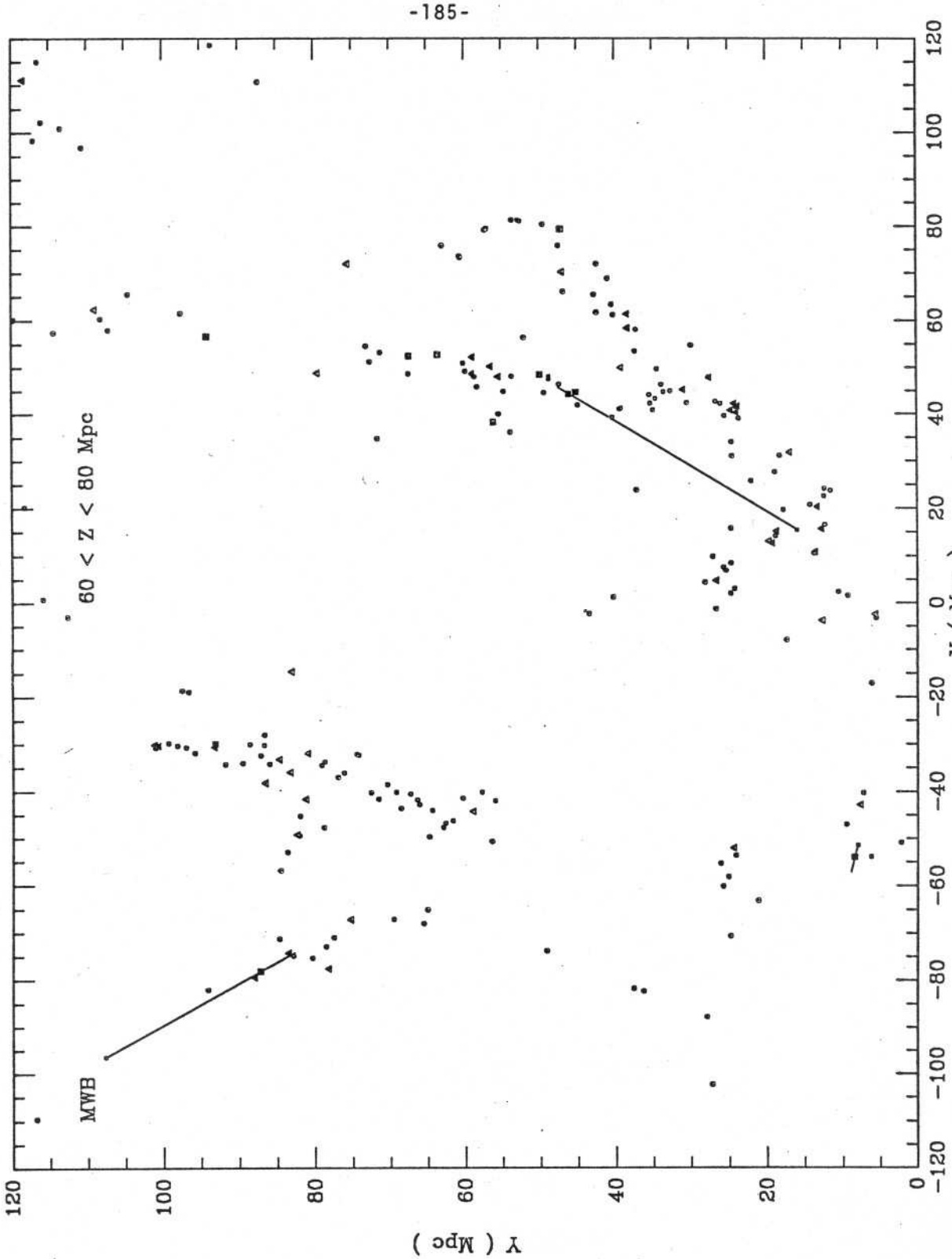

Fig.7 - continued

VII- Comentários Finais

Neste trabalho foram examinados alguns temas relacionados às propriedades estruturais de galáxias "early-type". No capítulo II foi feito um estudo das propriedades de galáxias S0 em regiões de alta densidade galáctica que, como visto, é fundamental para o desenvolvimento das teorias que tentam explicar a origem destes sistemas. As galáxias S0 estudadas no capítulo II não apresentaram nenhuma evidência de corte na sua distribuição de brilho, o que seria de se esperar se o disco é formado lentamente e tem seu crescimento interrompido devido a perda de seu reservatório de gas. Para este estudo os sistemas "edge-on" são mais adequados porque permitem investigar a estrutura do disco a maiores distâncias e também a sua estrutura vertical, fornecendo dados importantes sobre o processo de formação desta componente, o que neste trabalho foi feito no capítulo III utilizando a galáxia NGC 1381. No capítulo IV foram apresentados e discutidos os dados fotométricos obtidos a partir de um levantamento de 131 galáxias elípticas. Estes dados são de interesse tanto isoladamente como em conjunto com os dados espectroscópicos do SSRS. No capítulo V foi demonstrada a boa qualidade das medidas de velocidade de dispersão obtidas. Estes dados foram usados no capítulo VI para estudar o campo de velocidade peculiar, dando enfase a sua possível associação com o movimento das grandes estruturas observadas na distribuição de galáxias no hemisfério sul.

Os temas abordados neste trabalho envolveram um grande esforço pois são o resultado de dois grandes levantamentos que vem sendo realizados ao

longo dos últimos anos. Parte deste esforço ainda está em andamento, e é importante mencionar que o banco de dados fotométrico contém aproximadamente 500 imagens de galáxias S0 no hemisfério sul digitalizadas e reduzidas incluindo todas as galáxias early-type com dados disponíveis do SSRS. Este levantamento, concluido recentemente, em conjunto com o levantamento fotométrico das galáxias elípticas, formará a primeira base de dados homogênea de sistemas "early-type" no hemisfério sul.

Em prosseguimento a este projeto também obtivemos dados fotométricos (em colaboração com G. Djorgovski), utilizando uma câmara CCD no CTIO, para uma amostra de galáxias elípticas no aglomerado de Fornax, completa até magnitude 15. Para todos estes objetos medidas de velocidade dispersão já se encontram disponíveis a partir da extensão do SSRS que vem sendo atualmente realizada no Complejo Astronomico El Leoncito numa colaboração entre o ON e o Harvard-Smithsonian Center for Astrophysics.

Os dados dos programas acima mencionados permitirão dar continuidade aos vários temas abordados neste trabalho. Em particular, a análise das galáxias elípticas no aglomerado de Fornax e os parâmetros fotométricos que ficarão disponíveis para as galáxias S0 serão de grande importância para: 1) analisar em maior detalhe a possível influência do meio ambiente na estruttura interna das galáxias que deve se refletir em seu plano fundamental; 2) verificar se as galáxias S0 obedecem a uma lei tão bem definida quanto a expressa pelo plano fundamental das galáxias elípticas; 3) mapear em maior detalhe o campo de velocidade residual e a possível

existência de movimentos peculiares das estruturas de galáxias em grande-escala.

Todos os Interessados em Publicações do Observatório Nacional. Devem Dirigir-se à

NCT - CNPQ
Observatório Nacional
Biblioteca
Setor de Reprodução Gráfica
r. General José Cristino, 77 - CP. 23002
20921 - São Cristovão, RJ
BRASIL
Telf. 5807313 - r. 271